Comparison of Lateral Load Resisting Systems in Steel-Concrete Composite Tall Buildings

BY

Jenish Y. Patel

20MCLC10

DEPARTMENT OF CIVIL ENGINEERING

INSTITUTE OF TECHNOLOGY

SCHOOL OF ENGINEERING

NIRMA UNIVERSITY

AHMADABAD-382481

May 2022

Comparison of Lateral Load Resisting Systems in Steel-Concrete Composite Tall Buildings

Major Project

Submitted in partial fulfillment of the requirements

for the degree of

Master of Technology

in

Civil Engineering

(Computer Aided Structure Analysis and Design)

By

Jenish Y. Patel

20MCLC10

Under the guidance of

Prof. P. V. Patel

DEPARTMENT OF CIVIL ENGINEERING

INSTITUTE OF TECHNOLOGY

SCHOOL OF ENGINEERING

NIRMA UNIVERSITY

AHMADABAD-382481

May 2022

Declaration

This is to certify that

a The major project comprises my original work towards the Degree of Master of Technology in Civil Engineering (Computer Aided Structural Analysis And Design) at Nirma University and has not been submitted elsewhere for a degree.

b Due acknowledgement has been made in text to all mother material used.

Jenish Y. Patel

Certificate

This is to certify that the Major Project Report entitled **"Comparison of Lateral Load Resisting Systems in Steel-Concrete Composite Tall Buildings"** submitted by **Jenish Y. Patel (20MCLC10)**, towards the partial fulfillment of the requirements for the degree of Master of Technology in Civil Engineering (Computer Aided Structural Analysis And Design) of Nirma University is the record of work carried out by him under our supervision and guidance. The work submitted has in our opinion reached a level required for being accepted for examination. The results embodied in this major project work to the best of our knowledge have not been submitted to any other University or Institution for award of any degree or diploma.

Dr. P. V. Patel
Guide & Professor,
Dept. of Civil Engg.,
Institute of Technology,
Nirma University,
Ahmedabad.

Dr. Urmil V. Dave
Professor & Head,
Dept. of Civil Engg.,
Institute of Technology,
Nirma University,
Ahmedabad.

Dr R. N. Patel
Director,
Institute of Technology,
Nirma University,
Ahmedabad.

_____
Examiner

_____
Date of Examination

Abstract

The rising urbanization of the world's population, the high cost of land, and the competition to build smart, sustainable, and distinctive skyscrapers have contributed to a surge in tall building development. Designing and constructing a skyscraper is a challenging task. Along with architectural design considerations such as core planning, slenderness ratio, and building forms, structural design considerations such as structural materials and structural systems play a significant role in making tall buildings smart, sustainable, and resilient. The evolution of structural systems, materials, and construction technology has pushed the height barrier of skyscrapers over the last few decades. In general, the stiffness of tall structures is equally important as their strength because the lateral stiffness requirements for tall structures to resist lateral loads induced by wind or earthquakes governs as the structure's height increases. So, the selection of suitable structural systems and materials becomes essential.

Due to natural phenomena like wind storms and earthquakes, buildings are affected greatly, causing significant loss globally. Building authorities are constantly taking measures against such severe hazards. In the last few years, the Bureau of Indian standards has brought revisions in the wind and seismic codes such as IS 875 (Part 3): 2015 and IS 1893 (Part 1): 2016 along with IS 16700: 2017 for design criteria of tall structures.

One of the objective of present project work is to understand various approaches for evaluation of wind loading on tall buildings. The evaluation of along and across wind forces acting on tall buddings is carried out utilizing the gust factor method from IS 875 (Part 3): 2015. In addition to codal specifications, wind time history data based on wind tunnel studies available at Tokyo Polytechnic University (TPU) Aerodynamic database is used. The present study considers nine different tall buildings with different number of story and aspect ratios for comparison of wind load obtained from IS 875 (Part 3): 2015 and wind tunnel study based TPU database. Three distinct methodologies are used to calculate along and across wind forces using the TPU database's wind time history data: maximum sum of pressure coefficients at particular time instant, peak pressure coefficients and mean pressure coefficients. It is observed that along wind forces calculated from pressure coefficients using the TPU database match with the wind forces evaluated

from the gust factor method from IS 875 (Part 3): 2015, while for across wind forces, difference is observed between wind forces calculated from IS 875 (part 3): 2015 and TPU database.

The main objective of the present study is to gain a better understanding about the behaviour and design of steel-concrete composite tall building structural systems, including the impact of lateral loads induced by wind and earthquakes. The present study analyses and designs tall buildings with four basement floors, ground floors and 19, 39 and 59 upper stories with different lateral load resisting structural systems such as Structural Wall-Moment Frame system, Tubular system, and Outrigger and Belt Truss system. The location of tall buildings is considered as Ahmedabad (Seismic zone III and basic wind speed 39 m/s). Response Spectrum analysis in accordance with IS 1893 (Part 1): 2016 as well as Site-specific Response Spectrum and Time History analysis are performed for seismic lateral load analysis. For analysis and design purposes, both along and across wind forces in accordance with IS 875 (Part 3): 2015 are considered concurrently. All building models are modelled, analysed and designed in line with applicable Indian standards, including IS 16700: 2017, IS 875 (Part 3): 2015, IS 1893 (Part 1): 2016, IS 456: 2000, and IS 13920: 2016, as well as the composite design code AISC 360-10 using ETABS software. Excel sheets are also developed for design of various composite structural elements like composite slab, composite beam, composite columns etc.

The Structural Wall-Moment Frame, Tubular and Outrigger, and Belt Truss systems are compared in terms of building response characteristics such as time period, base shear, modal mass participating ratio, top story displacement, inter-story drift ratio, design forces, contribution of structural walls in resisting lateral loads, and structural weight. For 24 story buildings, the design governed either by the strength parameters of structural members or the torsional mode time period values, but for 44 and 64 story buildings with any structural system, the design is governed by the top story displacement in all structural systems. Based on concrete and steel quantity estimates, the structural wall-moment frame system and tubular system are correspondingly more cost-effective structural system for 24-story tall building. Outrigger structural system can become cost-effective by altering location of outrigger from mid-height to the optimum location of outrigger in

the building. The outrigger system is the cost-effective and efficient structural system for 44-story and 64-story tall buildings considered in the present study.

Acknowledgement

In the name of *the almighty* who founded this puzzling mother earth to grace us with the power to solve its mysteries and helped me to reinvent myself time to time.

This project would not have been possible without the support of many people. I would first of all like to thank my guide **Dr. P. V. Patel**, Professor, Department of Civil Engineering,Institute of Technology, Nirma University who read my numerous revisions and helped make some sense of the confusion. His insightful remarks and assistance aided me in honing my professional writing skills and completing this project flawlessly.

I also extend my thanks to **Dr. Urmil V.Dave**, Head and Professor and **Dr. Sharad P. Purohit**, Professor, Department of Civil Engineering, Institute of Technology,Nirma University, Ahmedabad, for their valuable guidance and continual encouragement throughout my major project work. I further extend my thanks to **Dr. R. N. Patel**, Director, Institute of Technology, Nirma University, Ahmedabad.

I would also like to thank my fellow classmates of M.Tech (CASAD), batch 2020-22, Nirma University, for their support, help and for encouraging me in every ways.

I am highly indebted to my family members and my friends by whose blessings, endless love and support, help me to complete my study and encouraged me in all possible way.

Jenish Y. Patel

20MCLC10

Abbreviation, Notation and Nomenclature

SM ..... Structural Wall-Moment Frame
RF ..... Rigid Frame
TT ..... Tube-in-tube
TB ..... Tubular
OR ..... Outrigger and Belt Truss
RCC ..... Reinforced cement Concrete
G ..... Gust Factor
SWLA ..... Static Wind Load Analysis
DGF .Dynamic wind load analysis using Gust Factor method from IS 875 (Part 3):2015
DTHA ... Dynamic wind load Time History Analysis using TPU aerodynamic database
SSRSA .....Site-specific Response Spectrum Analysis
LLRS .....Lateral Load Resisting System
MMPR ..... Modal Mass Participating Ratio
f_y .....Yeild strength of the section
f_{ck} ..... Characteristic strength of concrete cube
k_2 ..... Terrain roughness and height factor
p_d .....Design wind pressure
$\overline{k_{2,i}}$ ..... Hourly mean wind speed factor
$\overline{p_{d,i}}$ ..... Design hourly mean wind pressure
E .....Modulus of Elasticity
I .....Moment of Inertia
B .....Width of the Column
D .....Depth of the Column
T ..... Thickness of steel tube

Contents

List of Figures

List of Tables

Chapter 1

Introduction

1.1 General

Globally, high-rise buildings have been developed as a result of advancements in construction technology, the evolution of efficient structural systems, and the scarcity of urban land. Along with gravitational loading, lateral loading caused by wind or earthquakes governs the design of high-rise buildings. There is no universally accepted definition for tall buildings or high-rise structures; however, there are some characteristics that can be used to express tallness. These are the following elements: Height relative to context, Proportion, and Technologies. Even 20-story buildings are considered tall structures in cities like Ahemdabad, not in Chicago or Hongkong. The proportion of any structure can be expressed as the ratio of the building's height to its lateral dimension. This means that buildings of the same height cannot be tall if the lateral dimension of one is quite large and the lateral dimension of another is quite small. A skyscraper is generally defined as a structure with a slenderness ratio greater than or equal to 6. A building can also be classified as tall if it incorporates technologies such as special vertical transport and structural wind bracing.[6] Fig. 1.1 shows classification of tall, super tall and mega tall buildings as per CTBUH [6].

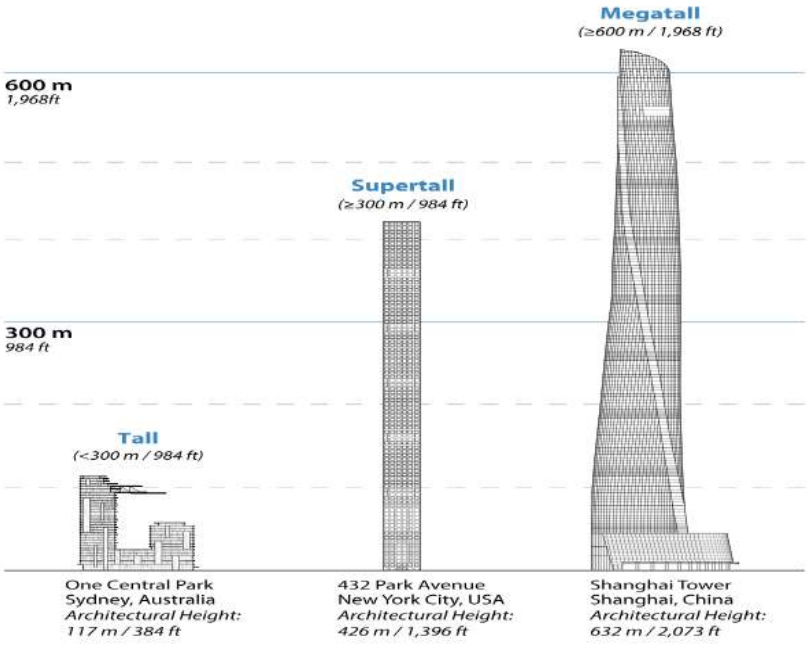

Figure 1.1: Classification of tall, super tall and mega tall buildings as per CTBUH[6]

1.2 Structural Systems in Tall Buildings

As the height of the building increase, the lateral loads become more critical than the gravity loads, and the total material used for floor framing increase rapidly with the increase in the height of the building. Thus the conventional rigid frame structures used for low rise to medium-rise buildings cannot be used in high rise buildings. There is a need to explore new structural systems for high rise buildings. The choice of structural system depends on several factors like the geometry of the building, site conditions, functional requisites and aesthetics of the building. The various structural systems can be broadly classified as gravity load resisting systems and lateral load resisting systems[34].

1.2.1 Concrete Structural Systems

Concrete offers a wide range of structural systems which are suitable for tall buildings. Concrete is favoured in low-rise to medium-rise buildings due to advantages like the flexibility to create any shape and size, high fire resistance and less requirement of skilled labours.[34] The gravity load resisting systems in concrete tall buildings are:

a. Flat plates

b. Flat slabs

c. Waffle system

d. Ribbed slabs

e. Skip joist system

f. Band beam system

g. Haunch girder and joist system

h. Beam and slab system

i. Pre-stressed concrete system

The lateral load resisting systems in concrete tall buildings are:

a. Flat slab frame system

b. Rigid frame system

c. Infilled frame system

d. Widely spaced perimeter tube

e. Rigid frames with haunch girders

f. Flat slab frame with shear walls

g. Wall-frame system

h. Tubular system

i. Outrigger-braced system

j. Hybrid system

1.2.2 Steel Structural Systems

After the second world war, the use of structural steel has been rapidly increased. Steel structures have advantages over concrete structures like high strength to weight ratio, ease of fabrication, fast erection and installation and no requirement of form works. The gravity load resisting systems in steel tall buildings are:

a. Open web joist system

b. Wide flange beams

c. Columns

The lateral load resisting systems in concrete tall buildings are:

a. Frames with semi-rigid connections

b. Rigid frame system

c. Braced frame system

d. Staggered truss system

e. Braced rigid frame system

f. Steel plate shear wall system

g. Outrigger and belt truss systems

h. Frame tube system

i. Trussed tube systems

j. Bundled tube system

k. Diagrid structural system

1.2.3 Composite Structural Systems

The term Composite construction refers to a structural system with members composed of more than one material, and they are rigidly connected to each other such that no relative movement can occur. Nowadays, steel-concrete composite systems have become

quite popular because of their advantages against conventional construction practices like concrete and steel construction. Some of the advantages of composite systems are mentioned below:

a. High bearing capacity

b. Effective utilization of materials

c. Absorbs energy released due to seismic forces

d. Fast rate of construction

e. Possible to construct a large span structure that gives the large column-free area

f. The low weight of the structure and low cost of the foundation Good quality control

g. Higher stiffness that gives less deflection

The disadvantages of composite construction are as follows:

a. Required of skilled labor

b. Extensive care required during design and construction

In earlier days, composite structural members consisted of steel beams and reinforced concrete slabs connected with shear connectors in between. The composite system is called composite floor system, first developed for bridge construction. Its success inspired engineers to develop composite systems by combining steel and concrete for various structural members of the building. Now, most of the tall buildings are built by using steel-concrete composite structural material. Composite gravity load systems are enlisted below:

a. Composite metal deck

b. Composite beam/girder

c. Composite haunched beam

d. Composite column

e. Composite shear wall

f. Composite truss

The systems which are employed to resist lateral loads in composite construction are given below:

a. Braced frames

b. Shear wall systems

c. Shear wall – frame interacting systems

d. Tube systems

e. Vertically mixed systems

f. Mega frames with super columns

1.3 Case Study on Structural Systems

There are a variety of structural systems that are suitable for tall buildings, each with its own set of advantages. The following are some case studies involving the tallest of high-rise buildings located all over the world.

1.3.1 Burj Khalifa

With a height of 828 metres and a total of 163 floors, the Burj Khalifa is the world's tallest structure. The tower is a mixed-use development with a total floor area of 460,000 m2, including residential, hotel, commercial, office, entertainment, shopping, and leisure establishments. This was the first time in human history that such a large structure was attempted. Aerial view of Burj Khalif is shown in Fig. 1.2. This compelled the designers to use cutting-edge technology and innovative structural design.

Figure 1.2: Aerial View of Burj Khalifa[56]

The following section discusses the Burj Khalifa's structural features.

1.3.1.1 Burj Khalifa Project Details

The structure is located in Dubai, United Arab Emirates. The structural features include:

- 160 + story tower
- Podium structure adjacent
- Have a six story office adjacent
- A two story pool facility near

The tower is 2,80,000 square metres in size. This area is home to 700 residential apartments ranging in height from 45 to 108 stories. Corporate officers occupy the remaining spaces up to the 160^{th} floor. The estimated total cost of the project is US$20 billion. The

construction of the tower alone will cost $4.2 billion. The structural elements that were used and their quantity are listed below:

- Concrete Used = 250000 cubic meter
- Curtain Walls = 83,600 sq.m of glass and 27,900 sq.m of metal
- Steel Rebars Used = 39,000 tones
- Man-Hours = 22 million man-hours

1.3.1.2 Structural System of Burj Khalifa

The Burj Khalifa's floor plan is shaped like a 'Y'. This plan offers increased performance and a panoramic view of the Persian Gulf. The shape and upward setbacks assist the structure in mitigating the wind forces acting on it. The final shape was determined through a series of wind tunnel tests. Burj Khalifa's structural system is referred to as the Buttressed Core System. The entire system is made of high-performance concrete walls. Each wing is buttressed against the other by a hexagonal central core, as illustrated in the Fig. 1.3. The central core exhibits a greater resistance to torsional forces. The structure is more suited to withstand wind forces and their associated effects. Corridor walls run the length of the wing, from the central core to the end. Finally, these walls are thickened with hammer walls. These walls act similarly to the web and flanges of the beams in resisting wind shears and moments. There are perimeter columns that run along the perimeter of the building and connect to the mechanical floors. Outrigger walls connect the perimeter columns to the mechanical floors. This contributes to the ability of the structure to withstand greater wind loads laterally. The depth of the outrigger is three storeys. The outrigger system comes into contact with the tower on a periodic basis.

1.3.1.3 High Performance Concrete Used in Concrete

Burj Khalifa's high-performance concrete ensures minimal permeability and increased durability. Concrete with a cube strength of C80 and C60 is used, along with fly ash, Portland cement, and locally sourced aggregates. The C80 concrete provides a young's modulus of 43800 MPa. Concrete was pumped to a height of 600 metres using the world's

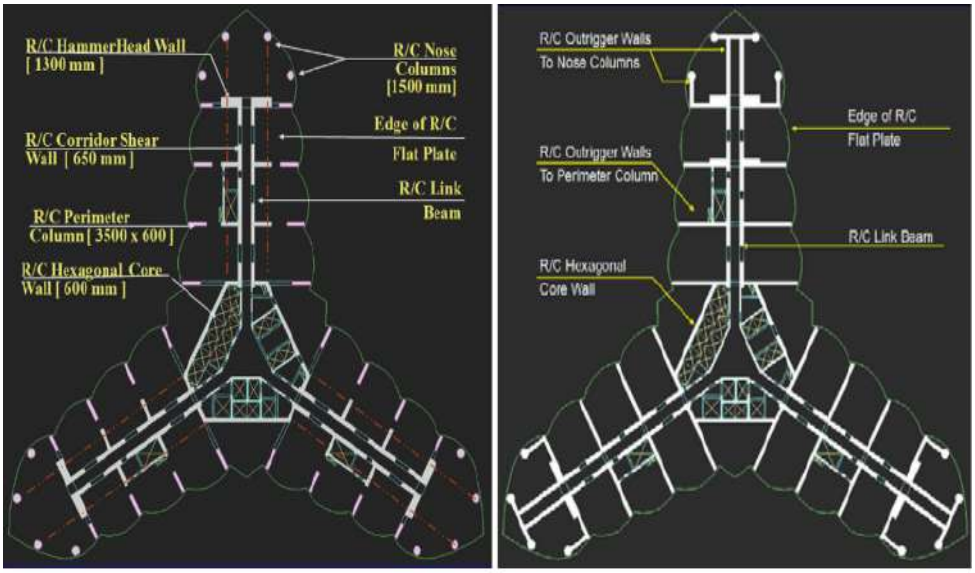

Figure 1.3: Typical Floor Framing Plans at a) typical hotel level and at b) Typical Mechanical Level[30]

largest concrete pumps. This type of pump was used in two different numbers. Due to the location's high temperature (Dubai), shrinkage cracks were possible. As a result, the concrete pouring took place at night, when the temperature was cooler. Ice was added to the concrete mix to achieve the desired temperature. Special concrete mixes were used to withstand the excessive pressure generated by the building's weight. Prior to distribution, each batch was tested.

1.3.1.4 Foundation of Burj Khalifa

A massive reinforced concrete raft supports burj Khalifa's superstructure. This raft is then reinforced by concrete piles that have been bored into the ground. The 3.7m-thick raft was constructed in four separate pours. The grade of self-consolidating concrete used in the concrete raft is C50. The raft is made of 12,500 cubic metres of concrete. One hundred ninety-four piles were used. The piles were 1.5 metres in diameter and 43 metres in length. Each pile is 3000 tonnes in capacity. The piles were constructed using C60 SCC concrete placed using the tremie method. This process was carried out using a polymer slurry. Cathodic protection was installed beneath the raft to mitigate the negative effects of chemicals[30].

1.3.2 Shanghai Tower

The Shanghai tower in China is the world's second-tallest finished structure and the tallest in the country. Shanghai Tower is 128 floors high and 5 stories deep; the architectural and total heights are both 632 metres, the structural height is 580 metres, and the highest accessible point is 587 metres. Shanghai Tower's structural height is not the highest in China; the tower's uppermost section is a parapet, a structure that cannot support any floors; the tower's roof is really 587 metres tall. The tallest structure in China is a 597-meter-tall tower in Tianjin called Goldin Finance 117. The aerial view of shanghai tower is shown in Fig. 1.4 The Shanghai tower in China is the world's second-tallest finished

Figure 1.4: Aerial View of Shanghai Tower[57]

structure and the tallest in the country. Shanghai Tower is 128 floors high and 5 stories deep; the architectural and total heights are both 632 metres, the structural height is 580 metres, and the highest accessible point is 587 metres. Shanghai Tower's structural height is not the highest in China; the tower's uppermost section is a parapet, a structure that cannot support any floors; the tower's roof is really 587 metres tall. The tallest structure in China is a 597-meter-tall tower in Tianjin called Goldin Finance 117. Fig. 1.5 shows Shanghai Center Tower elevation and typical floor plans. Shanghai Tower has 128 floors above ground, with a total floor area of 380,000 square metres. The shape of the tower is spiral; each floor is roughly a round triangle and is slightly revolved about the below floor; as a result, the highest floor is rotated by up to 120 degrees in relation to the bottom

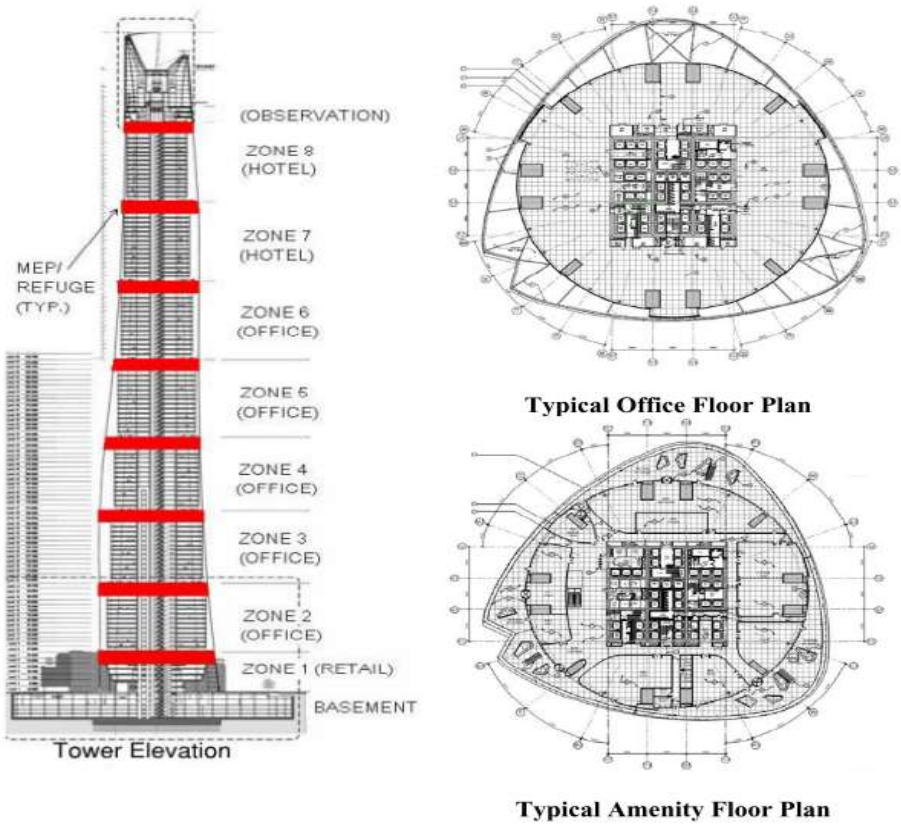

Figure 1.5: Shanghai Center Tower Elevation and Typical Floor Plans[31]

floor, giving the tower an appearance of being twisted. This type of design effectively mitigates the impact of wind, and additionally, the spiral shape can help reduce noise. Shanghai Tower cost 2.4 billion US dollars to build, nearly twice the nearby Shanghai World Financial Center cost.

The structural systems are centrally located around a 30m × 30m square core. These cores work in conjunction with four pairs of orthogonal twin super columns. Additionally, each floor features four inclined super columns. The concrete core is 1200 mm thick, while the mega columns measure 4800mm × 3200mm and are constructed of high strength concrete. The tower is divided vertically into nine zones of 12-15 storeys each. The top of each zone (which serves as a mechanical level) houses a two-story deep outrigger and a one-story deep radial belt truss connecting all perimeter super columns. This arrangement of core, outrigger, and belt provides the building's lateral resistance[31].

1.3.3 432 Park Avenue

432 Park Avenue is the western hemisphere's second-tallest residential tower and the sixth-tallest structure in North America. The ultra-slim structure, which stands at 1,396 feet tall, has 86 residential floors and 104 condominium apartments. The estimated total cost of construction is $1.25 billion. The building has a 1:15 slenderness ratio, a 93.5-foot identical width and length, and a 1,396-foot total height. The architectural concept, the building's aspect ratio, and the required structural performance created interesting challenges that necessitated the development of several novel structural engineering solutions. The building's design incorporates energy efficiency and renewable technology strategies, earning LEED certification. The aerial view of 432 park Avenue is shown in Fig. 1.6. The structural concept utilised a dual tube-in-tube system comprised of an exoskeleton

Figure 1.6: 432 Park Avenue[58]

of perimeter moment frames connected by spandrel beams and columns and connected to the interior shear wall core via outriggers located at critical elevations. This configuration enabled virtually every floor to have unobstructed open space. The interior tube, measuring 9m × 9m, serves as the building's core, housing the elevators and egress stairs. Its reinforced concrete walls, which range in thickness from 760mm at the base to 300mm at

the top, provide considerable stiffness. The outer tube is the perimeter beam-and-column frame of the tower, which is also extremely stiff, even with the windows punched out. On each 12th floor, these tubes are connected by stiffening beams that are housed in double-height plant rooms to avoid encroaching on the apartments.

The structure is made of reinforced cast-in-place concrete. It is surrounded by architecturally exposed white concrete columns and a central shear wall core that surrounds the elevator shafts and staircases that serve as the building's spine. The residential floors are ten-inch thick reinforced concrete two-way flat plates supported by the exterior columns and central core. The central core was cast three stories ahead of the perimeter moment frame in the construction sequence.

Given the building's slenderness and height, which is more than twice that of neighboring structures and thus more exposed to high winds, it was necessary to pay special attention to wind-induced dynamic motion control. Additionally, other wind-related effects such as lateral accelerations, vibrations, and the occupants' perception of movement had to be addressed. To ensure the building's strength and lateral stiffness, five outriggers, each spanning two stories, were designed throughout the tower's height to act as beneficial linkages between the interior core and the perimeter framing, thereby improving the structure's overall performance. The location of the outriggers is denoted in Fig. 1.7 by red rectangles.

Additionally, five two-story open floors along the building's height resulted in significant reductions in wind requirements and their effect on the structure, most notably by reducing the vortex shedding phenomenon. Finally, it was determined that installing two 660-ton opposed pendulum tuned mass dampers in the top portion of the building was the best engineering solution for maintaining lateral accelerations within the industry-accepted limits.

The superstructure was constructed using over 70,000 cubic yards of concrete and approximately 12,500 tonnes of reinforcing bars. The structural elements' specified concrete compressive strength ranges from 14,000 psi in the lower 38 stories to 10,000 psi in the upper levels. The 432 Park Avenue project's concrete was designed for increased durability by reducing the water-to-cementitious material ratio to as little as 0.25. Additionally, to ensure proper concrete placement at each casting location and to enhance the finish on exposed structural elements, the concrete had to be pumpable, self-consolidating, and

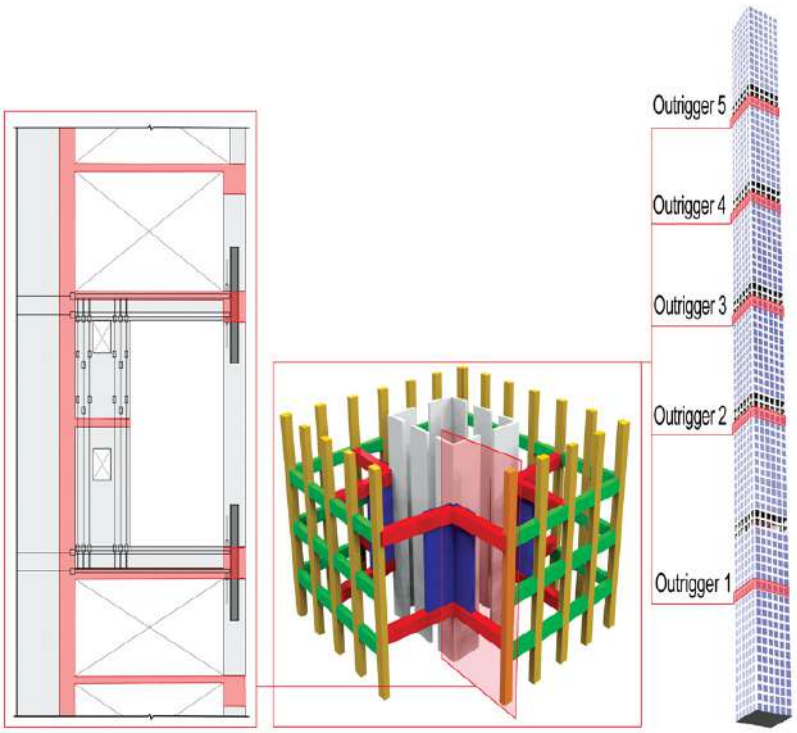

Figure 1.7: General depiction, structural detail and location of outriggers[59]

have a low heat of hydration. Producing high-strength, pumpable white concrete successfully was undoubtedly one of the most difficult construction challenges on the project[59].

1.4 Need for the study

Tall building construction involves a very high demand for money, human resources and technology, and the economy in such a project plays an important role. To achieve a better economy, selecting suitable structural materials and efficient structural systems according to location, type of building, geometrical dimension, and available construction technology makes a tall building smart, resilient, and sustainable. Benefits like fewer sizes of structural components, low foundation cost, less form work requirement, and faster construction speed make steel-concrete composite material preferable structural material in tall buildings.

Stiffness and stability requirements under lateral loads caused by wind or earthquakes in tall structures increase exponentially as height increases. Thus, understanding the behaviour of different lateral load resisting systems becomes essential to determine efficient

structural systems in tall structures. To make tall buildings strong, stiff and resilient against lateral loads, codal provisions are updated and new provisions are added in relevant Indian standards. Three different structural systems subjected to wind and seismic loading in seismic zone III are studied to determine various structural systems' efficiency and study revised codal provisions of Indian standards to guide practising engineers and researchers.

1.5 Objective of the Study

The main objectives of present study are:

- To study structural aspects of IS 16700 : 2017.
- To evaluate along and across wind forces utilising gust factor method as per IS 875 (Part 3): 2015 and wind time history method based on wind tunnel studies accessible at Tokyo Polytechnic University Aerodynamic database.
- To understand behaviour of high-rise lateral load resisting structural systems using static and dynamic analysis under wind and seismic loading.
- To understand cost-effectiveness of various lateral load resisting structural systems used in high-rise steel-concrete composite buildings.

1.6 Scope of Work

The scope of major project work is as follows:

- Deciding typical floor plan of steel-concrete tall buildings considering architectural, structural and building authorities' requirements.
- Understanding structural aspects of IS 16700 : 2017 regarding general and special guidelines for tall buildings and considered lateral load resisting systems.
- Evaluation of along and across wind forces acting on tall buildings in accordance with IS 875 (Part 3): 2015 and TPU Aerodynamic database.

- Modeling and analysis various structural systems (Structural Wall-Moment Frame, Tubular and Outrigger and Belt Truss) with plan dimension 48 m x 48 m for 24, 44 and 64 storey buildings using commercial software ETABS.

- Comparison of three structural systems (Structural Wall-Moment Frame, Tubular, Outrigger and Belt Truss) in terms of designed sections, drift ratios, top story displacements, base shear, story shear, time period, modal mass participating ratio, contribution of shear walls in resisting lateral loads and structural weight.

- Design of composite structural elements of various structural systems as per AISC 360-10.

1.7 Organization of Report

The Major Project report is organized into various chapter as follows:

Chapter 1 gives general information about tall buildings and structural systems for concrete, steel and composite construction. It presents case studies of existing tall buildings in the world with various structural systems. It includes It also includes need, objective and scope of work.
The literature review on the different relevant topics is presented in **Chapter 2**. The literature review is divided into various topics like the general discussion on structural systems, structural wall-moment frame system, tubular system, outrigger and belt truss system, wind and seismic lateral loads.
Chapter 3 presents step-wise procedure of evaluation of along and across wind forces using three methods which are static wind force calculation as per IS 875 (Part 3): 2015, dynamic wind force calculation using gust factor method specified in IS 875 (Part 3): 2015 and dynamic wind load calculation as per wind time history pressure coefficients given in TPU Aerodynamic Database.
Chapter 4 presents the behavior of Shear Wall-Moment Frame, Tubular and Outrigger and Belt Truss Systems.
Chapter 5 includes modelling, analysis and design of Structural Wall-Moment Frame System, Tubular System and Outrigger and Belt Truss System for 24, 44 and 64 story

buildings. Lateral load calculations and design of structural members are discussed in this chapter **Chapter 5**. Axial force variations due to shear lag effect in tubular structural system are also discussed in **Chapter 5**.

Chapter 6 includes a comparison of analysis results in terms of the , base shear, time period, modal mass participating ratio, top storey displacements, inter storey drift , contribution of shear walls in resisting lateral loads and structural weight of various structural systems considered in this study.

Finally, a summary of the project, conclusions and future scope of work is discussed in **Chapter 7**.

Chapter 2

Literature Review

2.1 General

In this chapter critical review of literature related to lateral load resisting structural systems in steel-concrete composite tall buildings is presented. To understand behaviour of various lateral load resisting systems various research papers, books and codes have been referred. The literature review includes a review of literature related to : structural systems, structural wall-moment frame system, tubular system, outrigger and belt truss system, diagrid system, evaluation of wind loads and major project reports submitted at Nirma University.

2.2 Structural Systems

Ilgın et al. (2021) [**13**] studied primary architectural design considerations and structural considerations of 93 completed or under construction super tall buildings registered in the CTBUH database. Analysis of architectural design considerations included building function, core planning, slenderness ratio and building forms, while analysis of structural considerations included structural materials and structural systems. The authors also analysed interrelations among design considerations such as building form and structural system, building height and structural system, building height and aspect ratio, structural system and structural material and aspect ratio and structural system. The authors had concluded from an analysis of architectural design considerations that most of the considered super tall buildings were centrally cored, prismatic or tapped with a slender-

ness ratio varying from 7 to 10. From the analysis of structural design considerations, it was found that 64% of buildings were constructed with composite structural material. In comparison, RCC and steel percentages were 32% and 4%, respectively, as shown in Fig. 2.1a. The authors also presented various structural systems used in considered buildings shown in Fig. 2.1b. This proved that outrigger, tube, diagrid and shear-frame structural systems were primarily utilised in super tall buildings.

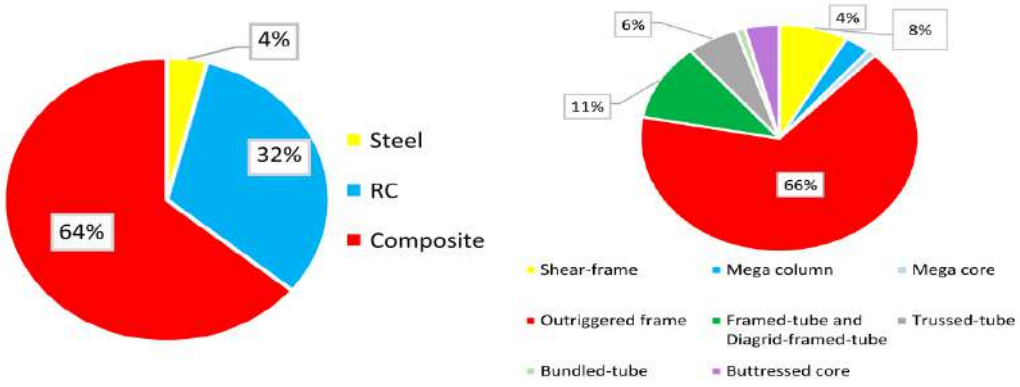

(a) Analysis of selected super-tall buildings by structural material

(b) Analysis of selected super-tall buildings by structural system

Gupta et al. (2020) [11] reviewed the recently launched first tall building code of India, IS 16700: 2017 [48]. The study mainly aimed to understand some of the critical structural aspects of the code to develop a better understanding in practitioners and design engineers about it. A brief interpretation of the critical clauses related to structural design had been provided along with the comparison of the same with the existing international standards such as ASCE 7-16 [37], and ACI 318 [36]. The authors discussed structural parameters like lateral drift, limiting height and slenderness ratio for various structural systems, floor diaphragm openings, vertical shaking considerations in high seismic zones, and cracked RC section properties. They concluded that despite a reasonable effort of bringing the Indian design community at the same base scale as the international community, a clear depiction of certain aspects of code was observed lacking.

Ali and Moon (2011) [23] discussed the development of structural systems and brief history for tall buildings. They also presented the new classification of the structural systems as interior and exterior structure based on the distribution of the primary lateral load resisting system of the building. The behaviour of interior structural systems like

structural wall-moment frame, core supported outriggers, tube and bundled tube systems were explained in detail with relevant schematic diagrams. Different damping strategies for structural systems were presented. Recent developments in the forms of tall buildings like aerodynamic forms, twisted forms, free forms and future prospects of sustainable and efficient tall buildings were discussed in this paper.

2.3 Structural wall-moment frame system

Ahamad and Pratap (2020) [**1**] investigated the usage of Shear walls at different locations in a G + 20 plan irregular multi-storied residential building and the nature of the structure exposed to the earthquake by adopting Response Spectrum Analysis. They modelled and analysed the whole structure in all the seismic zones of India prescribed by IS 1893 (Part-1): 2016 using prominent FEM integrated software named Etabs 2015. Results were presented in terms of the fundamental time period, storey drift, base shear, maximum allowable displacement and torsional irregularity. They concluded that building with shear walls at both sides resists lateral seismic load efficiently compared to building without shear walls and building with shear walls at one side. They also concluded that building with shear walls at one side performed well in torsional check due to irregularity in the plan.

Reshma et al. (2021) [**26**] studied the behaviour of 20 floor RCC structures with two basements considering with and without shear walls at different locations in seismic zones from II to V. Response spectrum analysis was carried out as per IS 1893 (Part 1):2016 using commercial software ETABS. The different locations of shear walls considered in this study were corners, the periphery of the lift and the faces of the building. Time period, storey displacement and inter-storey drift of building with shear walls at the corner positions were observed to a minimum and building with shear walls at the periphery of the lift were observed to the maximum in all seismic zones. The authors concluded that the building with the corner position of the shear wall performed better than all other positions and was the best feasible location. Buildings under zone V was prone to severe damage during seismic activity.

Ren et al. (2018) [**25**] studied the non-linear behaviour of 20 storey tall buildings under severe earthquakes using ABAQUS software. The authors carried out a uniaxial compressive and tensile test of concrete to identify compressive strength parameters of concrete. Load-displacement hysteretic loops were also developed and compared. To perform comparative studies of the seismic behaviours for different structures, four structural design schemes regular reinforced concrete (RC), RC with steel reinforced columns (SRC), RC with steel plate reinforced shear walls (SPRSW) and RC with SRC and SPRSW, were considered in the study. Non-linear time history analyses were carried out with four horizontal earthquake ground motions with PGA = 400 cm/s^2 and PGA = 600 cm/s^2. The authors concluded that RC structural elements should be designed with particular attention in bottom stories. At the same time, steel plate RC composite shear wall structures should be enhanced at transit and top stories for certain earthquakes.

2.4 Tubular system

In this study, **Fu (2018)** [**10**] explained detailed descriptions of different types of tube systems, such as tube-in-tube, framed tube, braced tube, bundled tube, and hybrid tube system. The author discussed the case studies of the Twin Towers and One World Trade Center (the replacement of the Twin Towers). The author modelled three-dimensional of Petronas Twin Towers in ETABS using the available drawings and introduction documents on the web. The author gave a detailed explanation of the shear lag effect of the framed tube through a case study of the World Trade Centre. The author presented axial load distribution of exterior tube columns of the WTC1 building model using ETABS. The author suggested a braced tube structural system to reduce the shear lag effect and allow larger spacing of columns in tube structure to resist lateral loads. The concept of super tall building design and bundled tube were also illustrated in the study.

Moon (2014) [**24**] compared structural efficiency of braced tube, diagrid and outrigger structural systems to meet the lateral stiffness requirements. Moon presented optimal section sizes of diagonal braces, columns and diagrids using stiffness-based design requirements. In order to investigate the structural efficiency of each system comparatively depending on the building heights and height-to-width aspect ratios, moon designed braced

tubes, diagrids and outrigger structures in tall buildings of 40, 60, 80 and 100 storeys. The author presented required structural steel amounts in all buildings as per Table 2.1. Moon concluded that as the building height increases, the required quantity of structural steel increases drastically. Braced tube and diagrid structures were more efficient than outrigger systems. Moon also concluded that diagrid structures were more efficient to resist lateral load when the aspect ratio was less than 7, while braced tubes were more efficient for very tall buildings with an aspect ratio greater than 8.

Table 2.1: Required steel amount for 40 to 100 storey buildings

Storey	**Type of Building**	**H/B**	**Required steel in ton**	**Required steel in psf**
40	Braced Tube	4.3	3,620	13.9
40	Diagrid	4.3	3370	12.9
40	Outrigger	4.3	5460	20.9
60	Braced Tube	6.5	8,370	21.3
60	Diagrid	6.5	7,970	20.3
60	Outrigger	6.5	13,360	34
80	Braced Tube	8.7	17,390	33.3
80	Diagrid	8.7	18,550	35.5
80	Adujusted diagrid	8.7	19,170	36.6
80	Outrigger	8.7	33,690	64.4
100	Braced Tube	10.8	34,750	53.1
100	Diagrid	10.8	37,990	58.1
100	Adujusted diagrid	10.8	38,800	59.4
100	Outrigger	10.8	74,110	113.8

Elansary et al. (2021) [8] analysed eight reinforced concrete buildings ranging between 10 and 50 with different lateral load resisting systems using one-step analysis and staged-construction analysis. To account for time-dependent effects such as shrinkage, creep, and strength gain in buildings with total plan dimensions 30 m $\times$ 30 m with the total number of storey varying from 10 to 50, the authors extended SCA analysis to SCAT analysis. The comparison included column shortening, beam differential settlement, and the differences in straining actions yielded from the analyses. Buildings were modelled in MIDAS GEN software, and time-dependent material properties were assumed based on

ACI 318-19 standards. Maximum shortening obtained from SCAT was more extensive than that obtained from OSA by a percentage reaching 143%, 153%, 116%, and 154% for RC buildings with a rigid frame, shear wall, wall-frame, and Tube-in-tube lateral load resisting systems, respectively, while maximum differential displacement experienced in the buildings with RF, SW, WF, and TT was 2.28 mm, 6.37 mm, 12.13 mm, and 13.03 mm, respectively. The authors concluded that analysis of RC buildings using OSA yields unsafe solutions in certain element zones.

2.5 Outrigger and belt truss system

Kavyashree et al. (2021) [**17**] reviewed the evolution of the outrigger system from the conventional outrigger to damped outrigger concepts. Outrigger structural system development from the conservative design as a rigid connection to a virtual connection with passive control, active control system, semi-active control system to hybrid control system was deliberated. They briefly over viewed the history of outriggers, types of the outrigger, analysis of tall buildings without outriggers, formulation of equations for outrigger structure to simplify analysis were elaborated. They discussed different approaches to locate optimum positioning of outriggers in tall structures, analysis of outriggers to study its behaviour in high-rise buildings using different methods and damped outrigger systems. The authors highlighted the advantages of outrigger structure with semi-active control and performance enhancement of the outrigger system with effective devices. They summarized that there is a need for more precise semi-active and hybrid control techniques incorporating adaptive control stochastic control to make the outrigger structural system perform better and more economically feasible.

Alhaddad et al. (2020) [**2**] investigated various aspects related to the outrigger and belt-truss system through a comprehensive review to provide guidance for designers and researchers. The authors illustrated the components, configurations, types of outrigger system from structural materials, response and the way of linking between external and internal structural system points of view. The structural behaviour of the outrigger and belt-truss system under various gravity and lateral loading were also elaborated. The advantages of the outrigger system and its disadvantages associated with the solutions

were presented. They also discussed factors impacting the performance of the outrigger system and future research scopes of the outrigger and belt-truss systems.

İnam et al. (2021) [**14**] studied the estimation of the optimum location of the outriggers in 35, 40 and 45 storey buildings to minimise lateral displacement. The finite element models of the tall steel building were created with the aid of the software ETABS. Dynamic time history analysis was performed with a set of 11 strong ground motions from the Pacific Earthquake Engineering Research Center (PEER) database to determine the optimum location of outriggers. It was concluded that the optimum location of a single outrigger considering the lateral deflection results was varied from 0.56H to 1.0H for all the buildings considered in this study. In contrast, the optimum location for the first and second outriggers for two-outrigger systems was 0.67H and 0.85H for a 40 storey building.

Samadi and Jahan (2021) [**27**] investigated the reliability of modal response spectrum analysis (MRSA) in predicting actual seismic behaviour of tall buildings with outrigger and belt truss in buildings with braced or reinforced concrete shear wall core with 28 and 56 stories. Results obtained from MRSA were discussed and compared to results obtained from nonlinear time history analysis (NLTHA) using ten near-fault earthquake records. They concluded that the maximum lateral displacements of the structures from NLTHA with braced core were less than buildings with RC shear walls. In contrast, more maximum inter-storey drift, residual displacements, and residual inter-storey drift were found in braced core buildings than RC shear wall core buildings. They also concluded that MRSA unrealistically overestimated the influence of outriggers on the drift reduction of tall buildings with braced cores.

2.6 Diagrid system

Liu et al. (2018) [**21**] reviewed the evolution of the diagrid system and its behaviour during seismic loading. Various calculation theories regarding the stiffness of diagrid structures were discussed. The structural optimization of diagrid structures was studied to improve the bearing capacity of structures and material utilization by considering parameters like the angle of inclined columns, the aspect ratio and the plane form of

structures, and the presence of corner columns. From the experimental results, it was found that the yield order of failure during the plastic state of the diagrid structural system was coupling beam, inclined column and core tube. The authors proposed a separate connection design emphasising stronger and weaker components. They advised using concrete-filled steel tube columns as the columns in diagrid structural systems for tall buildings based on the favourable performance of concrete-filled steel tubes.

Asadi and Adeli (2017) [**5**] reviewed various diagrid configurations, the main factors affecting their behaviours, and related design parameters and approaches. They explained that diagrid structures provided more significant lateral stiffness and less shear lag effect than tubular structures. It was suggested that the diagonal angle in the range of 60° to 75° was more efficient than others for the structures in the 36–60-story range. It was concluded that for an efficient diagrid system, grid density should be higher in the bottom levels while low in the upper level of the buildings. The authors discussed the preliminary analysis and design methods. They also discussed steel, RC and CFST diagrid connections. Diagrid applications for free-form steel and concrete structures were introduced, showing the diagrid applicability for complex structures. The authors also highlighted diagrid nonlinear behaviour, a new tubular and diagrid systems-hexagrids.

Heshmati et al. (2020) [**12**] evaluated the seismic performance of 36-story diagrid structures with varying angles from 53° to 79° using pushover and nonlinear time history analysis in PERFORM-3D software. In order to evaluate the effect of diagrid core on the behaviour of structures, interior gravity frames were replaced with diagrid frames with angle 69°. From the pushover analysis, enhanced the hardening behaviour of structures was observed when the angles of perimeter panels were lower or equal than those of the core compared to the conventional diagrids. It was concluded that as the angle of panels increased in models without core, the formation of plastic hinges moved towards the bottom stories, while in the core diagrid structures, the plastic hinges spread in upper stories. They also concluded that interior diagrid frames contributed more to inelastic energy dissipation in building with higher angles of diagrids.

Dabbaghchian et al. (2021) [**7**] presented the benefits of the newly introduced sys-

tem, diagrid, with a fused-shear link called eccentric diagrid system (EDS). A series of nonlinear pushover and time history analyses were performed to compare EDS with the conventional diagrid system (CDS). For two separate 12 and 18 storey buildings, three different EDS and CDS layouts with diagrid angles of 45°, 63.4°, and 71.6° were chosen. The models were created using R-factors of 3.6 and 5, respectively, for CDS and EDS frames. According to Federal Emergency Management Agency P695, the assumed R-factor for EDS was confirmed. The authors observed that EDS significantly improved the structure's post-yield performance and seismic characteristics compared to CDS, with ductility and over strength ratio increased by more than 2.5 and 1.3 times, respectively.

2.7 Evaluation of Wind loads

Kumar (2020) [19]reviewed the newly brought out third revision of the Indian Standard for wind loading IS 875 (III): 2015[43]. The author explained updates, like the along and across wind loading calculation using Gust Factor approach, importance factor for the cyclonic region, the interference factors by comparisons and compared to previous wind load code IS 875 (III): 1987 and Australian wind loading standards. The author suggested revision/amendment in areas such as the importance factor for the cyclonic region (k_4), the interference factor, the local peak pressure coefficient provided in Table 5 of the standard, the force coefficient provided in Figure 4 of the standard, the across wind calculation using empirical equations, the torsional loading provisions and the wind load combinations.

Jafari and Alipour (2021) [15]reviewed various methodologies developed to control the wind-induced vibration of tall buildings. Authors classified various methodologies to control wind-induced vibration of tall buildings into two broad categories - passive or active auxiliary damper and aerodynamic modification. They discussed various active, semi-active and passive control dampers and their advantages and disadvantages. It was found that the application of conventional dampers needs to be reassessed to ensure their efficiency in dissipating the energy, especially caused by wind loads. They also presented various shape and cross-section aerodynamic modifications used to reduce wind-induced vibrations in tall buildings. Explanations about wind tunnel tests and CFD simulations

used to study the effect of aerodynamic modifications and their efficiency in reducing wind-induced vibrations were given in the study. They also highlighted future advances in wind-induced vibration mitigation systems such as smart double facades and machine learning-based algorithms to measure the impact of the wind-induced vibration.

Alinejad and Kang (2020) [**3**] investigated improved base moment gust load factor method (MGLF) with conventional gust load factor (GLF) method adopted in ASCE 7-16[37]. The authors explained the step-wise procedure for calculating static and dynamic wind load by gust load factor method given in relevant ASCE standards and base moment gust load factor method. They calculated wind load from both methods for building with plan dimension 48 m × 48 m and the number of storey varying from 6 to 48. They compared approaches and results side by side. It was concluded that the mean force is always more significant than the background and resonant forces from the GLF method, whereas the resonant force has a different pattern. The resonant force from the MGLF is stronger in upper stories and weaker in lower stories.

2.8 Major Project Reports Submitted at Nirma University

Patel (2019) [**49**] evaluated the Diagrid structural system's performance under wind loading. The study considered the G+50-story Diagrid building with a plan dimension of 36 m 36 m. The building's performance was determined through static, dynamic, and time history wind analyses and the application of appropriate performance criteria from the available literature. Buildings were evaluated for their structural component performance and serviceability performance in terms of human comfort. The structural component's performance level was determined using the essential wind speed, and the serviceability comfort level was determined using the allowable floor acceleration range for people evacuation during windstorms. Wind time history data were collected and analysed using the TPU (Tokyo Polytechnic University) aerodynamic database. Wind time history varies according to the height and face of the building in terms of wind direction. SAP2000 software was used to conduct modelling and nonlinear analysis to evaluate the performance of diagrid structural systems. Additionally, a parametric study

was conducted by varying the angle of diagrid columns in structural systems. For this purpose, a G+50 storey building with varying angles of diagonal columns on the building's periphery was considered, including 74.47°, 78.23°, and 80.53° with 6,8,10 storey modules respectively. The time period, base shear, storey drift ratio, lateral displacement, and floor acceleration of various diagrid structural systems were compared. Based on the analysis results, it was determined that G+50 storey diagrid buildings with column angles of 74.47° and 80.53° performed better than those with column angles of 78.23°.

Modi (2017) [**50**] modelled and designed G+60-storey buildings using four structural systems: steel plate wall-frame, outrigger & belt, diagrid, and hybrid. At the periphery of hybrid structural system buildings, diagrids were used, while steel plate shear walls, boundary elements, outriggers, and belt trusses were used at the periphery. The analysis results were compared in terms of the time period, base shear, storey displacement, and inter-story drift for wall-frame, diagrid, outrigger & belt, and hybrid structural systems. When designing structural elements, critical load combinations were taken into account. Additionally, the shear lag effect was investigated in hybrid structural systems. The hybrid system proved to be the superior alternative to the four structural systems considered for the G+60 storey building. When the steel plate wall thickness and diagrid diameter were varied, the top storey displacement and inter-story drift remained within the permissible ranges, indicating that the hybrid structural system could be further optimised for economy. According to the steel usage comparison, the diagrid structural system required the least steel of all four structural systems, 36.10% less steel than the Steel Plate Shear Wall (SPSW) structural system, and 33.15% less steel than the SPSW structural system. The existence of a shear lag effect in hybrid structural systems was demonstrated in this study. At the base of the building, a maximum shear lag ratio of 1.37 was observed, and after 1/4th of the building's height, a negative shear lag effect was observed.

Khatri (2016) [**51**] analysed and designed five distinct structural systems used in high-rise buildings, considering secondary effects and sequential loading. A cruciform-shaped 110-story building with plan dimensions of 48m × 48m and a 20m × 20m core was designed for five systems using the MIDAS Gen software. A comparison of member sizes, building drift, time periods, material consumption, and an efficiency factor was conducted to deter-

mine the most efficient structural system. This study also included the performance-based design of common structural systems in high-rise buildings. Wind data records from a typhoon were presented, and a time history function was generated for the structure's nonlinear dynamic analysis. To determine the most efficient structural system, two new parameters were developed: the efficiency factor, which measures the building's stiffness in relation to normalised cost, and the performance parameter, which measures the structure's resilience to normalised cost. According to inter-storey drift ratios, plastic rotation in beams, and human comfort performance criteria, the High-Efficiency structure was the most efficient in terms of building performance. In contrast, the Wall frame structure was the least efficient of the structural systems considered in this study.

Gurule (2014) [**52**] analysed and designed three different structural systems, including an RCC frame tube, a steel frame tube, and a composite mega frame with a super column. A 96-story building with plan dimensions of 60.96 m × 36.576 m and a height of 380.16 m was used to compare the structural performance of these systems. Along with gravity loading, lateral loading due to earthquakes and wind was considered. The structural elements were modelled and designed using ETABS software. The analysis results were compared for all three structural systems in terms of the natural time period, storey shear, overturning moment, lateral drift, storey displacement, and forces in critical members. Euro Code 4 specifications were followed in the design of the composite structure. The consumption of basic materials such as concrete and steel was compared for all three structural systems based on their design. Additionally, the cost of the building's three structural systems was presented. Gravity load intensity was also calculated per unit floor area to help understand variation in dead load. According to the study, the mega frame with the super column was more cost-effective and efficient than the RCC frame tube and steel frame tube for the building in question. Although the steel frame tube had the lowest gravity load intensity, it was also the most expensive. The RCC frame tube exhibited a greater gravity load intensity, which may increase foundation costs.

Saiyed (2011) [**53**] analysed and designed a 50-story tall building with a moment-resisting steel frame system, a steel plate shear-wall system, and an outrigger structural system. The dynamic wind load was calculated by IS: 875 (III)-1987 and by IS: 875-Draft

code. The design of members was carried out as per IS: 800-2007. The parametric study was carried out by changing the periphery and core column sizes to satisfy the stiffness requirement. The effect of sequential loading in the analysis of structure was studied by considering the single-storey construction sequence. The optimum location of one outrigger and two outrigger systems subjected to uniform lateral loading was also presented. The comparisons of the moment-resisting frame, steel plate shear-wall frame and outrigger systems in terms of building response like time period, top storey displacement, drift and design forces were carried out. The Shear-Wall frame system required 8% less steel, and the Outrigger system required 10% less steel compared to the moment-resisting frame system for the 50-story building considered in this study.

Jivani (2008) [**54**] investigated the effect of the site-specific response spectrum on the analysis of a shear wall frame structure measuring 18 m x 18 m. The study assessed ground response at eleven locations throughout Ahmedabad using the one-dimensional equivalent linear analysis software ProSHAKE. Acceleration time history taken on 26^{th} January 2001 at Ahmedabad's Passport office building of the Bhuj earthquake was used as the input motion for various sites to obtain the acceleration time history of the ground and the response spectra. ETABS software was used to analyse the site-specific response spectrum and acceleration time history of shear wall building. The time period, base shear, and design forces in shear walls were compared using site-specific response spectrum analysis, time history analysis, and the response spectrum from IS: 1893 (Part I)-2002. ETABS was utilised to undertake parametric study on building height and shear wall position, and pushover analysis was used to determine the building's inelastic deformation capability. These analyses indicated that local subsoil characteristics influenced acceleration time histories on the ground and response spectra. In the case of certain buildings, design forces in sheer walls were governed by time history analysis and response spectrum analysis.

2.9 Summary

Literature review gives a proper understanding on: structural aspects to be considered for tall buildings, behaviour of different lateral load resisting systems subjected to gravity

and lateral loads, calculation of lateral loads according Indian Standards and its impact on tall building.

Chapter 3

Evaluation of Wind Forces on Tall Buildings

3.1 General

This chapter discusses the evaluation of along and across wind forces acting on tall buildings using three methods; Static Wind Load Analysis as per IS 875 (Part 3): 2015[43], Dynamic Wind Load Analysis as per IS 875 (Part 3): 2015[43] using Gust Factor Method: 2015 and Dynamic Wind Load Time History Analysis using Tokyo Polytechnic University Aerodynamic Database. This chapter also includes a parametric study of the along and across wind forces calculated using these three methods on tall buildings with varying heights and aspect ratios.

3.2 Static and Dynamic Wind Load Analysis

Wind speeds vary randomly in time and space; therefore, the design of numerous buildings and structures needs to assess wind loads and predict wind response. As wind pressure increases with altitude, taller structures must be able to withstand greater lateral loads. The wind consists of mean and fluctuating components, and it has been observed that the mean wind speed tends to increase with altitude, whereas the gustiness tends to decrease with altitude. The variation of wind speed with height is depicted in Fig. 3.1. Flexibility and, consequently, fundamental time period increase as the height of the structure

rises. The low-frequency energy content of wind flow fluctuations is more significant than seismic load. Therefore, taller buildings are more susceptible to wind-induced vibration. However, the vast majority of structures encountered in practice do not experience wind-induced oscillations and thus do not require investigation of the dynamic action of wind. Static wind analysis has proven to be an accurate method for estimating loads for such typical, small, and heavy structures. Numerous structures or their components, including certain tall buildings, cooling towers, chimneys, transmission towers, lattice towers, guyed masts, long-span bridges, communication towers, etc., require the study of wind-induced oscillations [43]. The Gust Factor Method must be used to determine the impact of dynamic turbulence on the along wind loads (drag loads) for these structures. A building with an irregular shape or subject to across-wind loading, vortex shedding, or instability due to galloping or fluttering must undergo wind tunnel testing [3]. However, wind tunnel testing, in general, is expensive and time-consuming. Consequently, alternative methods to evaluate along and across dynamic wind loads, such as computational fluid dynamics or dynamic wind load analysis using a database of wind time history, started to emerge. This section discusses three types of wind load analysis procedures, including static wind load analysis following IS 875 (Part 3): 2015, dynamic wind load analysis per IS 875 (Part 3): 2015 employing the gust factor method and dynamic wind load time history analysis utilising the Tokyo Polytechnic University Aerodynamic Database.

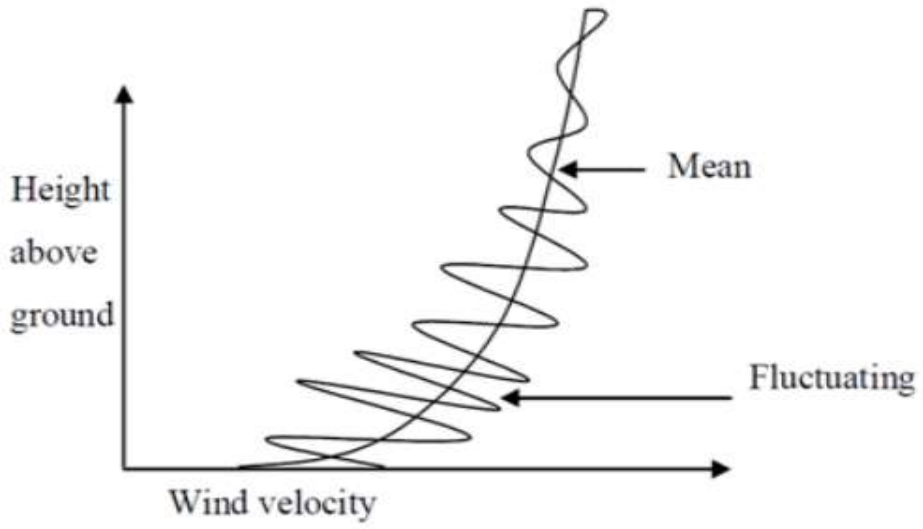

Figure 3.1: Variation of wind velocity with height[55]

3.2.1 Static Wind Load Analysis (SWLA)

In the static method, the equivalent wind load is estimated as a pressure that varies with structure height. It solely considers the mean component of wind speed and ignores the variable component. The static wind load is calculated using the wind force coefficient method in IS 875 (Part 3): 2015[43]. Following are the steps to estimate wind forces on rectangular clad type tall buildings in accordance with IS 875 (Part 3): 2015[43]'s static wind load analysis.

1. Find out Basic Wind Speed (V_b) from fig. 1 of IS 875 (Part 3): 2015[43].
2. Find out Risk Coefficient (k_1) from Table 1 of IS 875 (Part 3): 2015[43]. (*Note: Risk coefficient (k_1) depends upon class of structures and wind speed zone.*)
3. Evaluate Terrain Roughness and Height factor (k_2) from Table 2 of IS 875 (Part 3): 2015[43]. (*Note: Terrain Roughness and Height Factor (k_2) varies with height and terrain category. So for each story levels in building will have varying terrain roughness and height factor (k_2).*)
4. Evaluate Topography Factor (k_3) as per clause 6.3.3 and Annex C of IS 875 (Part 3): 2015[43].
5. Find out Importance Factor for Cyclonic Region (k_4) as per clause 6.3.4 of IS 875 (Part 3): 2015[43].
6. Calculate Design Wind Speed (V_z) as per equation 3.1 given in clause 6.3 of IS 875 (Part 3): 2015[43].

$$V_z = V_b k_1 k_2 k_3 k_4 \tag{3.1}$$

7. Calculate Wind Pressure (p_z) as per equation 3.2 given in clause 7.2 of IS 875 (Part 3): 2015[43].

$$p_z = 0.6 {V_z}^2 \tag{3.2}$$

8. Find out Wind Directionality Factor (K_d) as per clause 7.2.1 of IS 875 (Part 3): 2015[43].

9. Evaluate Area Averaging Factor (K_a) from clause 7.2.2 of IS 875 (Part 3): 2015[43] according to tributary area of building. (*Note: For overall structure, tributary area shall be taken as the centre to centre distances between frames multiplied by the individual panel dimension in the other direction together with overall pressure coefficients.*)

10. Find out Combination Factor (K_c) from clause 7.3.3.13 of IS 875 (Part 3): 2015[43].

11. Evaluate Interference Factor (IF) as per clause 8.2 and 8.3 for low-rise and tall buildings respectively.

12. Calculate Design Wind Pressure ($p_{d_{(z)}}$) as per equation 3.3 given in clause 7.2 of IS 875 (Part 3): 2015[43].

$$p_{d_{(z)}} = (K_d K_a K_c p_z) \tag{3.3}$$

(*Note: Multiply Interference Factor (IF) with Design Wind Pressure (p_d) given in equation 3.3 to evaluate final Design Wind Pressure ($p_{d_{(z)}}$).*)

13. Evaluate Force Coefficient ($C_{f_{(z)}}$) for rectangular clad building as per clause 7.4.2.1 of IS 875 (Part 3): 2015[43] shown in Fig. 3.2.

14. Calculate Static Wind Load Force ($F_{(z)}$) as per equation 3.4 given in clause 7.4 of IS 875 (Part 3): 2015[43].

$$F_{(z)} = C_{f_{(z)}} A_{e_{(z)}} p_{d_{(z)}} \tag{3.4}$$

(*Note: $A_{e_{(z)}}$ is effective area of buildings in the direction perpendicular to wind.*)

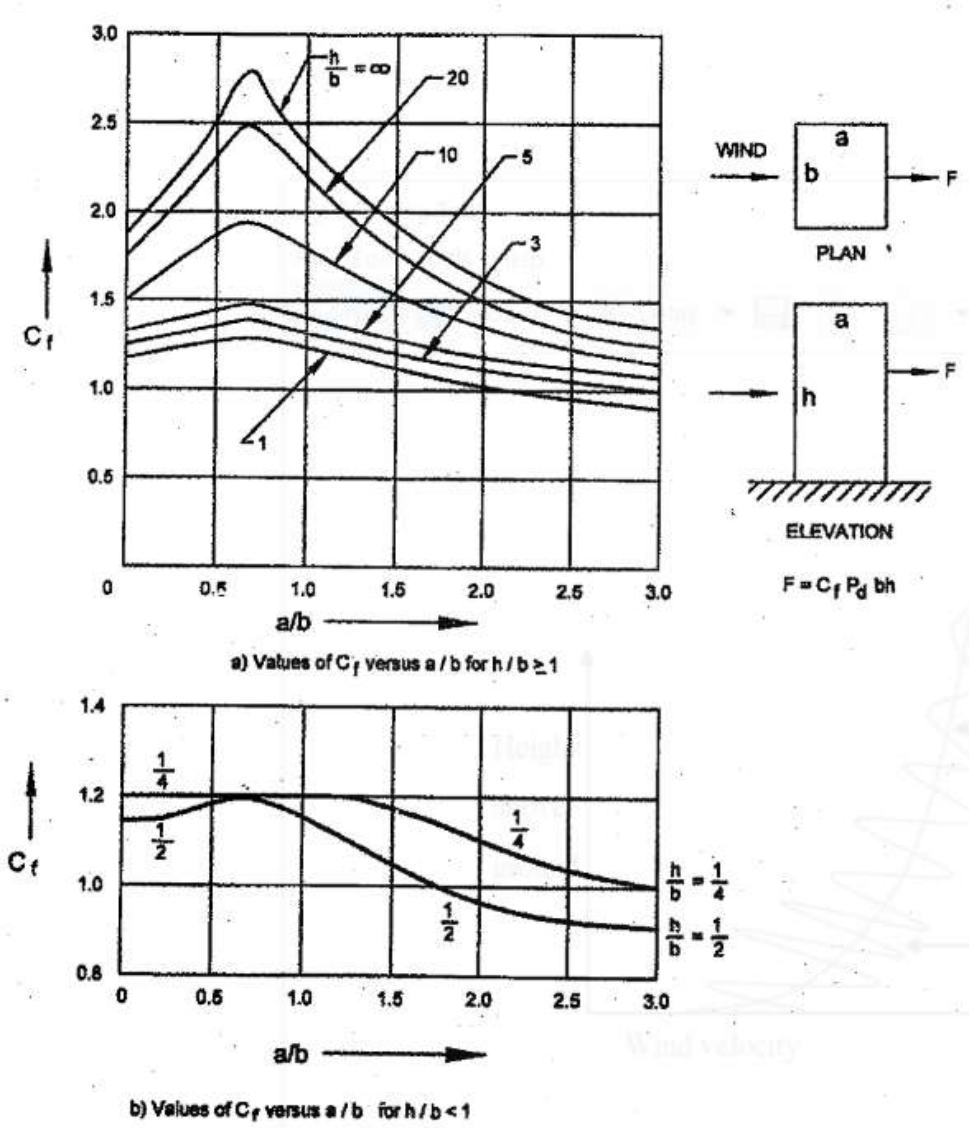

Figure 3.2: Force Coefficients in Rectangular Clad Building in Uniform Flow[43]

3.2.2 Dynamic Wind Load Analysis by Gust Factor Method (DGF)

The importance of wind-induced oscillations or excitations in both the along- and across-wind directions will be assessed concerning flexible, slender structures and structural elements. According to clause 9.1 of IS 875 (Part 3): 2015, buildings and closed structures having a height to minimum lateral dimension ratio of more than approximately 5.0, or buildings and structures whose natural frequency in the first mode is less than 1.0 Hz, shall be evaluated for dynamic wind effects. IS 875 (Part 3): 2015 includes dynamic impacts such as galloping, fluttering, ovaling, and vortex shedding in its gust factor-based

dynamic wind load analysis. The subsequent sections explain the along and across wind response according to the gust factor approach of IS 875 (Part 3): 2015[43].

3.2.2.1 Along Wind Response as per Gust Factor Method

Following are the steps to calculate along wind forces as per Gust Factor Method.

1. Find out Equivalent Aerodynamic Roughness Height ($z_{0,i}$) as per clause 6.3.2.1 of IS 875 (Part 3): 2015[43].

2. Calculate Hourly Mean Wind Speed Factor ($\overline{k_{2,i}}$) from equation 3.5 given in clause 6.4 of IS 875 (Part 3): 2015[43].

$$\overline{k_{2,i}} = 0.1423 \left[\ln \left(\frac{z}{z_{0,i}} \right) \right] (z_{0,i})^{0.0706} \tag{3.5}$$

3. Calculate Hourly Mean Wind Speed ($\overline{V_{z,H}}$) as per equation 3.6 given in clause 6.4 of IS 875 (Part 3): 2015[43].

$$\overline{V_{z,H}} = \overline{k_{2,i}} V_b \tag{3.6}$$

(*Note: V_b shall be calculated from step 1 given in 3.2.1.*)

4. Evaluate Design Hourly Mean Wind Speed ($\overline{V_{z,d}}$) as per equation 3.7 given in clause 6.4 of IS 875 (Part 3): 2015[43].

$$\overline{V_{z,d}} = \overline{V_{z,H}} k_1 k_3 k_4 \tag{3.7}$$

(*Note: k_1, k_3 and k_4 shall be calculated from steps 2, 4 and 5 given in 3.2.1.*)

5. Calculate Design Hourly Mean Wind Pressure ($\overline{p_d}$) as per equation 3.8 given in clause 10.2 of IS 875 (Part 3): 2015[41].

$$\overline{p_d} = 0.6 \overline{V_{z,d}}^2 \tag{3.8}$$

6. Evaluate Measure of Effective Turbulence Length Scale at the height h (L_h) as per equation 3.9 given in clause 10.2 of IS 875 (Part 3): 2015[43].

$$L_h = \begin{cases} 85 \left(\frac{h}{10} \right)^{0.25} & \text{for terrain category 1 to 3} \\ 70 \left(\frac{h}{10} \right)^{0.25} & \text{for terrain category 4} \end{cases} \tag{3.9}$$

7. Evaluate Background Factor B_s as per equation 3.10 given in clause 10.2 of IS 875 (Part 3): 2015[43].

$$B_s = \frac{1}{\left[1 + \frac{\sqrt{0.26(h-s)^2 + 0.46{b_{sh}}^2}}{L_h}\right]} \tag{3.10}$$

(*Note: Here, b_{sh} is average breadth of the building/ structure between heights s and h and height notions for z, h and s are shown in Fig. 3.3.*)

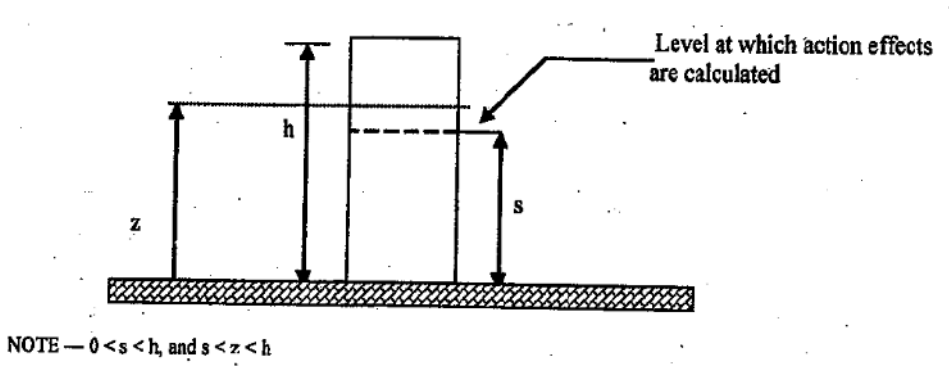

Figure 3.3: Height Notations[43]

8. Find out Peak Factor for Upwind Velocity Fluctuation g_v from equation 3.11 given in clause 10.2 of IS 875 (Part 3): 2015[43].

$$g_v = \begin{cases} 3.0 & \text{for terrain category 1 and 2} \\ 4.0 & \text{for terrain category 3 and 4} \end{cases} \tag{3.11}$$

9. Calculate Turbulence Intensity $I_{h,i}$ from equation 3.12 given in clause 10.2 of IS 875 (Part 3): 2015[43].

$$\begin{aligned} I_{z,1} &= 0.3507 - 0.0535 \log\left(\frac{z}{z_{0,1}}\right) \\ I_{z,4} &= 0.466 - 0.1358 \log\left(\frac{z}{z_{0,4}}\right) \\ I_{z,2} &= I_{z,1} + \frac{1}{7}\left(I_{z,4} - I_{z,1}\right) \\ I_{z,3} &= I_{z,1} + \frac{3}{7}\left(I_{z,4} - I_{z,1}\right) \end{aligned} \tag{3.12}$$

10. Evaluate Factor Account for Second Order Turbulence Intensity ϕ as per equation 3.13 given in clause 10.2 of IS 875 (Part 3): 2015[43].

$$\phi = \frac{g_v I_{h,i} \sqrt{B_s}}{2} \tag{3.13}$$

11. Evaluate Height Factor for Resonance Response H_s as per equation 3.14 given in clause 10.2 of IS 875 (Part 3): 2015[43].

$$H_s = 1 + \left(\frac{s}{h}^2\right) \tag{3.14}$$

12. Evaluate Peak Factor for Resonant Response g_R as per equation 3.15 given in clause 10.2 of IS 875 (Part 3): 2015[43].

$$g_R = \sqrt{[2 \ln (3600 f_a)]} \tag{3.15}$$

(*Note: Here, f_a is first mode natural frequency of the building/structure in along wind direction.*)

13. Calculate Size Reduction Factor S as per equation 3.16 given in clause 10.2 of IS 875 (Part 3): 2015[43].

$$S = \frac{1}{\left[1 + \frac{3.5 f_a h}{V_{h,d}}\right]\left[1 + \frac{4 f_a b_{0h}}{V_{h,d}}\right]} \tag{3.16}$$

(*Note: b_{0h} is average breadth of the building/ structure between 0 and h.*)

14. Calculate Spectrum of Turbulence in the approaching wind stream E as per equation 3.17 given in clause 10.2 of IS 875 (Part 3): 2015[43].

$$N = \frac{f_a L_h}{V_{h,d}}$$
$$E = \frac{\pi N}{(1 + 70.8 N^2)^{\frac{5}{6}}} \tag{3.17}$$

15. Find out Damping Coefficient of the building/ structure β as per Table 36 of IS 875 (Part 3): 2015[43].

16. Calculate Gust Factor G as per equation 3.18 given in clause 10.2 of IS 875 (Part 3): 2015[43].

$$G = 1 + r \sqrt{\left[{g_v}^2 B_s (1 + \phi)^2 + \frac{H_s {g_R}^2 S E}{\beta}\right]} \tag{3.18}$$

(*Note: Here, r is Roughness Factor which is twice the Longitudinal Turbulence Intensity* $I_{h,i}$.)

17. Calculate Design Peak Along Wind Load $F_{z,along}$ from equation 3.19 given in clause 10.2 of IS 875 (Part 3): 2015[43].

$$F_{z,along} = C_{f_{(z)}} A_{e_{(z)}} \overline{pd_{(z)}} G \tag{3.19}$$

(*Note:* $C_{f_{(z)}}$ *and* $A_{e_{(z)}}$ *shall be calculated from steps 13 and 14 given in 3.2.1.*)

3.2.2.2 Across Wind Response as per Gust Factor Method

Following are the steps to calculate across wind forces as per Gust Factor Method.

1. Evaluate Peak factor g_h from equation 3.20 given in clause 10.3 of IS 875 (Part 3): 2015[43].

$$g_h = \sqrt{[2 \ln (3600 f_c)]} \tag{3.20}$$

(*Note: Here,* f_c *is first mode natural frequency of the building/structure in across wind direction.*)

2. Find out Mode Shape Power Exponent k as per clause 10.3 of IS 875 (Part 3): 2015[43].

3. Evaluate Across Wind Force Spectrum Coefficient C_{fs} from Figures 3.4 and 3.5 given in clause 10.3 of IS 875 (Part 3): 2015[43].

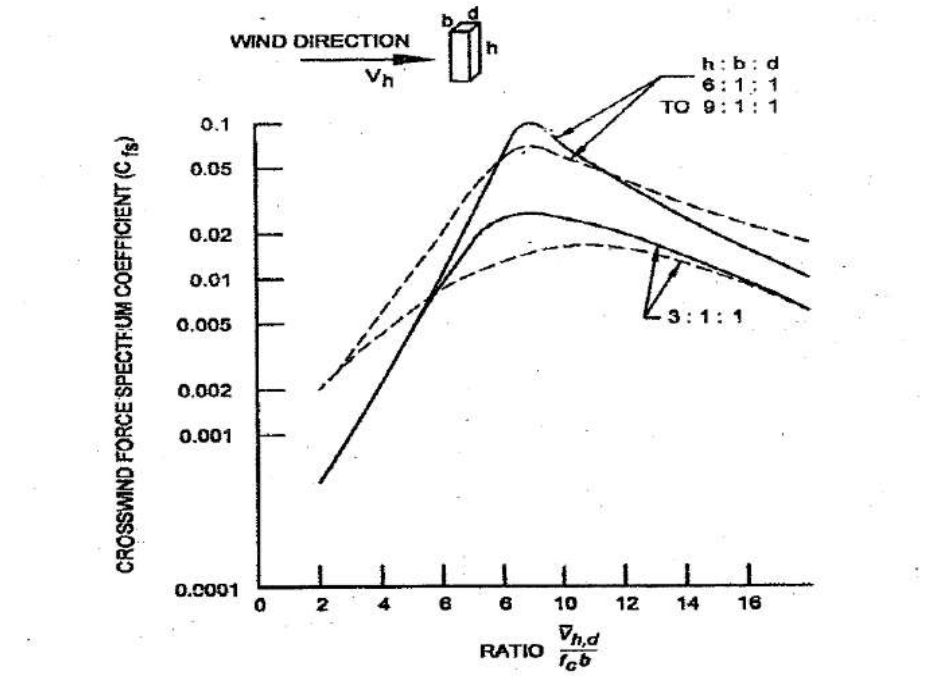

FIG. 10 VALUES OF THE CROSS WIND FORCE SPECTRUM COEFFICIENT FOR SQUARE SECTION BUILDINGS

Figure 3.4: Values of the Cross Wind Spectrum Coefficient for square section buildings[41]

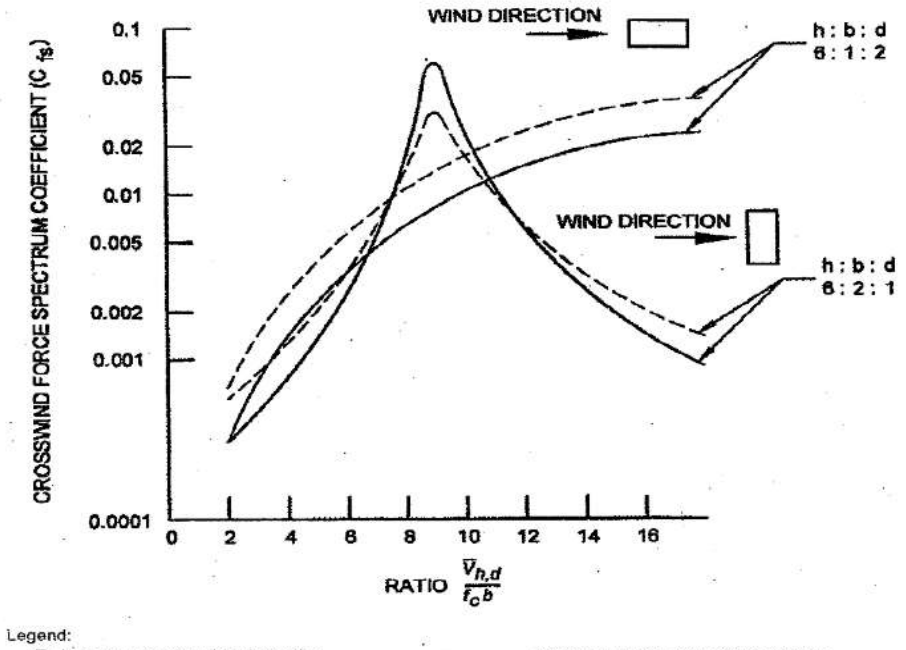

FIG. 11 VALUES OF THE CROSS WIND FORCE SPECTRUM COEFFICIENT FOR 2:1 AND 1 : 2 RECTANGULAR SECTION BUILDINGS

Figure 3.5: Values of the Cross Wind Spectrum Coefficient for 1:2 and 2:1 rectangular section buildings[43]

4. Calculate Across Wind Design Peak Base Bending Moment M_c from equation 3.21 given in clause 10.3 of IS 875 (Part 3): 2015[43].

$$M_c = 0.5 g_h \overline{p_h} b h^2 (1.06 - 0.06k) \sqrt{\frac{\pi C_{fs}}{\beta}} \tag{3.21}$$

(*Note: $\overline{p_h}$ and β shall be calculated from steps 5 and 15 given in section 3.2.2.1.*)

5. Calculate Across Wind Load $F_{z,across}$ as per equation 3.22 given in clause 10.3 of IS 875 (Part 3): 2015[43].

$$F_{z,across} = \left(\frac{3M_c}{h^2}\right)\left(\frac{z}{h}\right) \tag{3.22}$$

3.2.3 Dynamic Wind Time History Analysis using TPU Aerodynamic Database (DTHA)

For tall, slender structures, wind loads become increasingly significant. Therefore, it is vital to study the response of tall buildings to dynamic wind effects. Several techniques such as Anemometers, Doppler Radar, Laser-based LIDAR, and wind tunnel testing are employed in practice for estimating wind time history data. However, these processes are all time-consuming and costly. This section describes an alternative to conventional methods, an analytical procedure for generating wind time history point load data.

The Tokyo Polytechnic Aerodynamic database[60] is an online web resource that provides wind tunnel test data for low-rise and high-rise building wind loads. It includes a graph of area-averaged wind pressure coefficients, contours of statistical values of local wind pressure coefficients on all four sides of the structure, and time-series data of point wind pressure coefficients. This webpage presents statistics corresponding to multiple aspect ratios of the model and different wind directions. Figures 3.6 and 3.7 depicts the typical data page for the high-rise building database on this website.

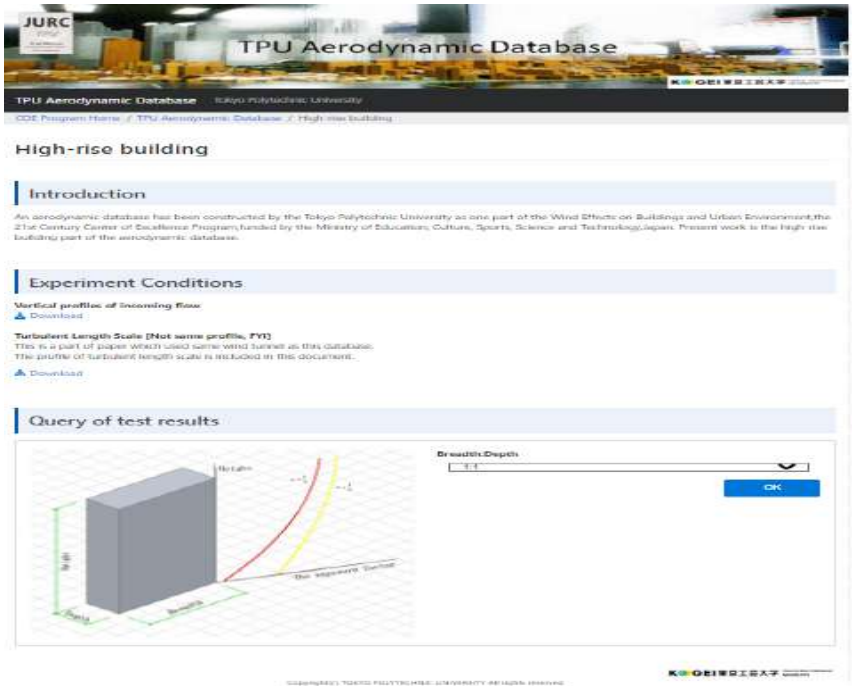

Figure 3.6: TPU Aerodynamic High-Rise Building Database[60]

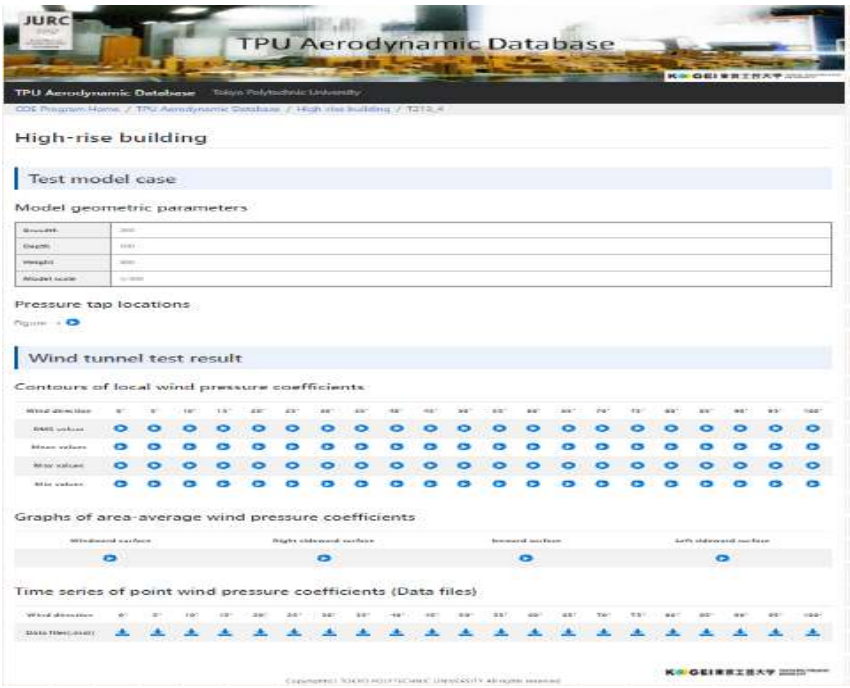

Figure 3.7: TPU wind time history data for high-rise building with 1:2 aspect ratio and 1:3 slenderness ratio[60]

Using the TPU Aerodynamic High-rise Building Database, the procedure to calculate wind time histories along and across wind forces is described below.

1. Download wind time history pressure coefficient data from TPU Aerodynamic database[60] by providing dimensions of building as shown in Figures 3.8 and 3.9.

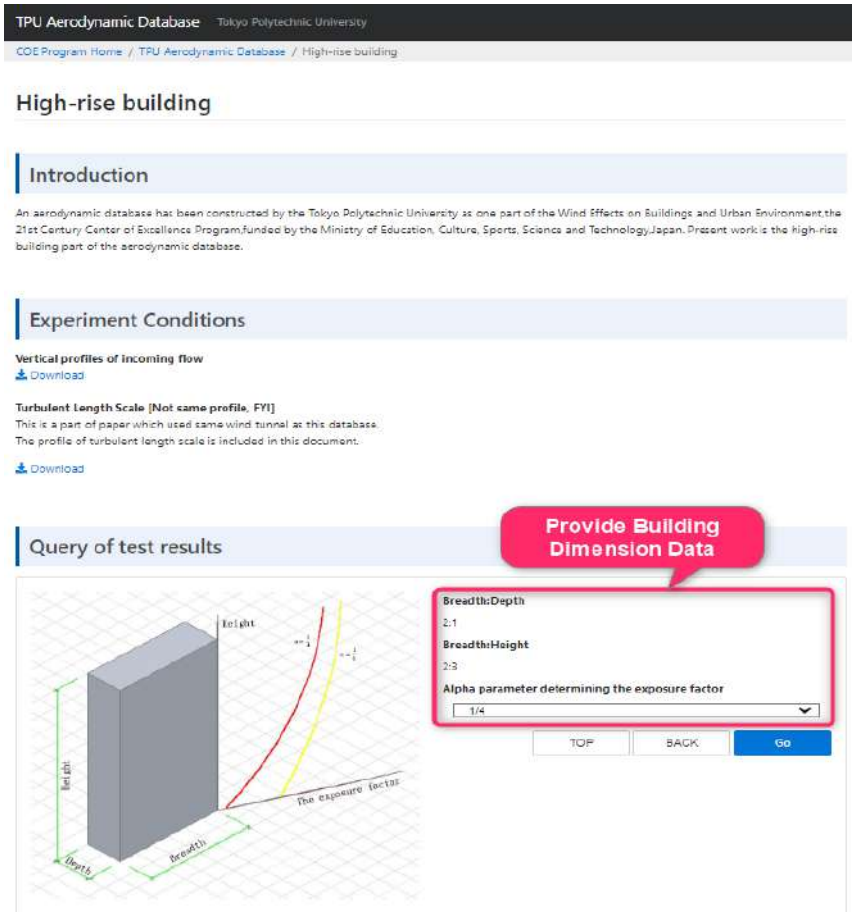

Figure 3.8: TPU Aerodynamic High-Rise Building Database[60]

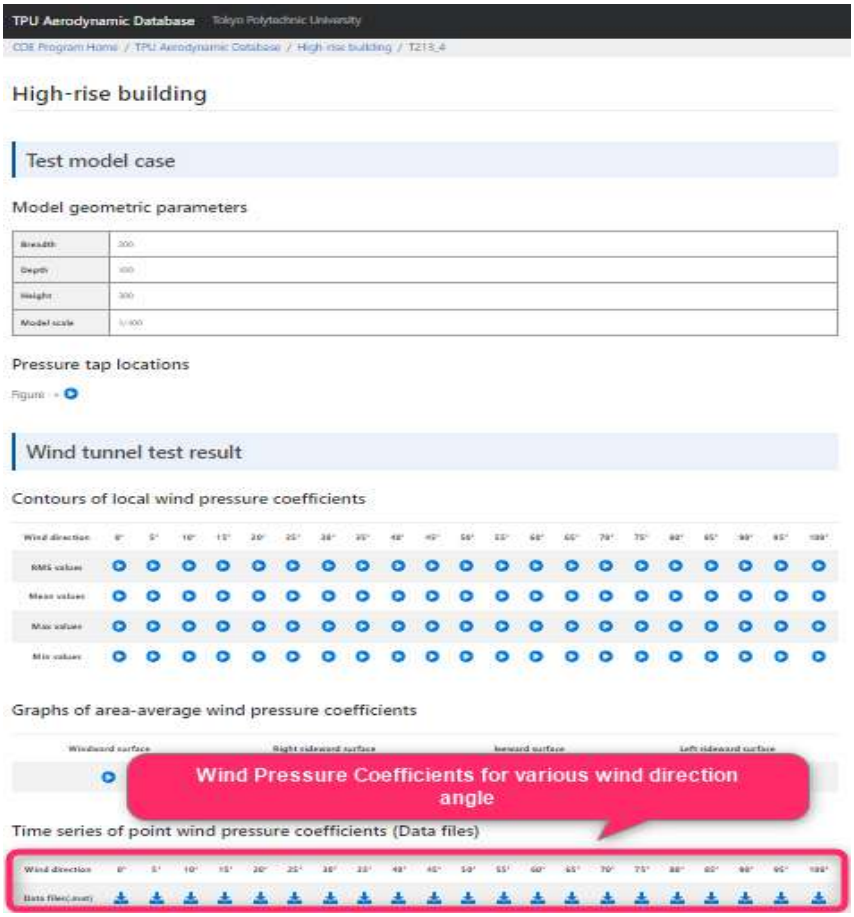

Figure 3.9: TPU wind time history data for high-rise building with 1:2 aspect ratio and 1:3 slenderness ratio[60]

Pressure tap locations can also be located from the figure under Pressure tap locations in Fig. 3.9. Pressure tap locations for high-rise building with 1:2 aspect ratio and 1:3 slenderness ratio is shown in Fig. 3.10.

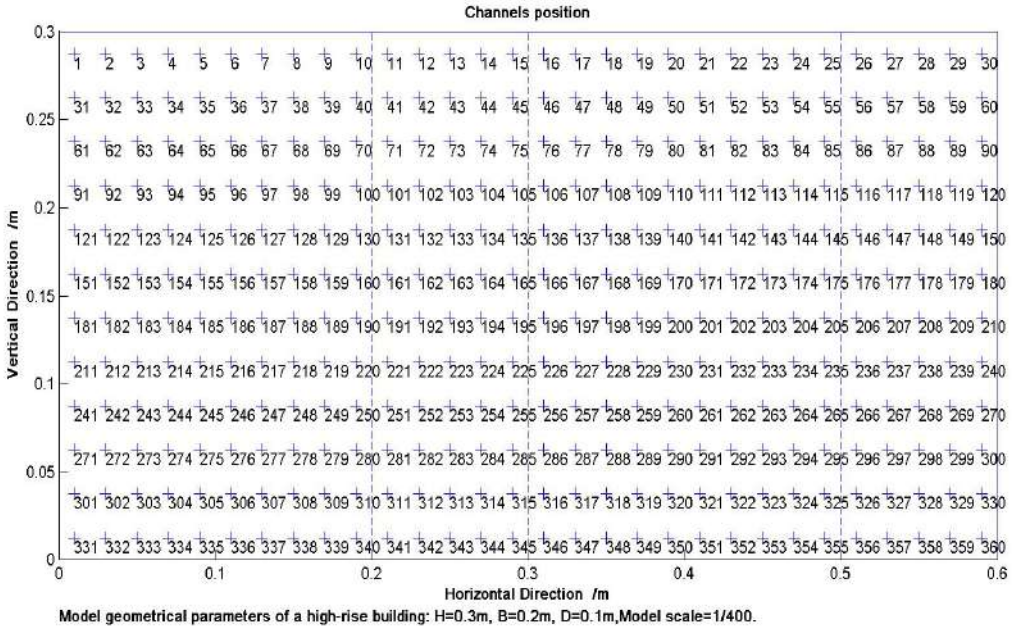

Figure 3.10: Pressure tap locations[60]

2. Evaluate along and across wind pressure coefficients at each story levels. Three different approaches to calculate along and across wind pressure coefficients are adopted.

   (a) Maximum Sum of Wind Pressure Coefficients Approach

   This method takes into account wind pressure coefficients in along and across wind directions at each story level at the time when the sum of wind pressure coefficients in along wind direction reaches its maximum. Steps to calculate along and across wind pressure coefficients according this approach are as follows:

   i. Evaluate average of wind pressure coefficients on each face at each story levels for all time series data from t = 0 to t = T sec as shown in Fig. 3.11 where T = total time of recorded wind time history data.

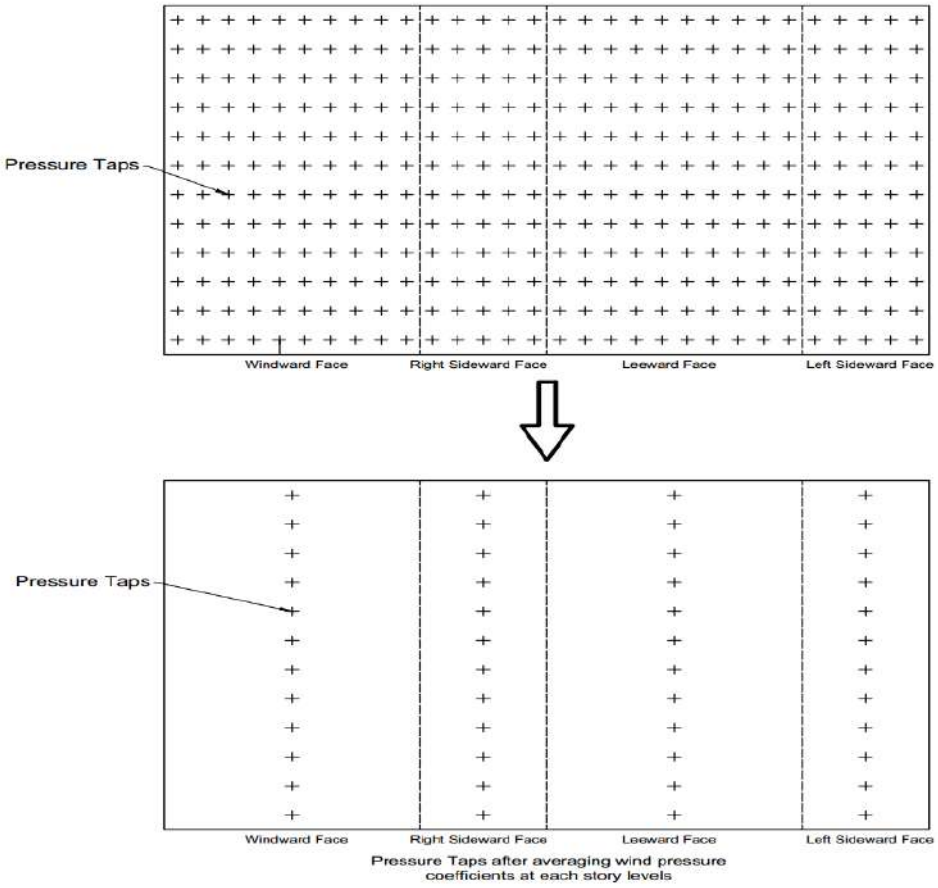

Figure 3.11: Averaged Wind Pressure Taps Locations

ii. Calculate along and across wind pressure coefficients by using equations 3.23.

$$C_{(f,along)} = C_{(f,windward)} - C_{(f,leeward)}$$
$$C_{(f,across)} = C_{(f,rightside-ward)} - C_{(f,leftside-ward)} \tag{3.23}$$

The Fig. 3.12 shows along wind pressure coefficients and the Fig. 3.13 shows across wind pressure coefficients for considered building at top story level.

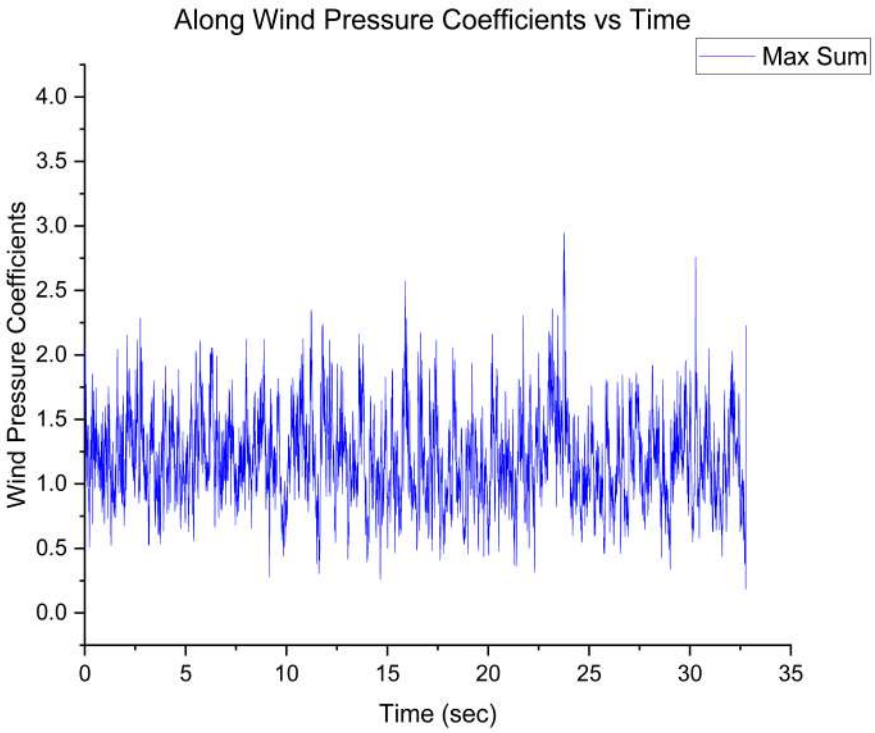

Figure 3.12: Along Wind Pressure Coefficient by Maximum Sum Approach

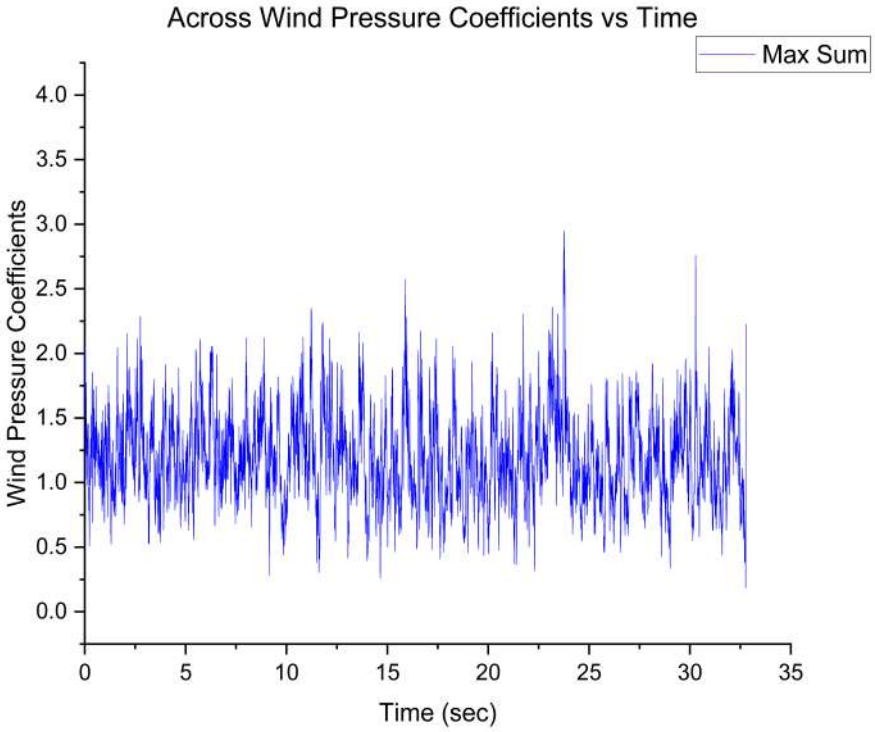

Figure 3.13: Across Wind Pressure Coefficient by Maximum Sum Approach

iii. Find out times at when sum of along and across wind pressure coefficients of all story levels becomes maximum. Table 3.1 shows both the time when maximum sum of along and across wind pressure coefficients are obtained.

Table 3.1: Time and sum of wind pressure coefficients at time when maximum sum of pressure coefficient are obtained

Max Sum Approach (Time at when maximum sum of pressure coefficient are obtained)		
Wind_Type	**Time (sec)**	**Pressure Coefficient Sum**
Along	23.743	28.84
Across	23.440	-19.34

iv. Consider along and across wind pressure coefficients at time considered in Table 3.1 as wind pressure coefficients to calculate wind force at each story level. The Table 3.2 shows final along and across wind pressure coefficients by Maximum Sum Approach

Table 3.2: Along and Across Wind Pressure Coefficients by Maximum Sum Approach

Maximum Sum of Along Wind Coefficients			**Maximum Sum of Across Wind Coefficients**	
Height(m)	**Along_coeff**	**Across_coeff**	**Along_coeff**	**Across_coeff**
0.287	2.809	0.035	1.410	-0.963
0.262	3.196	0.216	1.887	-1.282
0.237	3.083	0.237	2.001	-1.484
0.213	2.931	0.288	1.940	-1.661
0.188	2.788	0.267	1.938	-1.636
0.162	2.574	0.321	1.962	-1.560
0.138	2.458	0.309	1.992	-1.693
0.112	2.101	0.238	1.863	-2.018
0.087	1.764	0.444	1.696	-1.758
0.063	1.674	0.749	1.585	-1.758
0.038	1.660	0.220	1.521	-1.744
0.013	1.806	0.147	1.536	-1.782

(b) Peak Wind Pressure Coefficients Approach

This method evaluates peak wind pressure coefficients in along and across wind directions at every story level for entire time-series data and finalise maximum

along and across wind pressure coefficients for every story level. Steps to calculate along and across wind pressure coefficients according this approach are as follows:

i. Evaluate maximum and minimum wind pressure coefficients on each face at each story levels for all time series data from t = 0 to t = T sec.

ii. Evaluate along and across wind pressure coefficients at each story levels for all time series data from t = 0 to t = T sec using equation 3.24.

$$C_{(f,along)} = C_{(f,max_windward)} - C_{(f,min_leeward)}$$
$$C_{(f,across)} = C_{(f,max_rightside-ward)} - C_{(f,min_leftside-ward)} \quad (3.24)$$

Along and across wind pressure coefficients calculated as per equation 3.24 are shown in Figures 3.14 and 3.15 respectively for top story level.

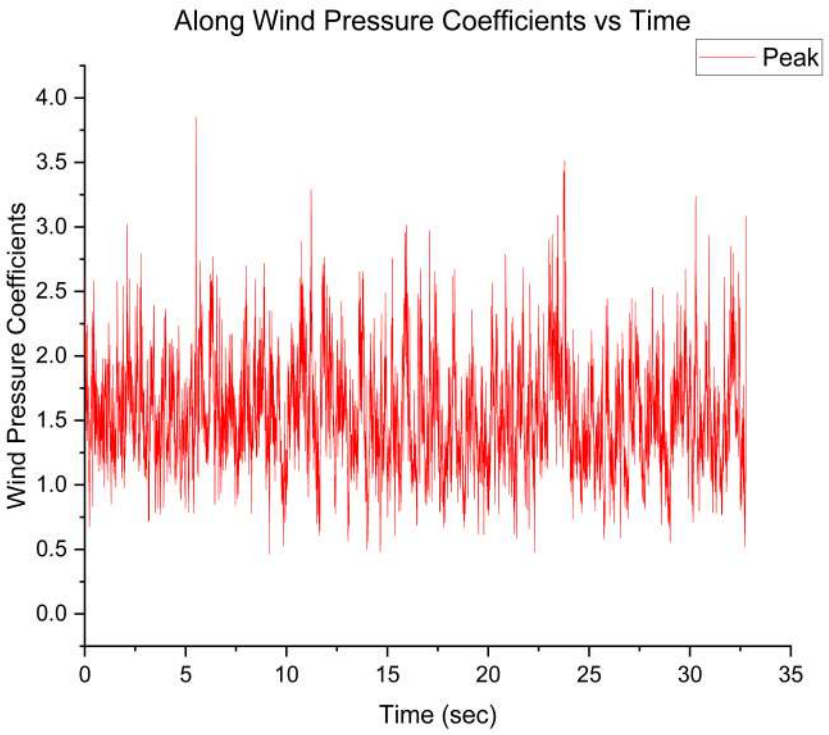

Figure 3.14: Along Wind Pressure Coefficient by Peak Coefficient Approach

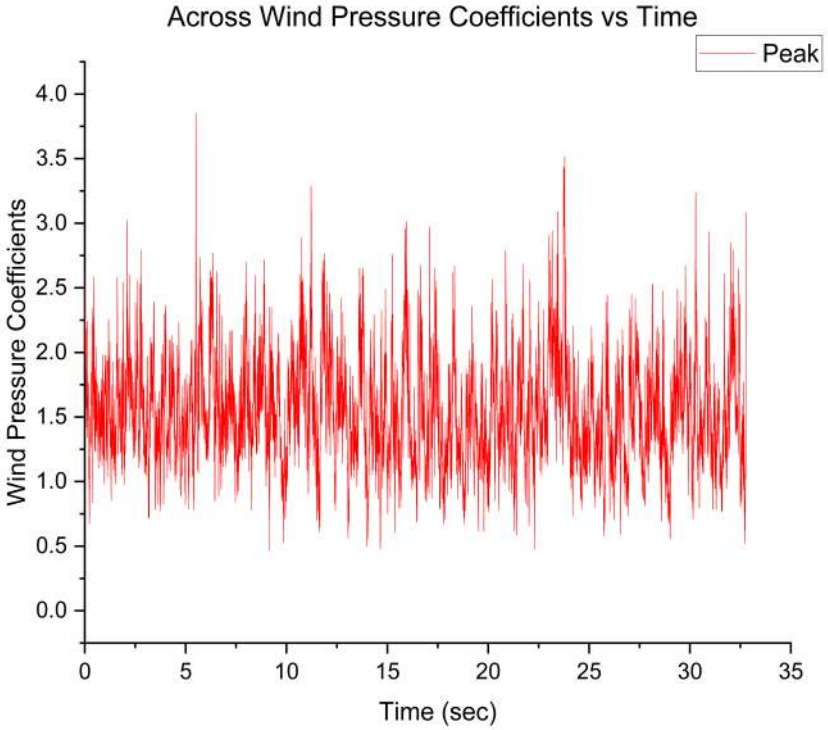

Figure 3.15: Across Wind Pressure Coefficient by Peak Coefficient Approach

iii. Find out peak along and across wind pressure coefficients at each story levels among time t = 0 to t = T sec. Table 3.3 shows peak along and across wind pressure coefficients calculated by Peak Coefficient Approach.

Table 3.3: Along and Across Wind Coefficients by Peak Coefficient Approach

Peak Coefficient Approach		
Height(m)	**Along_coeff**	**Across_coeff**
0.2875	3.85463929	3.63616908
0.2625	3.80395496	2.77083755
0.2375	3.86529589	2.85044861
0.2125	3.87071788	2.69052535
0.1875	3.53907502	2.6280424
0.1625	3.48906922	2.6609183
0.1375	3.58803642	2.89950341
0.1125	3.49446464	2.74342191
0.0875	3.28566706	3.52709907
0.0625	3.40862691	3.51991761
0.0375	3.10998356	3.45054013
0.0125	3.10776722	3.55211693

(c) Mean Wind Pressure Coefficients Approach

This method evaluates mean wind pressure coefficients in along and across wind directions at every story level for entire time-series data and finalise mean along and across wind pressure coefficients for every story level. Steps to calculate along and across wind pressure coefficients according this approach are as follows:

i. Evaluate mean wind pressure coefficients on each face at each story levels for all time series data from t = 0 to t = T sec.

ii. Evaluate along and across wind pressure coefficients at each story levels for all time series data from t = 0 to t = T sec using equation 3.25.

$$C_{(f,along)} = C_{(f,mean_windward)} - C_{(f,mean_leeward)}$$
$$C_{(f,across)} = C_{(f,mean_rightside-ward)} - C_{(f,mean_leftside-ward)} \quad (3.25)$$

Along and across wind pressure coefficients calculated as per equation 3.25 are shown in Figures 3.16 and 3.17 respectively for top story level.

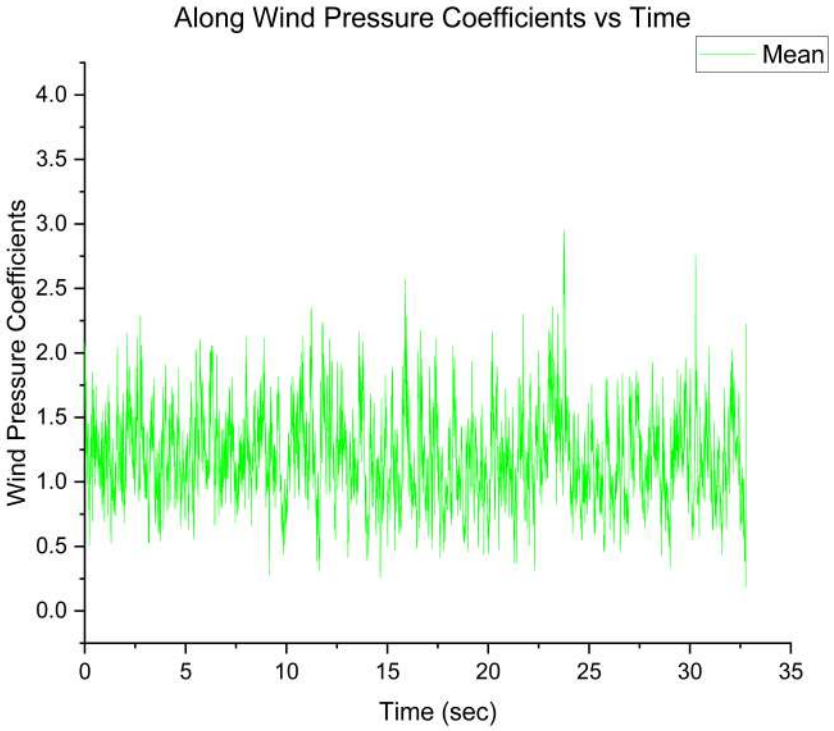

Figure 3.16: Along Wind Pressure Coefficient by Mean Coefficient Approach

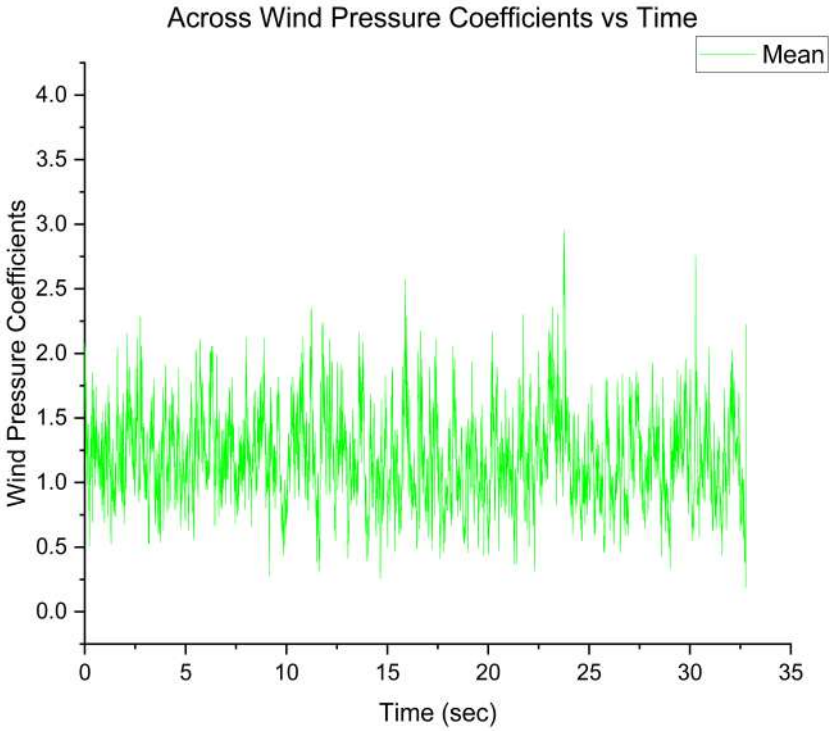

Figure 3.17: Across Wind Pressure Coefficient by Mean Coefficient Approach

iii. Find out mean along and across wind pressure coefficients at each story levels among time t = 0 to t = T sec. Table 3.4 shows mean along and across wind pressure coefficients calculated by Mean Coefficient Approach.

Table 3.4: Along and Across Wind Coefficients by Mean Coefficient Approach

Mean Coefficient Approach		
Height(m)	**Along_coeff**	**Across_coeff**
0.2875	1.19755223	0.02559126
0.2625	1.36627566	0.03429686
0.2375	1.37292689	0.03238811
0.2125	1.33190159	0.03044692
0.1875	1.27931562	0.02819047
0.1625	1.21248196	0.02822255
0.1375	1.14886303	0.03055072
0.1125	1.08121781	0.02923399
0.0875	1.02003274	0.02774708
0.0625	0.96483914	0.03126418
0.0375	0.93983263	0.02340359
0.0125	1.00270471	0.01730387

3. Evaluate $A_{e_{(z)}}$ and $p_{d_{(z)}}$ as per steps 12 and 14 in the section 3.2.1 respectively.

4. Calculate along and across wind force as per equation 3.26. Here $C_{f_{(z)}}$ can be taken as along and across wind pressure coefficients calculated from three approaches for wind pressure coefficient time history data.

$$F_{(z)} = C_{f_{(z)}} A_{e_{(z)}} p_{d_{(z)}} \tag{3.26}$$

(*Note: MATLAB Code for evaluation of along and across wind pressure coefficients from TPU Wind Time History Database is given in Appendix C.*)

3.3 Parametric Study on Along and Across Wind Force Evaluation

In this section, the parametric study on wind load evaluation of tall buildings with three different aspect ratios 1:1 (A1), 1:2 (A2), and 1:3 (A3) with varying number of stories: 35 story, 40 story, and 45 story is performed and explained using static wind load analysis (SWLA), dynamic wind load analysis by gust factor method (DGF) and dynamic wind time history analysis from TPU aerodynamic database (DTHA).

Total of nine tall buildings situated in Bhuj city are considered for this investigation. The plans and elevations of these buildings with aspect ratio 1:1 (A1), 1:2 (A2), and 1:3 (A3) are shown in Figures 3.18, 3.19 and 3.20 respectively.

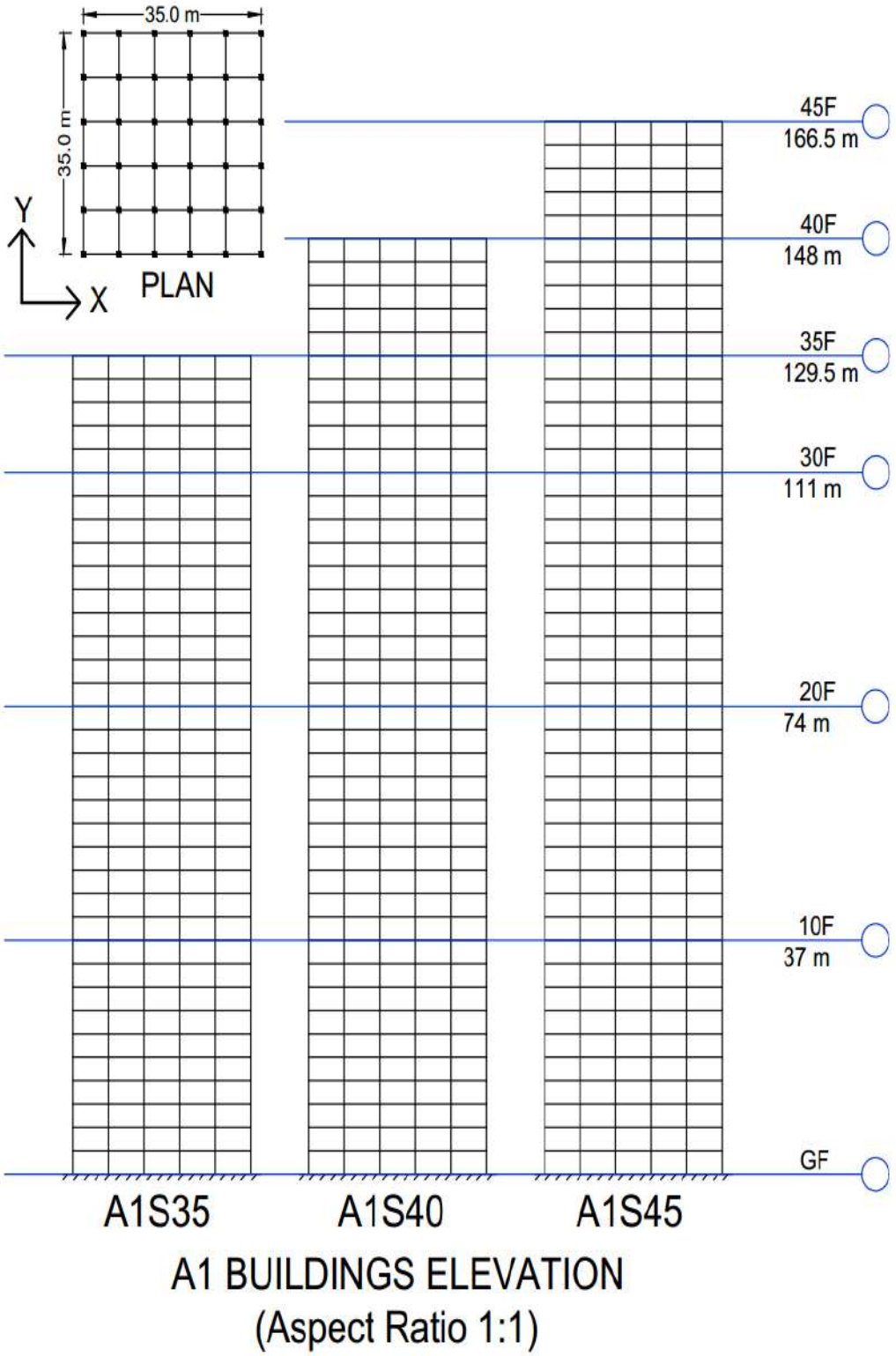

Figure 3.18: Plan and Elevation A1 Type Buildings (Aspect Ratio = 1:1)

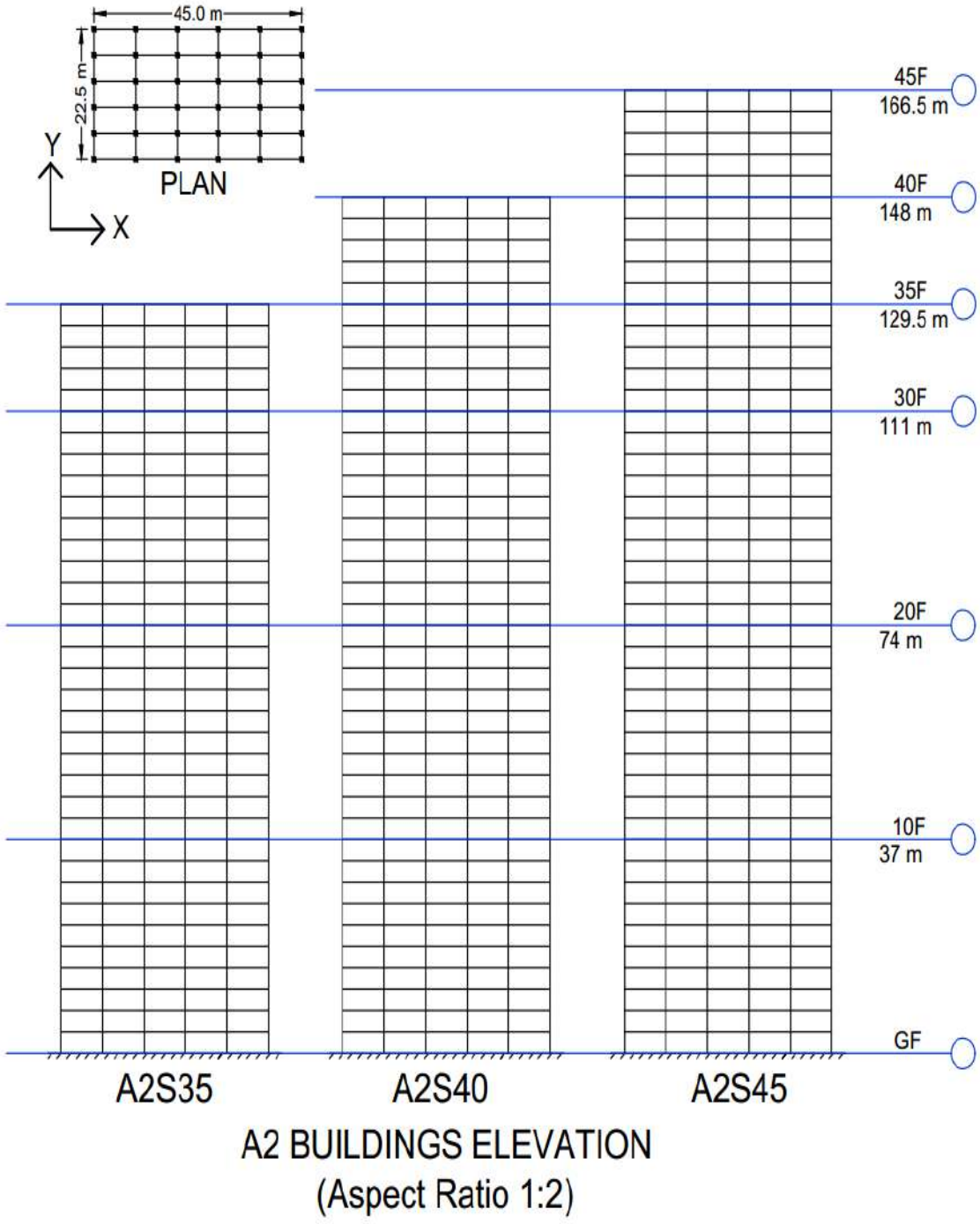

Figure 3.19: Plan and Elevation A2 Type Buildings (Aspect Ratio = 1:2)

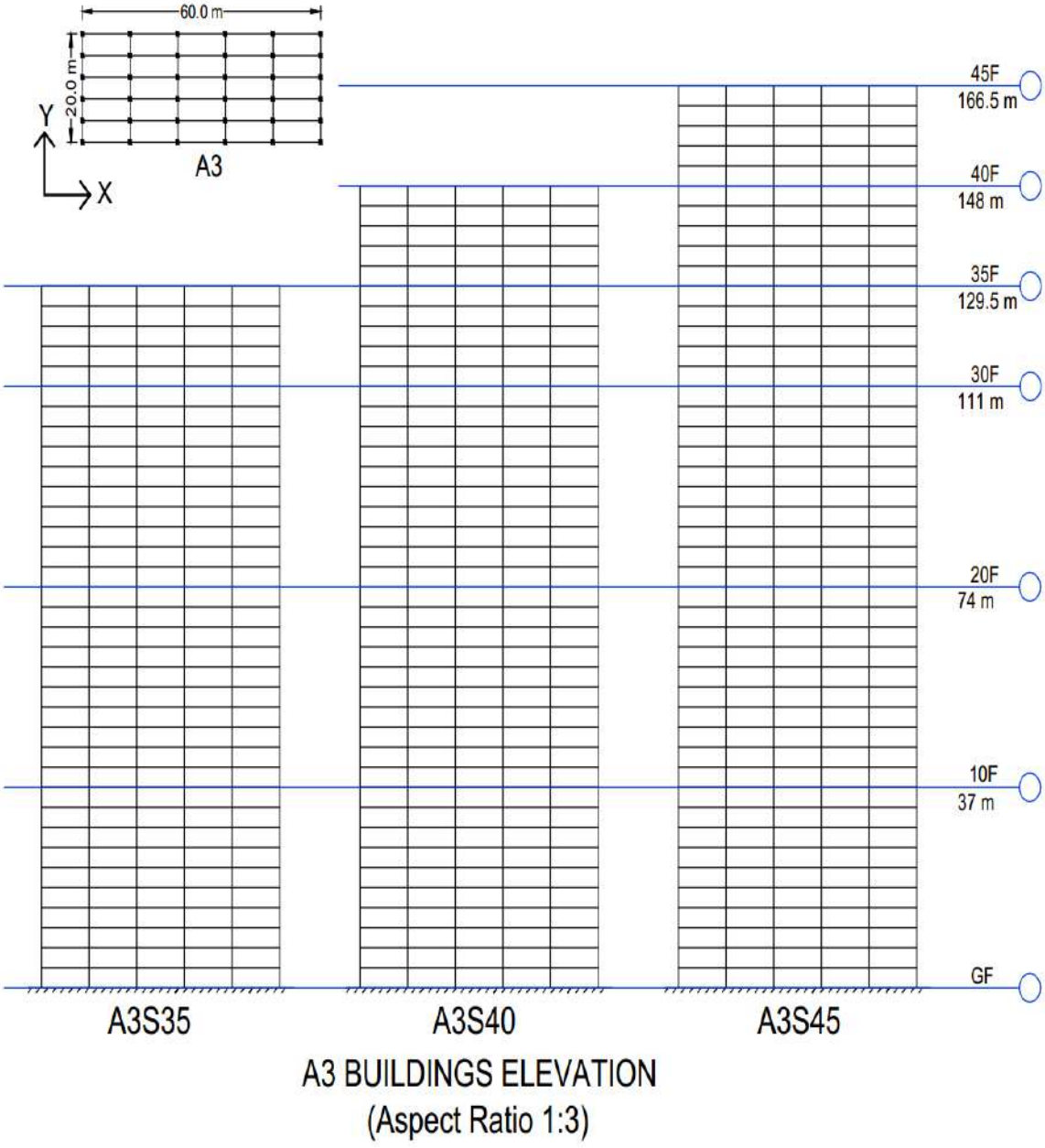

Figure 3.20: Plan and Elevation A3 Type Buildings (Aspect Ratio = 1:3)

General building dimension data and basic data for wind load calculations are shown in Tables 3.5 and 3.6 respectively.

Table 3.5: General Building Dimension Data

General Building Dimension Data							
Building Type	**Model Name**	**Dimension along X (m)**	**Dimension along Y (m)**	**Aspect Ratio**	**Nos of story**	**Story Height (m)**	**Slenderness Ratio**
A1	**A1S35**	35	35	1:1	35	3.7	3.70
	A1S40	35	35	1:1	40	3.7	4.23
	A1S45	35	35	1:1	45	3.7	4.76
A2	**A2S35**	22.5	45	1:2	35	3.7	5.76
	A2S40	22.5	45	1:2	40	3.7	6.58
	A2S45	22.5	45	1:2	45	3.7	7.40
A3	**A3S35**	20	60	1:3	35	3.7	6.48
	A3S40	20	60	1:3	40	3.7	7.40
	A3S45	20	60	1:3	45	3.7	8.33

Table 3.6: Basic Wind Data

Basic Wind Data		
Description	**Value**	**Remarks**
Basic Wind Speed V_b (Bhuj) (m/s)	50	Annex A of IS 875 (Part 3) : 2015
k_1 (Risk Coefficient)	1	Table 1 of IS 875 (Part 3) : 2015
k_3 (Topography Factor)	1	Cl. 6.3.3 of IS 875 (Part 3) : 2015
k_4 (Importance Factor)	1	Cl. 6.3.4 of IS 875 (Part 3) : 2015
K_d (Wind Directionality factor)	0.9	Cl. 7.2.1 of IS 875 (Part 3) : 2015
K_c (Combination Factor)	0.9	Cl. 7.3.3.13 of IS 875 (Part 3) : 2015
Terrain Category	2	Cl. 6.3.2 of IS 875 (Part 3) : 2015

For understanding purpose, along an across wind load calculations of A2S35_X model with wind flowing along X-axis will be explained using static wind load analysis (SWLA), dynamic wind load analysis by gust factor method (DGF) and dynamic wind time history analysis from TPU aerodynamic database (DTHA).

3.3.1 Static Wind Load Analysis (SWLA) of A2S35(X) Model

General data for static wind load analysis of A2S35(X) model are shown in Table 3.7.

Table 3.7: A2S35_X Building General Data

A2S35_X Building General Data		
Description	**Value**	**Remarks**
Basic Wind Speed Vb (Bhuj) (m/s)	50	Annex A of IS 875 (Part 3) : 2015
K1 (Risk Coefficient)	1	Table 1 of IS 875 (Part 3) : 2015
K3 (Topography Factor)	1	Cl. 6.3.3 of IS 875 (Part 3) : 2015
K4 (Importance Factor)	1	Cl. 6.3.4 of IS 875 (Part 3) : 2015
Kd (Wind Directionality factor)	0.9	Cl. 7.2.1 of IS 875 (Part 3) : 2015
Kc (Combination Factor)	0.9	Cl. 7.3.3.13 of IS 875 (Part 3) : 2015
Terrain Category	2	Cl. 6.3.2 of IS 875 (Part 3) : 2015
Typical Storey height	3.7	m
a (Along Wind Building Dimension)	45	m
b (Across Wind Building Dimension)	22.5	m
Ka (Area Avg. Factor)	1.17	Cl. 7.2.2 of IS 875 (Part 3) : 2015
Ground Floor Level	0	m
Total nos of storeys	35	-
Total Building Height h	129.5	-
h/a	2.88	-
h/b	5.76	-
a/b	2	-

Static wind load calculations of A2S35(X) model are shown in Tables 3.8 and 3.9.

Table 3.8: Static Wind Load Calculations of A2S35(X) model

Static Wind Load Calculations of A2S35(X)					
Description	**Calculations**				**Remarks**
Force F acting in direction of wind at height z (kN)	$F_{(z)} = C_{f_{(z)}} A_{e_{(z)}} p_{d_{(z)}}$				Cl. 7.4
Force coefficient C_f	a/b	2	h/b	5.76	Fig. 4
	C_f		1.25		
Effective frontal area A_e (m2)	$A_{e_{(z)}}$				Cl. 7.4 Note 3
Basic wind speed V_b (m/s)	50				Annex A
Risk coefficient k_1	1				Table 1
Terrain roughness and height factor k_2	Vary with height z and terrain category				Table 2
Topography factor k_3	1				Cl. 6.3.3
Importance factor for the cyclonic region k_4	1				Cl. 6.3.4
Design wind Speed V_z (m/s)	$V_z = V_b k_1 k_2 k_3 k_4$				Cl. 6.3
Wind pressure at height z (kN/m2)	$p_z = 0.6 {V_z}^2$				Cl. 7.2
Wind directionality factor K_d	0.9				Cl. 7.2.1
Area average factor K_a	0.822333333				Cl. 7.2.2
Combination factor K_c	0.9				Cl. 7.3.3.13
Design wind pressure p_d with Interference effect (kN/m2)	$p_{d_{(z)}} = (K_d K_a K_c p_z)$				Cl. 7.2 & 8
	IF		1		
Force F	$F_{(z)} = C_{f_{(z)}} A_{e_{(z)}} p_{d_{(z)}}$				Clause 8

Table 3.9: Static Wind Load Calculations of A2S35(X)

Static Wind Load Calculations of A2S35(X)								
Storey	**Height z(m)**	k_2	V_z **(m/s)**	p_z **(kN/m^2)**	p_d **(kN/m^2)**	A_e **(m^2)**	C_f	F_z **(kN)**
35	129.5	1.26	63.18	2.395	1.595	41.625	1.25	83.01
34	125.8	1.26	63.03	2.384	1.588	83.25	1.25	165.23
33	122.1	1.26	62.88	2.373	1.580	83.25	1.25	164.46
32	118.4	1.25	62.74	2.361	1.573	83.25	1.25	163.69
31	114.7	1.25	62.59	2.350	1.566	83.25	1.25	162.91
30	111	1.25	62.44	2.339	1.558	83.25	1.25	162.15

Static Wind Load Calculations of A2S35(X)								
Storey	**Height z(m)**	k_2	V_z **(m/s)**	p_z **(kN/m^2)**	p_d **(kN/m^2)**	A_e **(m^2)**	C_f	F_z **(kN)**
29	107.3	1.25	62.29	2.328	1.551	83.25	1.25	161.38
28	103.6	1.24	62.14	2.317	1.543	83.25	1.25	160.61
27	99.9	1.24	61.99	2.306	1.536	83.25	1.25	159.83
26	96.2	1.23	61.73	2.287	1.523	83.25	1.25	158.50
25	92.5	1.23	61.48	2.268	1.510	83.25	1.25	157.17
24	88.8	1.22	61.22	2.248	1.498	83.25	1.25	155.85
23	85.1	1.22	60.96	2.229	1.485	83.25	1.25	154.53
22	81.4	1.21	60.70	2.211	1.472	83.25	1.25	153.22
21	77.7	1.21	60.44	2.192	1.460	83.25	1.25	151.92
20	74	1.20	60.18	2.173	1.447	83.25	1.25	150.62
19	70.3	1.20	59.92	2.154	1.435	83.25	1.25	149.33
18	66.6	1.19	59.66	2.136	1.423	83.25	1.25	148.04
17	62.9	1.19	59.40	2.117	1.410	83.25	1.25	146.76
16	59.2	1.18	59.14	2.099	1.398	83.25	1.25	145.48
15	55.5	1.18	58.89	2.080	1.386	83.25	1.25	144.21
14	51.8	1.17	58.63	2.062	1.374	83.25	1.25	142.94
13	48.1	1.17	58.26	2.037	1.357	83.25	1.25	141.17
12	44.4	1.16	57.80	2.005	1.335	83.25	1.25	138.94
11	40.7	1.15	57.34	1.973	1.314	83.25	1.25	136.73
10	37	1.14	56.88	1.941	1.293	83.25	1.25	134.53
9	33.3	1.13	56.41	1.909	1.272	83.25	1.25	132.35
8	29.6	1.12	55.90	1.875	1.249	83.25	1.25	129.96
7	25.9	1.10	54.98	1.813	1.208	83.25	1.25	125.69
6	22.2	1.08	54.05	1.753	1.168	83.25	1.25	121.50
5	18.5	1.06	53.20	1.698	1.131	83.25	1.25	117.71
4	14.8	1.05	52.40	1.647	1.097	83.25	1.25	114.19
3	11.1	1.01	50.55	1.533	1.021	83.25	1.25	106.27
2	7.4	1.00	50.00	1.500	0.999	83.25	1.25	103.97

Static Wind Load Calculations of A2S35(X)								
Storey	**Height z(m)**	k_2	V_z **(m/s)**	p_z **(kN/m^2)**	p_d **(kN/m^2)**	A_e **(m^2)**	C_f	F_z **(kN)**
1	3.7	1.00	50.00	1.500	0.999	41.625	1.25	51.99

3.3.2 Dynamic Wind Load Analysis by Gust Factor Method (DGF) of A2S35(X) Model

Along wind load calculations by gust factor method of A2S35(X) model are shown in Tables 3.10 and 3.11.

Table 3.10: Along Wind Load Calculations of A2S35(X)

Along Wind Load Calculations of A2S35(X)					
Description	**Calculations**				**Remarks**
Force F_z acting in direction of wind at height z (kN)	$F_{z,along} = C_{f_{(z)}} A_{e_{(z)}} \overline{pd_{(z)}} G$				Cl. 10.2
Force coefficient C_f	a/b	2	h/b	5.76	Fig. 4
	C_f		1.25		
Effective frontal area $A_{e_{(z)}}$ (m^2)	$A_{e_{(z)}}$)				Cl. 10.2
Hourly mean wind speed factor for terrain category i	$\overline{k_{2,i}} = 0.1423 \left[\ln \left(\frac{z}{z_{0,i}} \right) \right] (z_{0,i})^{0.0706}$				Cl. 6.4
Design hourly mean wind speed at height z (m/s)	$\overline{V_{z,d}} = \overline{V_{z,H}} k_1 k_3 k_4$				Cl. 6.4
Design hourly mean wind pressure (kN/m^2)	$\overline{p_d} = 0.6 \overline{V_{z,d}}^2$				Cl. 10.2
	IF	**1**			Cl 8
Turbulence intensity	$I_{z,i}$				Cl. 6.5
Roughness factor r	$r = 2 \times I_{z,i}$				Cl. 10.2
Peak factor for upwind velocity fluctuation g_v	3				Cl. 10.2

Along Wind Load Calculations of A2S35(X)			
Description	**Calculations**		**Remarks**
Measure of effective turbulence length scale at the height h Lh (m)	$L_h = \begin{cases} 85\left(\frac{h}{10}\right)^{0.25} & \text{for 1 to 3} \\ 70\left(\frac{h}{10}\right)^{0.25} & \text{for 4} \end{cases}$		Cl. 10.2
	Lh	161.25	
Background factor B_s	$B_s = \frac{1}{\left[1 + \frac{\sqrt{0.26(h-s)^2 + 0.46{b_{sh}}^2}}{L_h}\right]}$		Cl. 10.2
Factor accout for second order turbulence intensity	$\phi = \frac{g_v I_{h,i} \sqrt{B_s}}{2}$		Cl. 10.2
Height factor for resonance response H_s	$H_s = 1 + \left(\frac{s}{h}^2\right)$		Cl. 10.2
First mode natural frequency (Hz)	$f_a = \frac{\sqrt{d}}{0.09h}$		Cl 9.1 Notes
	f_a	0.576	
Peak factor for resonant response g_R	$g_R = \sqrt{[2\ln(3600 f_a)]}$		Cl. 10.2
	gR	3.908	
Size reduction factor S	$S = \frac{1}{\left[1 + \frac{3.5 f_a h}{\overline{V_{h,d}}}\right]\left[1 + \frac{4 f_a b_{0h}}{\overline{V_{h,d}}}\right]}$		Cl. 10.2
	S	0.073	
Effective reduced frequency N	$N = \frac{f_a L_h}{\overline{V_{h,d}}}$		Cl. 10.2
	N	1.959	
Spectrum of turbulence in the approching wind stream	$E = \frac{\pi N}{(1 + 70.8N^2)^{\frac{5}{6}}}$		Cl. 10.2

Along Wind Load Calculations of A2S35(X)			
Description	**Calculations**		**Remarks**
	E	0.0575	
Damping coefficient of the building/structure	β	0.02	T. 36
Force F	$F_{z,along} = C_{f_{(z)}} A_{e_{(z)}} \overline{p_{d_{(z)}}} G$		Clause 8

Table 3.11: Along Wind Load Calculations for A2S35(X)

Along Wind Load Calculations for A2S35(X)												
Floor	**Height z (m)**	B_s	H_s	**r**	ϕ	$\overline{k_{2,i}}$	$\overline{V_{z,d}}$ **(m/s)**	$\overline{p_d}$ **(kN/m^2)**	A_z **(m^2)**	C_f	**G**	$F_{z,(along)}$ **(kN)**
35	129.5	0.91354	2	0.22281	0.15972	0.94741	47.3707	1.34639	41.625	1.25	1.93209	135.3508545
34	125.8	0.91294	1.94367	0.22445	0.15967	0.94428	47.2142	1.33751	83.25	1.25	1.93386	269.1626991
33	122.1	0.91117	1.88898	0.22614	0.15951	0.94106	47.0531	1.32839	83.25	1.25	1.93543	267.5460171
32	118.4	0.90831	1.83592	0.22789	0.15926	0.93774	46.887	1.31903	83.25	1.25	1.93684	265.8534429
31	114.7	0.9045	1.78449	0.22969	0.15893	0.93431	46.7156	1.30941	83.25	1.25	1.93812	264.0887294
30	111	0.89988	1.73469	0.23154	0.15852	0.93077	46.5386	1.2995	83.25	1.25	1.93934	262.2565686
29	107.3	0.89459	1.68653	0.23347	0.15805	0.92711	46.3556	1.2893	83.25	1.25	1.94056	260.361661
28	103.6	0.88876	1.64	0.23546	0.15754	0.92332	46.1662	1.27879	83.25	1.25	1.94184	258.4080547
27	99.9	0.88253	1.5951	0.23752	0.15698	0.9194	45.9699	1.26794	83.25	1.25	1.94323	256.3987659
26	96.2	0.87598	1.55184	0.23966	0.1564	0.91532	45.7661	1.25672	83.25	1.25	1.94479	254.3356102
25	92.5	0.8692	1.5102	0.24188	0.15579	0.91109	45.5544	1.24512	83.25	1.25	1.94658	252.2191591
24	88.8	0.86225	1.4702	0.24419	0.15517	0.90668	45.3341	1.23311	83.25	1.25	1.94863	250.0487507
23	85.1	0.8552	1.43184	0.24661	0.15453	0.90209	45.1043	1.22064	83.25	1.25	1.95101	247.8225098
22	81.4	0.84807	1.3951	0.24912	0.15389	0.89729	44.8644	1.20769	83.25	1.25	1.95375	245.5373481
21	77.7	0.84092	1.36	0.25176	0.15324	0.89227	44.6133	1.19421	83.25	1.25	1.95691	243.1889296
20	74	0.83375	1.32653	0.25453	0.15258	0.887	44.3499	1.18015	83.25	1.25	1.96053	240.7715885

Along Wind Load Calculations for A2S35(X)												
Floor	**Height z (m)**	B_s	H_s	**r**	ϕ	$\overline{k_{2,i}}$	$\overline{V_{z,d}}$ **(m/s)**	$\overline{p_d}$ **(kN/m^2)**	A_z **(m^2)**	C_f	**G**	$F_{z,(along)}$ **(kN)**
19	70.3	0.8266	1.29469	0.25743	0.15193	0.88146	44.073	1.16546	83.25	1.25	1.96469	238.2781916
18	66.6	0.81949	1.26449	0.2605	0.15127	0.87562	43.7812	1.15007	83.25	1.25	1.96942	235.6999322
17	62.9	0.81242	1.23592	0.26374	0.15062	0.86945	43.4726	1.13392	83.25	1.25	1.97482	233.0260371
16	59.2	0.8054	1.20898	0.26718	0.14997	0.86291	43.1454	1.11691	83.25	1.25	1.98095	230.2433648
15	55.5	0.79845	1.18367	0.27083	0.14932	0.85594	42.797	1.09895	83.25	1.25	1.9879	227.3358538
14	51.8	0.79157	1.16	0.27474	0.14867	0.84849	42.4246	1.07991	83.25	1.25	1.9958	224.283766
13	48.1	0.78477	1.13796	0.27894	0.14803	0.84049	42.0246	1.05964	83.25	1.25	2.00476	221.0626368
12	44.4	0.77805	1.11755	0.28348	0.1474	0.83185	41.5925	1.03796	83.25	1.25	2.01496	217.6417953
11	40.7	0.77141	1.09878	0.28841	0.14677	0.82246	41.1228	1.01465	83.25	1.25	2.02659	213.9822312
10	37	0.76485	1.08163	0.29382	0.14614	0.81217	40.6083	0.98942	83.25	1.25	2.03992	210.0334389
9	33.3	0.75838	1.06612	0.29979	0.14552	0.80079	40.0396	0.9619	83.25	1.25	2.05527	205.7285957
8	29.6	0.752	1.05224	0.30646	0.14491	0.78808	39.4038	0.9316	83.25	1.25	2.07312	200.9768995
7	25.9	0.74571	1.04	0.31403	0.1443	0.77366	38.683	0.89783	83.25	1.25	2.09409	195.6507988
6	22.2	0.7395	1.02939	0.32277	0.1437	0.75702	37.8509	0.85962	83.25	1.25	2.11912	189.5634032
5	18.5	0.73338	1.02041	0.3331	0.14311	0.73734	36.8668	0.8155	83.25	1.25	2.14966	182.4253589
4	14.8	0.72735	1.01306	0.34575	0.14252	0.71325	35.6623	0.76308	83.25	1.25	2.18812	173.753735
3	11.1	0.7214	1.00735	0.36206	0.14193	0.68219	34.1094	0.69807	83.25	1.25	2.23904	162.6499772

Along Wind Load Calculations for A2S35(X)												
Floor	**Height z (m)**	B_s	H_s	**r**	ϕ	$\overline{k_{2,i}}$	$\overline{V_{z,d}}$ **(m/s)**	$\overline{p_d}$ **(kN/m^2)**	A_z **(m^2)**	C_f	**G**	$F_{z,(along)}$ **(kN)**
2	7.4	0.71554	1.00327	0.38504	0.14135	0.63841	31.9207	0.61136	83.25	1.25	2.31259	147.1257743
1	3.7	0.70976	1.00082	0.42433	0.14078	0.56358	28.1791	0.47644	41.625	1.25	2.44129	60.52

Across wind load calculations by gust factor method of A2S35(X) model are shown in Tables 3.12 and 3.13 respectively.

Table 3.12: Across Wind Load Calculations of A2S35(X)

Across Wind Load Calculations of A2S35(X)			
Description	**Calculations**		**Remarks**
First mode natural frequency (Hz)	$f_c = \frac{\sqrt{d}}{0.09h}$		Cl 9.1 Notes
	f_c	0.407	
Peak factor g_h	3.818		Cl. 10.3
Peak hourly mean wind pressure at height h (kN/m^2)	$\overline{p_h} = 0.6\overline{V_{h,d}}^2$		Cl. 10.3
	$\overline{p_h}$	1.346	
Mode shape power exponent k	1		Cl. 10.3
Damping coefficient of the building/structure	β	0.02	T. 36 & Cl. 6.2 of IS 16700 : 2017
Cross wind force spectrum coefficient C_{fs}	2/3 h (m)	86.33	Fig. 10
	$I_{(2/3h),i}$	0.1221	
	$\overline{V_{h,d}}/(f_c b)$	5.17	
	C_{fs}	0.003	
Across Wind design peak base bending moment M_c (kNm)	$M_c = 0.5 g_h \overline{p_h} b h^2 (1.06 - 0.06k)\sqrt{\frac{\pi C_{fs}}{\beta}}$		Cl. 10.3
	M_c	665814.44	
Across wind load per unit height at height z	$F_{z,across} = \left(\frac{3M_c}{h^2}\right)\left(\frac{z}{h}\right)$		Cl. 10.3

Table 3.13: Across Wind Load Calculations for A2S35(X)

Across Wind Load Calculations for A2S35(X)		
Floor	**Height z (m)**	$F_{(z,across)}$ **(kN)**
35	129.5	119.11
34	125.8	115.70

Across Wind Load Calculations for A2S35(X)		
Floor	**Height z (m)**	$F_{(z,across)}$ **(kN)**
33	122.1	112.30
32	118.4	108.90
31	114.7	105.49
30	111	102.09
29	107.3	98.69
28	103.6	95.29
27	99.9	91.88
26	96.2	88.48
25	92.5	85.08
24	88.8	81.67
23	85.1	78.27
22	81.4	74.87
21	77.7	71.46
20	74	68.06
19	70.3	64.66
18	66.6	61.25
17	62.9	57.85
16	59.2	54.45
15	55.5	51.05
14	51.8	47.64
13	48.1	44.24
12	44.4	40.84
11	40.7	37.43
10	37	34.03
9	33.3	30.63
8	29.6	27.22
7	25.9	23.82
6	22.2	20.42

Across Wind Load Calculations for A2S35(X)		
Floor	**Height z (m)**	$F_{(z,across)}$ **(kN)**
5	18.5	17.02
4	14.8	13.61
3	11.1	10.21
2	7.4	6.81
1	3.7	3.40

3.3.3 Dynamic Wind Time History Analysis from TPU Aerodynamic Database (DTHA) of A2S35(X) Model

Slenderness ratio of A2S35(X) model is 2.88 which falls between 2 and 3. To get actual wind pressure coefficients by three approaches, interpolation of wind pressure coefficients of Max Sum, Peak and Mean approaches between 2 and 3 should be carried out. Table 3.14 shows final wind pressure coefficients of A2S35(X) model.

Table 3.14: Wind Pressure Coefficients of A2S35(X)

Wind Pressure Coefficients of A2S35(X)							
Floor	**Height (m)**	**Along Wind Pressure Coefficients**			**Across Wind Pressure Coefficients**		
		Max Sum	**Peak**	**Mean**	**Max Sum**	**Peak**	**Mean**
35	129.5	1.057828	3.500773	0.038052	1.406258	2.893777	0.961907
34	125.8	1.091976	3.406833	0.042385	1.469378	3.067786	0.985859
33	122.1	1.126123	3.312892	0.046718	1.532498	3.241794	1.00981
32	118.4	1.160271	3.218952	0.051052	1.595619	3.415803	1.033761
31	114.7	1.194419	3.125012	0.055385	1.658739	3.589812	1.057713
30	111	1.179732	3.099655	0.057329	1.707641	3.725135	1.067833
29	107.3	1.067377	3.211466	0.054495	1.728108	3.783086	1.050292
28	103.6	0.955022	3.323277	0.051661	1.748575	3.841037	1.032751
27	99.9	0.842667	3.435087	0.048827	1.769043	3.898988	1.01521
26	96.2	0.730312	3.546898	0.045993	1.78951	3.956939	0.997669
25	92.5	0.714909	3.568945	0.043472	1.826083	3.864317	0.98326
24	88.8	0.747982	3.546111	0.041108	1.870709	3.69641	0.970417
23	85.1	0.781054	3.523276	0.038744	1.915336	3.528502	0.957574
22	81.4	0.814127	3.500442	0.03638	1.959962	3.360594	0.944731
21	77.7	0.847199	3.477607	0.034016	2.004588	3.192686	0.931888
20	74	0.880787	3.419105	0.037749	1.956315	3.114121	0.915016

Wind Pressure Coefficients of A2S35(X)							
Floor	**Height (m)**	**Along Wind Pressure Coefficients**			**Across Wind Pressure Coefficients**		
		Max Sum	**Peak**	**Mean**	**Max Sum**	**Peak**	**Mean**
19	70.3	0.914375	3.360603	0.041482	1.908042	3.035555	0.898144
18	66.6	0.947963	3.302101	0.045215	1.859768	2.956989	0.881272
17	62.9	0.981551	3.243599	0.048948	1.811495	2.878423	0.8644
16	59.2	1.017603	3.218153	0.052401	1.77207	2.833358	0.846978
15	55.5	1.058582	3.258819	0.055294	1.750343	2.855292	0.828456
14	51.8	1.099561	3.299486	0.058187	1.728617	2.877227	0.809933
13	48.1	1.14054	3.340152	0.06108	1.70689	2.899162	0.791411
12	44.4	1.181519	3.380819	0.063973	1.685163	2.921097	0.772888
11	40.7	1.221074	3.387972	0.061621	1.638113	2.868502	0.749258
10	37	1.259918	3.37837	0.056646	1.5784	2.778643	0.723073
9	33.3	1.298761	3.368767	0.051672	1.518687	2.688784	0.696889
8	29.6	1.337604	3.359164	0.046698	1.458974	2.598925	0.670704
7	25.9	1.376448	3.349561	0.041723	1.399262	2.509066	0.64452
6	22.2	1.31394	3.604141	0.044322	1.415721	2.595184	0.647924
5	18.5	1.251432	3.858721	0.046921	1.432181	2.681301	0.651327
4	14.8	1.188925	4.1133	0.04952	1.44864	2.767418	0.654731
3	11.1	1.126417	4.36788	0.052118	1.4651	2.853535	0.658134

Wind Pressure Coefficients of A2S35(X)							
Floor	**Height (m)**	**Along Wind Pressure Coefficients**			**Across Wind Pressure Coefficients**		
		Max Sum	**Peak**	**Mean**	**Max Sum**	**Peak**	**Mean**
2	7.4	1.06391	4.622459	0.054717	1.481559	2.939652	0.661538
1	3.7	1.001402	4.877039	0.057316	1.498019	3.025769	0.664942

Figures 3.21a and 3.21b shows final along and across wind pressure coefficients for A2S35X model.

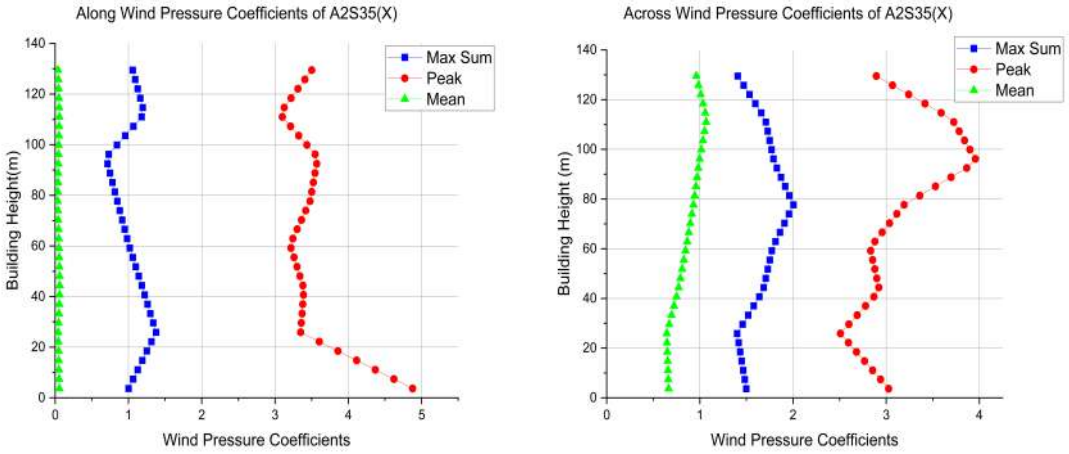

(a) Along Wind Pressure Coefficients (b) Across Wind Pressure Coefficients

Figure 3.21: Wind Pressure Coefficients of A2S35(X)

Along and across wind forces of A2S35X using various static and dynamic analysis are shown in Figures 3.22a and 3.22b respectively.

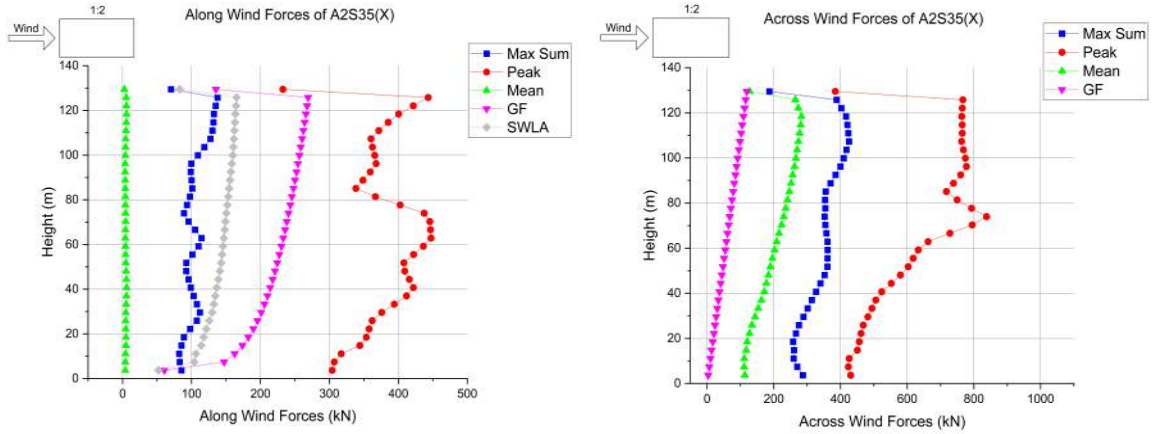

(a) Along Wind Forces (b) Across Wind Forces

Figure 3.22: Wind Forces of A2S35(X)

3.3.4 Results and Discussion

3.3.4.1 A1 Type Tall Buildings

Along and across wind forces of A1 Type (aspect ratio 1:1) tall buildings A1S35 (35 Story), A1S40 (40 Story) and A1S45 (45 Story) using various static and dynamic analysis are shown in Figures 3.23, 3.24 and 3.25 respectively.

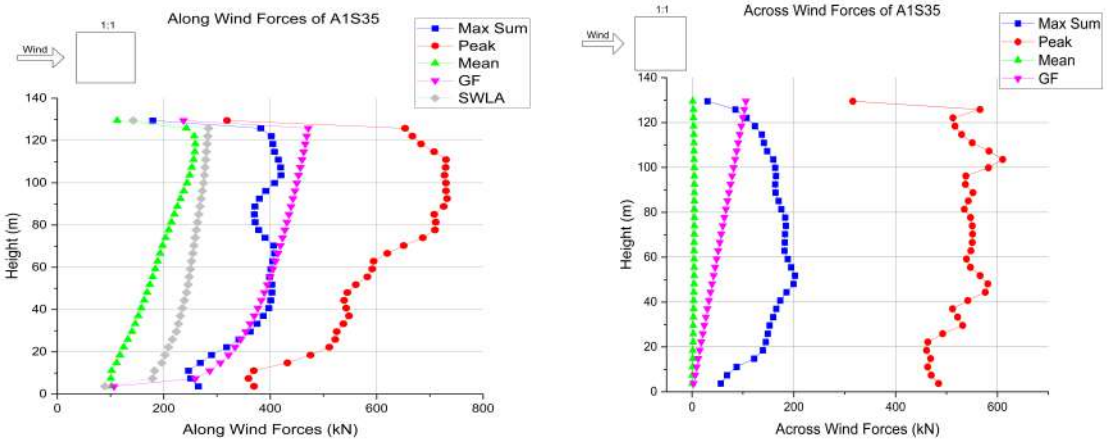

(a) Along Wind Forces (b) Across Wind Forces

Figure 3.23: Wind Forces of A1S35

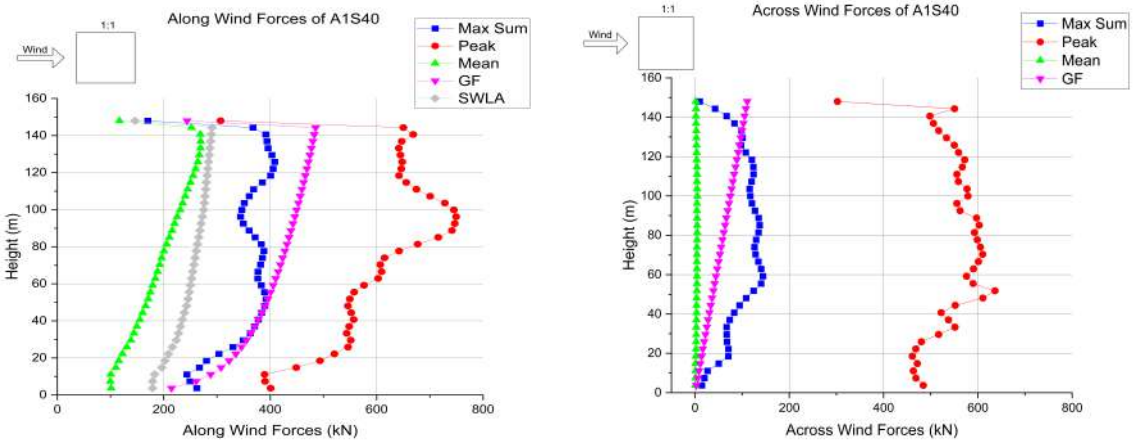

(a) Along Wind Forces (b) Across Wind Forces

Figure 3.24: Wind Forces of A1S40

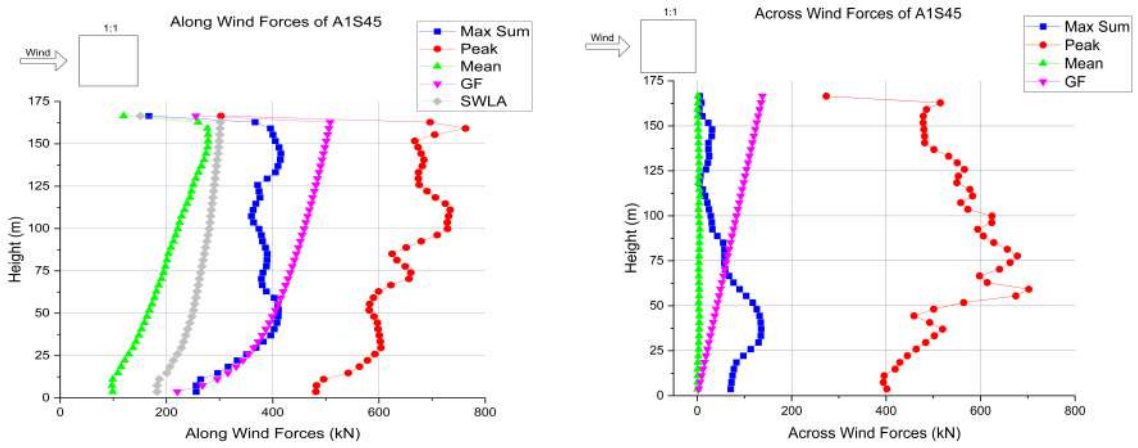

(a) Along Wind Forces (b) Across Wind Forces

Figure 3.25: Wind Forces of A1S45

It is observed that the mean wind force coefficient approach yields the lowest along and across wind forces in square plan tall buildings, whereas the peak wind force coefficient approach yields the highest along and across wind forces. At the bottom stories of all three buildings, the along wind force calculated using the maximum sum of wind coefficient approach is nearly equivalent to the along wind force calculated using the gust factor method of IS 875 (Part 3): 2015[43]; however, at the top stories, the along wind force calculated using the maximum sum of wind coefficient approach yields a smaller wind force than the gust factor method. In the case of across-wind forces, the maximum sum of wind coefficients yields more wind forces than the gust factor method in all three buildings, with the exception of the top storeys.

3.3.4.2 A2 Type Tall Buildings

Along and across wind forces of A2 Type (aspect ratio 1:2) tall buildings; A2S35(X)(35 Story), A2S40(X)(40 Story) and A2S45(X)(45 Story) using various static and dynamic analysis are shown in Figures 3.26, 3.27 and 3.28 respectively. In these three building models, wind is blowing along longer dimension of buildings.

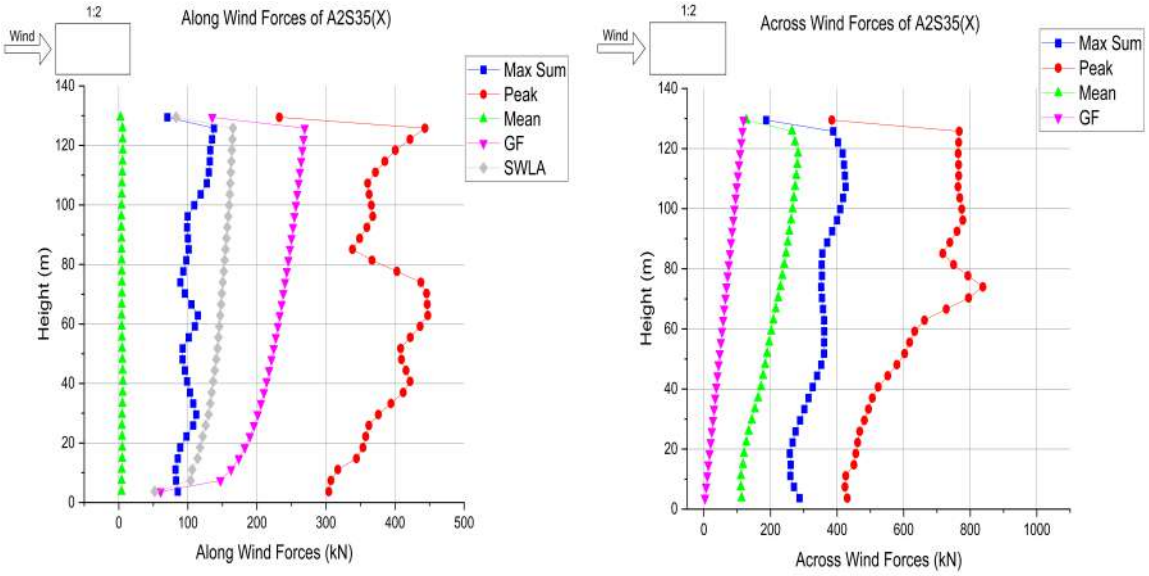

(a) Along Wind Forces (b) Across Wind Forces

Figure 3.26: Wind Forces of A2S35(X)

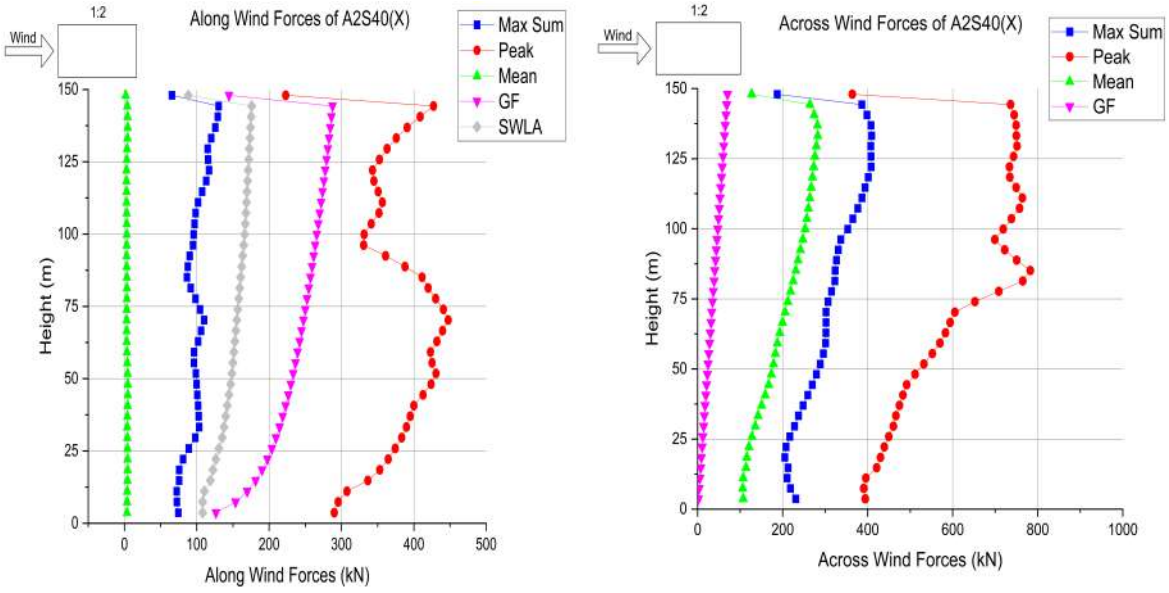

(a) Along Wind Forces (b) Across Wind Forces

Figure 3.27: Wind Forces of A2S40(X)

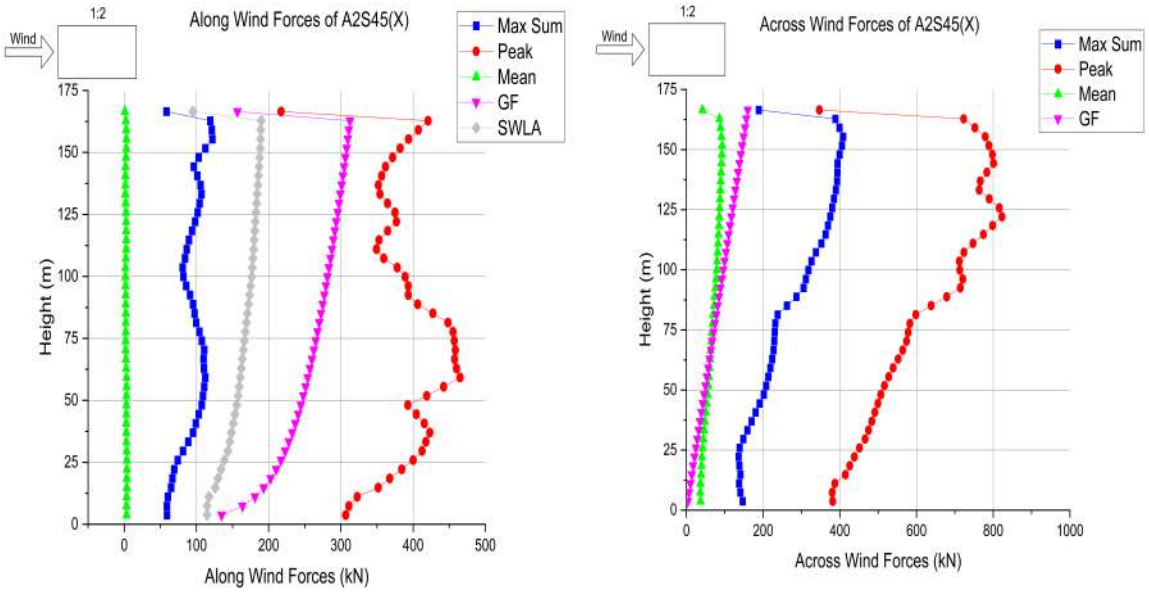

(a) Along Wind Forces (b) Across Wind Forces

Figure 3.28: Wind Forces of A2S45(X)

The mean wind fore coefficient approach results in the lowest along wind forces in rectangular plan tall buildings, while the peak wind force coefficient approach results in the highest along wind forces. In the case of across wind forces, the gust factor method yields the least wind forces, whereas the peak coefficient method yields the most. In all three buildings, the along wind force calculated using the maximum sum of wind coefficient approach is considerably less than the along wind force calculated using the gust factor method of IS 875 (Part 3): 2015[43]. On the other hand, the across wind force calculated using the maximum sum of wind coefficient approach yields a greater wind force than the gust factor method.

Along and across wind forces of A2 Type (aspect ratio 1:2) tall buildings; A2S35(Y)(35 Story), A2S40(Y)(40 Story) and A2S45(Y)(45 Story) using various static and dynamic analysis are shown in Figures 3.29, 3.30 and 3.31 respectively. In these three building models, wind is blowing along shorter dimension of buildings.

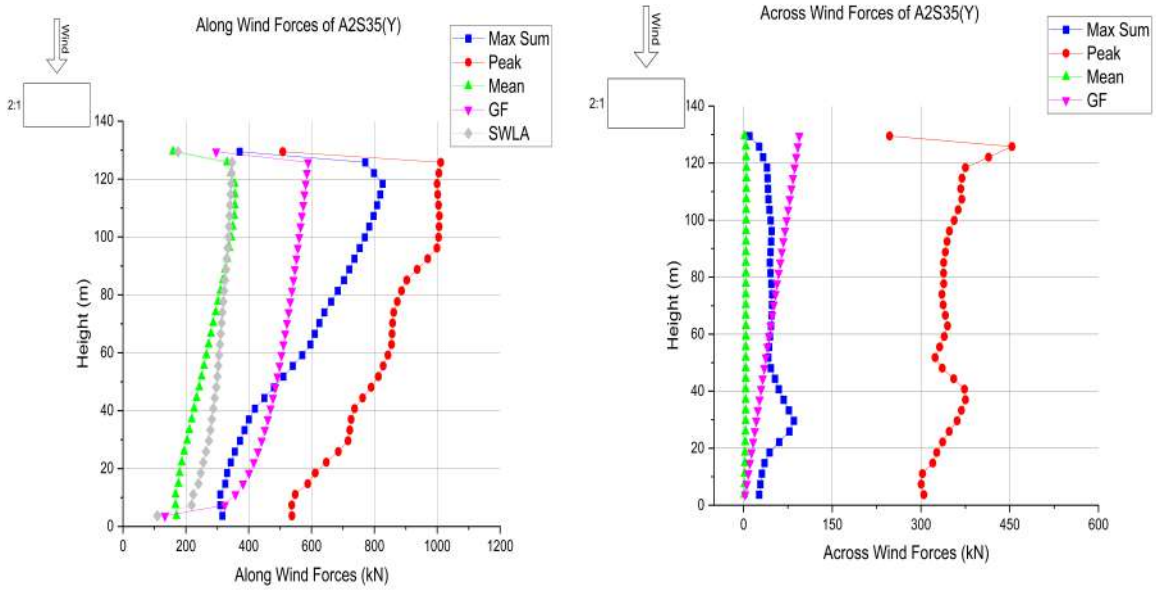

(a) Along Wind Forces (b) Across Wind Forces

Figure 3.29: Wind Forces of A2S35(Y)

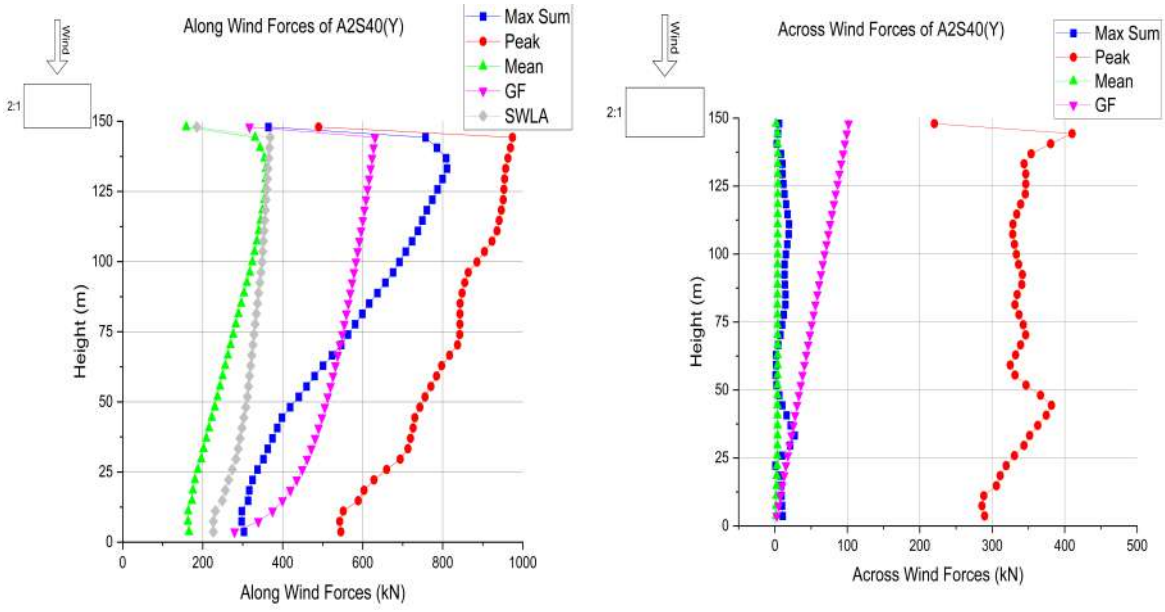

(a) Along Wind Forces (b) Across Wind Forces

Figure 3.30: Wind Forces of A2S40(Y)

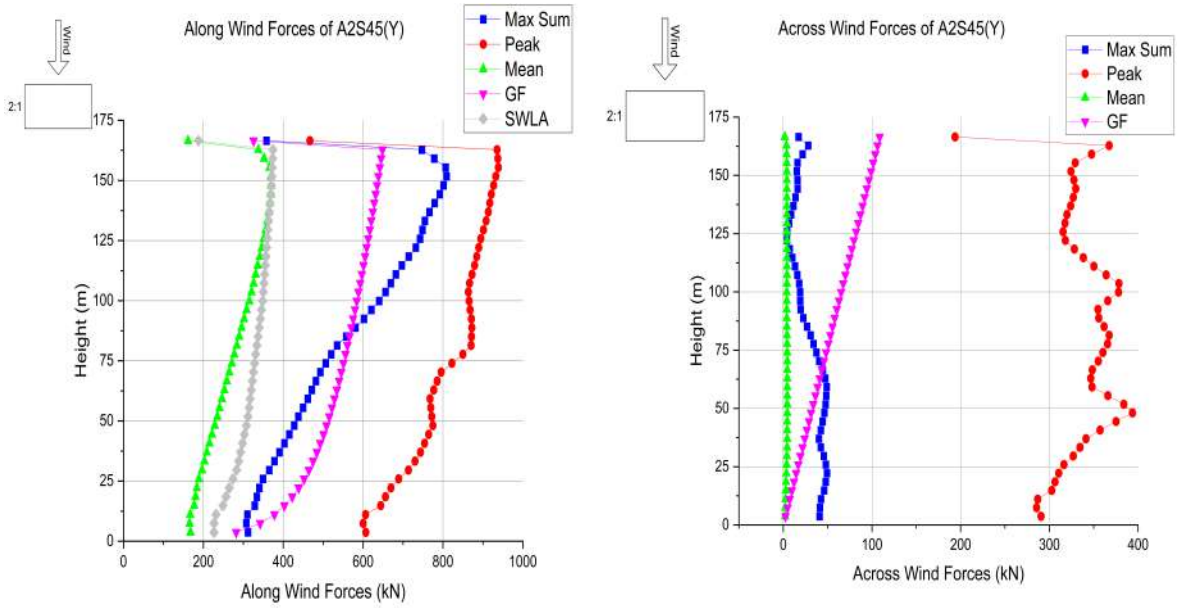

(a) Along Wind Forces (b) Across Wind Forces

Figure 3.31: Wind Forces of A2S45(Y)

In rectangular plan tall buildings, the mean wind force coefficient approach yields the lowest along wind forces, whereas the peak wind force coefficient approach yields the highest along wind forces. In the case of across wind forces, the gust factor method produces the lowest wind forces while the peak coefficient method produces the highest. In each of the three structures, the along wind force estimated utilising the maximum sum of wind coefficient approach is less than the along wind force computed using the gust factor method of IS 875 (Part 3): 2015[43] for the lower stories and more for the upper stories. In contrast, the across wind force estimated using the maximum sum of wind coefficients produces a higher value than the gust factor technique in lower levels and a lower value in upper stories compared to the gust factor approach.

3.3.4.3 A3 Type Tall Buildings

Along and across wind forces of A3 Type (aspect ratio 1:3) tall buildings; A3S35(X)(35 Story), A3S40(X)(40 Story) and A3S45(X)(45 Story) using various static and dynamic analysis are shown in Figures 3.32, 3.33 and 3.34 respectively. In these three building models, wind is blowing along longer dimension of buildings.

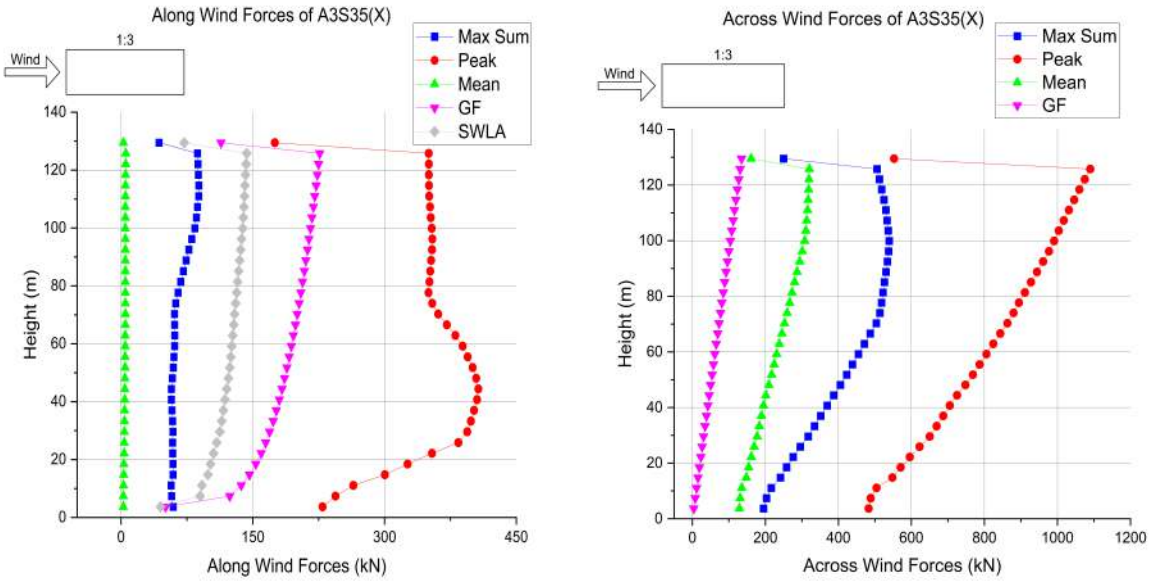

(a) Along Wind Forces (b) Across Wind Forces

Figure 3.32: Wind Forces of A3S35(X)

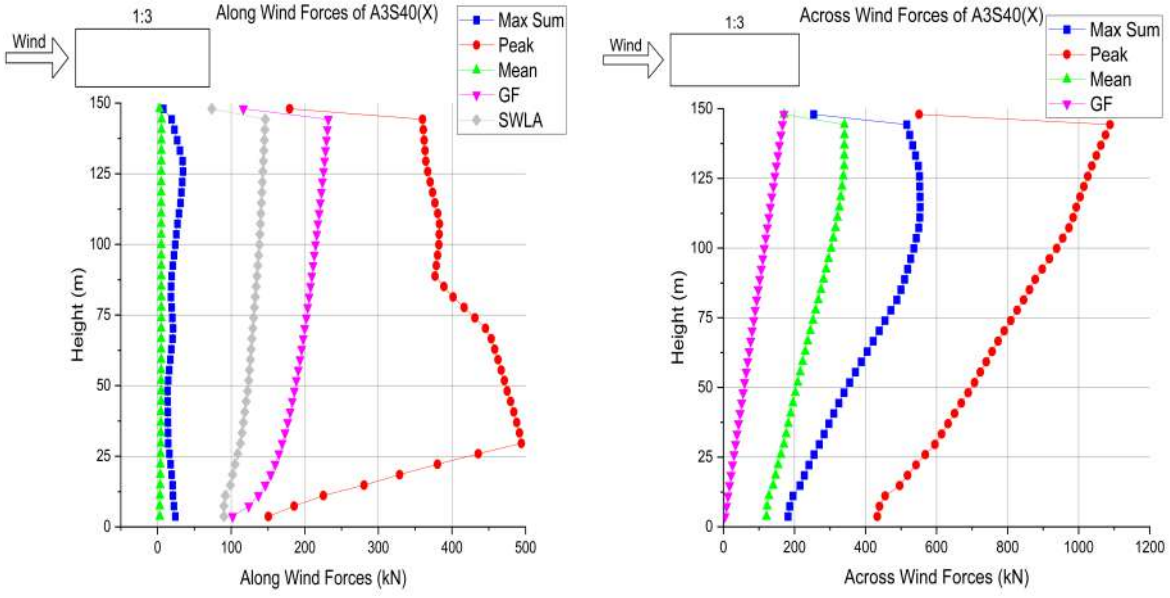

(a) Along Wind Forces (b) Across Wind Forces

Figure 3.33: Wind Forces of A3S40(X)

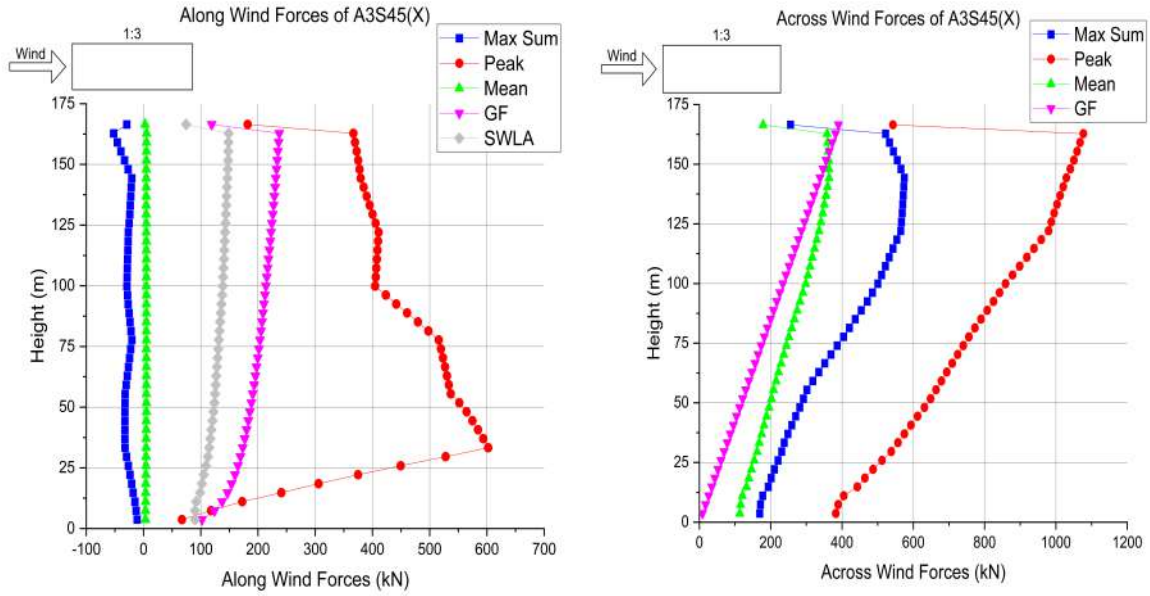

(a) Along Wind Forces

(b) Across Wind Forces

Figure 3.34: Wind Forces of A3S45(X)

In rectangular plan tall buildings, the mean wind force coefficient method produces the lowest along wind forces, while the peak wind force coefficient approach produces the highest along wind forces. In terms of across wind forces, the gust factor approach produces the smallest, while the peak coefficient method produces the highest wind forces. The along wind force computed using the maximum sum of wind coefficient approach is significantly smaller than the along wind force calculated using the gust factor method of IS 875 (Part 3): 2015[41] in all three buildings. The across wind force estimated using the greatest sum of wind coefficients method, on the other hand, produces a stronger wind force than the gust factor method.

Along and across wind forces of A3 Type (aspect ratio 1:3) tall buildings; A3S35(Y)(35 Story), A3S40(Y)(40 Story) and A3S45(Y)(45 Story) using various static and dynamic analysis are shown in Figures 3.35, 3.36 and 3.37 respectively. In these three building models, wind is blowing along shorter dimension of buildings.

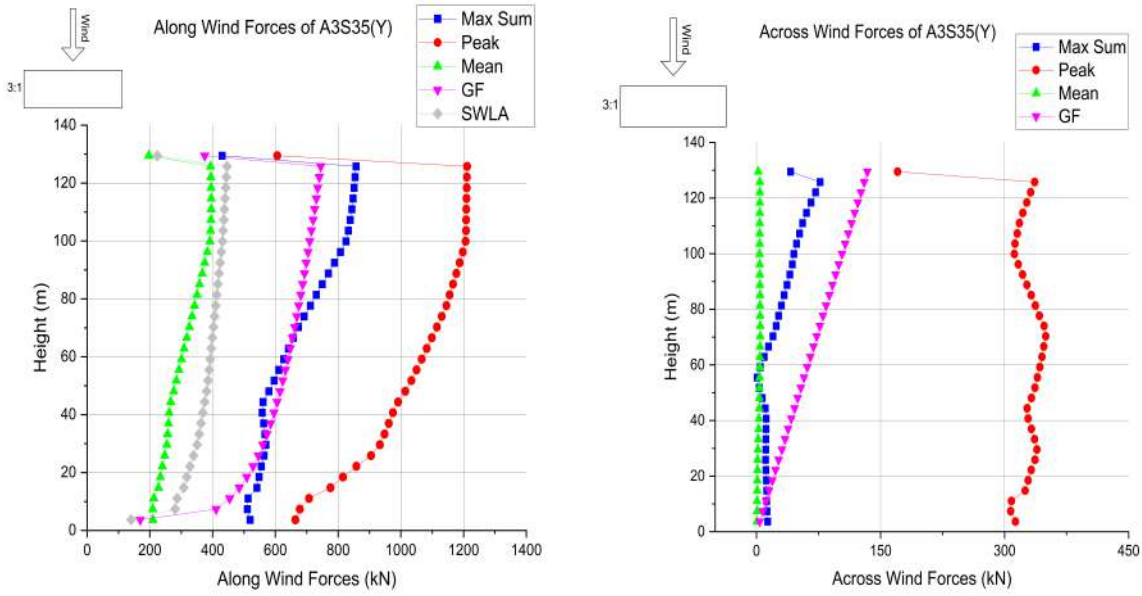

(a) Along Wind Forces (b) Across Wind Forces

Figure 3.35: Wind Forces of A3S35(Y)

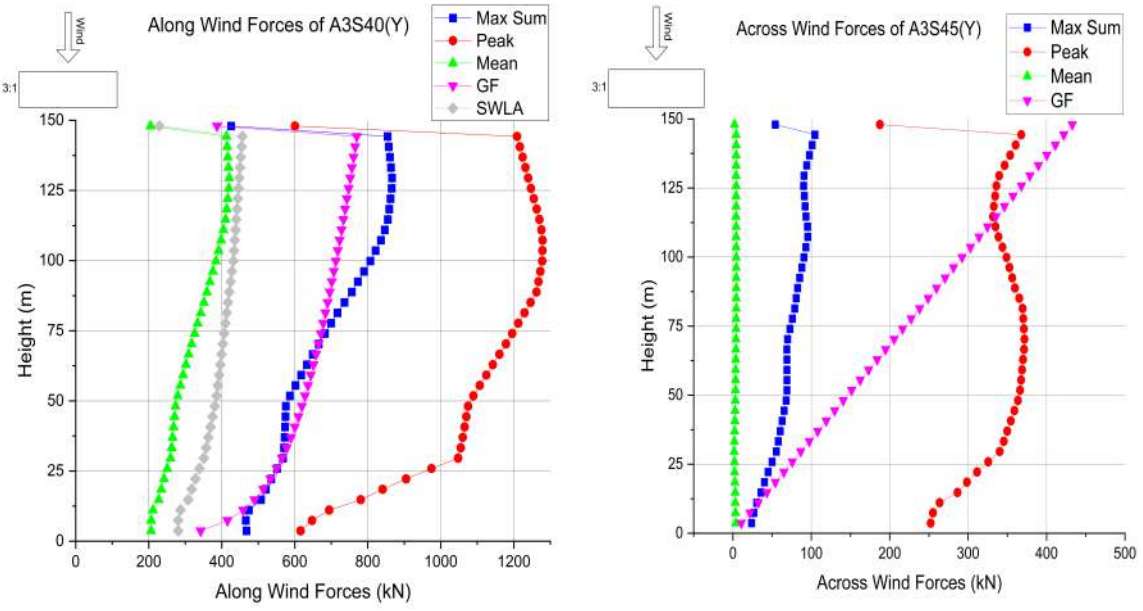

(a) Along Wind Forces (b) Across Wind Forces

Figure 3.36: Wind Forces of A3S40(Y)

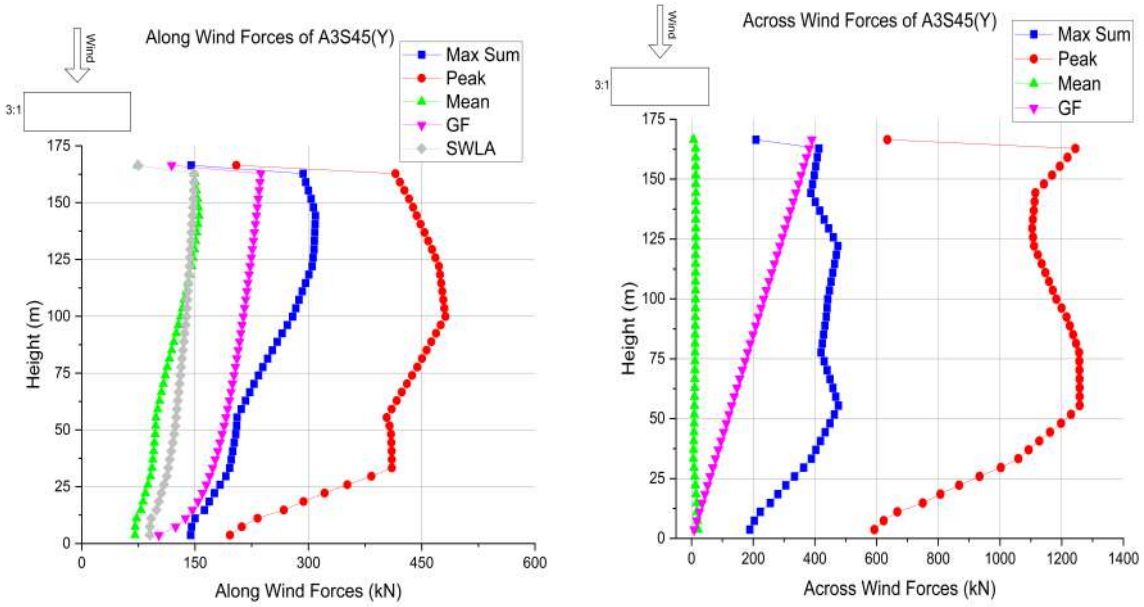

(a) Along Wind Forces

(b) Across Wind Forces

Figure 3.37: Wind Forces of A3S45(Y)

The mean wind force coefficient approach gives the lowest along and across wind forces in rectangular plan tall buildings, but the peak wind force coefficient approach yields the highest along and across wind forces. At the bottom and middle stories of all three buildings, the along wind force calculated using the maximum sum of wind coefficient approach is nearly equivalent to the along wind force calculated using the gust factor method of IS 875 (Part 3): 2015[41]; however, at the top stories, the along wind force calculated using the maximum sum of wind coefficient approach results in a slightly greater wind force than the gust factor method. In the case of across-wind forces, the maximum sum of wind coefficients yields less wind forces than the gust factor approach for buildings of 35 and 40 stories, but yields more wind forces than the gust factor method for buildings of 45 stories.

3.4 Summary

In this chapter, static and dynamic wind load evaluation methods such as static wind load analysis (SWLA), the dynamic gust factor method (DGF), and wind time history analysis utilising maximum sum, peak, and mean coefficient approaches are described, as well as the procedure for conducting wind evaluation using these methods. A parametric

examination is conducted to examine the efficacy of wind evaluation methods on a variety of tall buildings with variable aspect ratios and heights. For square-shaped structures, the gust factor method (DGF) or wind time history analysis utilising the peak coefficient approach is more safe and effective, whereas for rectangular-shaped tall buildings, the gust factor method is the most reliable way for evaluating along and across winds.

3.5 Concluding Remarks

The following concluding remarks are made from the wind load evaluation parametric study using static wind load analysis (SWLA)method from IS 875 (Part 3): 2015[41], dynamic wind load analysis by gust factor method (DGF) from IS 875 (Part 3): 2015[41] and dynamic wind load time history analysis (DTHA) from TPU aerodynamic database[60].

1. Compared to the static wind load analysis (SWLA) approach, the dynamic gust factor method (DGF) generates between 148 and 267.5 percent of along wind forces due to static wind load analysis in tall structures. This demonstrates that the gust factor approach is more relevant than the SWLA method for evaluating the along-wind forces of tall buildings.

2. Along wind forces in A1-type buildings from maximum sum, peak coefficient, and mean coefficient methods are between 69.7% to 128.8%, 125.7% to 186.9%, and 34.8% to 56.4% percent, respectively, when compared to along wind forces determined using DGF. While across wind forces in A1-type buildings from maximum sum, peak coefficient, and mean coefficient approaches range from 89.3% to 521.8%, 272.1% to 1711.7%, and 1.3% to 13.3%, respectively, when compared to across wind forces evaluated by DGF.

3. In A2-type buildings where wind direction is along to longer dimension of plan, along wind forces from maximum sum, peak coefficient, and mean coefficient methods are between 35.1% to 56.7%, 128.1% to 208.3%, and 1.41% to 2.81% percent, respectively, when compared to along wind forces determined using DGF. While across wind forces in A1-type buildings from maximum sum, peak coefficient, and mean coefficient approaches range from 288.4% to 1276.8%, 662.3% to 2264.5%, and

108.1% to 768.5%, respectively, when compared to across wind forces evaluated by DGF.

4. In A2-type buildings where wind direction is along to shorter dimension of plan, along wind forces from maximum sum, peak coefficient, and mean coefficient methods are between 79.6% to 126.4%, 144.5% to 175.8%, and 42.1% to 58.3% percent, respectively, when compared to along wind forces determined using DGF. While across wind forces in A1-type buildings from maximum sum, peak coefficient, and mean coefficient approaches range from 6.3% to 586.3%, 345.1% to 1872.7%, and 3.9% to 26.1%, respectively, when compared to across wind forces evaluated by DGF.

5. In A3-type buildings where wind direction is along to longer dimension of plan, along wind forces from maximum sum, peak coefficient, and mean coefficient methods are between 14.8% to 41.6%, 154.1% to 230.8%, and 2.1% to 5.2% percent, respectively, when compared to along wind forces determined using DGF. While across wind forces in A1-type buildings from maximum sum, peak coefficient, and mean coefficient approaches range from 162.8% to 1028.9%, 298.4% to 1096.8%, and 117.1% to 628.3%, respectively, when compared to across wind forces evaluated by DGF.

6. In A3-type buildings where wind direction is along to shorter dimension of plan, along wind forces from maximum sum, peak coefficient, and mean coefficient methods are between 107.1% to 133.5%, 166.2% to 233.1%, and 52.4% to 66.4% percent, respectively, when compared to along wind forces determined using DGF. While across wind forces in A1-type buildings from maximum sum, peak coefficient, and mean coefficient approaches range from 113.1% to 550.7%, 326.3% to 1260.8%, and 3.95% to 12.3%, respectively, when compared to across wind forces evaluated by DGF.

7. In tall buildings with a square plan, the DGF method and the maximum sum of pressure coefficient approaches are preferred for evaluating along wind loads, whilst the maximum sum of pressure coefficient approach is more reliable for evaluating across wind.

8. In rectangular-shaped structures, the gust factor method (DGF) is more dependable and safer than other approaches for evaluating along and across winds.

Chapter 4

Behaviour of Structural Systems

4.1 General

This chapter discusses the behaviour of various structural systems when subjected to lateral loading. Each structural system behaves differently and has its own load transmission mechanism. In general, stiffness requirements in terms of inter-story drift, top-story displacements, and torsional stability are critical criteria to govern in high-rise constructions. As a result, the structural system should be chosen in such a way that it satisfies strength requirements, serviceability requirements, and optimum usage of structural elements. This chapter discusses the behaviour of the Structural Wall-Moment Frame, Tubular, Outrigger and Belt Truss systems.

4.2 Structural Wall-Moment Frame (SWMF) System

A structure, whose resistance to horizontal loading is provided by a combination of shear walls and rigid frames may be categorized as a structural wall-moment frame structure. A wall-frame structure is resistant to lateral loading through shear walls (or braces) and perimeter columns. Shear walls are frequently used around elevator and service cores, while frames with somewhat large spandrels are used around the structure's exterior. When a wall-frame structure is loaded laterally, the unique deflected forms of the walls and frames can be highly successful at reducing lateral deflection to the point where buildings of up to 50 stories or more are economically feasible [33].

The potential benefits of a wall-frame construction are determined by the degree of hor-

izontal interaction, which is determined by the relative stiffness of the walls and frames and the structure's height. Both the wall and frame exhibit distinct deflection modes; the wall exhibits flexural deflection while the frame exhibits shear deflection. As we ascend, the stiffness of the core decreases by the cube of the height, whilst the stiffness of the frame remains proportional to the height. As a result, for systems with more than 40-50 storeys, the relative stiffness of the wall-frame contact decreases, and the system becomes ineffective in the combined action.

The wall bends in a flexural mode, with the steepest slope at the top of the structure, showing that the shear wall system delivers the most negligible stiffness to this region. While the frame deflects in a shear mode, the deflection slope is most significant near the structure's base, where the most significant shear is acting. When the rigid beam and wall are joined through pin terminated connections, the assembly's deflected shape exhibits a flexural profile at the bottom and a shear profile at the top. Due to the shear wall's and frame's distinct deflection characteristics, the shear wall is pulled back by the frame in the top portion of the building and pushed forward in the lower portion. The pin terminated link assists the wall in minimising bottom deflection and the rigid frame minimising maximum deflection. The combined action of the wall can be seen in Fig. 4.1

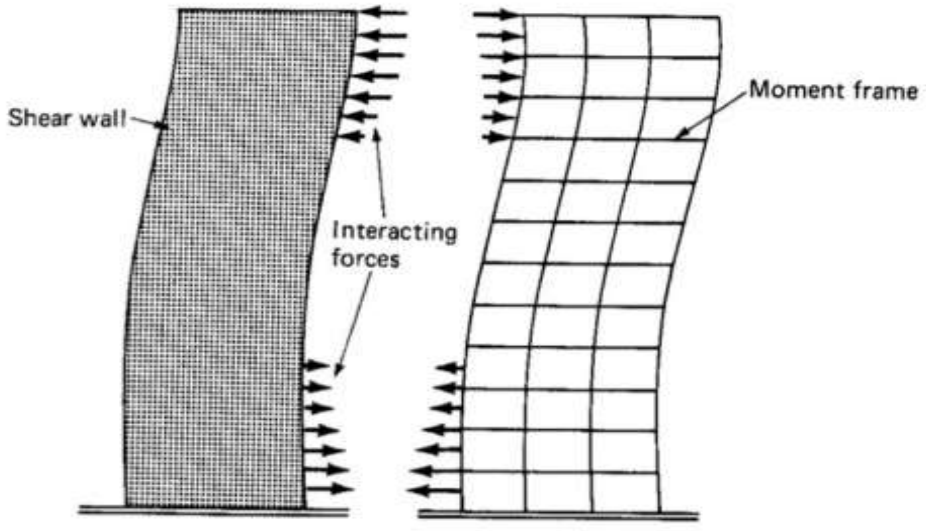

Figure 4.1: Wall-Frame Interaction[28]

4.3 Tubular (TB) System

The basic tubular form is a framed tube system consisting of closely spaced columns and deep spandrel beams that are rigidly connected across the outside frames. To maximise resistance, the perimeter columns are positioned with their primary axes parallel to the direction of the load. The parallel edge to the load serves as the web, while the opposing edge serves as the system's flange. While the perimeter columns of the perforated tube resist the lateral load, creating tension and compression on columns on either side of the neutral axis, the inner and exterior columns of the perforated tube resist the gravity load, depending on their tributary areas. Fig. 4.2 shows schematic plan and isometric view of a framed tube structure.

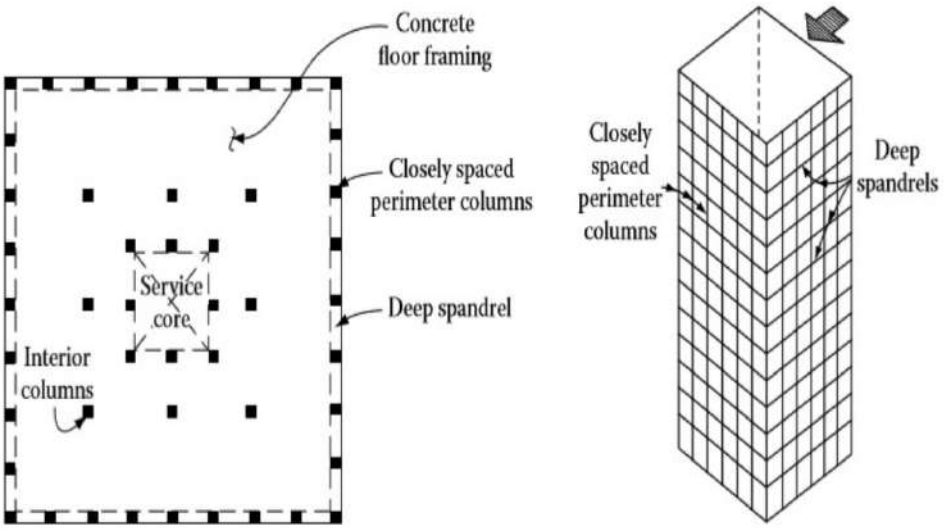

Figure 4.2: Wall-Frame Interaction[51]

Additionally, this technique has a significant drawback known as shear lag. The shear lag effect is relevant to any slender box element loaded laterally with framed tube core walls. The beam theory presupposes that a plane remains flat before and after bending. As a result of this assumption, the bending force is distributed linearly over the beam's cross-section. In a box section, this assumption remains true only if the shear stiffness of the cross-section is unbounded and if there is no shear force inside the box. Shear flow develops over the flange and web panels. The shear lag increases the axial load in the web's and flange's corner columns. This increases the axial load on the corner columns due to the engineer's desire to have columns with uniform cross-sections along with the

same vertical level for aesthetic purposes. As a result, all columns (interior and corner) must have the same cross-sectional area, rendering the building economically unviable. The non linear stress distribution along the flange and web can be seen in the Fig. 4.3.

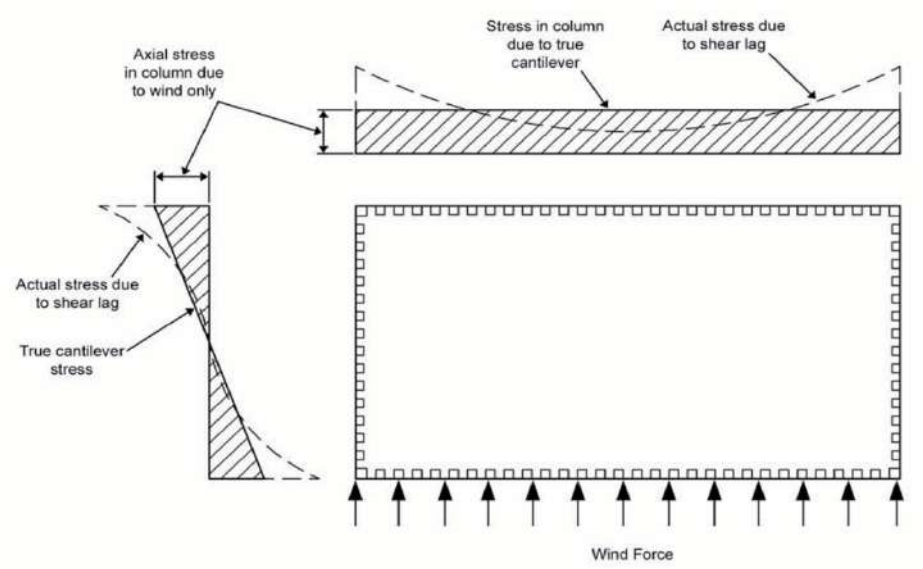

Figure 4.3: Shear lag in tubular system[23]

4.4 Outrigger and Belt Truss (OR) System

Outriggers are interior lateral structural devices used to increase the rigidity and strength of high-rise structures during overturning. It is a lateral load resisting system concealed within the structure. The entire system is composed of a core structure attached to the building's outer columns via structural elements called outriggers. Outriggers may be horizontal beams, trusses, or walls. Outriggers are classified as interior structural systems capable of supporting up to 150 stories. It is a proven and reliable arrangement for high-rise construction. The core may be located centrally or with offsets with outriggers extending to both sides or one side connecting the building columns as shown in Fig. 4.4.

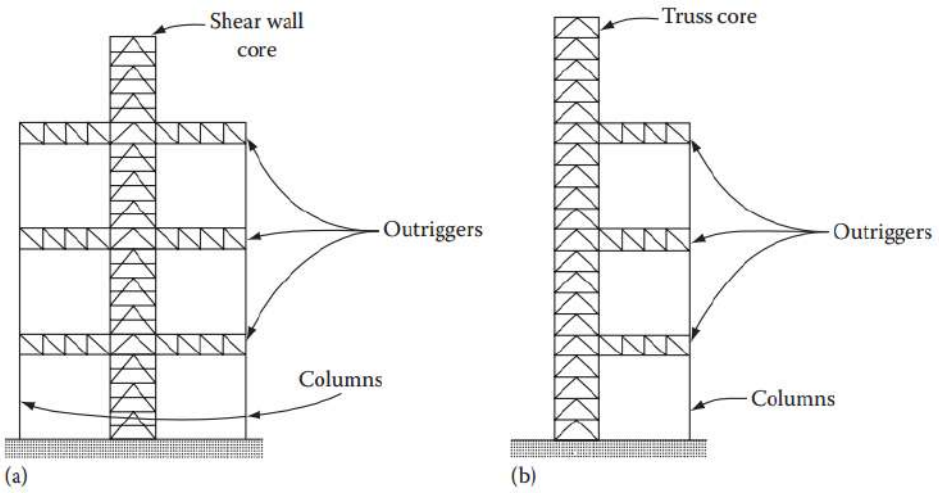

Figure 4.4: Core and outrigger system: (a) centrally located core; (b) offset core[33]

When the system is subjected to lateral forces, the outriggers constrain the core's rotation through their contact with the columns, resulting in lower core deflections and bending moments than if the core stood alone to resist the lateral pressures. When a structure with an outrigger system is loaded laterally, the lateral force generated by the core structure is transferred to the perimeter columns via the outriggers and subsequently to the ground, as illustrated in Fig. 4.5.

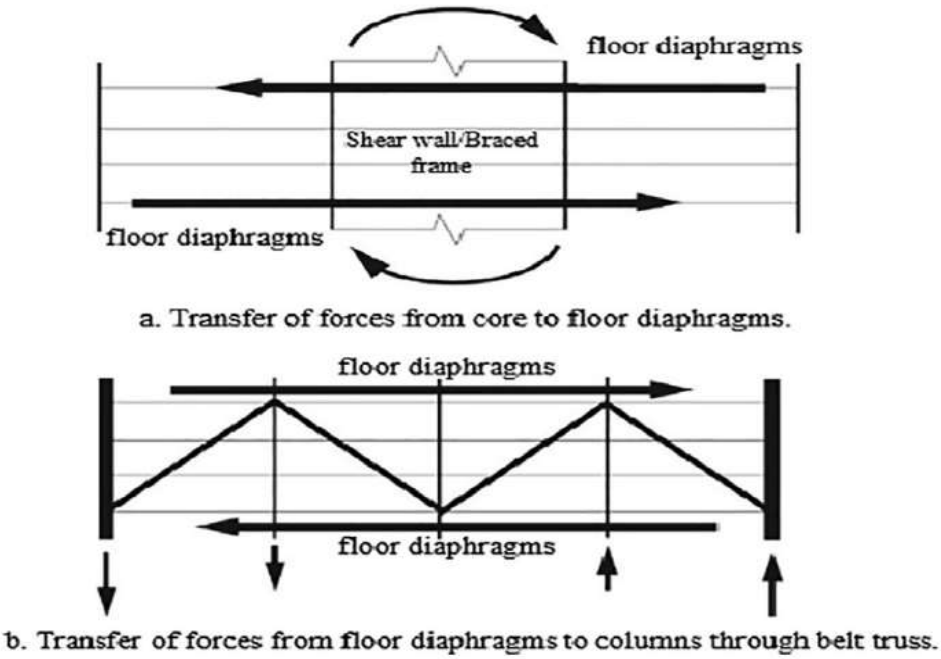

Figure 4.5: Lateral force transfer in Outrigger and Belt Truss system[2]

The lateral stresses are now resisted by core deformation and the lever arm action,

creating axial tension and compression in the external columns attached to the rigid outriggers. As a result of the development of tension in the windward columns and compression in the leeward columns, the effective depth of the structure for resisting bending is increased, as illustrated in Fig. 4.6. Additionally to the connected exterior column resisting core bending, all perimeter columns can be employed to resist core bending by linking them with a one- or two-story deep 'Belt wall' that rigidly connects all perimeter columns to function as a single unit.

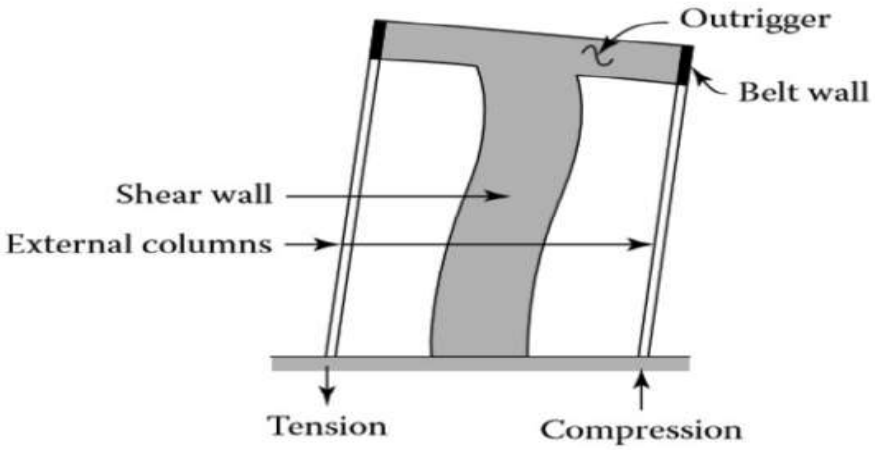

Figure 4.6: Lateral force transfer in Outrigger and Belt Truss system[51]

The tensile and compressive forces are mathematically equal to a restoring pair resisting the core's rotation. As a result, the cap truss can be thought of as an equivalent spring positioned at the top of the cantilever. Its stiffness, defined as a restoring couple caused by the core rotating in a unit circle, can be calculated. Considering the cap truss is infinitely rigid, the columns' axial compression and tension are equal to the product of the core's rotation and their distance from the core's centre. If the columns are located at a distance of d/2 from the center of the core, the axial deformation of the columns is equal to $\theta \times \frac{d}{2}$ where θ is the rotation of the core and d is the distance between the exterior columns.Since by our definition, for $\theta = 1$, the axial deformation is equal to d/2 units. The axial load P in the columns corresponding to this deformation is

$$P = \frac{AEd}{2L} \tag{4.1}$$

where P is the axial load in the columns

A is the area of columns

E is the modulus of elasticity of the column material

d is the distance between the exterior columns

L is the height of the building

The restoring couple which is the rotational stiffness of the cap truss is given by summation of the product of the axial load in the columns and their distance from the center of core. Using the notation K for the rotational stiffness we get

$$K = \sum Pd_iK = P \times \frac{d}{2} \times 2K = Pd$$

4.4.1 Outrigger Located at Top

The conceptual model is shown in Fig. 4.7. The rotation compatibility condition at Z = L can be written as

$$\theta_L = \theta_W - \theta_S \tag{4.2}$$

where θ_W is the rotation of the cantilever at Z = L due to uniform lateral load W, in radians

θ_S is the rotation due to spring restraint located at Z = L, in radians.

The negative sign indicates that the rotation of the cantilever due to the spring stiffness acts in a direction opposite of the rotation due to external load

θ_L is the final rotation of the cantilever at Z = L, in radians

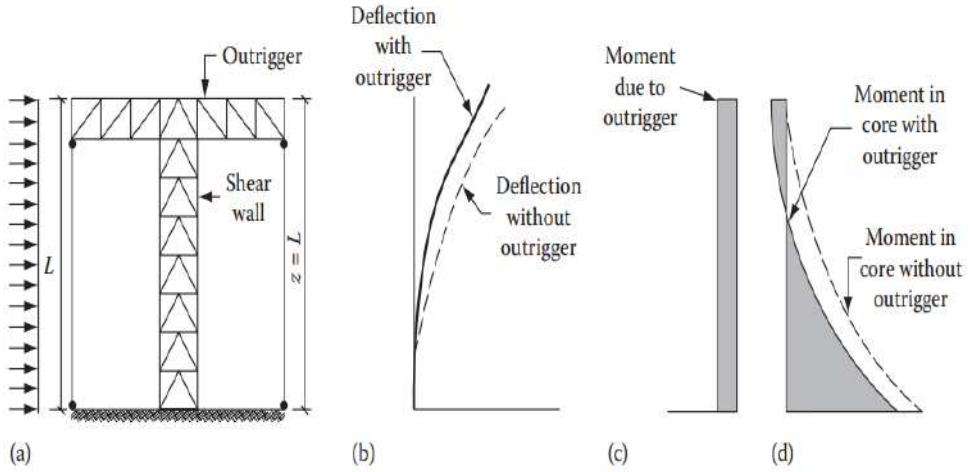

Figure 4.7: Outrigger located at top: (a) analytical model; (b) deflected shape; (c and d) moment diagrams[33]

For a cantilever with uniform moment of inertia I, and modulus of elasticity E subject to uniform horizontal load W,

$$\theta_W = \frac{WL^3}{6EI}$$

If M_1 and K_1 represent the moment and stiffness of the spring located at Z = L, the rotational compatibility equation can be written thus

$$\begin{aligned} \frac{WL^3}{6EI} - \frac{M_1 L}{EI} &= \frac{M_1}{K_1} \\ M_1 &= \frac{WL^3}{\frac{1}{K_1} + \frac{L}{EI}} \end{aligned} \tag{4.3}$$

The resulting drift Δ_1 at the building top can be obtained by superposing the deflection of the cantilever due to external uniform load W and the deflection due to the moment induced by the spring; thus,

$$\begin{aligned} \Delta_1 &= \Delta_{load} - \Delta_{spring} \\ &= \frac{WL^4}{8EI} - \frac{M_1 L^2}{2EI} \\ \Delta_1 &= \frac{L^2}{2EI}\left(\frac{WL^2}{4} - M_1\right) \end{aligned} \tag{4.4}$$

4.4.2 Outrigger at Mid-Height

The conceptual model is shown in Fig. 4.8. The rotation at Z = L/2 due to external load W can be shown to be equal to $7WL^3/48EI$, giving the rotation compatibility equation

$$\frac{7WL^3}{48EI} - \frac{M_3 L}{2EI} = \frac{M_3}{K_3}$$

where M_3 and K_3 represent the moment and stiffness of the spring at Z = L/2. Noting that $K_3 = 2K_1$, the expression for M3 works out as

$$M_3 = \frac{\frac{WL^3}{6EI}}{\frac{1}{K_1} + \frac{L}{EI}} \times \frac{7}{4} \tag{4.5}$$

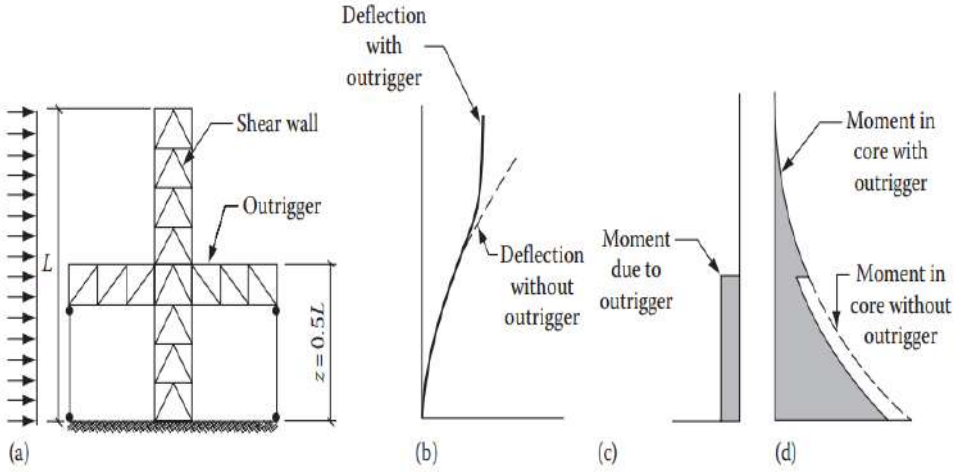

Figure 4.8: Outrigger located at mid-height: (a) analytical model; (b) deflected shape; (c and d) moment diagrams[33]

Since the expression in the parentheses in equation 4.5 is equal to M_1, M_3 can be expressed in terms of M_1

$$M_3 = 1.75M_1$$

The drift is given by the equation

$$\Delta_3 = \frac{WL^4}{8EI} - \frac{M_3 L}{2EI}\left(L - \frac{L}{4}\right)$$
$$\Delta_3 = \frac{L^2}{2EI}\left(\frac{WL^2}{4} - 1.31M_1\right) \tag{4.6}$$

4.5 Summary

In this chapter, structural behavior of Structural Wall-Moment Frame, Tubular and Core with Outrigger and Belt Truss systems are presented here, which helps to understand the analysis and design of structural members of system.

Chapter 5

Analysis and Design of Steel-Concrete Composite Tall Buildings

5.1 General

This chapter presents the analysis and design of 24-, 44-, and 64-story steel-concrete composite tall buildings with three structural systems: the Structural Wall-Moment Frame system, the Tubular system, and the Outrigger and belt truss system. The analysis is performed with ETABS v.18.0 software. Steel and composite structural components are designed according to IS 800: 2007[45] and AISC 360-10[35], respectively. IS 456: 2000[44] and IS 13920: 2016[46] are used to design RC shear walls, considering all required load combinations for strength and serviceability. The static and dynamic wind and earthquake loads are analysed based on Indian standards. This chapter presents the designed sections of structural members, design forces, and governing load scenarios for each structural system.

5.2 Building Configuration

The selection of building geometry is an important stage in the study and comparison of various structural systems. The building geometry encompasses the form, inter-story height, aspect ratio, plan, and core size of the structure. Tall structure floor plans and

story heights are controlled by a number of architectural, structural, and constructional restrictions. Case studies for floor layouts of some of the world's current tall towers are being conducted [34]. Along with previous tall building case studies, the codal criteria of NBC (Volume 1): 2016[38], NBC (Volume 2): 2016[39], Model Building Bye-Laws (2016)[40], and IS 16700: 2017[48] are also taken into account while selecting a typical floor design for tall buildings in this research. Fig. 5.1 depicts the building's architectural layout.

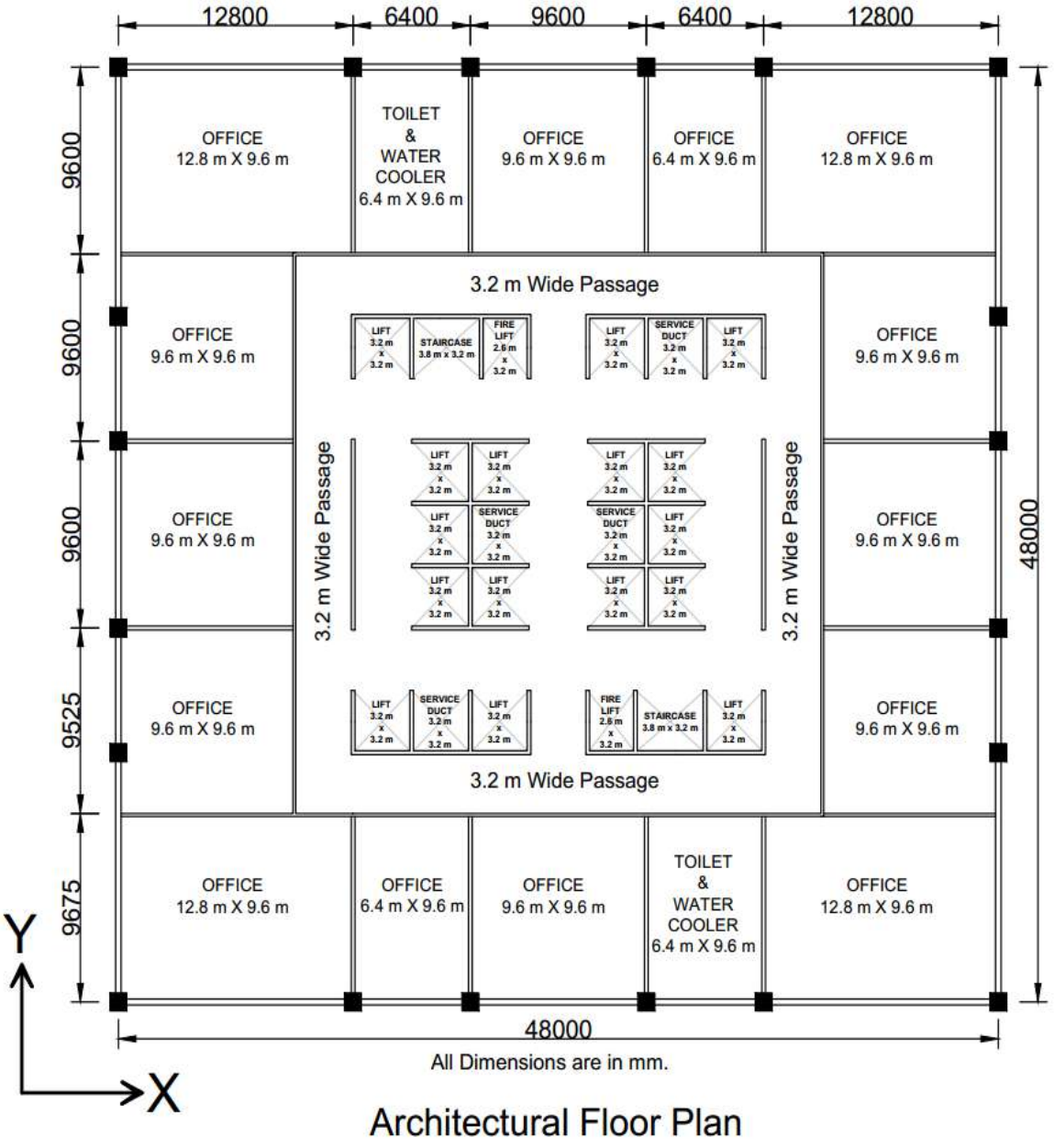

Figure 5.1: Architectural Floor Plan of Tall Building

5.2.1 General Building Data

- Location of building = Ahmedabad
- Type of building function = Business Group E1[38]
- Typical floor plan dimension = 48 m × 48 m
- Core plan dimension = 22.4 m × 22.4 m
- Total number of story = 24, 44 and 64
- Number of basements = 4
- Refuge floors = Every 4_{th} floors starting from 3_{rd} floor ($7th$ story)
- Typical floor story height = 3.7 m
- Basement floor story height = 5.2 m
- Fire Lift dimension = 2.6 m × 3.2 m
- Passenger & Service lift dimension = 3.2 m × 3.2 m
- Service duct dimension = 3.2 m × 3.2 m
- Staircase dimension = 3.8 m × 3.2 m
- Software used for analysis and design = ETABS v.18.0

5.2.2 Material Data

- Concrete = M60
- Structure steel = Fe540 (E410)

5.3 Loading Data

5.3.1 Dead and Imposed Loads

Dead load and Imposed load are derived from IS 875 (Part 1): 1987[41] and IS 875 (Part 2): 1987[42], respectively. Special considerations of NBC 2016 (Volume 1 & 2)([38] & [39])

for refuge floors are also considered. Dead load consists of 1.2 kN/m^2 floor finish and 0.8 kN/m^2 partition wall including glass cladding on perimeter. Dead load and imposed loads are shown in Table.5.1.

Table 5.1: Dead Load and Imposed Load Data

Dead load on typical floors	2 kN/m^2
Dead load on terrace and basement floors	1.5 kN/m^2
Imposed load typical floors	2.5 kN/m^2
Imposed load on the refuge and basement floors	5 kN/m^2
Imposed load on the terrace	1.5 kN/m^2

5.3.2 Seismic Load

Buildings are situated in seismic zone III. Table. 5.2 shows seismic load data. Static equivalent static analysis (ESA) and dynamic response spectrum analysis (RSA) for seismic loads are carried out in ETABS as per IS 1893 (Part 1): 2016[47]

Table 5.2: Seismic load data

Seismic Zone (Z)	V
Importance Factor (I)	1.2
Response Reduction Factor (R)	3
Soil Type	Medium
Damping Ratio of materials	2 %

Dipak Jivani conducted site-specific response analysis for three separate locations in Ahmadabad: N.I.T. (Nirma Institute of Technology), Old Passport Office, and IIM Ahmedabad.[54]. One-dimensional equivalent linear site response model is utilised for the investigation. This approach is utilised by the ProSHAKE software. The input motion is the strong motion recorded on the ground level at the Passport Office location in Ahmedabad during the Bhuj earthquake on January 26, 2001, as illustrated in Fig.5.2.

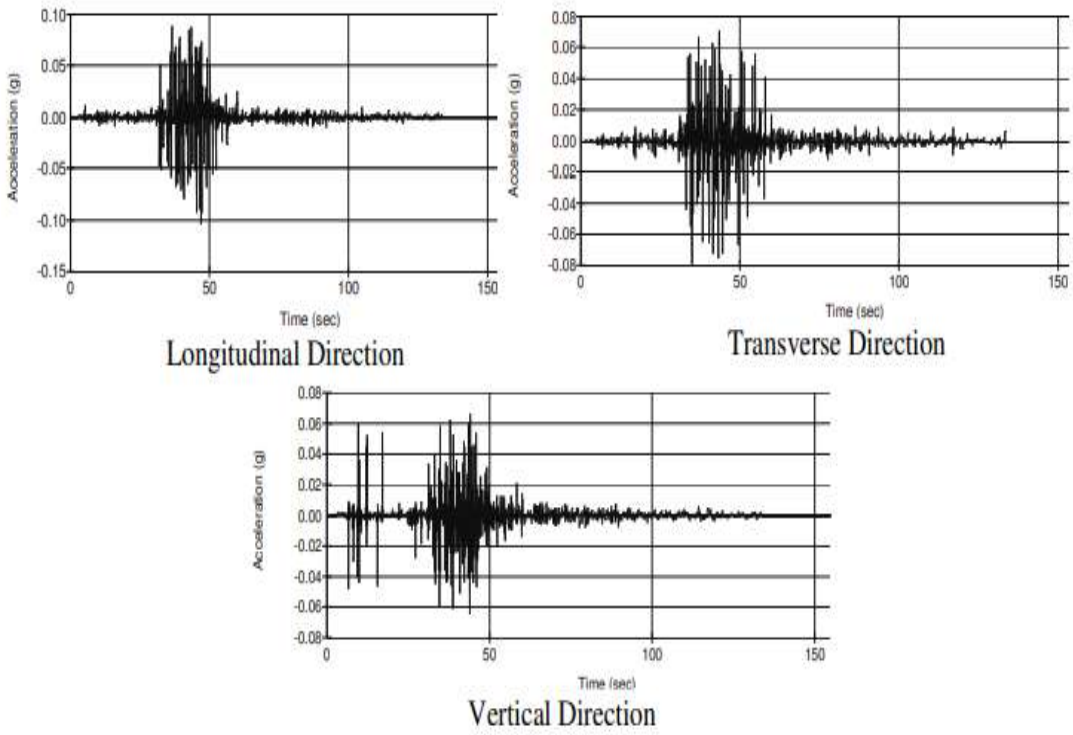

Figure 5.2: Passport Office Site- Acceleration Time History (Ground Surface)[54]

Three site-specific response spectra obtained from a one-dimensional linear equivalent site response model are depicted in Figures 5.3a, 5.3b and 5.3c. These site-specific response spectra are entered into ETABS as response spectrum functions. In ETABS, the time history functions derived from the response spectrum functions are also taken into account for the analysis of composite tall structures.

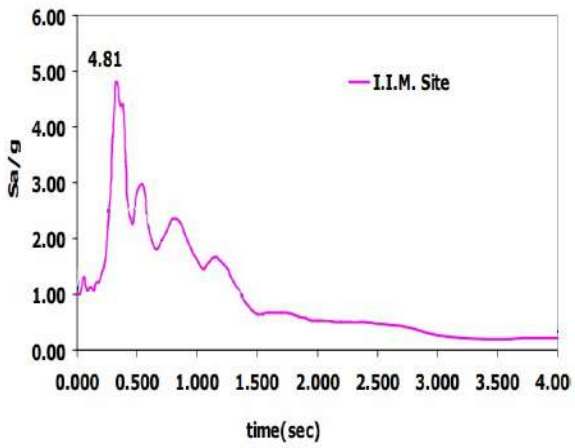

(a) IIM Site

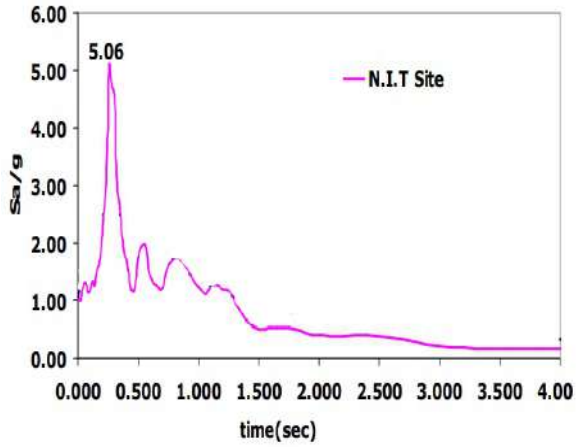

(b) NIT Site

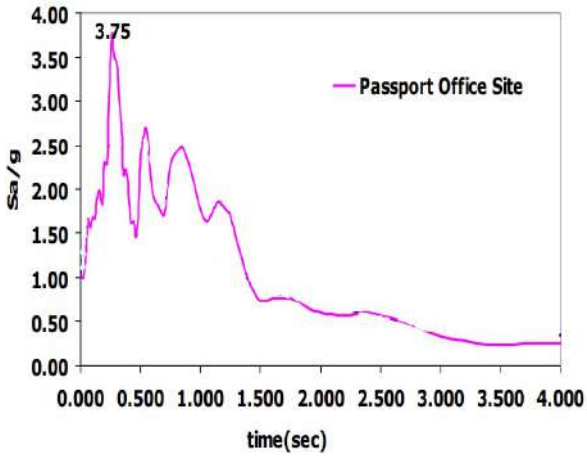

(c) Passport Site

Figure 5.3: Site-specific Response Spectrums

5.3.3 Wind Load

Wind loads on buildings are assessed using two approaches, namely static wind load and dynamic along and across wind loads via the gust factor method given in IS 875 (Part): 2015[43]. Table 5.3 provides wind load parameters considered for evaluation of 24, 44, and 64-story composite tall structures.

Table 5.3: Wind load data

Decription	**Value**
Basic Wind Speed V_b	39
Risk Coefficient k_1	1
Topography Factor k_3	1
Importance Factor k_4	1
Wind Directionality factor K_d	1
Area Avg. Factor K_a	0.8
Combination Factor K_c	0.9
Terrain Category	2

Steps to carry out Static Wind Load Analysis (SWLA) and Dynamic wind load analysis by Gust Factor method (DGF) are illustrated in sections 3.2.1 and 3.2.2 respectively in accordance to IS 875 (Part 3): 2015[43]. Wind forces in accordance to SWLA and DGF in 24, 44 and 64 story steel-concrete tall buildings are shown in Figures 5.4, 5.5 and 5.6 respectively.

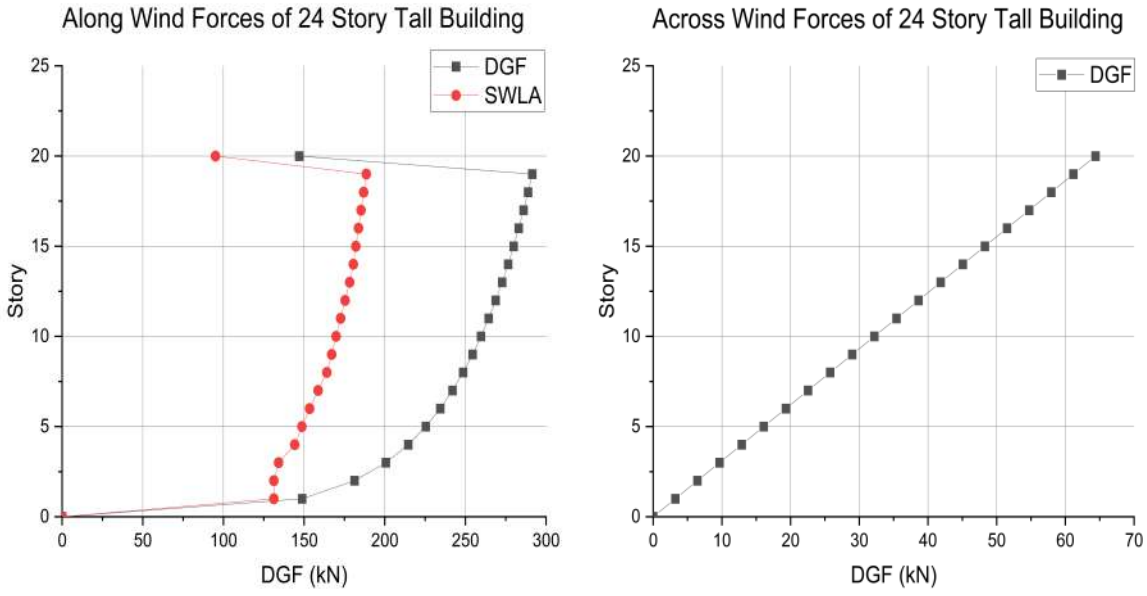

(a) Along wind forces of 24 story building (b) Across wind forces of 24 story building

Figure 5.4: Wind Forces on 24 Story Tall Building

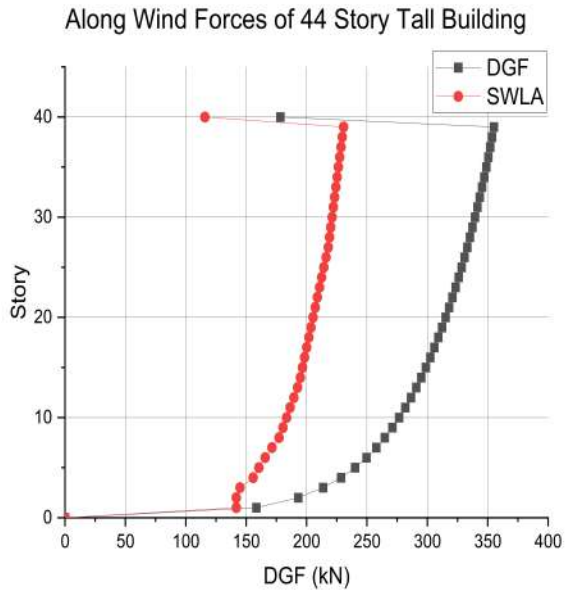

(a) Along wind forces of 44 story building

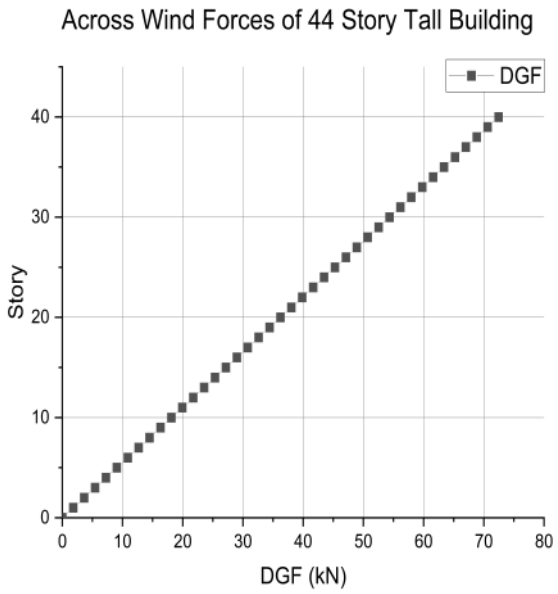

(b) Across wind forces of 44 story building

Figure 5.5: Wind Forces on 44 Story Tall Building

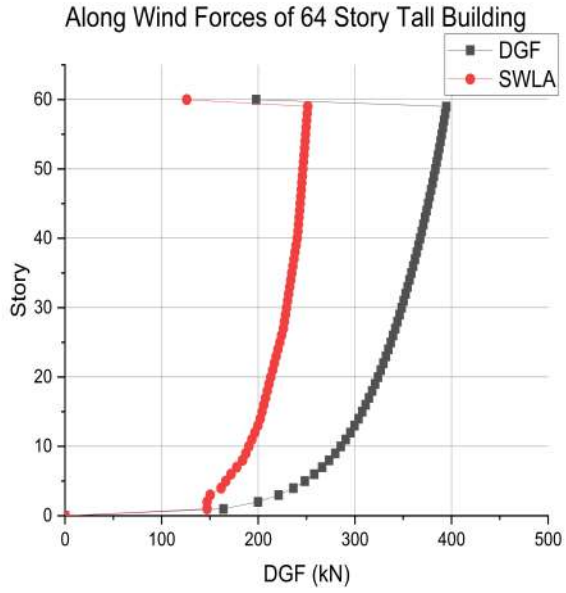

(a) Along wind forces of 64 story building

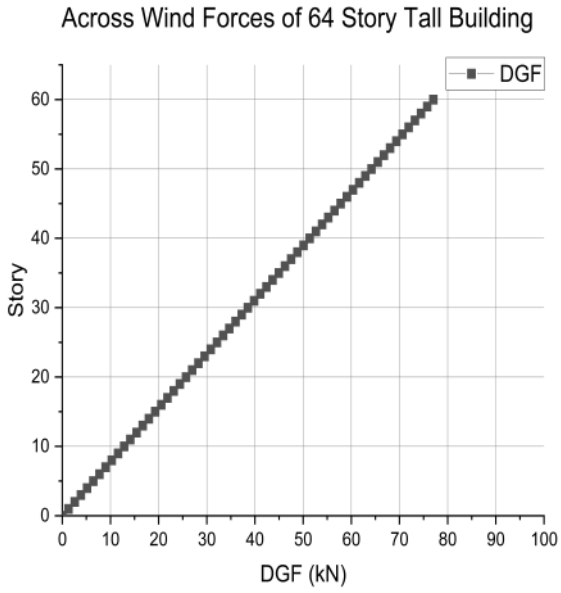

(b) Across wind forces of 64 story building

Figure 5.6: Wind Forces on 64 Story Tall Building

5.4 Load Combinations

Load combinations for design of RCC shear walls are as per table 18 of IS 456: 2000[44] shown in Table. 5.4 and for steel primary beams are as per Table 4 of IS 800: 2007[45] shown in Table. 5.5. Design and service load combinations for composite slab and composite beam considered are $(1.5DL + 1.5LL)$ and $(DL + LL)$, respectively. Composite columns are designed for combined RC and Steel design and service load combinations.

Table 5.4: Load Combinations for RCC Structural Elements

RCC Load Combinations	
Design Load Combinations	**Service Load Combinations**
1.5DL + 1.5LL	DL + LL
1.2 DL + 1.2LL ± 1.2WLX	DL ± WLX
1.2DL + 1.2LL ± 1.2WLY	DL ± WLY
1.2DL + 1.2LL ± 1.2DWLX	DL ± DWLX
1.2DL + 1.2LL ± 1.2DWLY	DL ± DWLY
1.5DL ± 1.5WLX	DL ± EQX
1.5DL ± 1.5WLY	DL ± EQY
1.5DL ± 1.5DWLX	DL + 0.8LL ± 0.8WLX
1.5DL ± 1.5DWLY	DL + 0.8LL ± 0.8WLY
0.9DL ± 1.5WLX	DL + 0.8LL ± 0.8DWLX
0.9DL ± 1.5WLY	DL + 0.8LL ± 0.8DWLY
0.9DL ± 1.5DWLX	DL + 0.8LL ± 0.8EQX
0.9DL ± 1.5DWLY	DL + 0.8LL ± 0.8EQY
1.2DL + 1.2LL ± 1.2EQX ± 0.36EQY	-
1.2DL + 1.2LL± 1.2EQY ± 0.36EQX	-
1.5DL ± 1.5EQX ± 0.42 EQY	-
1.5DL ± 1.5EQY ± 0.42EQX	-
0.9DL ± 1.5EQX ± 0.42 EQY	-
0.9DL ± 1.5EQY ± 0.42EQX	-

Table 5.5: Load Combinations for Steel Structural Elements

Steel Load Combinations	
Design Load Combinations	**Service Load Combinations**
1.5DL + 1.5LL	DL+LL
1.2 DL + 1.2LL ± 0.6WLX	DL±WLX
1.2DL + 1.2LL ± 0.6WLY	DL±WLY
1.2DL + 1.2LL ± 0.6DWLX	DL±DWLX
1.2DL + 1.2LL ± 0.6DWLY	DL±DWLY
1.2 DL + 1.2LL ± 1.2WLX	DL±EQX
1.2DL + 1.2LL ± 1.2WLY	DL±EQY
1.2DL + 1.2LL ± 1.2DWLX	DL+0.8LL±0.8WLX
1.2DL + 1.2LL ± 1.2DWLY	DL+0.8LL±0.8WLY
1.5DL ± 1.5WLX	DL+0.8LL±0.8DWLX
1.5DL ± 1.5WLY	DL+0.8LL±0.8DWLY
1.5DL ± 1.5DWLX	DL+0.8LL±0.8EQX
1.5DL ± 1.5DWLY	DL+0.8LL±0.8EQY
0.9DL ± 1.5WLX	-
0.9DL ± 1.5WLY	-
0.9DL ± 1.5DWLX	-
0.9DL ± 1.5DWLY	-
1.2DL + 1.2LL ± 1.2EQX ± 0.36EQY	-
1.2DL + 1.2LL± 1.2EQY ± 0.36EQX	-
1.5DL ± 1.5EQX ± 0.42 EQY	-
1.5DL ± 1.5EQY ± 0.42EQX	-
0.9DL ± 1.5EQX ± 0.42 EQY	-
0.9DL ± 1.5EQY ± 0.42EQX	-

In Tables 5.4 and 5.5, "EQ" load case consists of various seismic load case which includes static earthquake load case as per IS 1893 (Part 1): 2016[47] (EQ), dynamic response spectrum load case as per IS 1893 (Part 1): 2016[47] (RS), site-specific response spectrum load cases of three sites (NIT_RS, PASSPORT_RS and IIM_RS) and site-specific time history load cases of three sites (NIT_TH, PASSPORT_TH and IIM_TH).

5.5 Modelling of Tall Buildings

In this section, modelling of steel-composite tall building is discussed. Modeling is done in ETABS.The steps followed for modelling and analysis of structure is as follows:

- Define material properties and sectional properties for structural elements.
- Prepare the three dimensional structural model as per typical floor plan and elevation of structural systems.
- Assign the support conditions and sections properties to 3D model.
- Define and assign the loads to the structure as mentioned in the section 5.3.
- Analyze the Model.
- From analysis results, structural elements are designed and if required, sections are modified and analysis is carried out again

Figure 5.7 shows number of steel-concrete tall building models modelled, analysed and designed for various lateral load resisting system in consideration.

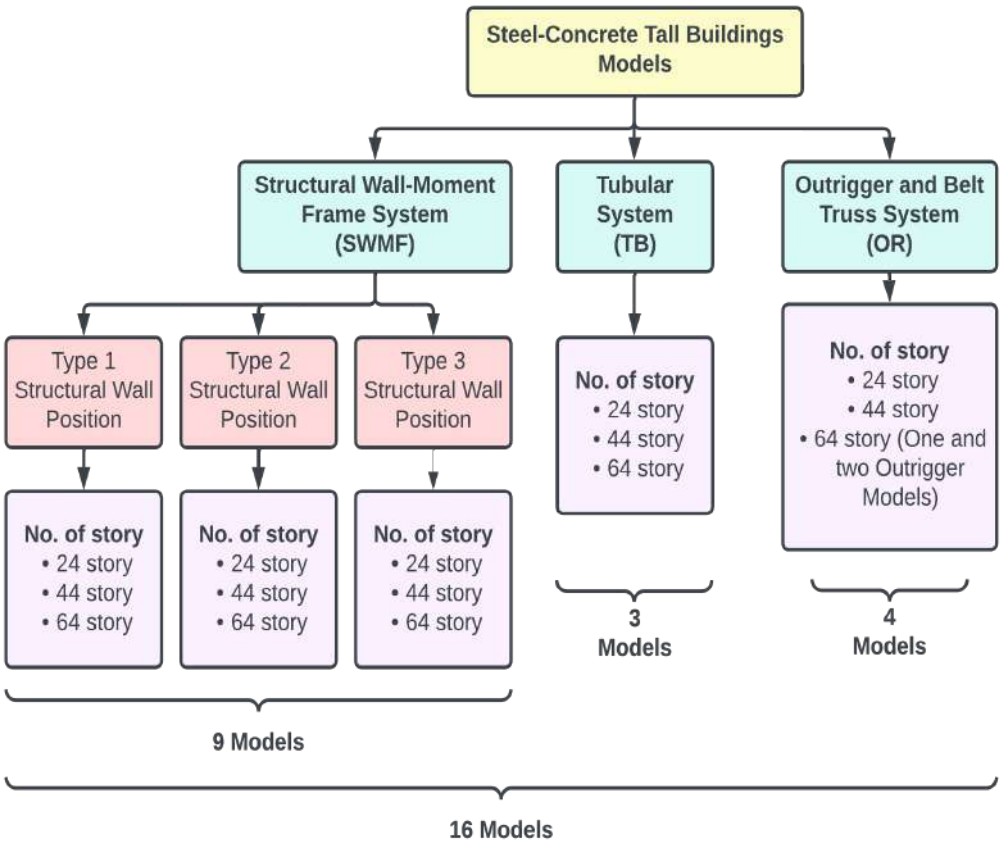

Figure 5.7: Steel-Concrete Tall Buildings Models

5.6 Analysis of Tall Buildings

Before designing the structural components of tall structures, many forms of study are necessary. Figure 5.8 shows the different gravity and lateral load analyses considered during the assessment of sixteen tall steel-concrete tall buildings.

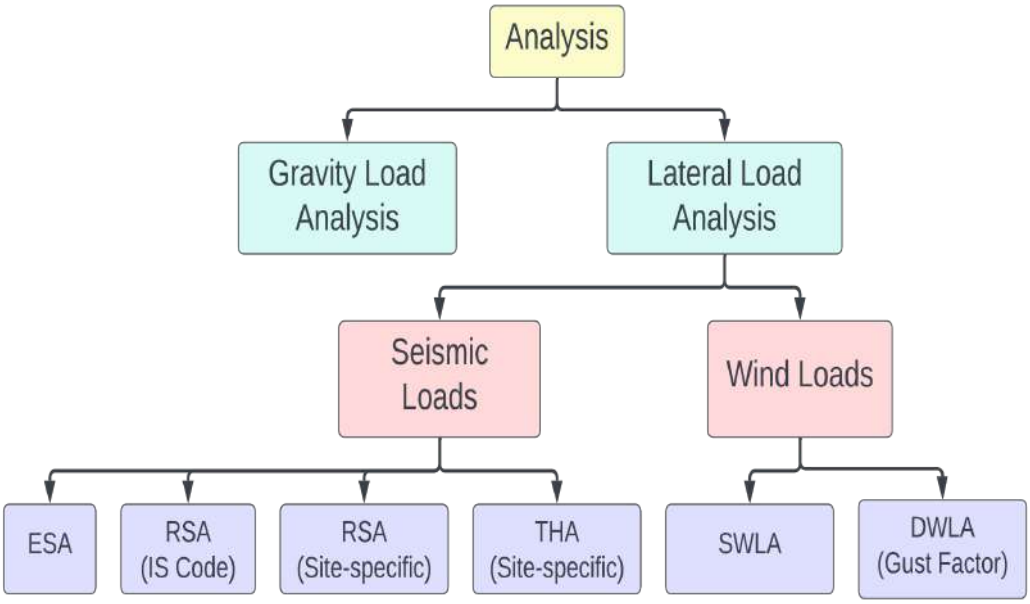

Figure 5.8: Types of analysis considered for analysis of tall buildings

5.7 Design of structural members

5.7.1 Composite slab

The slab is designed as a composite metal deck. The following steps are involved in the design of metal deck.

1. Select the deck profile and list the decking sheet data (preferably from manufacturer's data).

2. Find out the loading acting on the slab.

3. Design the profiled sheeting as shuttering.

   - Calculate the effective length l_e of the span

$$l_e = (l - B + d_{ap})/2 \tag{5.1}$$

   where,

   l = Actual span of the composite floor

   B = Width of top flanges of the steel beams

   d_{ap} = The depth of the sheeting

- Calculate factored moments and shear acting of profiled sheeting.
- Check for moment

  Moment capacity (M_{pa}/γ_{ap}) > factored moment.

  where,

  M_{pa} = plastic moment of resistance of sheet

  γ_{ap} = partial safety factor

- Check for shear

  Shear capacity (V_{pa}/γ_{ap}) > factored shear.

- Check for deflection.

4. Design of composite slab

- Calculate the effective length l_e of the span.

  Effective length = Center to center between supports or clear distance between supports + effective depth of slab whichever is less.

- Calculate factored moments and shear.
- Check for moment

  Bending resistance

$$M_{p.Rd} = N_{cf}(d_p - 0.42x) > factored\ moment \tag{5.2}$$

  where,

  $N_{cf} = \dfrac{A_p f_{yp}}{\gamma_{ap}}$

  A_p = Effective area per meter width

  f_{yp}= yield strength of steel

  d_p = effective depth of slab

  x = depth of neutral axis = $N_{cf}/b(0.36f_{ck})$

- Check for shear

  Shear resistance

$$V_{v.Rd} = (b_0/b)d_p\tau_{Rd}k_v(1.2 + 40\rho) > factored\ shear \tag{5.3}$$

Where,

b = one typical wavelength of profiled sheeting

b_0 = average width of trough

tau_{Rd} = basic shear strength of concrete

$k_v = (1.6d_p) \geqslant 1$

$\rho = A_p/(b_0 d_p)$

A_p = effective area of sheeting within width b_0

- Check for longitudinal shear Longitudinal shear is checked by m-k method. The m-k method gives the vertical shear resistance $V_{i.Rd}$ as

$$V_{i,Rd} = bd_p \left(\frac{mA_p}{bl_s} + k \right) / \gamma_v s > factored\ shear \tag{5.4}$$

m and k values are generally provided by manufacturers of profiled sheet. This values are based on experimental results.

The design of composite metal deck slab is given in Appendix D.

5.7.2 Composite beam

Composite beam B2 is designed as per AISC 360-[35]. Following steps are involved in design of composite beam.

1. Calculate dead loads and imposed loads acting on composite slabs in pre-composite and composite conditions as per IS 875 (Part 1): 1987[41], IS 875 (Part 2): 1987[42] and data of composite slab from manufacturer.

2. Check composite deck and anchor requirements stipulated in AISC Specifications I1.3, I3.2c and I8.

3. Design for Pre-composite condition

   - Calculate uniform distributed dead load w_D, imposed load w_L and factored load w_u.

- Calculate factored design bending moment,

$$M_u = \frac{w_u L^2}{8} \tag{5.5}$$

here, L = span of beam

- Find out required plastic section modulus Z_x as per F2-1 of AISC Specifications.

$$Z_{xmin} = \frac{M_u}{\phi_b f_y} \tag{5.6}$$

where,

$\phi_b = 0.9$

f_y= yield strength of steel beam

- Select steel section as per minimum requirement of plastic section modulus.
- Calculate pre-composite deflection of beam which should not exceed L/360 as per AISC Design Guide 3. If exceeds, try changing sections or provide cambering of maximum of 80% of pre-composite dead load deflection.

$$\Delta_{nc} = \frac{5 w_D L^4}{384 EI} \tag{5.7}$$

where,

E = Young's modulus of elasticity of beam

I = Moment of inertia of beam

4. Design for composite condition

- Calculate uniform distributed dead load w_D, imposed load w_L and factored load w_u.
- Calculate factored design bending moment,

$$M_u = \frac{w_u L^2}{8} \tag{5.8}$$

here, L = span of beam

- Determine effective width b as per AISC Specifications Section I3.1a.
- Check for plastic distribution of beam as per equation 5.9 given in AISC Specification Section I3.2a.

$$h/t_w \leqslant 3.76\sqrt{E/f-y} \tag{5.9}$$

- Calculate stud compressive force as per equations AISC Specification Commentary Section I3.2a.
- Find out the location of plastic neutral axis (x) of section as per 5.10 and design moment capacity M_n as per AISC Specification Commentary Section I3.2a.

$$x = \frac{A_s f_y - C}{2 b_f f_y}$$
$$M_n = C(d_1 + d_2) + P_y(d_3 - d_2) \tag{5.10}$$

where,

x = location of plastic neutral axis from top of flange of beam

A_s = Section area of beam

f_y = Yield strength of beam

b_f = Width of flange of beam

C, d_1, d_2, d_3 and P_y are calculated as per AISC Specification Commentary Section I3.2a.

- Calculate composite live load deflection as per AISC Specification Commentary Section I3.2 which should be L/360 as per AISC Design Guide 3.

$$Y_{ENA} = \left[A_s d_3 + (\sum Q_n/f_y)(2d_3 + d_1)\right] / \left[A_s + (\sum Q_n/f_y)\right]$$
$$I_{LB} = I + A_s(Y_{ENA} - d_3)^2 + (\sum Q_n/f_y)(2d_3 + d_1 - Y_{ENA})^2$$
$$\Delta_{LL} = \frac{5 w_L L^4}{384 E I_{LB}} \tag{5.11}$$

where, d_1 = distance from the compression force in the concrete to the top of the steel section

d_3 = distance from the resultant steel tension force for full section tension yield

to the top of the steel

I_{LB} = lower bound moment of inertia

I = moment of inertia for the structural steel section

$\sum Q_n$ = sum of the nominal strengths of steel anchors between the point of maximum positive moment and the point of zero moment to either side

The sample design of composite beam is given in Appendix E.

5.7.2.1 Steel Beam

Steel beam B1 is designed as per IS 800: 2007[45]. Following steps are involved in the design of steel flexural member.

1. Calculate the design loads from the analysis, M_u and V_u.
2. Find out required plastic section modulus as per following equation

$$Z_p = \frac{M_u \gamma_{m0}}{f_y} \tag{5.12}$$

where, Z_p =Plastic sectional modulus of section γ_{m0} = Partial Safety factor

3. Select suitable section which has a section modulus equal to or more than Z_p.
4. Classify the section based on b_f/t_f and d/t_w ratio.
5. Selected section is checked for shear. IS: 800-2007 clause 8.4

$$V_d = \frac{A_v f_y}{\sqrt{3}\gamma_{m0}} \tag{5.13}$$

if $V_u \leqslant 0.6V_d$

$$M_d = \frac{\beta_b Z_p f_y}{\gamma m0} \leqslant \frac{1.2 Z_e f_y}{\gamma m0} \tag{5.14}$$

if $V_u > 0.6V_d$ For plastic and compact section,

$$M_{dv} = M_d - \beta_b (M_d - M_{fd} \leqslant \frac{1.2 Z_e f_y}{\gamma m0} \tag{5.15}$$

For semi compact section,

$$M_{dv} = \frac{Z_e f_y}{\gamma m0} \tag{5.16}$$

6. Check for web buckling and web crippling Web buckling strength,

$$F_{wb} = (b_1 + n_1)t_w f_{cd} > V_u \tag{5.17}$$

Where, b_1 = stiff bearing length

$n_1 = 1$, assuming 45° dispersion

t_w = web thickness

f_{cd} = allowable compressive stress

Web crippling strength

$$F_{crip} = (b_1 + n_2)t_w f_y/\gamma_{m0} > Vu$$
$$n2 = 2.5(R_1 + t_f) \tag{5.18}$$

Where, R_1 = root radius

The design of steel beam is given in Appendix F.

5.8 Structural Wall-Moment Frame System

Herein are described the structural configuration, designed sections, design forces, and governing load cases for 24, 44, and 64-story structural wall-moment frame steel-concrete tall structures. In addition, a parametric research is conducted to determine the optimal positions for shear walls in given architectural plans. Three distinct shear wall locations, designated SM1, SM2, and SM3 SWMF tall structures, were used for this investigation.

5.8.1 SM1 Steel-Concrete Composite SWMF Tall Buildings

Typical floor plan of SM1 tall buildings is shown in Fig. 5.9. Here, B2 beams shown in Fig. 5.9 are secondary composite beams while B1 and B3 are main primary beams. C1 represents composite columns and SW represents RCC shear walls.

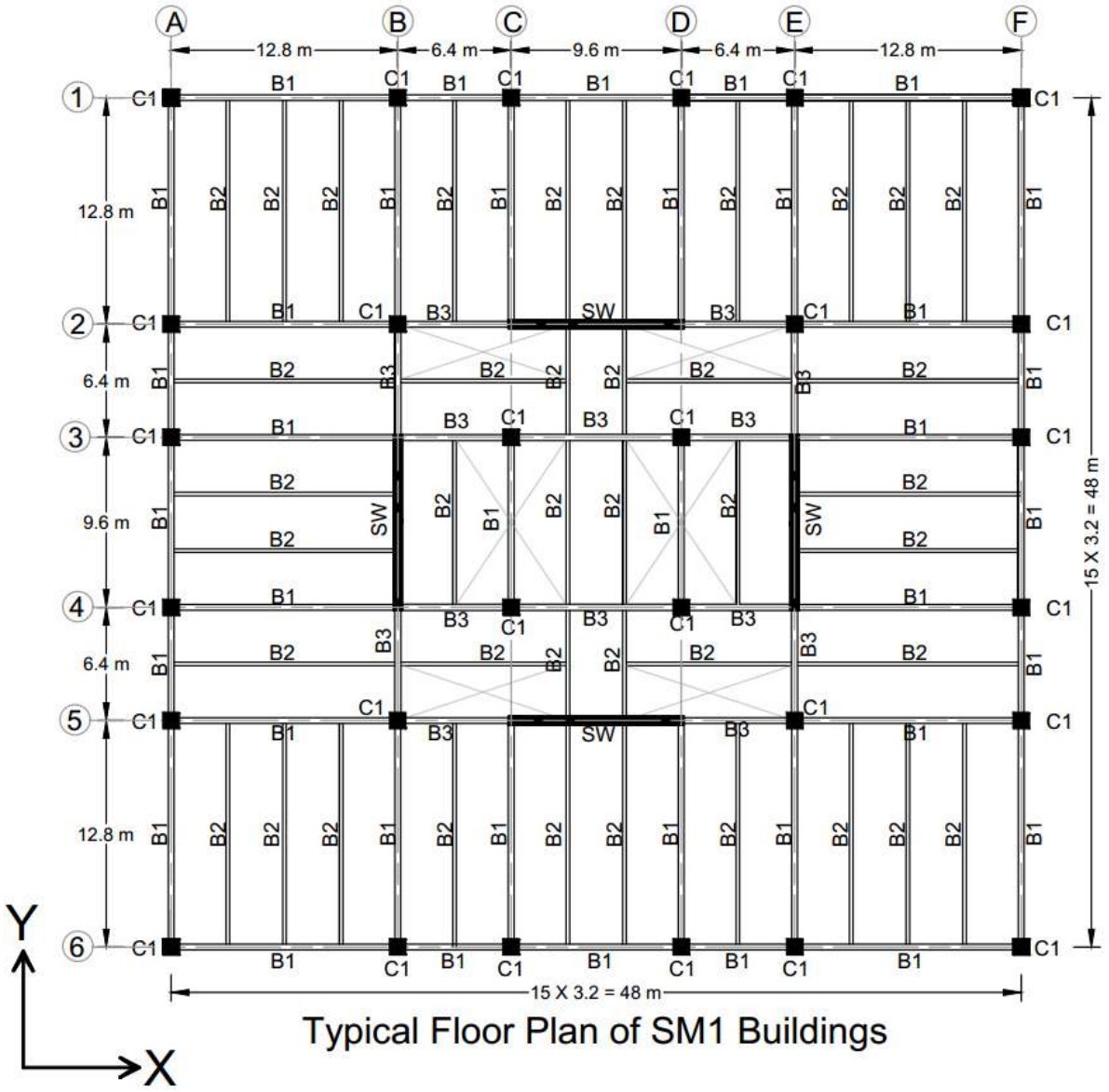

Figure 5.9: Typical Floor Plan of SM1 Tall Buildings

The SM1S24, SM1S44, and SM1S64 models of SM1 tall structures with 24, 44, and 64 floors respectively are analysed and developed in accordance with applicable Indian and AISC 360-10 requirements. Figure 5.10 shows an elevation view of three SM1 building models.

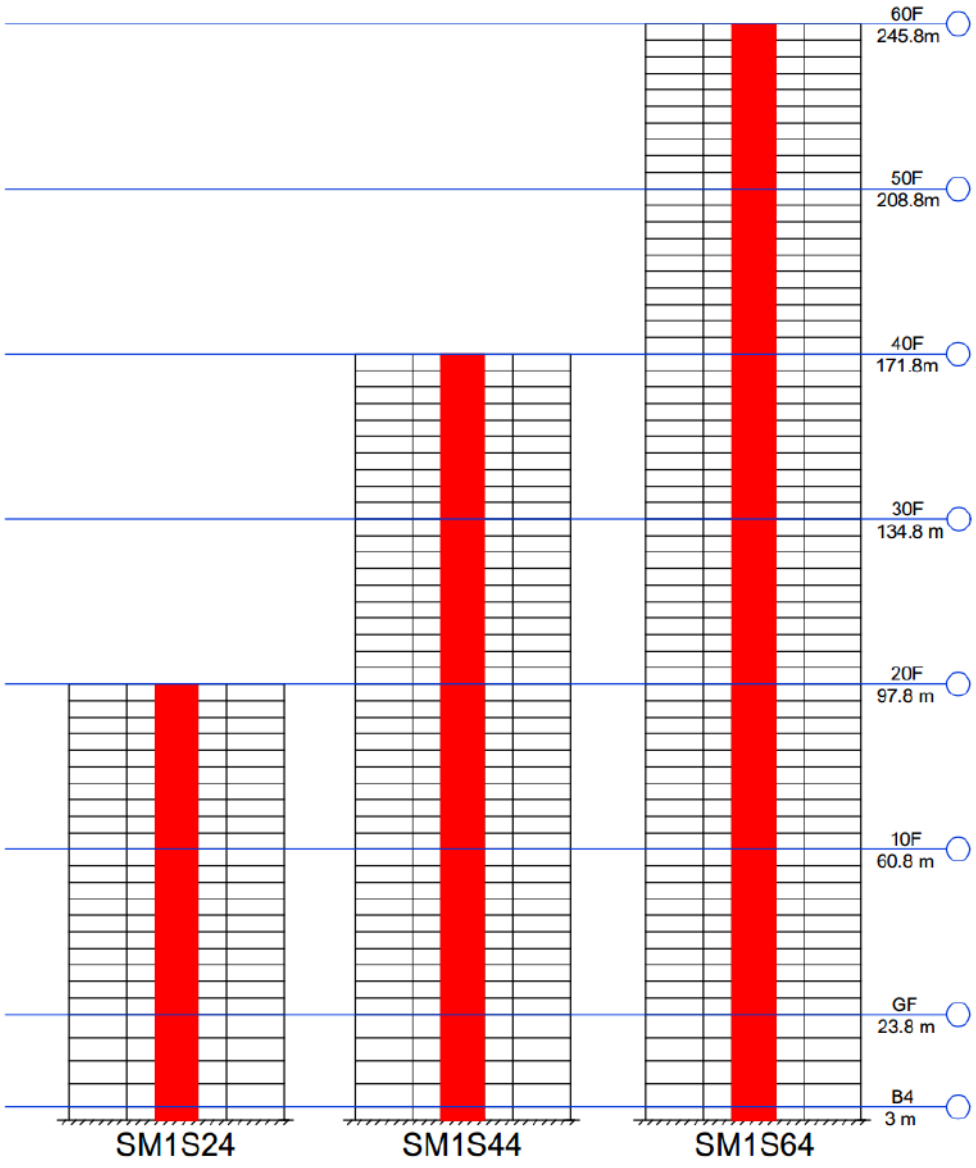

Figure 5.10: Elevation of SM1 Tall Buildings

Table 5.6 shows sectional properties of designed section of SM1S24, SM1S44 and SM1S64 tall buildings and Table **??** shows design forces of structural elements of SM1S24, SM1S44 and SM1S64 tall buildings.

Table 5.6: Designed Sections of SM1 Tall Buildings

Designed Section of SM1 Tall Buildings				
Building		SM1S24	SM1S44	SM1S64
Concrete Grade		M60	M60	M60
Steel Grade		Fe540	Fe540	Fe540
Rebar Grade		HYSD 550D	HYSD 550D	HYSD 550D
Composite Slab	Thickness (mm)	125	125	125
	Reinforcement (Main & Dist)	8ϕ @ 200 mm c/c	8ϕ @ 200 mm c/c	8ϕ @ 200 mm c/c
Beam B1	Total depth (mm)	500	650	700
	Flange Width (mm)	250	325	450
	Flange Thickness (mm)	40	40	60
	Web Thickness (mm)	20	20	30
Beam B2	Section	ISWB 450	ISWB 450	ISWB 450
	Shear stud	20 mm (65 Nos)	20 mm (65 Nos)	20 mm (65 Nos)
Beam B3	Total depth (mm)	500	700	750
	Flange Width (mm)	250	350	450
	Flange Thickness (mm)	45	50	60
	Web Thickness (mm)	25	25	30
Column C1 (B x D x T)	B4 to GF	700X700X45	900X900X50	1200X1200X70
	1F to 10F	700X700X45	900X900X50	1200X1200X70
	11F to 20F	500X500X40	800X800X50	1000X1000X60
	21F to 30F	-	700X700X45	850X850X60
	31F to 40F	-	600 x 600 x 40	750X750X55
	41F to 50F	-	-	600X600X50
	51F to 60F	-	-	500X500X40
Shear Wall Thickness	B4 to GF	350	450	650
	1F to 10F	350	450	650
	11F to 20F	250	400	550
	21F to 30F	-	400	450
	31F to 40F	-	300	400
	41F to 50F	-	-	350
	51F to 60F	-	-	300

Table 5.7: Design Forces of SM1 Tall Buildings

Design Forces of SM1 Tall Buildings				
Element	**Description**	**SM1S24**	**SM1S44**	**SM1S64**
B1	Storey	19F	15F	22F
	Axial Force Nu (kN)	0	0	0
	Shear Force Vu (kN)	615.8	379.6	350.9
	Bending Moment Mu (kNm)	1413.4	1689.1	2366.6
	Torsional Moment Tu (kNm)	0.0166	0.07	0.06
	Governing Load Case	1.5DL + 1.5LL	1.2DL + 1.2LL - 1.2DWLX	1.5DL + 1.5PASSPORT_RSY
B2	Storey	19F	39F	59F
	Axial Force Nu (kN)	0	0	0
	Shear Force Vu (kN)	298.2	297.8	296.8
	Bending Moment Mu (kNm)	952.83	952.83	952.83
	Torsional Moment Tu (kNm)	0	0	0
	Governing Load Case	1.5DL + 1.5LL	1.5DL + 1.5LL	1.5DL + 1.5LL
B3	Storey	1F	GF	1F
	Axial Force Nu (kN)	0	0	0
	Shear Force Vu (kN)	508	780.6	1482.2
	Bending Moment Mu (kNm)	1484.3	3075.5	5099.3
	Torsional Moment Tu (kNm)	0.1	0.034	0.05
	Governing Load Case	1.5DL + 1.5PASSPORT_RSY	1.5DL + 1.5PASSPORT_RSY	1.5DL + 1.5PASSPORT_RSY
C1	Storey	B4	B4	B4
	Axial Force Pu (kN)	22466.5	45419.3	83699.8
	Shear Force Vu (kN)	361.5	840.1	1688.3
	Bending Moment Mu2 (kNm)	442.1	2446.6	2950.8
	Bending Moment Mu3 (kNm)	1075.6	1107.3	6305.7
	Torsional Moment Tu (kNm)	0.473	1.55	0.07
	Governing Load Case	1.5DL + 1.5PASSPORT_RSY + 0.45PASSPORT_RSX	1.5DL - 1.5PASSPORT_RSY + 0.45PASSPORT_RSX	1.5DL - 1.5PASSPORT_RSX + 0.45PASSPORT_RSY
SW	Storey	B4	B4	B4
	Axial Force Pu (kN)	37087.1	67157.4	98864.6
	Shear Force Vu (kN)	10461.5	122681	17225.6
	Bending Moment Mu (kNm)	199373.2	223386.8	332176.6
	Governing Load Case	1.5DL - 1.5PASSPORT_RSY + 0.45PASSPORT_RSX	1.5DL - 1.5PASSPORT_RSY + 0.45PASSPORT_RSX	1.5DL - 1.5PASSPORT_RSY + 0.45PASSPORT_RSX

Figure 5.11 shows schematic cross-sections of structural members used in analysis and design of SWMF tall buildings.

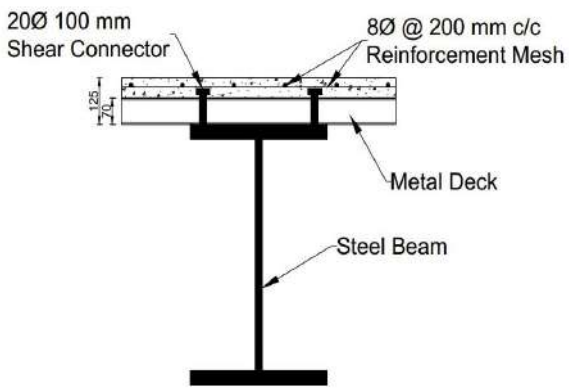

(a) Schematic Sections of Composite Slab and Beam

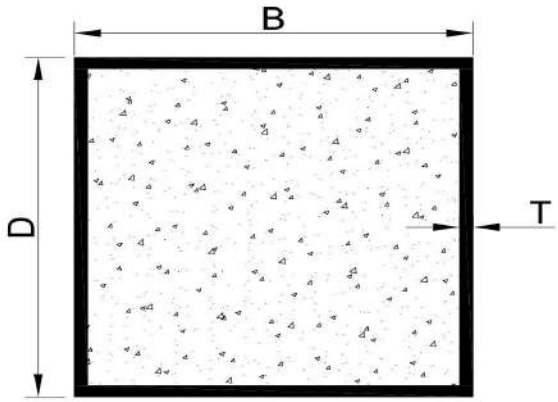

(b) Schematic Section of Composite Column

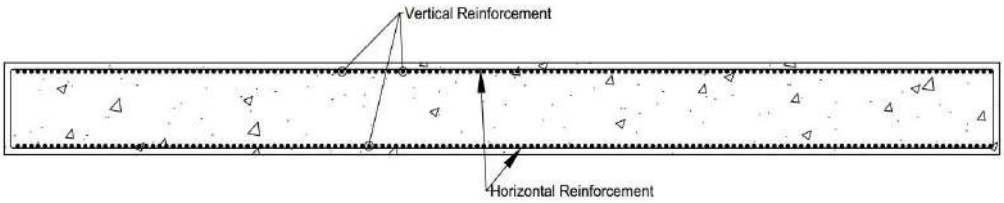

(c) Schematic Section of Structural Wall

Figure 5.11: Schematic Sections of Structural Members

5.8.2 SM2 Steel-Concrete Composite SWMF Tall Buildings

Typical floor plan of SM2 tall buildings is shown in Fig. 5.12. Here, B2 beams shown in Fig. 5.12 are secondary composite beams while B1 and B3 are main primary beams. C1 represents composite columns and SW represents RCC shear walls.

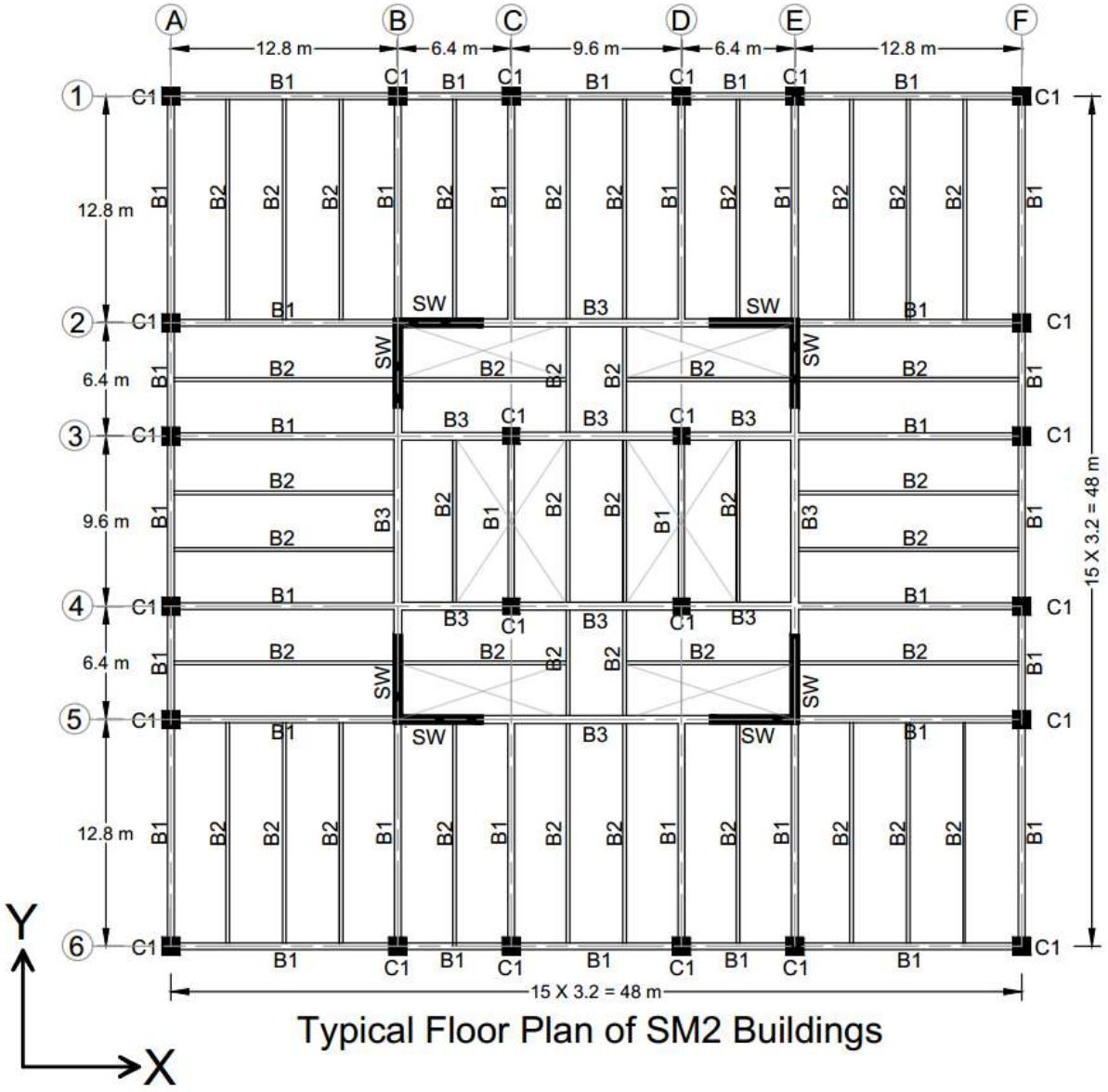

Figure 5.12: Typical Floor Plan of SM2 Tall Buildings

The SM2S24, SM2S44, and SM2S64 models of SM2 tall structures with 24, 44, and 64 floors respectively are analysed and developed in accordance with applicable Indian and AISC 360-10 requirements. Figure 5.13 shows an elevation view of three SM1 building models.

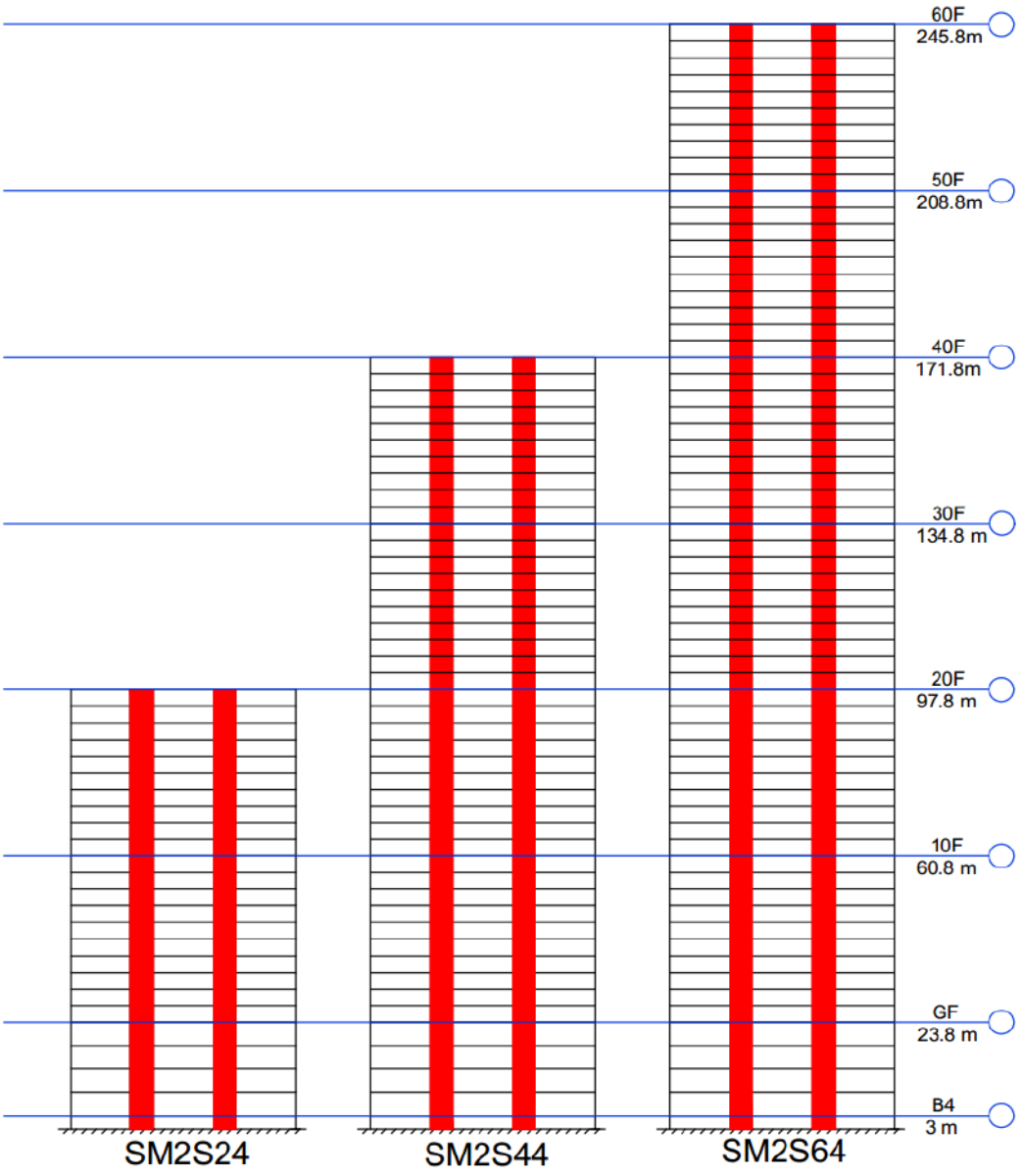

Figure 5.13: Elevation of SM2 Tall Buildings

Table 5.8 shows sectional properties of designed section of SM2S24, SM2S44 and SM2S64 tall buildings and Table 5.9 shows design forces of structural elements of SM2S24, SM2S44 and SM2S64 tall buildings.

Table 5.8: Designed Section of SM2 Tall Buildings

Designed Section of SM2 Tall Buildings				
Building		SM2S24	SM2S44	SM2S64
Concrete Grade		M60	M60	M60
Steel Grade		Fe540	Fe540	Fe540
Rebar Grade		HYSD 550D	HYSD 550D	HYSD 550D
Composite Slab	Thickness (mm)	125	125	125
	Reinforcement (Main & Dist)	8ϕ @ 200 mm c/c	8ϕ @ 200 mm c/c	8ϕ @ 200 mm c/c
Beam B1	Total depth (mm)	600	700	775
	Flange Width (mm)	300	375	500
	Flange Thickness (mm)	45	45	60
	Web Thickness (mm)	25	25	30
Beam B2	Section	ISWB 450	ISWB 450	ISWB 450
	Shear stud	20 mm (65 Nos)	20 mm (65 Nos)	20 mm (65 Nos)
Beam B3	Total depth (mm)	600	750	850
	Flange Width (mm)	300	450	500
	Flange Thickness (mm)	50	55	60
	Web Thickness (mm)	25	30	30
Column C1 (B x D x T)	B4 to GF	800X800X50	1000X1000X60	1200X1200X70
	1F to 10F	800X800X50	1000X1000X60	1200X1200X70
	11F to 20F	600X600X45	850X850X50	1000X1000X70
	21F to 30F	-	750X750X45	850X850X60
	31F to 40F	-	550X550X40	750X750X50
	41F to 50F	-	-	600X600X50
	51F to 60F	-	-	600X600X50
Shear Wall Thickness	B4 to GF	500	500	650
	1F to 10F	500	500	650
	11F to 20F	350	400	600
	21F to 30F	-	400	500
	31F to 40F	-	300	400
	41F to 50F	-	-	300
	51F to 60F	-	-	250

Table 5.9: Design Forces of SM2 Tall Buildings

Design Forces of SM2 Tall Buildings				
Element	**Description**	**SM2S24**	**SM2S44**	**SM2S64**
B1	Storey	3F	13F	19F
	Axial Force Nu (kN)	0	0	0
	Shear Force Vu (kN)	589.3	306.5	595.2
	Bending Moment Mu (kNm)	1813.1	2083.8	3731.5
	Torsional Moment Tu (kNm)	0.026	0.053	0.025
	Governing Load Case	1.2DL + 1.2LL + 1.2PASSPORT_RSX	1.5DL + 1.5PASSPORT_RSY	1.5DL + 1.5PASSPORT_RSY
B2	Storey	19F	39F	59F
	Axial Force Nu (kN)	0	0	0
	Shear Force Vu (kN)	298.2	297.8	296.8
	Bending Moment Mu (kNm)	952.83	952.83	952.83
	Torsional Moment Tu (kNm)	0	0	0
	Governing Load Case	1.5DL + 1.5LL	1.5DL + 1.5LL	1.5DL + 1.5LL
B3	Storey	3F	2F	GF
	Axial Force Nu (kN)	0	0	0
	Shear Force Vu (kN)	892.43	383.11	1764.5
	Bending Moment Mu (kNm)	2326.5	3635.8	6406.3
	Torsional Moment Tu (kNm)	1.3	0	8.71
	Governing Load Case	1.2DL + 1.2LL + 1.2PASSPORT_RSY	1.5DL + 1.5PASSPORT_RSY	1.5DL + 1.5PASSPORT_RSY
C1	Storey	B4	B4	B4
	Axial Force Pu (kN)	19085.6	40640.3	70486.5
	Shear Force Vu (kN)	256.7	491.3	928.4
	Bending Moment Mu2 (kNm)	543.7	3018.4	5881.93
	Bending Moment Mu3 (kNm)	1312	1272.6	2574.2
	Torsional Moment Tu (kNm)	1.3	0.6	8.54
	Governing Load Case	1.5DL - 1.5PASSPORT_RSX + 0.45PASSPORT_RSY	1.5DL - 1.5PASSPORT_RSY + 0.45PASSPORT_RSX	1.5DL - 1.5PASSPORT_RSY + 0.45PASSPORT_RSX
SW	Storey	B4	B4	B4
	Axial Force Pu (kN)	13904	68937.7	104753.6
	Shear Force Vu (kN)	5776.1	5628.4	8281.6
	Bending Moment Mu (kNm)	46058.6	48474.6	64498.6
	Governing Load Case	0.9DL - 1.5PASSPORT_RSX + 0.45PASSPORT_RSY	1.5DL - 1.5PASSPORT_RSX + 0.45PASSPORT_RSY	1.5DL - 1.5PASSPORT_RSY + 0.45PASSPORT_RSX

5.8.3 SM3 Steel-Concrete Composite SWMF Tall Buildings

Typical floor plan of SM3 tall buildings is shown in Fig. 5.14. Here, B2 beams shown in Fig. 5.14 are secondary composite beams while B1 and B3 are main primary beams. C1 represents composite columns and SW represents RCC shear walls.

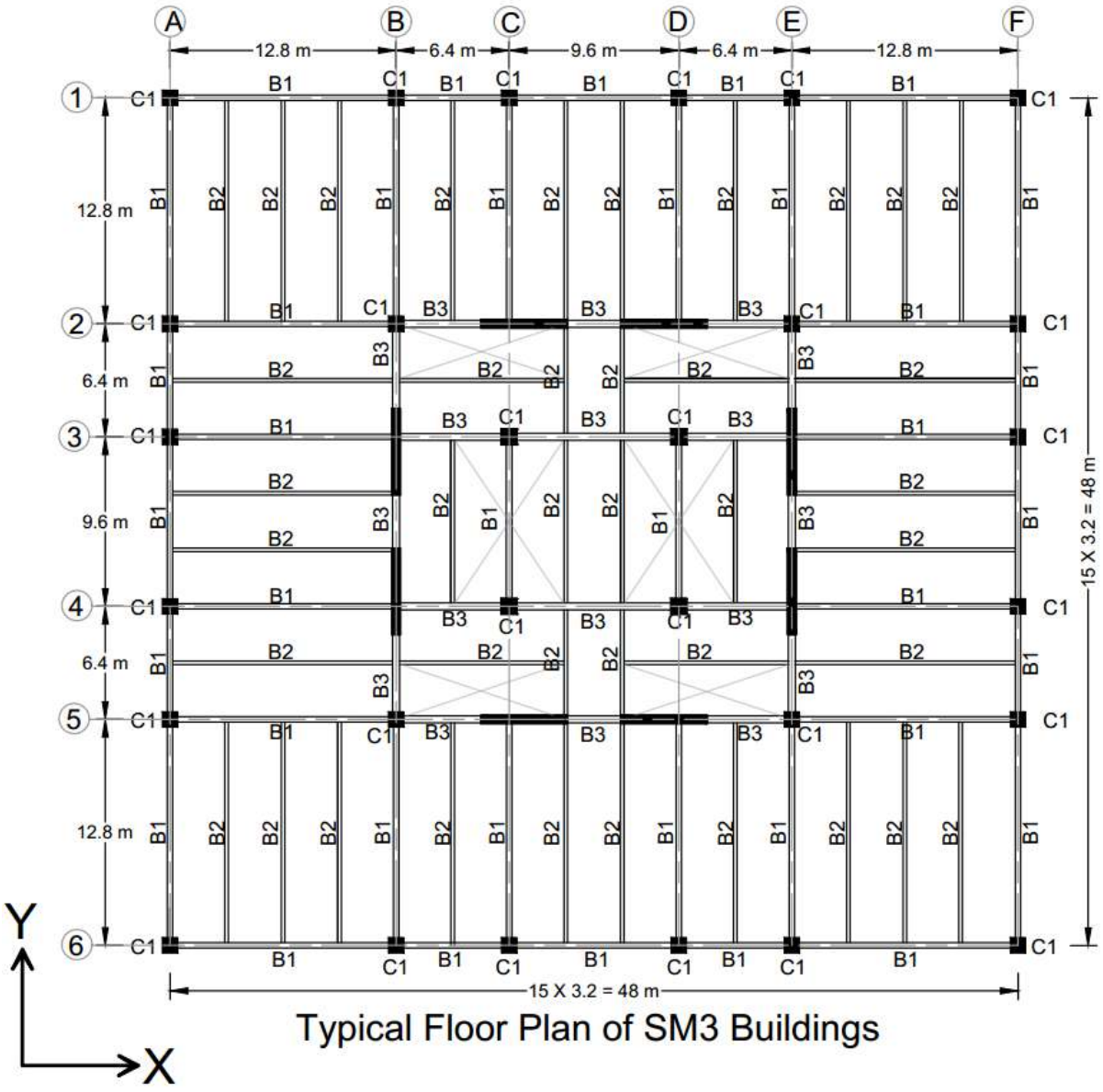

Figure 5.14: Typical Floor Plan of SM3 Tall Buildings

The SM3S24, SM3S44, and SM3S64 models of SM3 tall structures with 24, 44, and 64 floors respectively are analysed and developed in accordance with applicable Indian and AISC 360-10 requirements. Figure 5.15 shows an elevation view of three SM1 building models.

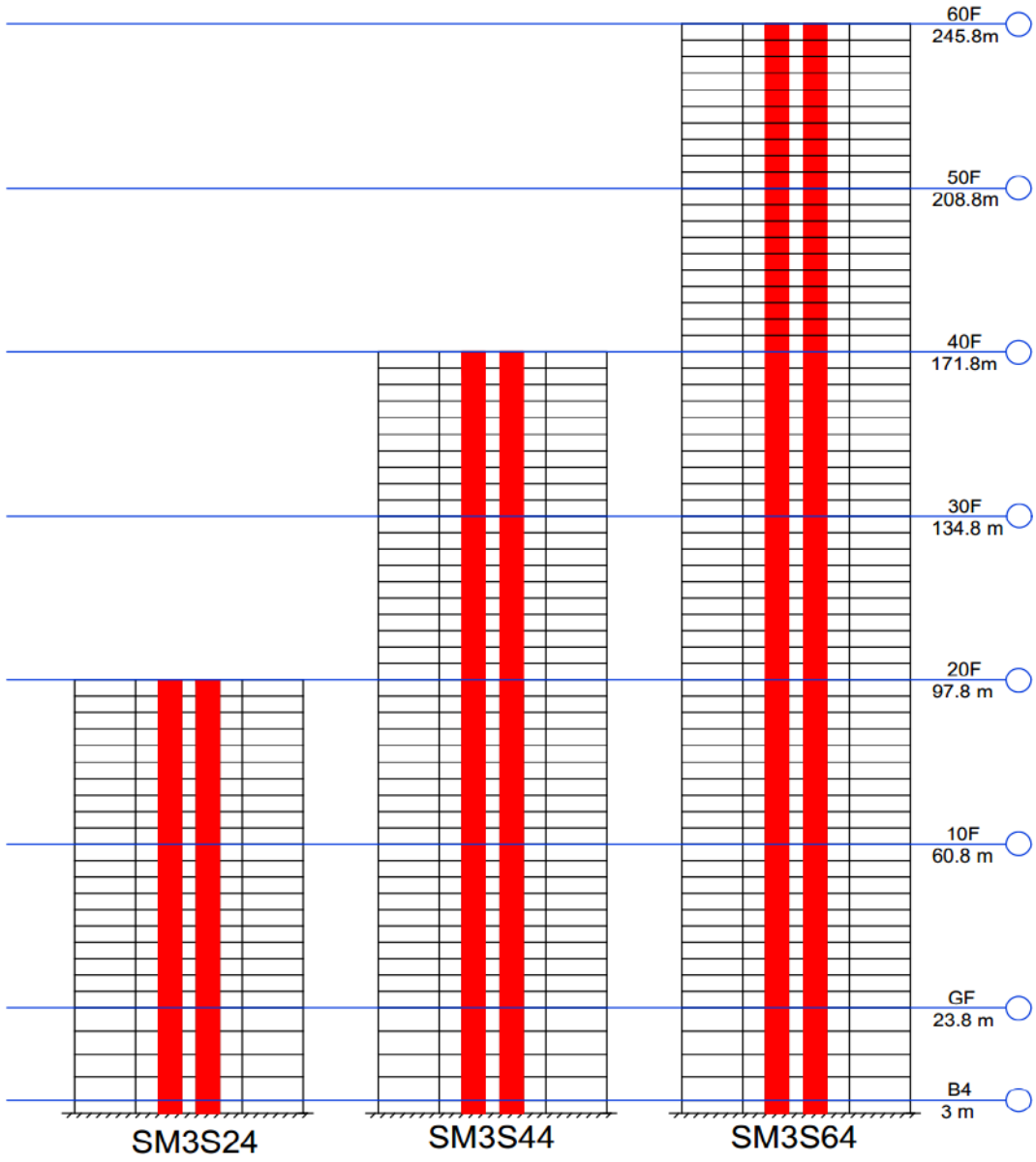

Figure 5.15: Elevation of SM3 Tall Buildings

Table 5.10 shows sectional properties of designed section of SM3S24, SM3S44 and SM3S64 tall buildings and Table 5.11 shows design forces of structural elements of SM3S24, SM3S44 and SM3S64 tall buildings.

Table 5.10: Designed Section of SM3 Tall Buildings

Designed Section of SM3 Tall Buildings				
Building		SM3S24	SM3S44	SM3S64
Concrete Grade		M60	M60	M60
Steel Grade		Fe540	Fe540	Fe540
Rebar Grade		HYSD 550D	HYSD 550D	HYSD 550D
Composite Slab	Thickness (mm)	125	125	125
	Reinforcement (Main & Dist)	8ϕ @ 200 mm c/c	8ϕ @ 200 mm c/c	8ϕ @ 200 mm c/c
Beam B1	Total depth (mm)	500	600	700
	Flange Width (mm)	250	300	450
	Flange Thickness (mm)	40	40	60
	Web Thickness (mm)	20	20	30
Beam B2	Section	ISWB 450	ISWB 450	ISWB 450
	Shear stud	20 mm (65 Nos)	20 mm (65 Nos)	20 mm (65 Nos)
Beam B3	Total depth (mm)	550	650	950
	Flange Width (mm)	300	400	650
	Flange Thickness (mm)	45	50	75
	Web Thickness (mm)	25	25	45
Column C1 (B x D x T)	B4 to GF	700X700X45	850X850X50	1000X1000X60
	1F to 10F	700X700X45	850X850X50	1000X1000X60
	11F to 20F	500X500X40	750X750X45	900X900X55
	21F to 30F	-	650X650X40	800X800X55
	31F to 40F	-	500X500X40	700X700X50
	41F to 50F	-	-	650X650X45
	51F to 60F	-	-	600X600X40
Shear Wall Thickness	B4 to GF	350	500	600
	1F to 10F	350	500	600
	11F to 20F	250	400	500
	21F to 30F	-	400	400
	31F to 40F	-	300	400
	41F to 50F	-	-	300
	51F to 60F	-	-	250

Table 5.11: Design Forces of SM3 Tall Buildings

Design Forces of SM3 Tall Buildings				
Element	**Description**	**SM3S24**	**SM3S44**	**SM3S64**
B1	Storey	19F	19F	27F
	Axial Force Nu (kN)	0	0	0
	Shear Force Vu (kN)	612.7	2330.5	406.3
	Bending Moment Mu (kNm)	1393.5	3694.6	2470.1
	Torsional Moment Tu (kNm)	0.022	0.02	0.02
	Governing Load Case	1.5DL + 1.5LL	1.5DL - 1.5PASSPORT_RSY + 0.45PASSPORT_RSX	1.2DL + 1.2LL + 1.2PASSPORT_RSX
B2	Storey	19F	39F	59F
	Axial Force Nu (kN)	0	0	0
	Shear Force Vu (kN)	297.8	297.8	297.8
	Bending Moment Mu (kNm)	952.8	952.8	952.8
	Torsional Moment Tu (kNm)	0	0	0
	Governing Load Case	1.5DL + 1.5LL	1.5DL + 1.5LL	1.5DL + 1.5LL
B3	Storey	B1	GF	B2
	Axial Force Nu (kN)	0	0	0
	Shear Force Vu (kN)	1630.3	2330.5	6624.1
	Bending Moment Mu (kNm)	2609.9	3694.6	10562
	Torsional Moment Tu (kNm)	0.02	0.07	1.36
	Governing Load Case	1.5DL - 1.5PASSPORT_RSY + 0.45PASSPORT_RSX	1.5DL - 1.5PASSPORT_RSY + 0.45PASSPORT_RSX	1.5DL + 1.5PASSPORT_RSY
C1	Storey	B2	B4	B4
	Axial Force Pu (kN)	22656.42	46689.4	85012.3
	Shear Force Vu (kN)	485.2	785.6	2081.7
	Bending Moment Mu2 (kNm)	1443.7	2561.4	2352.1
	Bending Moment Mu3 (kNm)	731.6	894.23	4841.4
	Torsional Moment Tu (kNm)	0	7.07	25.12
	Governing Load Case	1.5DL - 1.5PASSPORT_RSY + 0.45PASSPORT_RSX	1.5DL - 1.5PASSPORT_RSY + 0.45PASSPORT_RSX	1.5DL - 1.5PASSPORT_RSX + 0.45PASSPORT_RSY
SW	Storey	B4	B4	B4
	Axial Force Pu (kN)	25411	47678.5	75862.7
	Shear Force Vu (kN)	4238.7	5275.6	10308.6
	Bending Moment Mu (kNm)	45018.8	57120.3	58562.8
	Governing Load Case	1.5DL - 1.5PASSPORT_RSY + 0.45PASSPORT_RSX	0.9DL - 1.5PASSPORT_RSY + 0.45PASSPORT_RSX	1.5DL - 1.5PASSPORT_RSY + 0.45PASSPORT_RSX

Based on the results of SM1, SM2, and SM3 tall buildings in terms of strength and serviceability criteria, it can be concluded that SM1 tall buildings meet both strength and serviceability standards more effectively. Therefore, the same core structural plan is selected for tubular and outrigger systems as for SM1 tall buildings.

5.9 Tubular (TB) System

The structural configuration, designed sections, design forces, and governing load cases for 24-story, 44-story, and 64-story tall tubular steel-concrete composite tall buildings are described in this section. Typical floor plan of TB tall buildings is shown in Fig. 5.16. Here, B2 beams shown in Fig. 5.16 are secondary composite beams while B1 and B3 are main primary beams. C1 represents composite columns and SW represents RCC shear walls.

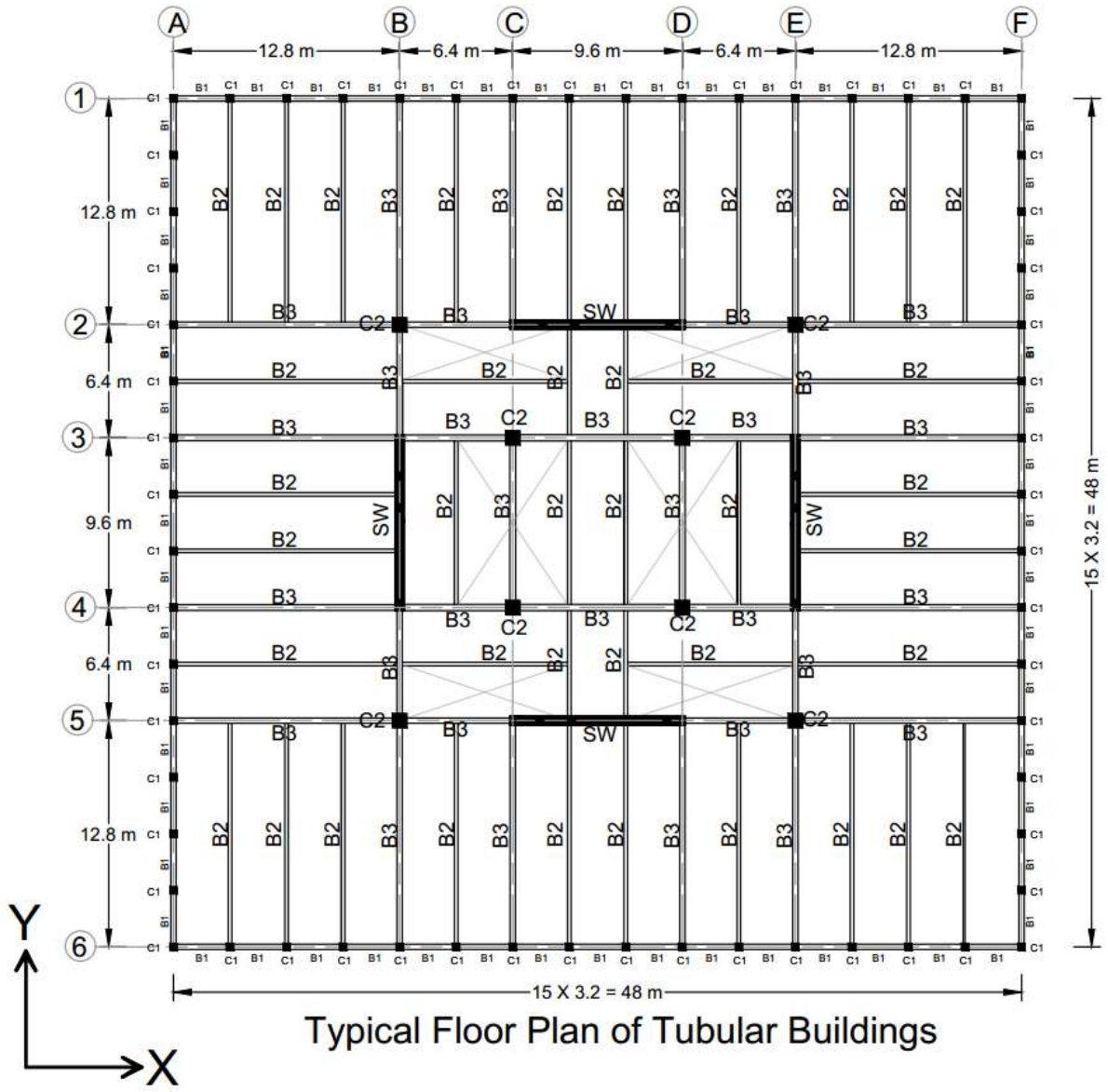

Figure 5.16: Typical Floor Plan of TB Tall Buildings

The TBS24, TBS44, and TBS64 models of TB tall structures with 24, 44, and 64

floors respectively are analysed and developed in accordance with applicable Indian and AISC 360-10 requirements. Figure 5.17 shows an elevation view of three SM1 building models.

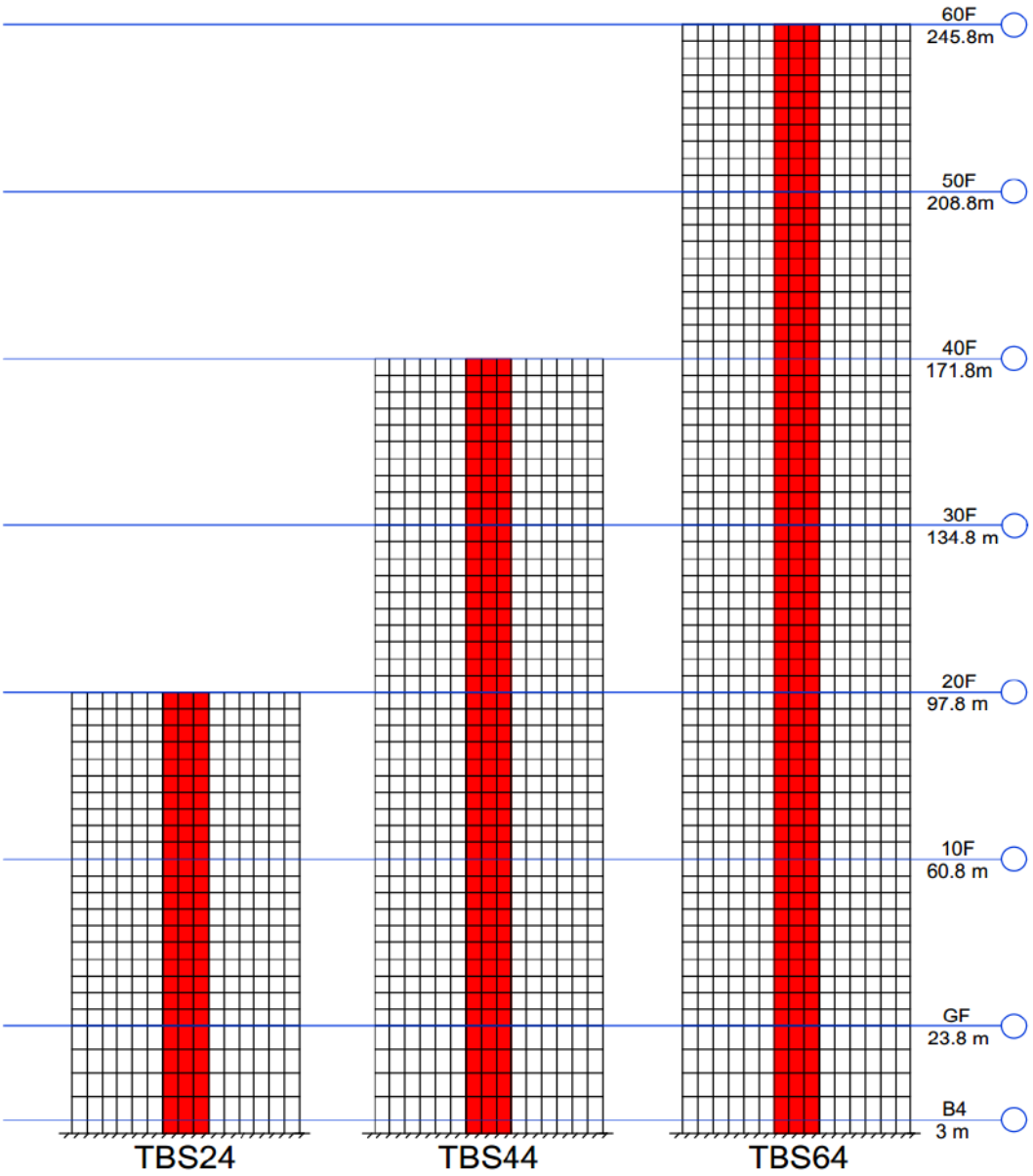

Figure 5.17: Elevation of TB Tall Buildings

Table 5.12 shows sectional properties of designed section of TBS24, TBS44 and TBS64 tall buildings and Table 5.13 shows design forces of structural elements of TBS24, TBS44 and TBS64 tall buildings.

Table 5.12: Designed Section of TB Tall Buildings

Designed Section of TB Tall Buildings				
Building		TBS24	TBS44	TBS64
Concrete Grade		M60	M60	M60
Steel Grade		Fe540	Fe540	Fe540
Rebar Grade		HYSD 550D	HYSD 550D	HYSD 550D
Composite Slab	Thickness (mm)	125	125	125
	Reinforcement (Main & Dist)	8ϕ @ 200 mm c/c	8ϕ @ 200 mm c/c	8ϕ @ 200 mm c/c
Beam B1	Total depth (mm)	500	450	500
	Flange Width (mm)	250	250	300
	Flange Thickness (mm)	40	40	50
	Web Thickness (mm)	20	25	25
Beam B2	Section	ISWB 450	ISWB 450	ISWB 450
	Shear stud	20 mm (65 Nos)	20 mm (65 Nos)	20 mm (65 Nos)
Beam B3	Total depth (mm)	350	550	650
	Flange Width (mm)	150	250	400
	Flange Thickness (mm)	30	50	55
	Web Thickness (mm)	15	25	30
Column C1 (B x D x T)	B4 to GF	350X350X30	450X450X35	600X600X40
	1F to 10F	350X350X30	450X450X35	600X600X40
	11F to 20F	350X350X25	450X450X30	550X550X40
	21F to 30F	-	400X400X30	550X550X30
	31F to 40F	-	350X350X25	450X450X30
	41F to 50F	-	-	400X400X30
	51F to 60F	-	-	400X400X25
Column C2 (B x D x T)	B4 to GF	600X600X40	800X800X50	1000X1000X60
	1F to 10F	600X600X40	800X800X50	1000X1000X60
	11F to 20F	450X450X30	700X700X45	900X900X60
	21F to 30F	-	650X650X45	850X850X55
	31F to 40F	-	550X550X40	750X750X55
	41F to 50F	-	-	600X600X50
	51F to 60F	-	-	500X500X40
Shear Wall Thickness	B4 to GF	400	500	650
	1F to 10F	400	500	650
	11F to 20F	250	400	600
	21F to 30F	-	350	500
	31F to 40F	-	250	400
	41F to 50F	-	-	350
	51F to 60F	-	-	250

Table 5.13: Design Forces of TB Tall Buildings

Design Forces of TB Tall Buildings				
Element	**Description**	**TBS24**	**TBS44**	**TBS64**
B1	Storey	3F	19F	9F
	Axial Force Nu (kN)	0	0	0
	Shear Force Vu (kN)	625.9	1530	1027.6
	Bending Moment Mu (kNm)	1420.3	560	1313.7
	Torsional Moment Tu (kNm)	0.045	0.1	0.05
	Governing Load Case	1.5DL + 1.5LL	1.2DL + 1.2LL + 1.2PASSPORT_RSx	1.5DL + 1.5DWLY
B2	Storey	19F	39F	59F
	Axial Force Nu (kN)	0	0	0
	Shear Force Vu (kN)	297.8	297.8	297.8
	Bending Moment Mu (kNm)	952.8	952.8	952.8
	Torsional Moment Tu (kNm)	0	0	0
	Governing Load Case	1.5DL + 1.5LL	1.5DL + 1.5LL	1.5DL + 1.5LL
B3	Storey	9F	9F	2F
	Axial Force Nu (kN)	0	0	0
	Shear Force Vu (kN)	479.63	664.5	1110
	Bending Moment Mu (kNm)	1364.3	1923.1	3230.5
	Torsional Moment Tu (kNm)	0.2	0.03	0.08
	Governing Load Case	1.5DL + 1.5PASSPRT_RSY	1.5DL + 1.5PASSPRT_RSY	1.5DL + 1.5PASSPRT_RSY
C1	Storey	B2	B2	GF
	Axial Force Pu (kN)	6492.4	10959.9	18336.6
	Shear Force Vu (kN)	238.3	268.3	367.2
	Bending Moment Mu2 (kNm)	14.6	35.84	384.1
	Bending Moment Mu3 (kNm)	645.32	774	994.4
	Torsional Moment Tu (kNm)	0	0	0
	Governing Load Case	1.5DL + 1.5LL	1.5DL + 1.5LL	1.5DL - 1.5PASSPORT_RSX + 0.45PASSPORT_RSY
C2	Storey	B2	B4	GF
	Axial Force Pu (kN)	18560.9	40329.3	48470.8
	Shear Force Vu (kN)	377.6	597.9	437.2
	Bending Moment Mu2 (kNm)	306.2	774.1	1142.61
	Bending Moment Mu3 (kNm)	1088.4	1788.3	1217.83
	Torsional Moment Tu (kNm)	0	1.98	0
	Governing Load Case	1.2DL + 1.2LL - 1.2PASSPORT_RSX	1.5DL - 1.5PASSPORT_RSX + 0.45PASSPORT_RSY	1.5DL - 1.5PASSPORT_RSY + 0.45PASSPORT_RSX
SW	Storey	B4	B4	B4
	Axial Force Pu (kN)	22694.91	74304.5	11590.7
	Shear Force Vu (kN)	11131.6	12388.6	17481.9
	Bending Moment Mu (kNm)	222215.9	272636.6	360601.4
	Governing Load Case	0.9DL - 1.5PASSPORT_RSY + 0.45PASSPORT_RSX	1.5DL - 1.5PASSPORT_RSY + 0.45PASSPORT_RSX	1.5DL - 1.5PASSPORT_RSY + 0.45PASSPORT_RSX

5.10 Outrigger and Belt Truss System (OR) System

The structural configuration, designed sections, design forces, and governing load cases for 24-story, 44-story, and 64-story tall outrigger steel-concrete composite tall buildings are described in this section. Typical floor plan of OR tall buildings is shown in Fig. 5.18 and floor plan of outrigger floors is shown in Fig. 5.19. Here, B2 beams shown in Figures 5.18 and 5.19 are secondary composite beams while B1,B3 and OB are main primary beams. OD represents diagonal bracing at outrigger floors, C1 represents composite columns and SW represents RCC shear walls. 3D view of outrigger floors of OR system is also shown in Fig. 5.20.

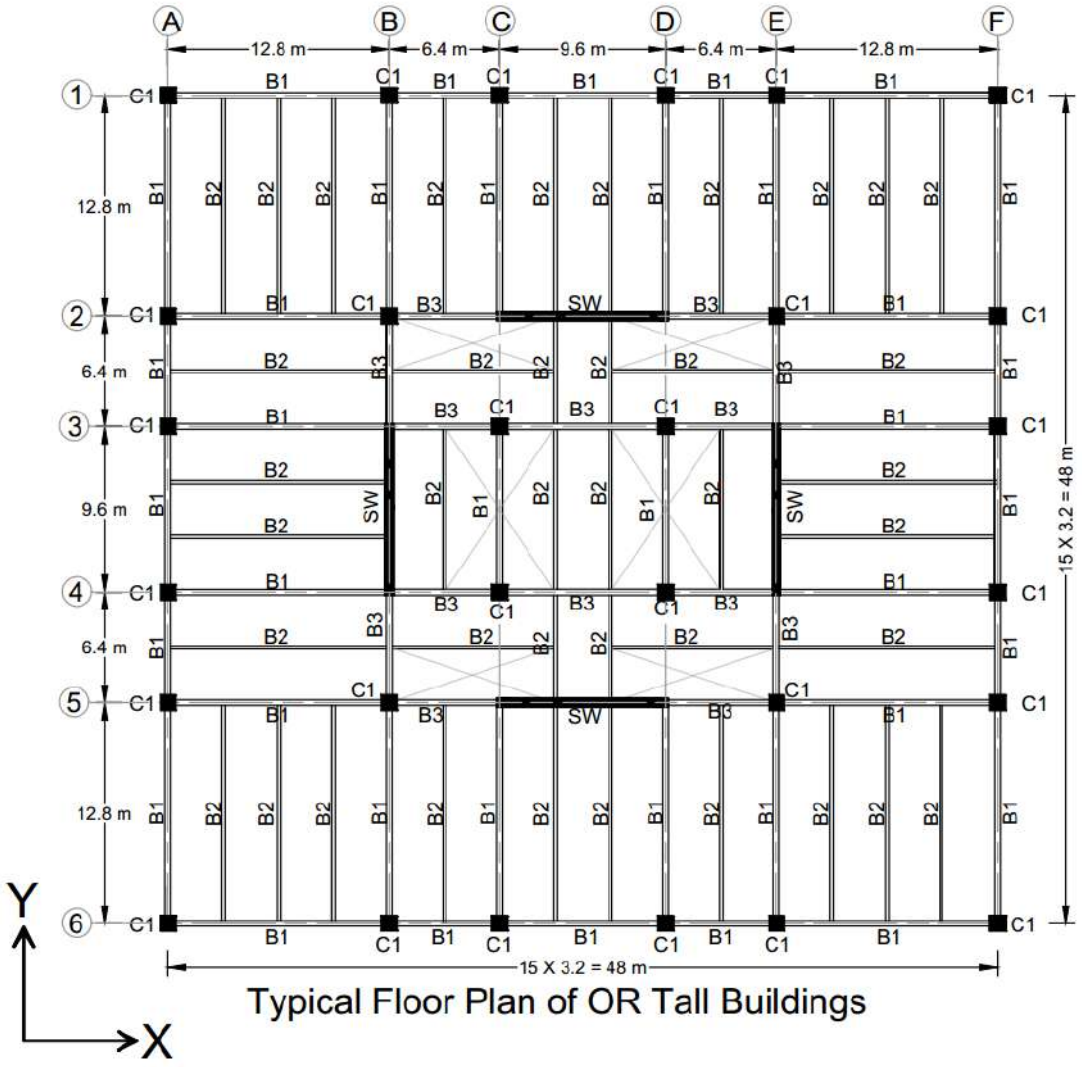

Figure 5.18: Typical Floor Plan of OR Tall Buildings

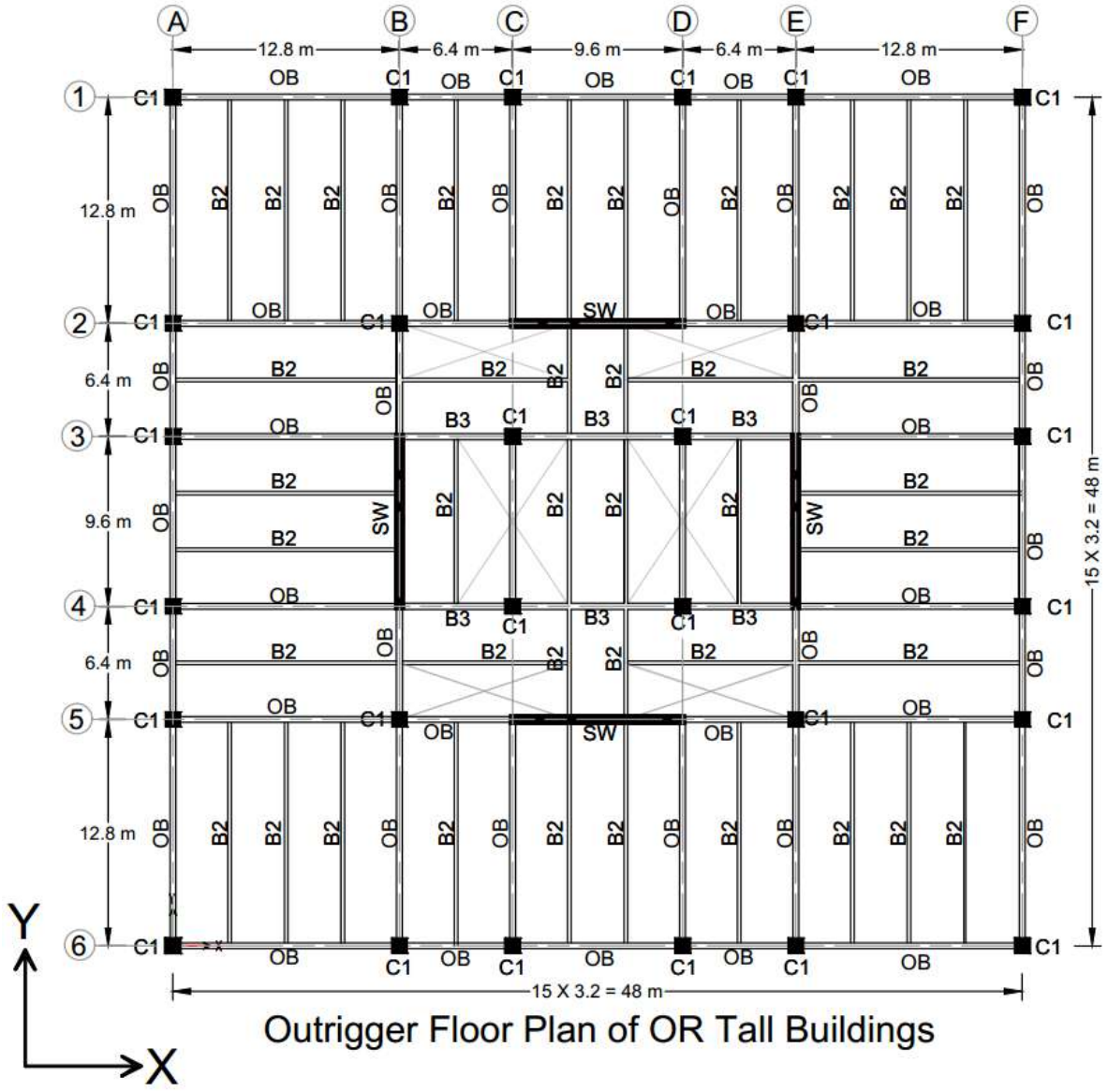

Figure 5.19: Outrigger Floor Plan of OR Tall Buildings

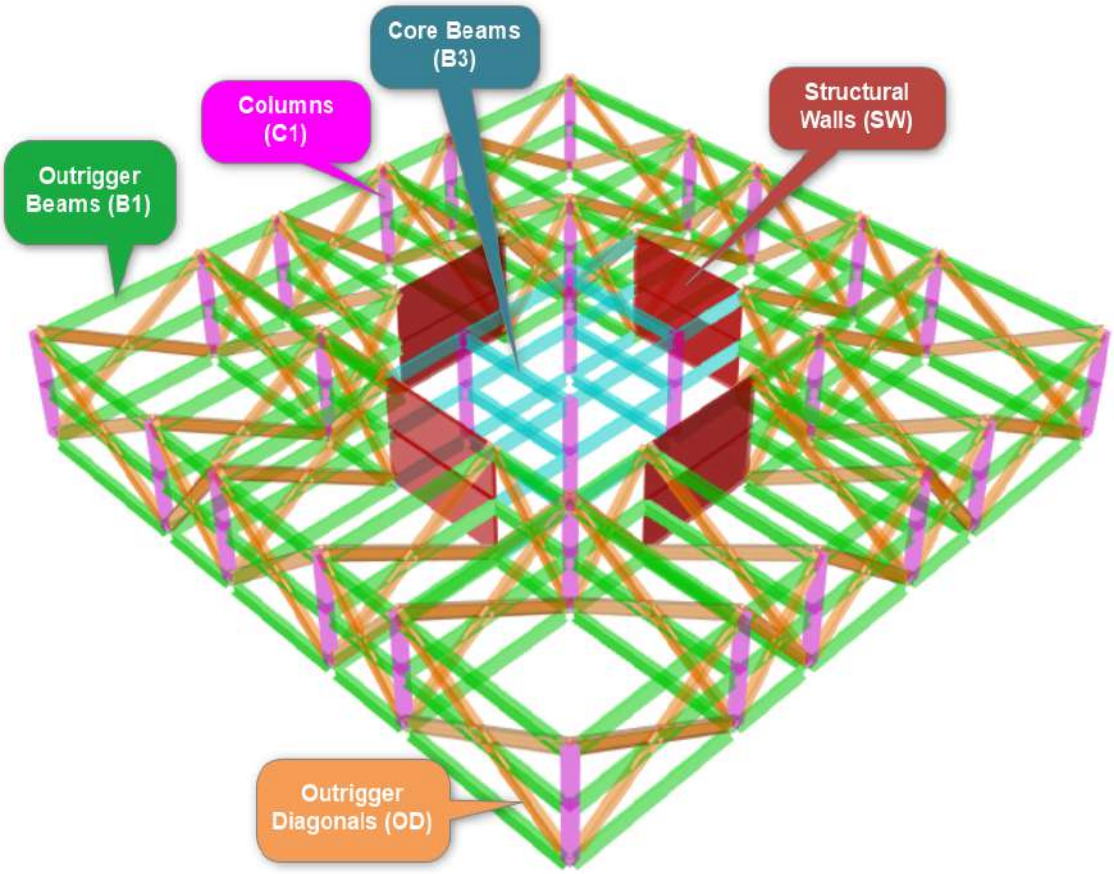

Figure 5.20: 3D View of Outrigger Floors

The OR724, OR17S44 and OR27S64 of OR tall structures with 24, 44 and 64 floors with one outrigger at 7^{th}, 17^{th} and 27^{th} floor respectively are analysed and developed in accordance with applicable Indian and AISC 360-10 requirements. Additional outrigger tall building OR27&59S64 with two outriggers at 27^{th} and 59^{th} floor is also analysed and designed to study the efficiency of outrigger with varying number of outriggers in tall buildings. Figure 5.21 shows an elevation view of three OR building models.

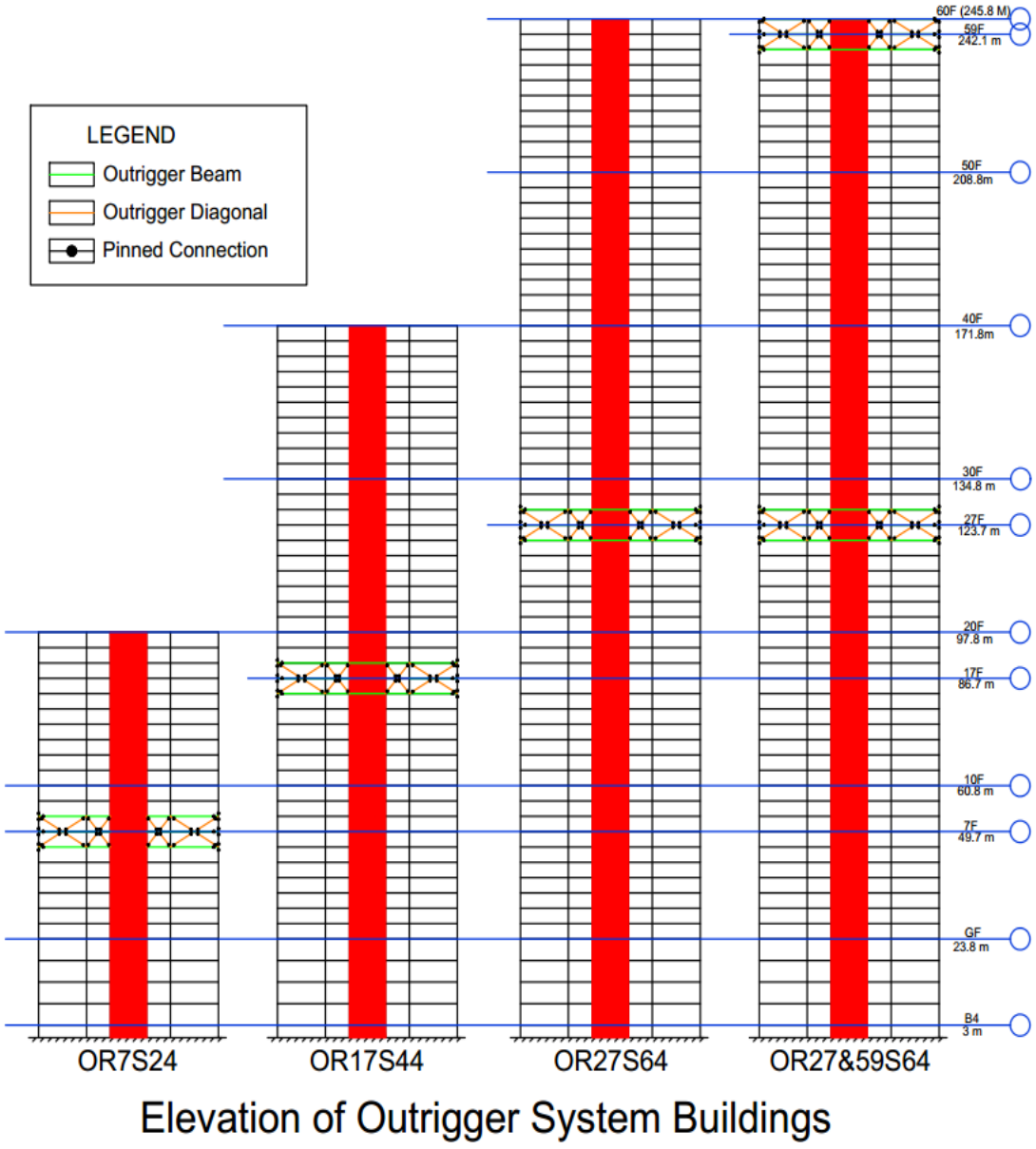

Figure 5.21: Elevation of OR Tall Buildings

Table 5.14 shows sectional properties of designed section of OR724, OR17S44, OR27S64 and OR59S64 tall buildings and Table 5.15 shows design forces of structural elements of OR724, OR17S44, OR27S64 and OR59S64 tall buildings.

Table 5.14: Designed Section of OR Tall Buildings

Designed Section of OR Tall Buildings					
Building		OR7S24	OR17S24	OR27S64	OR27&59S64
Concrete Grade		M60	M60	M60	M60
Steel Grade		Fe540	Fe540	Fe540	Fe540
Rebar Grade		HYSD 550D	HYSD 550D	HYSD 550D	HYSD 550D
Composite Slab	Thickness (mm)	125	125	125	125
	Reinforcement (Main & Dist)	8ϕ @ 200 mm c/c	8ϕ @ 200 mm c/c	8ϕ @ 200 mm c/c	8ϕ @ 200 mm c/c
Beam B1	Total depth (mm)	800	650	700	700
	Flange Width (mm)	450	300	450	450
	Flange Thickness (mm)	60	40	60	60
	Web Thickness (mm)	30	20	30	30
Beam B2	Section	ISWB 450	ISWB 450	ISWB 450	ISWB 450
	Shear stud	20 mm (65 Nos)	20 mm (65 Nos)	20 mm (65 Nos)	20 mm (65 Nos)
Beam B3	Total depth (mm)	800	650	750	750
	Flange Width (mm)	450	300	450	450
	Flange Thickness (mm)	60	40	60	60
	Web Thickness (mm)	30	20	30	30
Outrigger Beam OB	Total depth (mm)	800	650	750	750
	Flange Width (mm)	450	350	450	450
	Flange Thickness (mm)	60	50	60	60
	Web Thickness (mm)	30	25	30	30
Outrigger Diagonal OD	Total depth (mm)	800	700	750	750
	Flange Width (mm)	400	350	450	450
	Flange Thickness (mm)	60	50	60	60
	Web Thickness (mm)	30	25	30	30
Column C1 (B x D x T)	B4 to GF	700X700X45	700X700X50	950X950X60	950X950X60
	1F to 10F	700X700X45	700X700X50	950X950X60	950X950X60
	11F to 20F	500X500X40	600X600X45	850X850X55	850X850X55
	21F to 30F	-	500X500X40	750X750X50	750X750X50
	31F to 40F	-	450X450X40	650X650X45	650X650X45
	41F to 50F	-	-	600X600X40	600X600X40
	51F to 60F	-	-	500X500X40	500X500X40
Shear Wall Thickness	B4 to GF	450	450	625	625
	1F to 10F	300	450	625	625
	11F to 20F	250	350	450	450
	21F to 30F	-	300	400	400
	31F to 40F	-	250	350	350
	41F to 50F	-	-	300	300
	51F to 60F	-	-	250	250

Table 5.15: Design Forces of OR Tall Buildings

Design Forces of OR Tall Buildings					
Element	**Description**	**OR7S24**	**OR17S44**	**OR27S64**	**OR27&59S65**
B1	Storey	19F	3F	1F	11F
	Axial Force Nu (kN)	0	0	0	0
	Shear Force Vu (kN)	4068.75	388.7	352.1	351.3
	Bending Moment Mu (kNm)	2020.9	1658.4	2277.8	2273
	Torsional Moment Tu (kNm)	0.021	0.073	0.372	0.4
	Governing Load Case	1.5DL + 1.5PASSPORT_RSY	1.2DL + 1.2LL - 1.2DWLX	1.5DL - 1.5DWLY	1.5DL - 1.5DWLY
B2	Storey	19F	39F	59F	59F
	Axial Force Nu (kN)	0	0	0	0
	Shear Force Vu (kN)	298.2	297.8	296.8	296.8
	Bending Moment Mu (kNm)	952.83	952.83	952.83	952.83
	Torsional Moment Tu (kNm)	0	0	0	0
	Governing Load Case	1.5DL + 1.5LL	1.5DL + 1.5LL	1.5DL + 1.5LL	1.5DL + 1.5LL
B3	Storey	GF	3F	1F	1F
	Axial Force Nu (kN)	0	0	0	0
	Shear Force Vu (kN)	1597.6	823.7	1654.5	1651
	Bending Moment Mu (kNm)	5317.6	2529.1	5222.8	5211.4
	Torsional Moment Tu (kNm)	0.374	0.058	0.021	0.1
	Governing Load Case	1.5DL + 1.5PASSPORT_RSY	1.5DL - 1.5DWLY	1.5DL + 1.5PASSPORT_RSY	1.5DL + 1.5PASSPORT_RSY
OB	Storey	8F	18F	28F	60F
	Axial Force Nu (kN)	0	0	0	0
	Shear Force Vu (kN)	4068.8	713.4	913.3	125.1
	Bending Moment Mu (kNm)	2760.1	2996.2	5189.9	4444.81
	Torsional Moment Tu (kNm)	0.025	0	0	0
	Governing Load Case	1.5DL + 1.5LL	1.5DL + 1.5LL	1.5DL + 1.5LL	1.5DL + 1.5LL
OD	Storey	7F	17F	28F	28F
	Axial Force Nu (kN)	4439.6	2650.3	4181.6	3954.8
	Shear Force Vu (kN)	0	0	0	0
	Bending Moment Mu (kNm)	0	0	0	0
	Torsional Moment Tu (kNm)	0	0	0	0
	Governing Load Case	1.5DL + 1.5PASSPORT_RSY	1.5DL - 1.5DWLY	1.5DL + 1.5PASSPORT_RSX	1.5DL + 1.5PASSPORT_RSX
C1	Storey	B4	B4	B4	B4
	Axial Force Pu (kN)	22103.5	32933.2	67689.9	68110
	Shear Force Vu (kN)	1152.3	413.9	1272.5	1280.5
	Bending Moment Mu2 (kNm)	1044.1	1072.8	1857.95	1864.1
	Bending Moment Mu3 (kNm)	3018.9	489.9	3502.8	3523.2
	Torsional Moment Tu (kNm)	0.02	0.493	0.431	6.11
	Governing Load Case	1.5DL - 1.5PASSPORT_RSX + 0.45PASSPORT_RSY	1.5DL - 1.5PASSPORT_RSY + 0.45PASSPORT_RSX	1.5DL - 1.5PASSPORT_RSX + 0.45PASSPORT_RSY	1.5DL - 1.5PASSPORT_RSX + 0.45PASSPORT_RSY
SW	Storey	B4	B4	B4	B4
	Axial Force Pu (kN)	20831.6	38892.1	109495.9	110197.1
	Shear Force Vu (kN)	17844.1	11474.2	18484.6	18439.1
	Bending Moment Mu (kNm)	265087.6	234094.6	337581.8	337085.7
	Governing Load Case	0.9Dl - 1.5PASSPORT_RSY + 0.45PASSPRT_RSX	1.5DL - 1.5DWLY	1.5DL - 1.5PASSPORT_RSY + 0.45PASSPORT_RSX	1.5DL - 1.5PASSPORT_RSY + 0.45PASSPORT_RSX

5.11 Summary

This chapter contains a comprehensive analysis and design of three steel-concrete composite tall building systems of 24, 44, and 64 stories. It includes the building plan, elevations, estimations of gravity and lateral loads, sections of structural members, and design forces in structural members for the Structural Wall-Moment Frame (SM), Tubular (TB), and Outrigger and Belt Truss (OR) systems. It also contains design procedures for various structural elements.

Chapter 6

Results and Discussion

6.1 General

In this chapter, analysis results in terms of Time period, Modal Participating Mass Ratio, Base Shear, Storey Shear, Storey Displacements, Inter-Story Drift Ratio, Contribution of Structural Walls in resisting lateral loads and Structural Weight are presented and discussed for the Structural Wall-Moment Frame (SM), Tubular (TB), and Outrigger and Belt Truss (OR) systems. Comparative analysis of these three systems is also presented in this chapter.

6.2 Structural Wall-Moment Frame System

The parametric study to find out effective structural wall positions is carried out. Results of three different structural wall positions (SM1, SM2 and SM3) in SWMF system are shown in this section.

6.2.1 SM1 SWMF System

6.2.1.1 Base Shear

Base shear for various lateral load cases in SM1S24, SM1S44 and SM1S64 are shown in Figures 6.1a, 6.1b and 6.1c respectively. Story shear for various lateral load cases in SM1S24, SM1S44 and SM1S64 are shown in Figures 6.2a, 6.2b and 6.2c respectively.

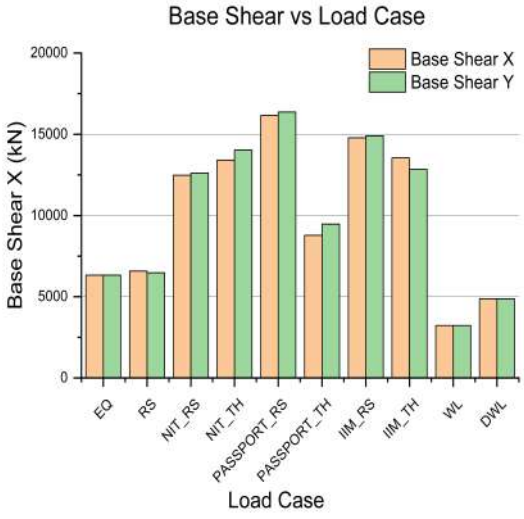

(a) Base Shear of SM1S24

(b) Base Shear of SM1S44

(c) Base Shear of SM1S64

Figure 6.1: Base Shear of SM1 Tall Buildings

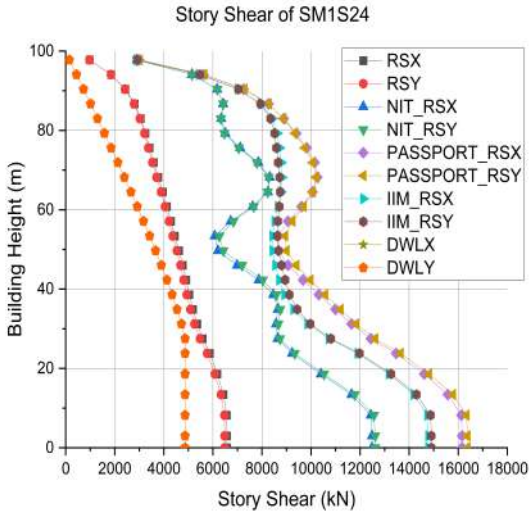

(a) Story Shear of SM1S24

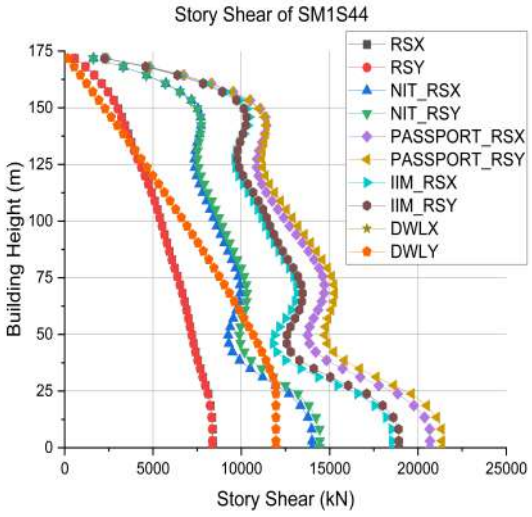

(b) Story Shear of SM1S44

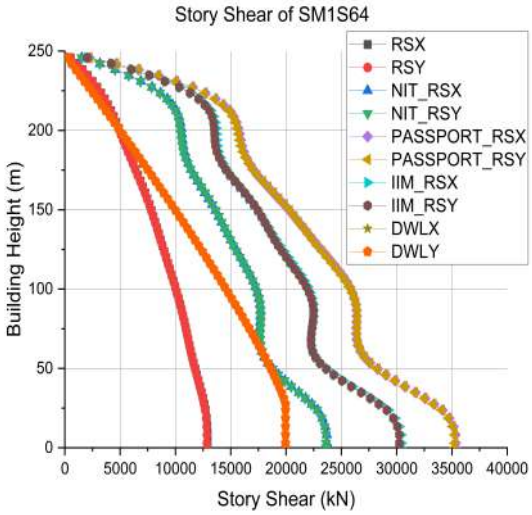

(c) Story Shear of SM1S64

Figure 6.2: Story Shear of SM1 Tall Buildings

From the results of Fig. 6.1 and Fig. 6.2, base shear of NIT_RS, PASSPORT_RS, IIM_RS and DWL are between 159.6% to 190%, 235.9% to 273.6%, 211.4% to 235.5% and 74.03% to 154.5% of RS load case respectively. This shows that, PASSPORT_RS from SSRSA gives maximum base shear and base shear due to DWL load case from DGF analysis increases exponentially as building height increases from 24 story SM1 tall building to 64 story SM1 tall building.

6.2.1.2 Natural Time Period and Modal Participating Mass Ratio

In accordance with clause 7.7.5.2 of IS 1893 (Part 1):2016[47], for the analysis of earthquake shaking in the considered direction, the number of modes shall be such that the sum of their modal masses is at least 90% of the overall seismic mass. The natural time period and modal participation mass ratios for SM1S24, SM1S44, and SM1S64 are depicted in Tables 6.1, 6.2, and 6.3, respectively. Based on the results of these tables, it can be stated that the number of modes addressed for analysis in all models is adequate for earthquake load analysis.

Table 6.1: Time Period and Modal Participating Mass Ratio of SM1S24

Mode	**Time Period (Sec)**	**UX**	**UY**	**RZ**
1	3.68	0.00	0.74	0.00
2	3.63	0.74	0.00	0.00
3	3.26	0.00	0.00	0.77
4	1.10	0.00	0.00	0.11
5	1.00	0.00	0.13	0.00
6	1.00	0.13	0.00	0.00
7	0.53	0.00	0.00	0.04
8	0.46	0.00	0.05	0.00
9	0.46	0.05	0.00	0.00
10	0.31	0.00	0.00	0.02
11	0.26	0.00	0.03	0.00
12	0.26	0.03	0.00	0.00

Table 6.2: Time Period and Modal Participating Mass Ratio of SM1S44

Mode	**Time Period (Sec)**	**UX**	**UY**	**RZ**
1	5.34	0.00	0.75	0.00
2	5.20	0.75	0.00	0.00
3	4.68	0.00	0.00	0.78
4	1.67	0.00	0.12	0.00
5	1.64	0.12	0.00	0.00
6	1.64	0.00	0.00	0.10
7	0.91	0.00	0.00	0.04
8	0.86	0.00	0.04	0.00
9	0.85	0.04	0.00	0.00
10	0.59	0.00	0.00	0.02
11	0.54	0.00	0.02	0.00
12	0.53	0.02	0.00	0.00

Table 6.3: Time Period and Modal Participating Mass Ratio of SM1S64

Mode	**Time Period (Sec)**	**UX**	**UY**	**RZ**
1	6.48	0.00	0.72	0.00
2	6.31	0.72	0.00	0.00
3	5.52	0.00	0.00	0.76
4	2.20	0.00	0.14	0.00
5	2.16	0.14	0.00	0.00
6	1.96	0.00	0.00	0.11
7	1.19	0.00	0.05	0.00
8	1.18	0.05	0.00	0.00
9	1.16	0.00	0.00	0.04
10	0.79	0.00	0.00	0.02
11	0.78	0.00	0.02	0.00
12	0.78	0.02	0.00	0.00

Figure 6.3 depicts the time period for the first three modes of vibration in buildings SM1S24, SM1S44, and SM1S64. From Fig. 6.3, it can be deduced that as building height grows, time period values increase and the probability of torsional mode of vibration occurring as the first fundamental mode of vibration of building diminishes.

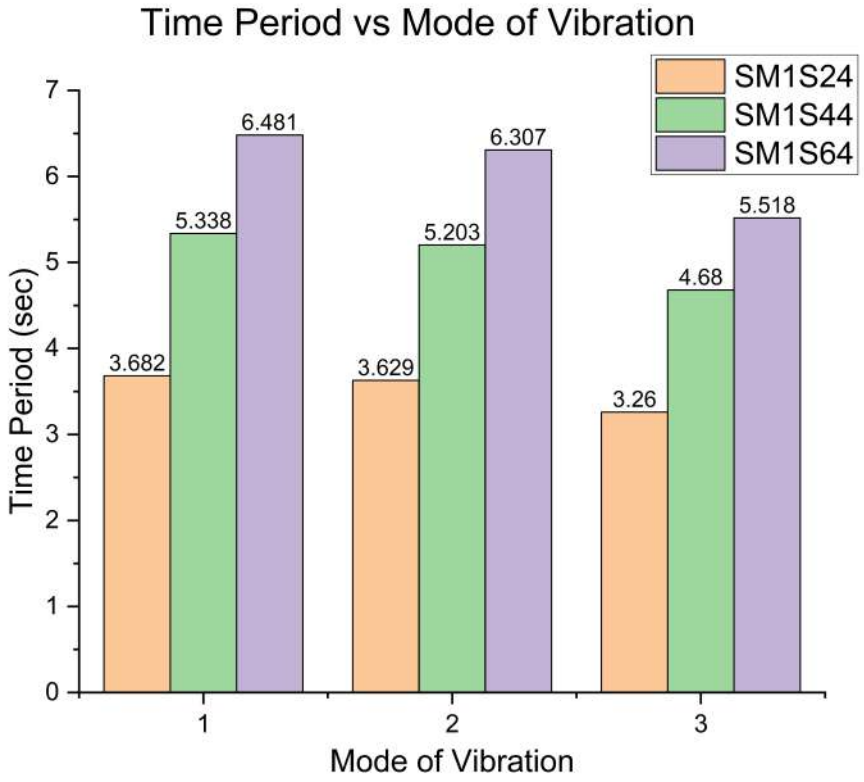

Figure 6.3: Time Period of SM1 Tall Buildings

6.2.1.3 Story Displacements

Story displacements are an essential criterion for tall building serviceability. As the height of a structure grows, top story displacement becomes the driving criterion for the majority of tall structures. In accordance with clause 20.5 of IS 456: 2000[44] and table 6 of IS 800: 2007[45], the displacement of the top storey of any building must be less than (building height)/500. So, the allowable maximum top storey displacement for models SM1S24, SM1S44 and SM1S64 are 195.6 mm, 269.6 mm and 343.6 mm, respectively. The Figures 6.4a, 6.4b, and 6.4c depict the story displacements of SM1S24, SM1S44, and SM1S64 tall buildings under various combinations of lateral loads respectively.

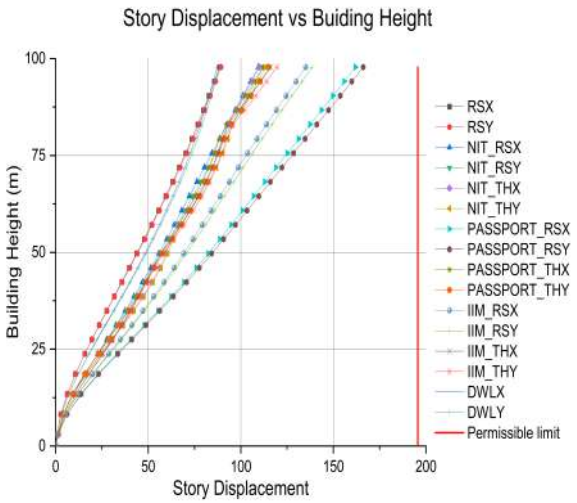

(a) Story Displacements of SM1S24

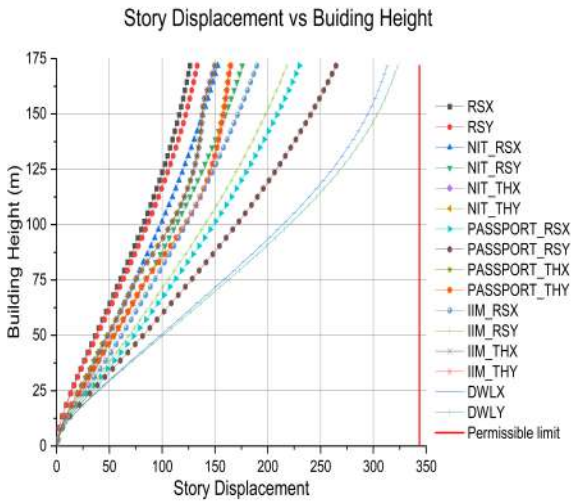

(b) Story Displacements of SM1S44

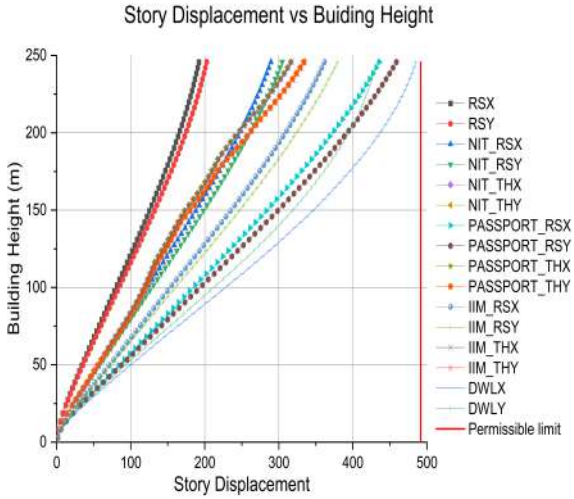

(c) Story Displacements of SM1S64

Figure 6.4: Story Displacements of SM1 Tall Buildings

From the results of story displacements, it can be determined that the story displacements of all SM1 tall structures fall within the allowable range. As the number of stories increases, the wind load combination utilising the DWL load case from the DGF analysis becomes increasingly significant, and the displacement of the top story owing to this load combination approaches the allowable limit.

6.2.1.4 Inter-Story Drift Ratio

Inter-story drift ratio has a significant influence in determining human comfort level and the design of non-structural components in tall buildings. According to clause 7.11 of IS

1893: 2016[47], the permitted limit for inter-story drift ratio of a structure under service loads is 0.004 times the height of each level. In addition, IS 16700: 2017[48] stipulates that the permitted maximum inter-story drift ratio of factored earthquake load combinations for tall buildings must not exceed storey height/250. Thus, allowable maximum ISDR for models SM1S24, SM1S44 and SM1S64 is 0.0148. Figures 6.5a, 6.5b, and 6.5c represent the ISDR for SM1S24, SM1S44, and SM1S64 tall structures for various load combinations under maximum codal requirements of IS 1893: 2016[47] and IS 16700: 2017[48]. It is observed that ISDR for all SM1 buildings are within limits and maximum ISDR is found in case of PASSPORT_RS load case.

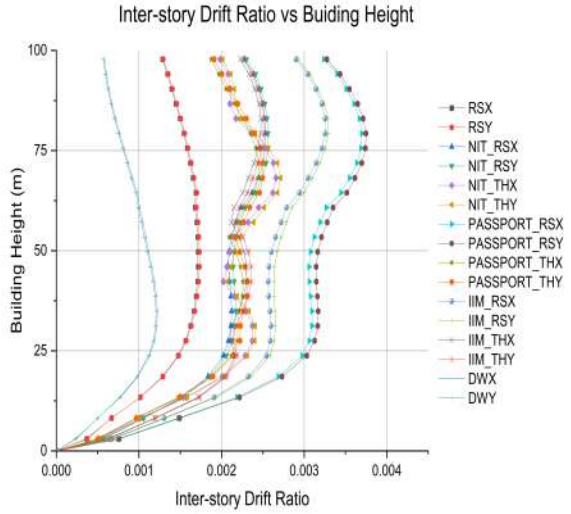

(a) ISDR of SM1S24

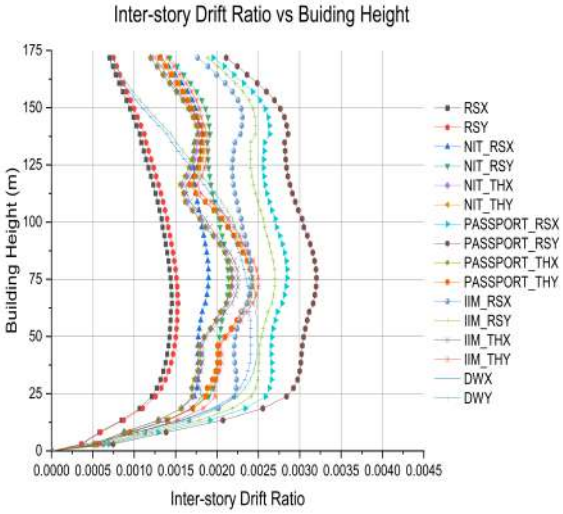

(b) ISDR of SM1S44

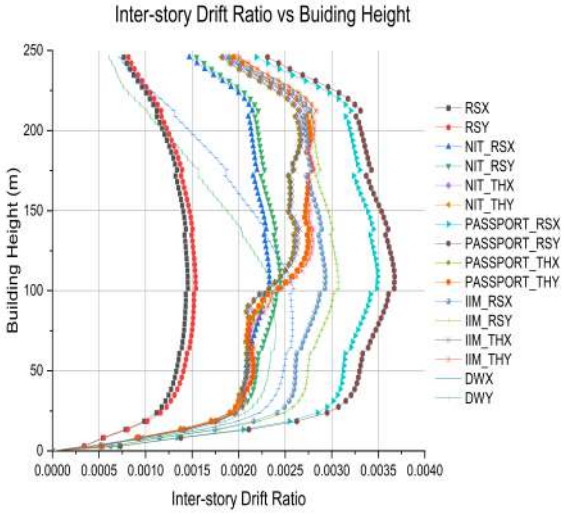

(c) ISDR of SM1S64

Figure 6.5: ISDR of SM1 Tall Buildings

6.2.2 SM2 SWMF System

6.2.2.1 Base Shear

Base shear for various lateral load cases in SM2S24, SM2S44 and SM2S64 are shown in Figures 6.6a, 6.6b and 6.6c respectively. Story shear for various lateral load cases in SM2S24, SM2S44 and SM2S64 are shown in Figures 6.7a, 6.7b and 6.7c respectively.

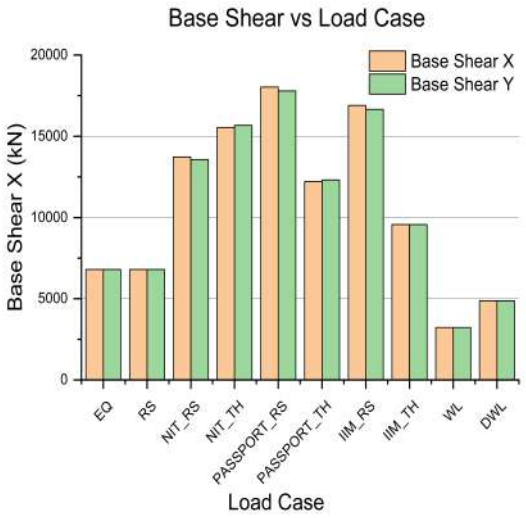

(a) Base Shear of SM2S24

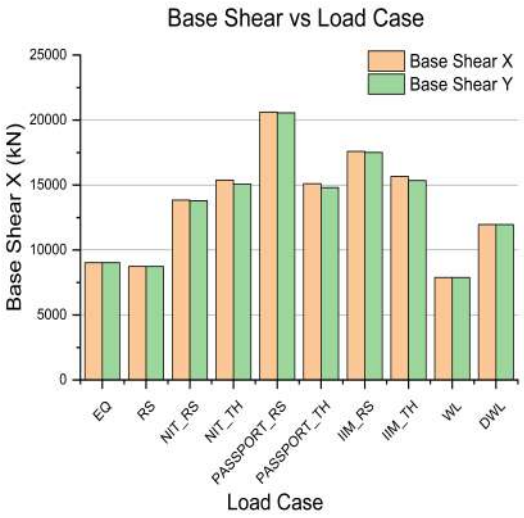

(b) Base Shear of SM2S44

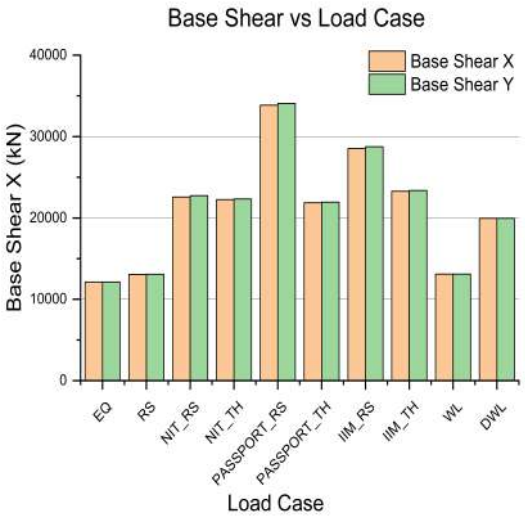

(c) Base Shear of SM2S64

Figure 6.6: Base Shear of SM2 Tall Buildings

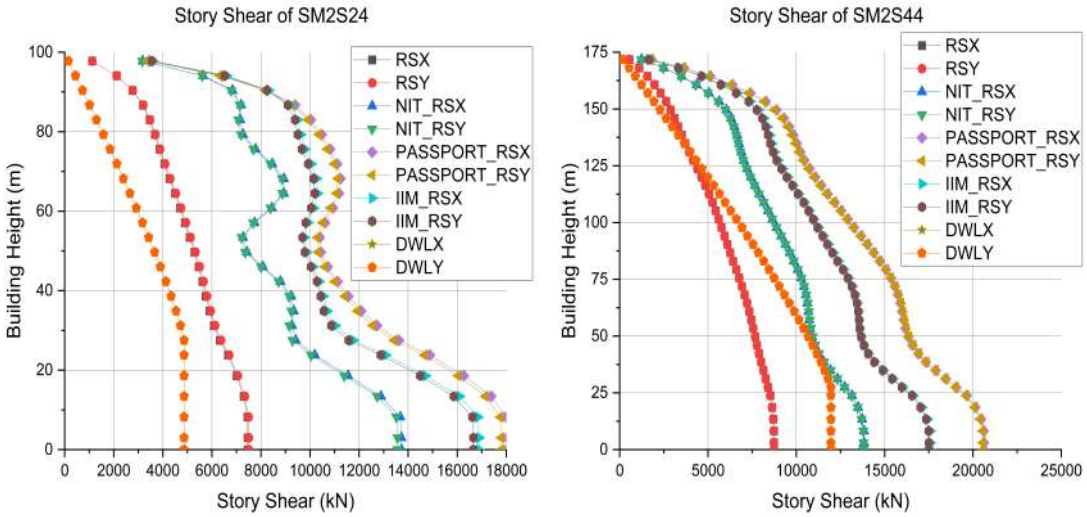

(a) Story Shear of SM2S24 (b) Story Shear of SM2S44

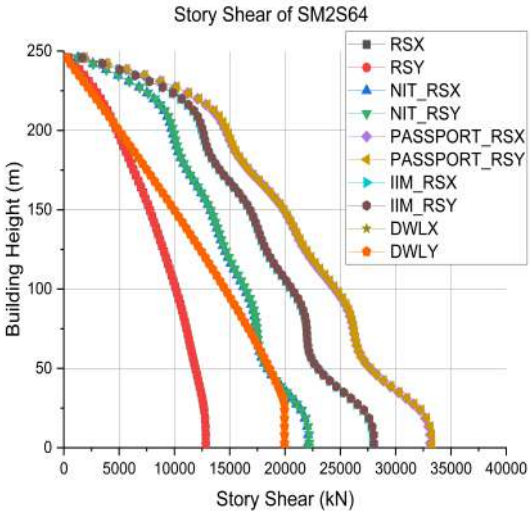

(c) Story Shear of SM2S64

Figure 6.7: Story Shear of SM2 Tall Buildings

From the results of Fig. 6.6 and Fig. 6.7, base shear of NIT_RS, PASSPORT_RS, IIM_RS and DWL are between 159.6% to 201.9%, 235.9% to 265.1%, 211.4% to 248.5% and 71.6% to 155.7% of RS load case respectively. This shows that, PASSPORT_RS from SSRSA gives maximum base shear and base shear due to DWL load case from DGF analysis increases exponentially as building height increases from 24 story SM1 tall building to 64 story SM1 tall building.

6.2.2.2 Natural Time Period and Modal Participating Mass Ratio

The natural time period and modal participation mass ratios for SM2S24, SM2S44, and SM2S64 are depicted in Tables 6.4, 6.5, and 6.6, respectively. Based on the results of these tables, it can be stated that the number of modes addressed for analysis in all models is adequate for earthquake load analysis.

Table 6.4: Time Period and Modal Participating Mass Ratio of SM2S24

Mode	**Time Period (Sec)**	**UX**	**UY**	**RZ**
1	3.636	0	0.747	0
2	3.607	0.747	0	0
3	3.136	0	0	0.768
4	1.023	0	0.123	0
5	1.018	0.123	0	0
6	0.934	0	0	0.111
7	0.476	0	0.048	0
8	0.475	0.048	0	0
9	0.457	0	0	0.043
10	0.27	0	0.025	0
11	0.27	0	0	0.024
12	0.27	0.025	0	0

Table 6.5: Time Period and Modal Participating Mass Ratio of SM2S44

Mode	**Time Period (Sec)**	**UX**	**UY**	**RZ**
1	5.761	0	0.76	0
2	5.612	0.76	0	0
3	4.779	0	0	0.77
4	1.865	0	0.11	0
5	1.825	0.11	0	0
6	1.602	0	0	0.10
7	0.997	0	0.04	0
8	0.978	0.04	0	0
9	0.896	0	0	0.04
10	0.632	0	0.02	0
11	0.621	0.02	0	0
12	0.583	0	0	0.02

Table 6.6: Time Period and Modal Participating Mass Ratio of SM2S64

Mode	**Time Period (Sec)**	**UX**	**UY**	**RZ**
1	6.642	0.74	0	0
2	6.628	0	0.74	0
3	5.344	0	0	0.77
4	2.272	0.13	0	0
5	2.258	0	0.13	0
6	1.891	0	0	0.11
7	1.252	0.04	0	0
8	1.243	0	0.04	0
9	1.101	0	0	0.04
10	0.836	0.02	0	0
11	0.83	0	0.02	0
12	0.75	0	0	0.02

Figure 6.8 depicts the time period for the first three modes of vibration in buildings SM2S24, SM2S44, and SM2S64. From Fig. 6.8, it can be deduced that the probability of torsional mode of vibration occurring as the first fundamental mode of vibration of SM2 tall building is less compared to SM1 tall buildings. Time period values of SM2 tall buildings are less in 24 story tall buildings and larger in case of 44 and 64 story tall buildings compared to SM1 tall buildings.

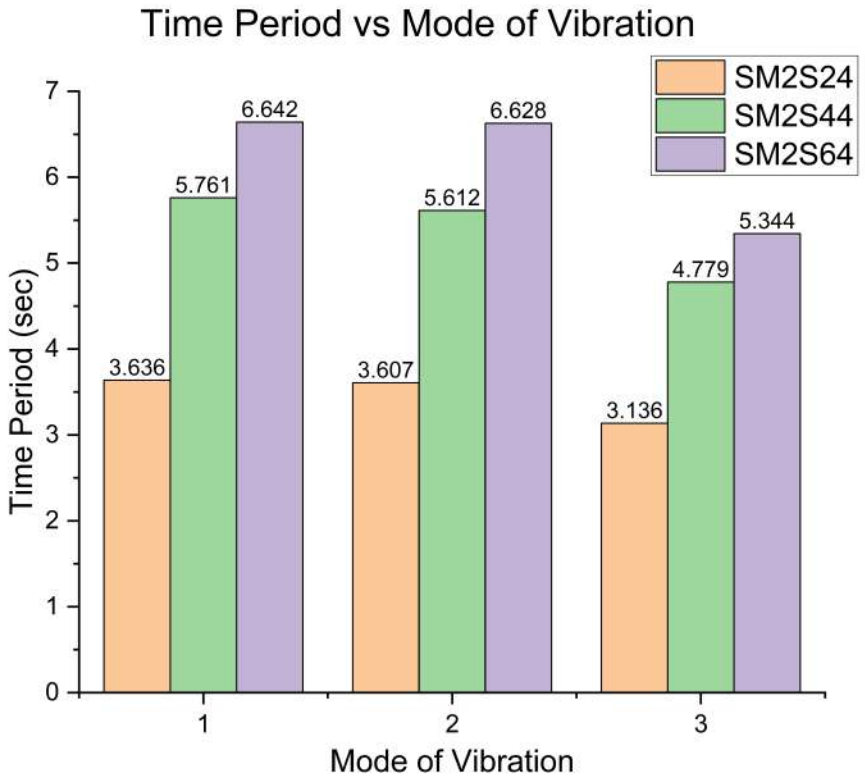

Figure 6.8: Time Period of SM2 Tall Buildings

6.2.2.3 Story Displacements

In accordance with clause 20.5 of IS 456: 2000[44] and table 6 of IS 800: 2007[45], the displacement of the top storey of any building must be less than (building height)/500. So, the allowable maximum top storey displacement for models SM2S24, SM2S44 and SM2S64 are 195.6 mm, 269.6 mm and 343.6 mm, respectively. The Figures 6.9a, 6.9b, and 6.9c depict the story displacements of SM2S24, SM2S44, and SM2S64 tall buildings under various combinations of lateral loads respectively.

(a) Story Displacements of SM2S24

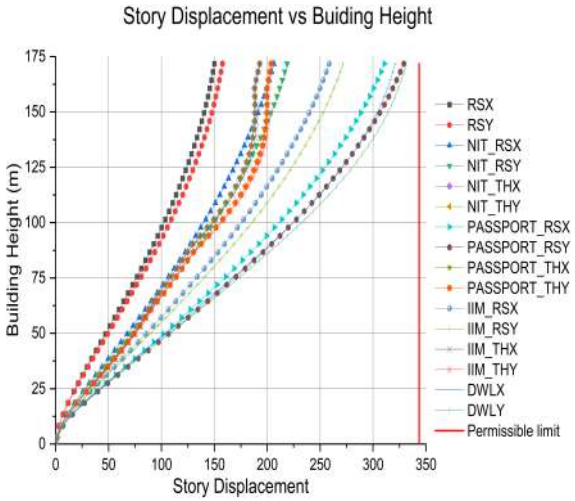

(b) Story Displacements of SM2S44

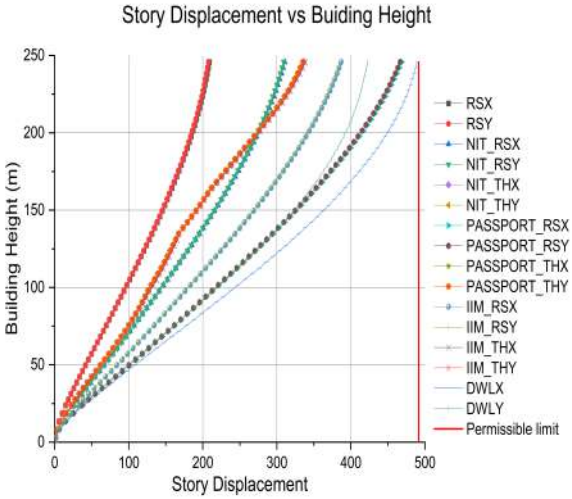

(c) Story Displacements of SM2S64

Figure 6.9: Story Displacements of SM2 Tall Buildings

From the results of story displacements, it can be determined that the story displacements of all SM2 tall structures fall within the allowable range. As the number of stories increases, the wind load combination utilising the DWL load case from the DGF analysis becomes increasingly significant, and the displacement of the top story owing to this load combination approaches the allowable limit. Top story displacements of SM2 tall buildings are significantly less compared to SM1 tall buildings.

6.2.2.4 Inter-Story Drift Ratio

According to clause 7.11 of IS 1893: 2016[47], the permitted limit for inter-story drift ratio of a structure under service loads is 0.004 times the height of each level. In addition, IS 16700: 2017[48] stipulates that the permitted maximum inter-story drift ratio of factored earthquake load combinations for tall buildings must not exceed storey height/250. Thus, allowable maximum ISDR for models SM2S24, SM2S44 and SM2S64 is 0.0148. Figures 6.10a, 6.10b, and 6.10c represent the ISDR for SM2S24, SM2S44, and SM2S64 tall structures for various load combinations under maximum codal requirements of IS 1893: 2016[47] and IS 16700: 2017[48]. It is observed that ISDR for all SM2 buildings are within limits and maximum ISDR is found in case of PASSPORT_RS load case.

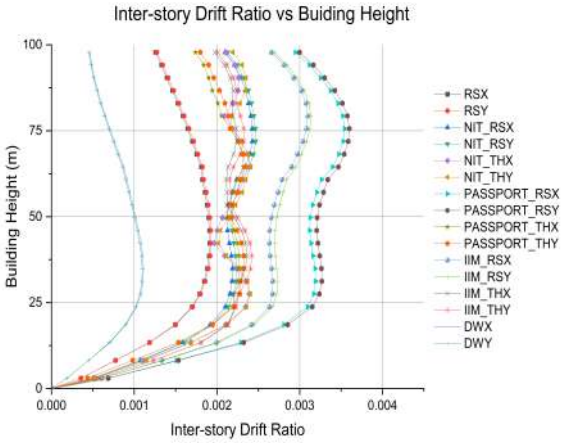

(a) ISDR of SM2S24

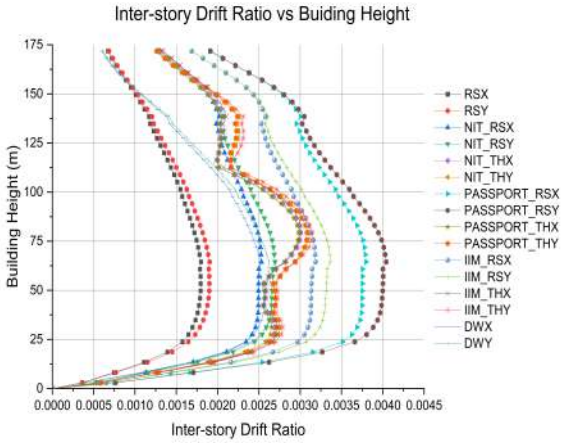

(b) ISDR of SM2S44

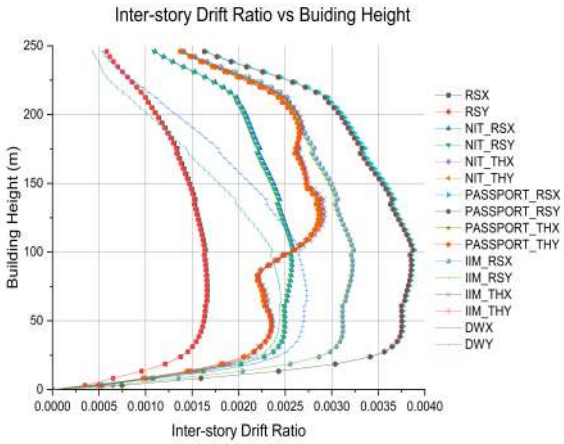

(c) ISDR of SM2S64

Figure 6.10: ISDR of SM2 Tall Buildings

6.2.3 SM3 SWMF System

6.2.3.1 Base Shear

Base shear for various lateral load cases in SM3S24, SM3S44 and SM3S64 are shown in Figures 6.11a, 6.11b and 6.11c respectively. Story shear for various lateral load cases in SM3S24, SM3S44 and SM3S64 are shown in Figures 6.12a, 6.12b and 6.12c respectively.

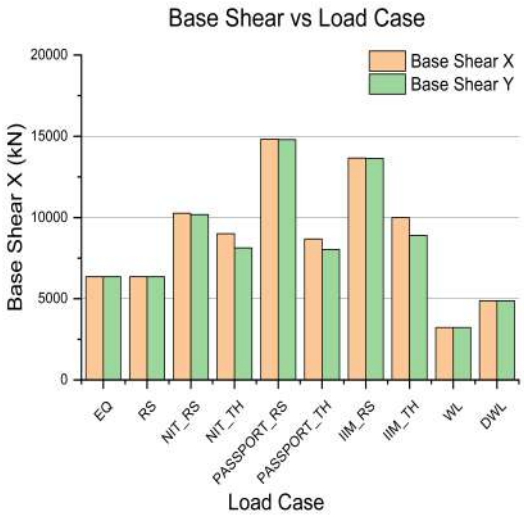

(a) Base Shear of SM3S24

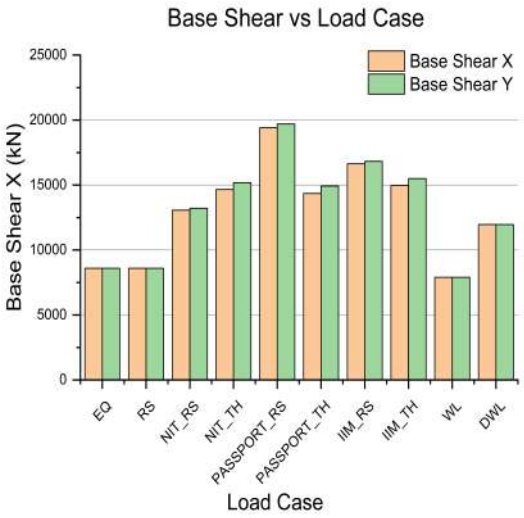

(b) Base Shear of SM3S44

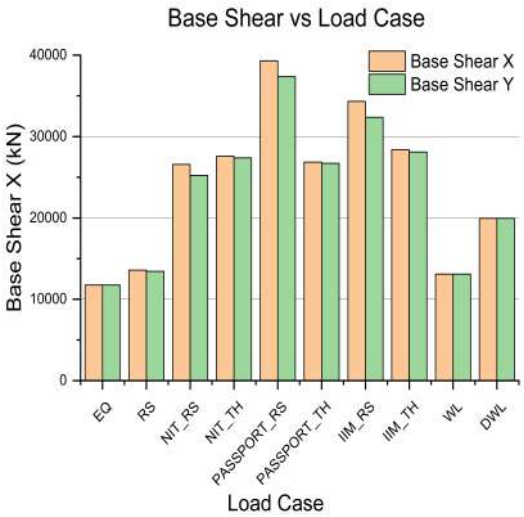

(c) Base Shear of SM3S64

Figure 6.11: Base Shear of SM3 Tall Buildings

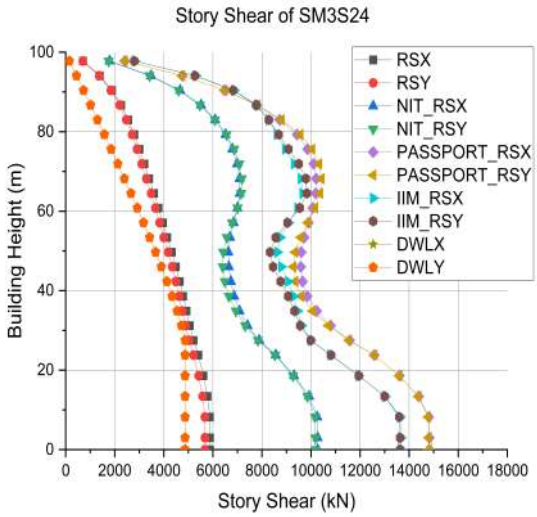

(a) Story Shear of SM3S24

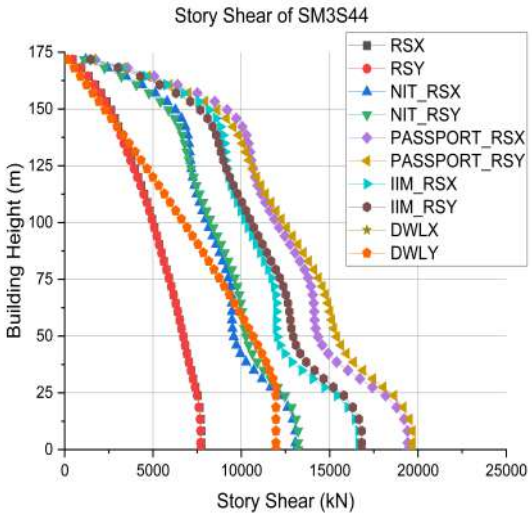

(b) Story Shear of SM3S44

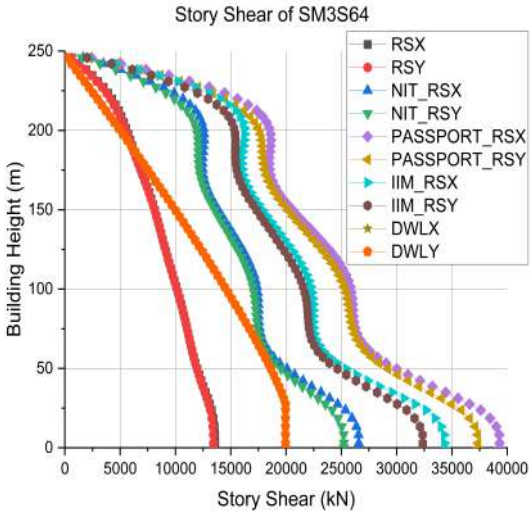

(c) Story Shear of SM3S64

Figure 6.12: Story Shear of SM3 Tall Buildings

From the results of Fig. 6.11 and Fig. 6.12, base shear of NIT_RS, PASSPORT_RS, IIM_RS and DWL are between 151.9% to 195.5%, 225.91% to 289.2%, 193.5% to 252.4% and 76.6% to 146.8% of RS load case respectively. This shows that, PASSPORT_RS from SSRSA gives maximum base shear and base shear due to DWL load case from DGF analysis increases exponentially as building height increases from 24 story SM1 tall building to 64 story SM1 tall building.

6.2.3.2 Natural Time Period and Modal Participating Mass Ratio

The natural time period and modal participation mass ratios for SM3S24, SM3S44, and SM3S64 are depicted in Tables 6.7, 6.8, and 6.9, respectively. Based on the results of these tables, it can be stated that the number of modes addressed for analysis in all models is adequate for earthquake load analysis.

Table 6.7: Time Period and Modal Participating Mass Ratio of SM3S24

Mode	**Time Period (Sec)**	**UX**	**UY**	**RZ**
1	3.57	0.00	0.80	0.00
2	3.44	0.80	0	0.00
3	3.308	0	0.00	0.82
4	1.149	0.00	0.00	0.09
5	1.077	0.00	0.10	0.00
6	1.044	0.10	0.00	0.00
7	0.613	0.00	0.00	0.03
8	0.55	0.00	0.03	0.00
9	0.534	0.03	0.00	0.00
10	0.393	0.00	0.00	0.02
11	0.344	0.00	0.02	0.00
12	0.336	0.02	0.00	0.00

Table 6.8: Time Period and Modal Participating Mass Ratio of SM3S44

Mode	**Time Period (Sec)**	**UX**	**UY**	**RZ**
1	4.264	0.00	0.75	0.00
2	4.039	0.74	0.00	0.00
3	3.895	0.00	0.00	0.80
4	1.441	0.00	0.14	0.00
5	1.388	0.00	0.00	0.10
6	1.356	0.15	0.00	0.00
7	0.813	0.00	0.00	0.03
8	0.783	0.00	0.04	0.00
9	0.733	0.04	0.00	0.00
10	0.557	0.00	0.00	0.01
11	0.521	0.00	0.02	0.00
12	0.489	0.02	0.00	0.00

Table 6.9: Time Period and Modal Participating Mass Ratio of SM3S64

Mode	**Time Period (Sec)**	**UX**	**UY**	**RZ**
1	5.603	0.00	0.71	0.00
2	5.489	0.70	0.00	0.00
3	4.342	0.00	0.00	0.80
4	1.772	0.00	0.17	0.00
5	1.714	0.17	0.00	0.00
6	1.528	0.00	0.00	0.10
7	0.928	0.00	0.05	0.00
8	0.906	0.00	0.00	0.03
9	0.894	0.05	0.00	0.00
10	0.635	0.00	0.00	0.02
11	0.616	0.00	0.02	0.00
12	0.592	0.02	0.00	0.00

Figure 6.13 depicts the time period for the first three modes of vibration in buildings SM3S24, SM3S44, and SM3S64. From Fig. 6.13, it can be deduced that time period of third mode of vibration values in SM3S24 and SM3S44 models are greater than 90% of time periods of the first two modes of vibrations, which is not acceptable as per IS 16700: 2017[48]. Time period values of SM3 tall buildings are significantly less compared to SM1 and SM2 tall buildings.

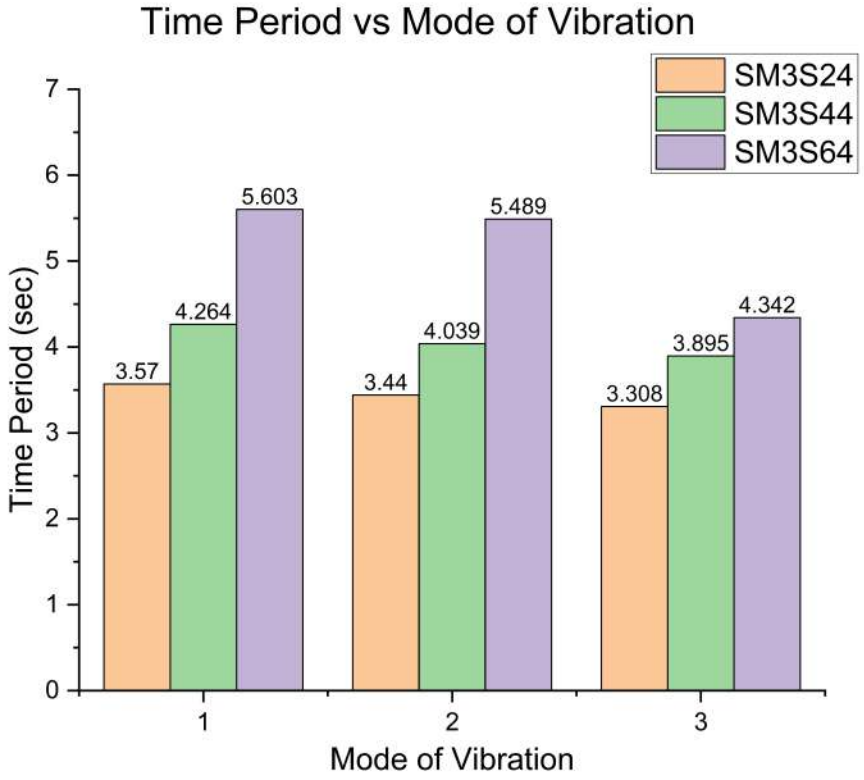

Figure 6.13: Time Period of SM3 Tall Buildings

6.2.3.3 Story Displacements

In accordance with clause 20.5 of IS 456: 2000[44] and table 6 of IS 800: 2007[45], the displacement of the top storey of any building must be less than (building height)/500. So, the allowable maximum top storey displacement for models SM2S24, SM2S44 and SM2S64 are 195.6 mm, 269.6 mm and 343.6 mm, respectively. The figures 6.14a, 6.14b, and 6.14c depict the story displacements of SM3S24, SM3S44, and SM3S64 tall buildings under various combinations of lateral loads respectively.

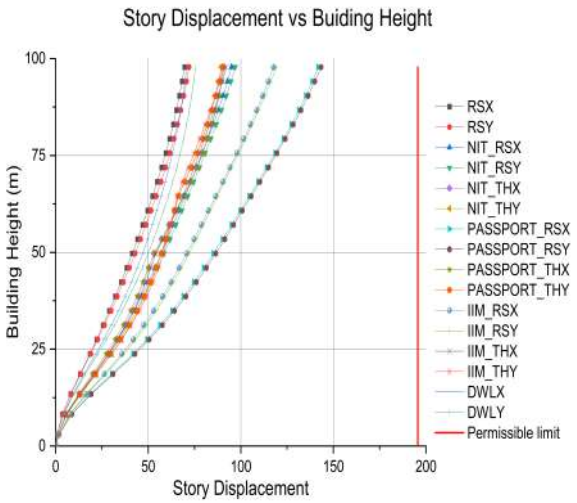

(a) Story Displacements of SM3S24

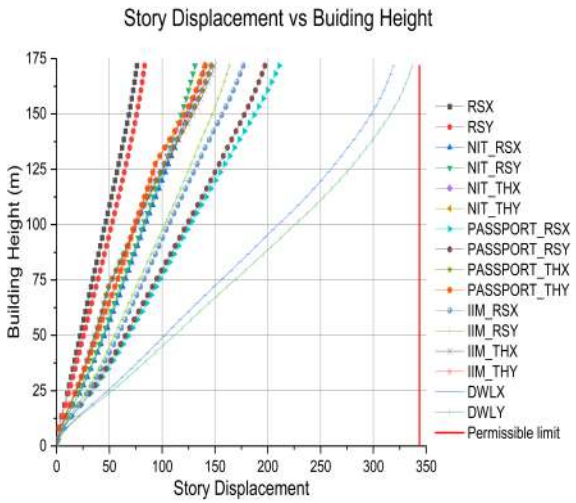

(b) Story Displacements of SM3S44

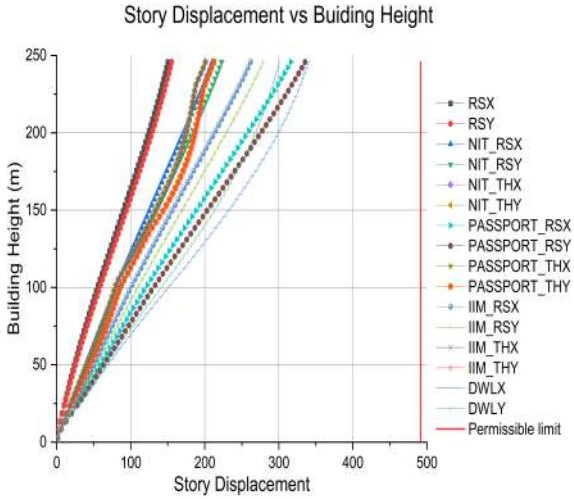

(c) Story Displacements of SM3S64

Figure 6.14: Story Displacements of SM3 Tall Buildings

From the results of story displacements, it can be determined that the story displacements of all SM3 tall structures fall within the allowable range. As the number of stories increases, the wind load combination utilising the DWL load case from the DGF analysis becomes increasingly significant, and the displacement of the top story owing to this load combination approaches the allowable limit.

6.2.3.4 Inter-Story Drift Ratio

According to clause 7.11 of IS 1893: 2016[47], the permitted limit for inter-story drift ratio of a structure under service loads is 0.004 times the height of each level. In addition,

IS 16700: 2017[48] stipulates that the permitted maximum inter-story drift ratio of factored earthquake load combinations for tall buildings must not exceed storey height/250. Thus, allowable maximum ISDR for models SM3S24, SM3S44 and SM3S64 is 0.0148. Figures 6.15a, 6.15b, and 6.15c represent the ISDR for SM3S24, SM3S44, and SM3S64 tall structures for various load combinations under maximum codal requirements of IS 1893: 2016[47] and IS 16700: 2017[48]. It is observed that ISDR for all SM3 buildings are within limits and maximum ISDR is found in case of PASSPORT_RS load case.

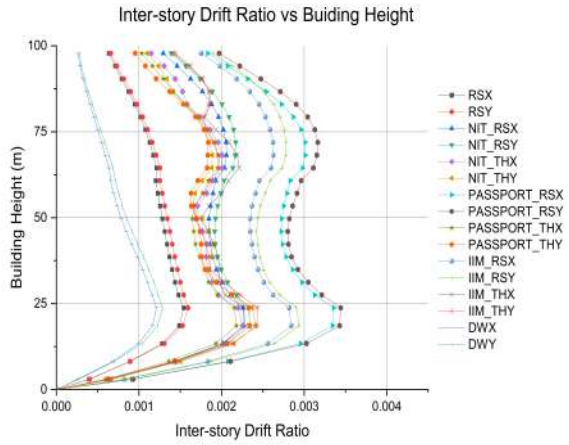

(a) ISDR of SM3S24

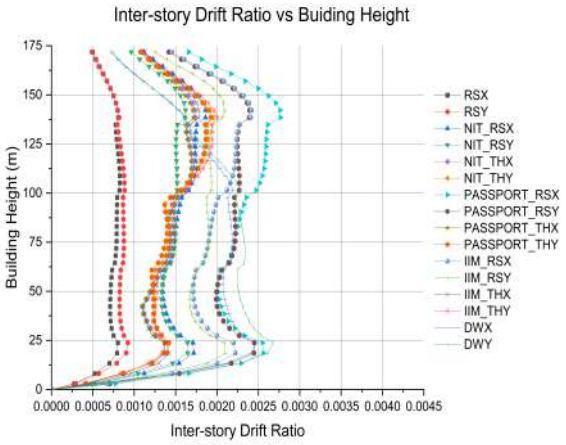

(b) ISDR of SM3S44

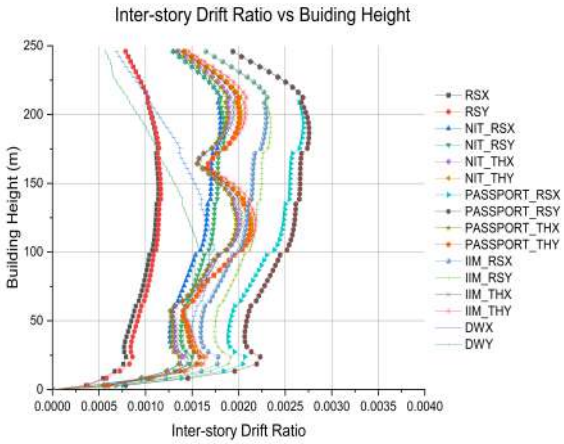

(c) ISDR of SM3S64

Figure 6.15: ISDR of SM3 Tall Buildings

6.3 Tubular System

Results of tubular structural system buildings TBS24, TBS44 and TBS64 in terms of base shear, time period, modal participating mass ratio, story displacement and inter-story drift ratio are presented and discussed in this section.

6.3.1 Base Shear

Base shear for various lateral load cases in TBS24, TBS44 and TBS64 are shown in Figures 6.16a, 6.16b and 6.16c respectively. Story shear for various lateral load cases in SM1S24, SM1S44 and SM1S64 are shown in Figures 6.17a, 6.17b and 6.2c respectively.

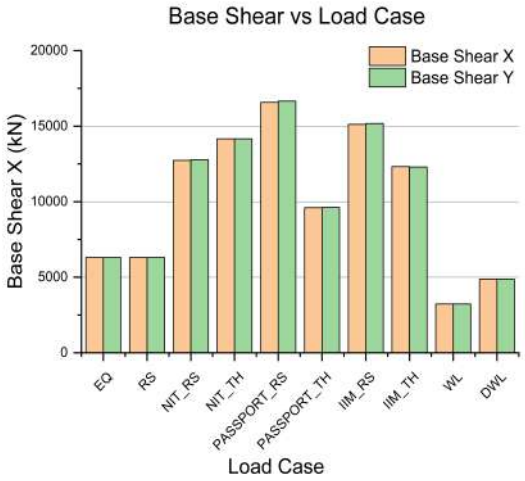

(a) Base Shear of TBS24

(b) Base Shear of TBS44

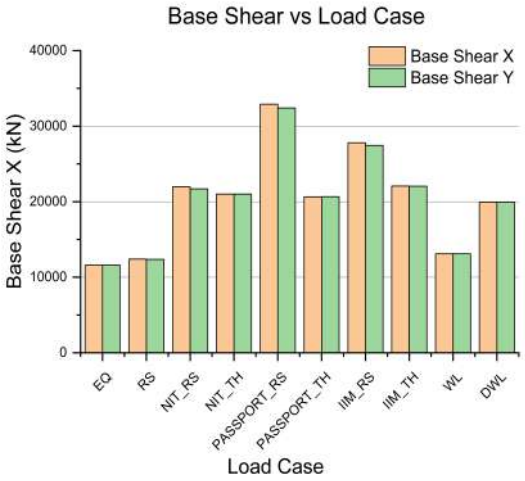

(c) Base Shear of TBS64

Figure 6.16: Base Shear of TB Tall Buildings

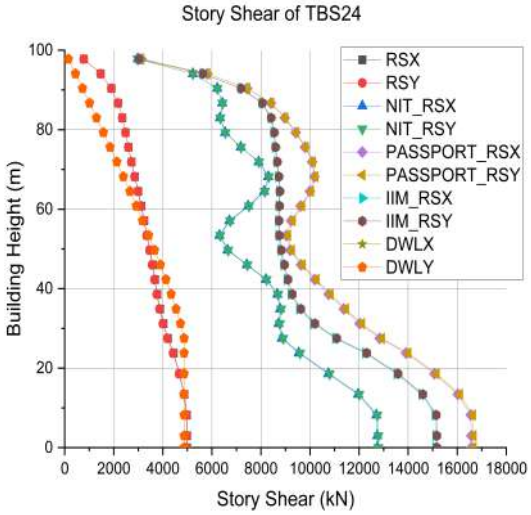

(a) Story Shear of TBS24

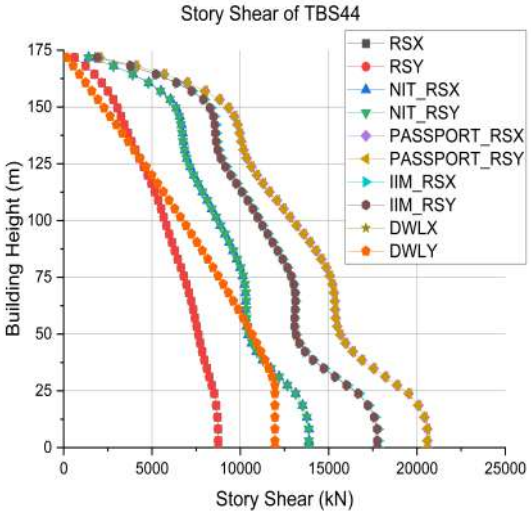

(b) Story Shear of TBS44

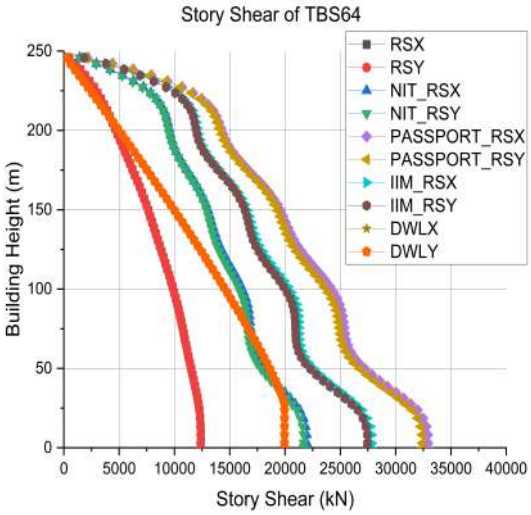

(c) Story Shear of TBS64

Figure 6.17: Story Shear of TB Tall Buildings

From the results of Fig. 6.16 and Fig. 6.17, base shear of NIT_RS, PASSPORT_RS, IIM_RS and DWL are between 158.8% to 201.6%, 235.4% to 265.6%, 203.7% to 239.7% and 77.2% to 161.1% of RS load case respectively. This shows that, PASSPORT_RS from SSRSA gives maximum base shear and base shear due to DWL load case from DGF analysis increases exponentially as building height increases from 24 story SM1 tall building to 64 story SM1 tall building.

6.3.2 Natural Time Period and Modal Participating Mass Ratio

In accordance with clause 7.7.5.2 of IS 1893 (Part 1):2016[47], for the analysis of earthquake shaking in the considered direction, the number of modes shall be such that the sum of their modal masses is at least 90% of the overall seismic mass. The natural time period and modal participation mass ratios for TBS24, TBS44, and TBS64 are depicted in Tables 6.10, 6.11, and 6.12, respectively. Based on the results of these tables, it can be stated that the number of modes addressed for analysis in all models is adequate for earthquake load analysis.

Table 6.10: Time Period and Modal Participating Mass Ratio of TBS24

Mode	**Time Period (Sec)**	**UX**	**UY**	**RZ**
1	3.56	0	0.739	0
2	3.52	0.739	0	0
3	3.17	0	0	0.783
4	1.01	0	0	0.105
5	0.97	0	0.132	0
6	0.97	0.131	0	0
7	0.51	0	0	0.041
8	0.44	0	0.051	0
9	0.44	0.051	0	0
10	0.30	0	0	0.023
11	0.25	0	0.026	0
12	0.25	0.026	0	0

Table 6.11: Time Period and Modal Participating Mass Ratio of TBS44

Mode	**Time Period (Sec)**	**UX**	**UY**	**RZ**
1	5.59	0	0.7439	0
2	5.50	0.7453	0	0
3	4.45	0	0	0.7953
4	1.77	0	0.1219	0
5	1.76	0.1207	0	0
6	1.52	0	0	0.0964
7	0.91	0	0.0448	0
8	0.91	0.0448	0	0
9	0.86	0	0	0.0352
10	0.57	0	0	0.0185
11	0.57	0	0.0244	0
12	0.57	0.0244	0	0

Table 6.12: Time Period and Modal Participating Mass Ratio of TBS64

Mode	**Time Period (Sec)**	**UX**	**UY**	**RZ**
1	6.67	0	0.7255	0
2	6.51	0.7265	0	0
3	5.01	0	0	0.7772
4	2.26	0	0.1365	0
5	2.23	0.1362	0	0
6	1.84	0	0	0.108
7	1.21	0	0.0454	0
8	1.20	0.0448	0	0
9	1.06	0	0	0.0385
10	0.80	0	0.0235	0
11	0.80	0.0234	0	0
12	0.74	0	0	0.0188

Figure 6.21 depicts the time period for the first three modes of vibration in buildings TBS24, TBS44, and TBS64. From Fig. 6.21, it can be deduced that the probability of torsional mode of vibration occurring as the first fundamental mode of vibration of TB tall building is less compared to SM1 tall buildings. Time period values of TB tall buildings are less in 24 story tall buildings and larger in case of 44 and 64 story tall buildings compared to SM1 tall buildings.

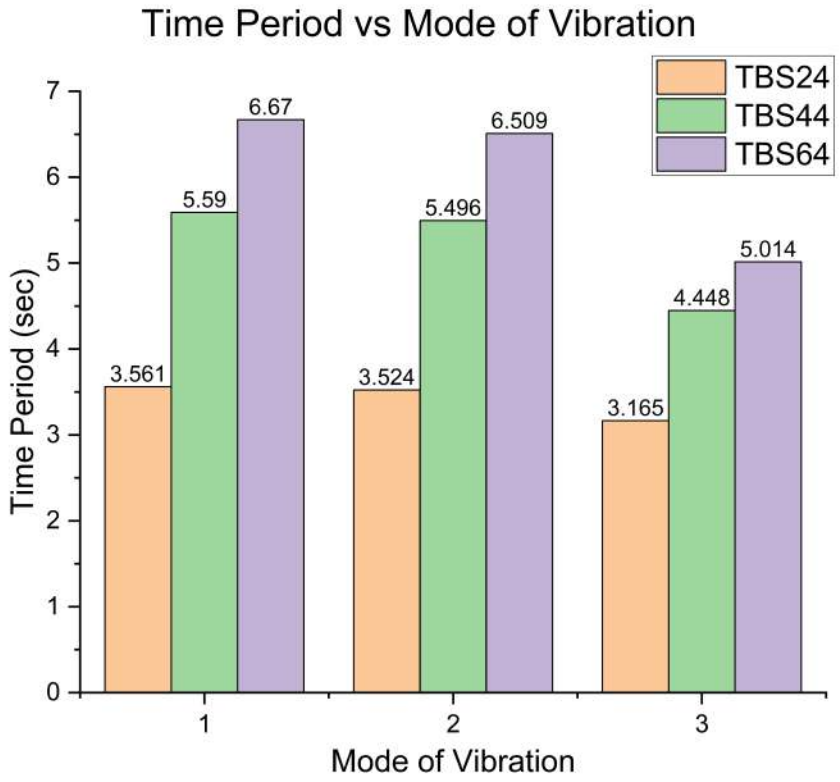

Figure 6.18: Time Period of TB Tall Buildings

6.3.3 Story Displacements

In accordance with clause 20.5 of IS 456: 2000[44] and table 6 of IS 800: 2007[45], the displacement of the top storey of any building must be less than (building height)/500. So, the allowable maximum top storey displacement for models TBS24, TBS44 and TBS64 are 195.6 mm, 269.6 mm and 343.6 mm, respectively. The Figures 6.19a, 6.19b, and 6.19c depict the story displacements of TBS24, TBS44, and TBS64 tall buildings under various combinations of lateral loads respectively.

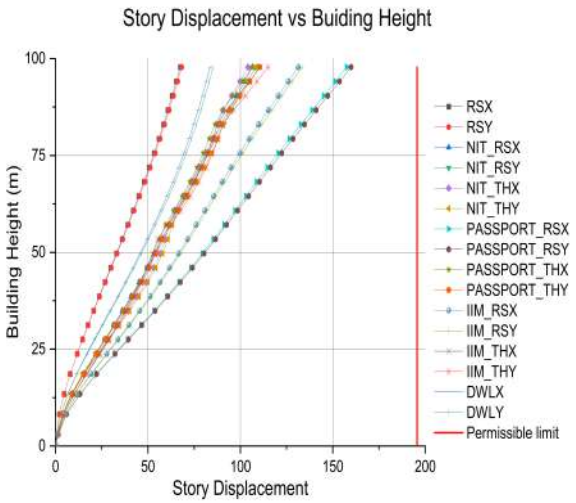

(a) Story Displacements of TBS24

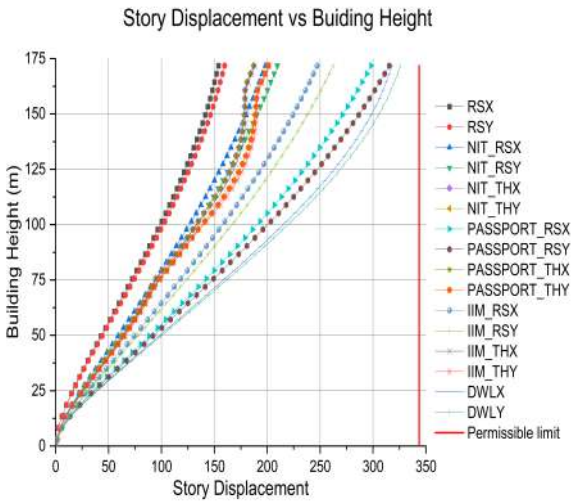

(b) Story Displacements of TBS44

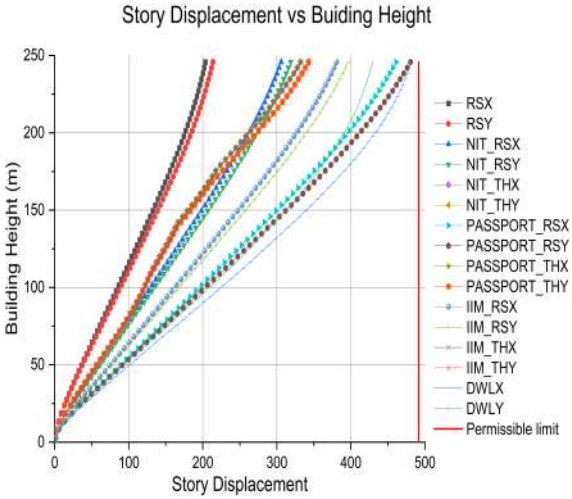

(c) Story Displacements of TBS64

Figure 6.19: Story Displacements of TB Tall Buildings

From the results of story displacements, it can be determined that the story displacements of all TB tall structures fall within the allowable range. As the number of stories increases, the wind load combination utilising the DWL load case from the DGF analysis becomes increasingly significant, and the displacement of the top story owing to this load combination approaches the allowable limit.

6.3.4 Inter-Story Drift Ratio

According to clause 7.11 of IS 1893: 2016[47], the permitted limit for inter-story drift ratio of a structure under service loads is 0.004 times the height of each level. In addition, IS

16700: 2017[48] stipulates that the permitted maximum inter-story drift ratio of factored earthquake load combinations for tall buildings must not exceed storey height/250. Thus, allowable maximum ISDR for models TBS24, TBS44 and TBS64 is 0.0148. Figures 6.20a, 6.20b, and 6.20c represent the ISDR for TBS24, TBS44, and TBS64 tall structures for various load combinations under maximum codal requirements of IS 1893: 2016[47] and IS 16700: 2017[48]. It is observed that ISDR for all TB buildings are within limits and maximum ISDR is found in case of PASSPORT_RS load case.

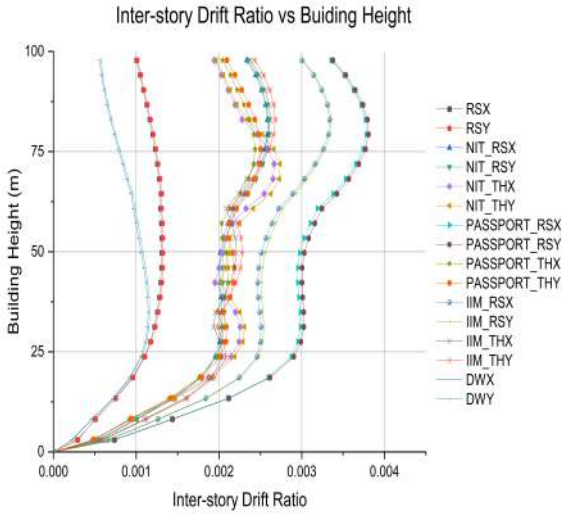

(a) ISDR of TBS24

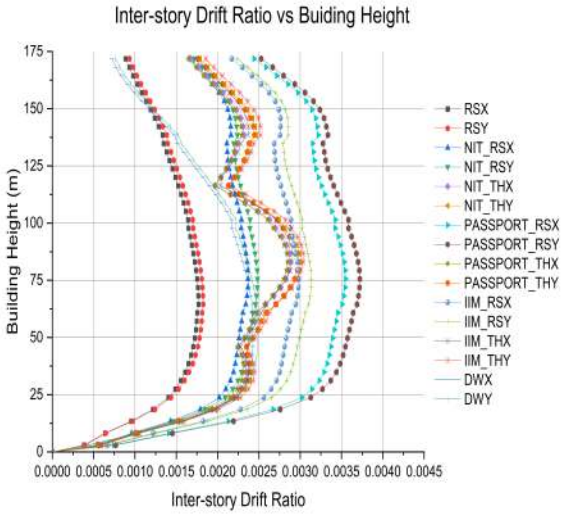

(b) ISDR of TBS44

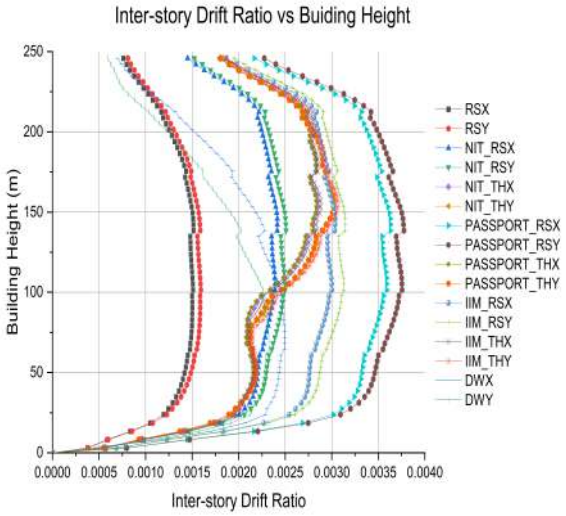

(c) ISDR of TBS64

Figure 6.20: ISDR of TB Tall Buildings

6.3.5 Shear lag effect in Tubular Tall buildings

In tubular buildings, shear lag effect becomes significant which cause unequal distribution of lateral forces. Shear lag effect in TB tall buildings are studied in terms of axial force variation. Axial force variations under critical lateral loads PASSPORT_RS and DWL at bottom most column in TB tall buildings are considered for this study. Column numbers for axial force variation in tubular tall buildings are shown in Fig. **??**.

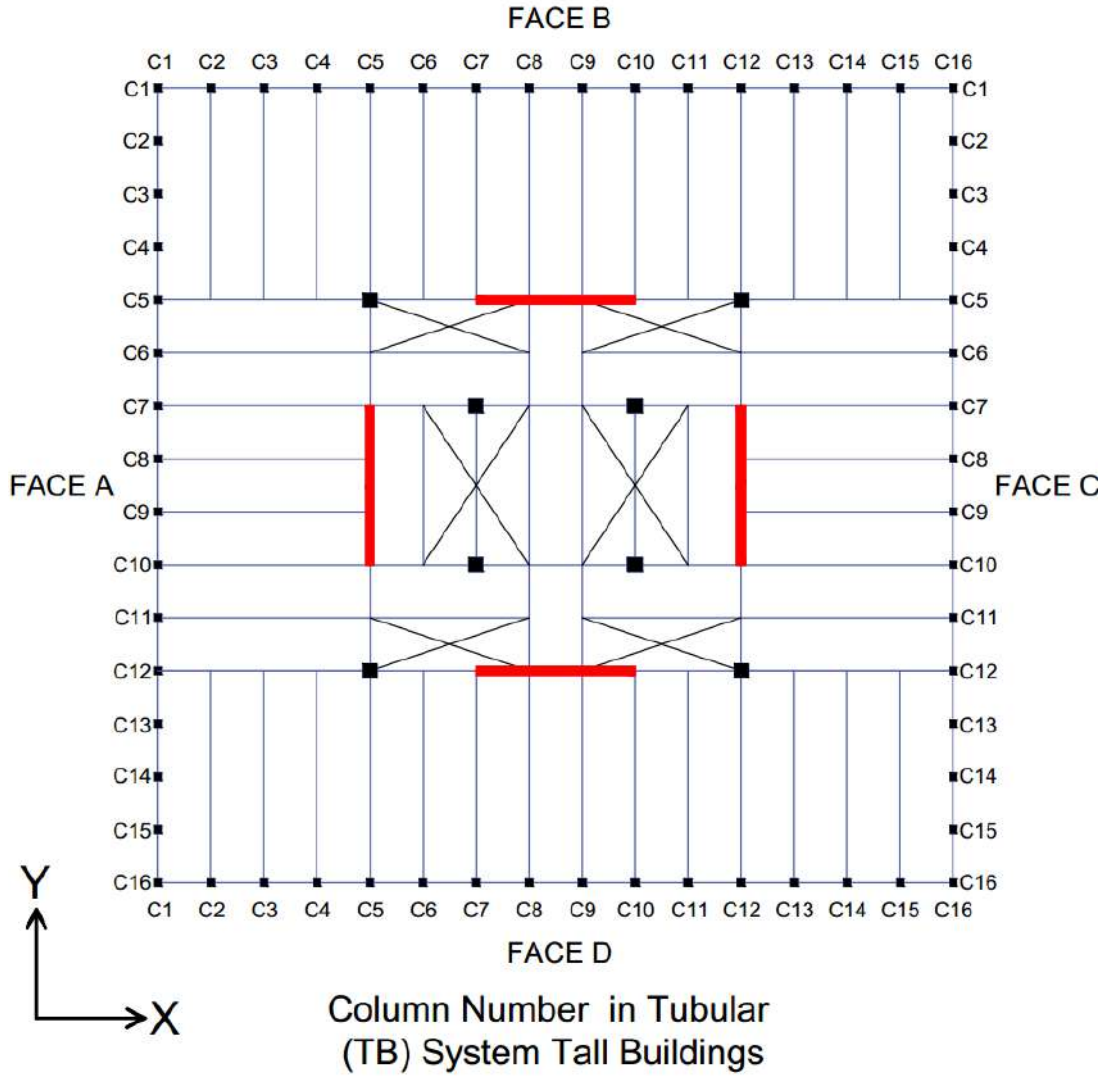

Figure 6.21: Time Period of TB Tall Buildings

Axial force variation in all tubular system buildings in all four faces (Face A, Face B, Face C and Face D) for load cases PASSPORT_RSX, PASSPORT_RSY, DWLX and DWLY are shown in Figures 6.22, 6.23, 6.24 and 6.25 respectively.

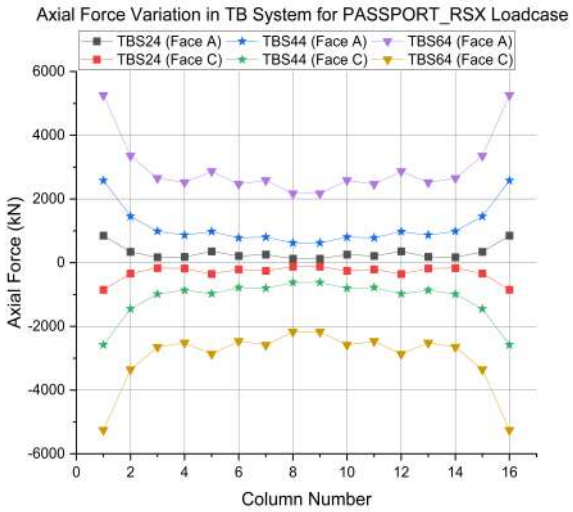

(a) Axial Force Variation in Face A and C

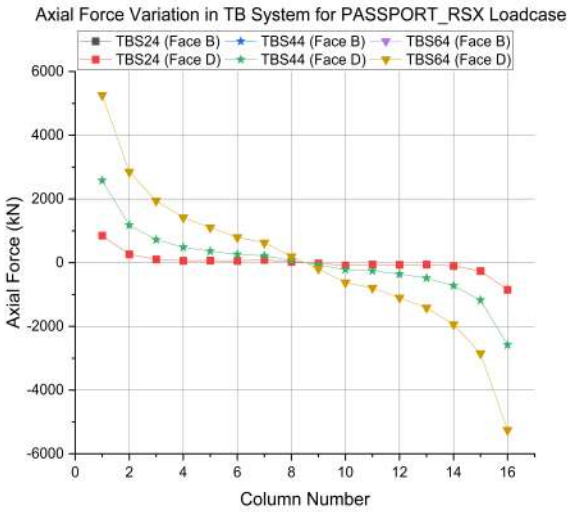

(b) Axial Force Variation in Face B and D

Figure 6.22: Axial Force Variation of TB buildings for PASSPORT_RSX Loadcase

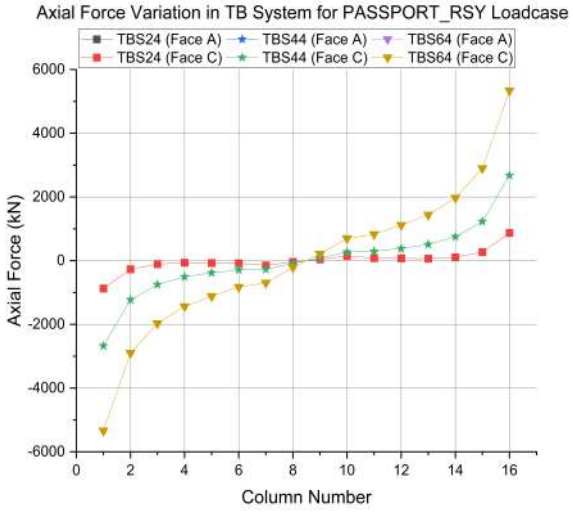

(a) Axial Force Variation in Face A and C

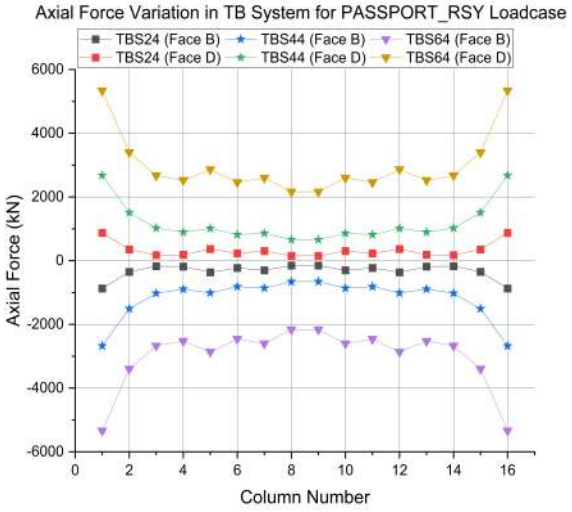

(b) Axial Force Variation in Face B and D

Figure 6.23: Axial Force Variation of TB buildings for PASSPORT_RSY Loadcase

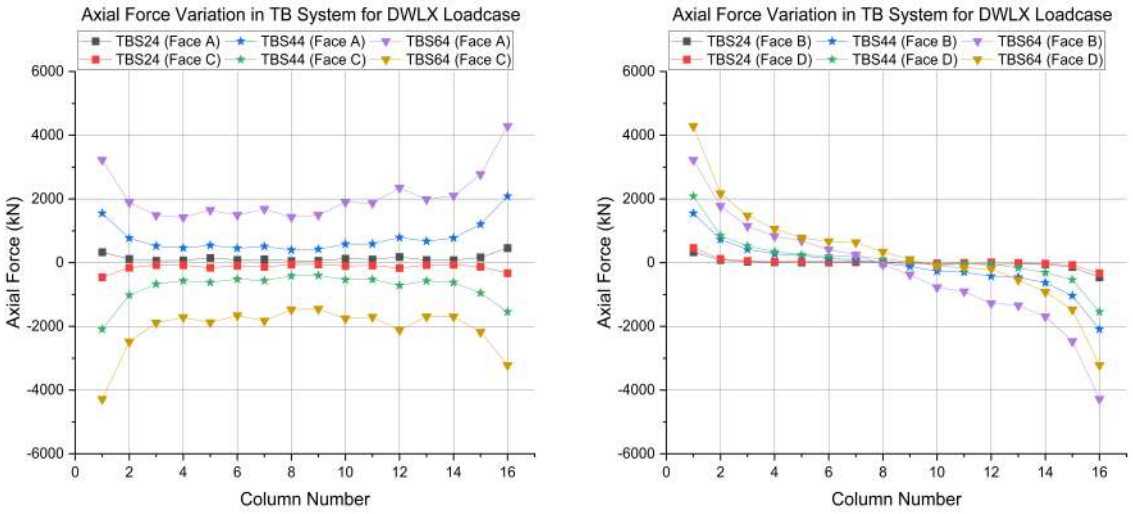

(a) Axial Force Variation in Face A and C (b) Axial Force Variation in Face B and D

Figure 6.24: Axial Force Variation of TB buildings for DWLX Loadcase

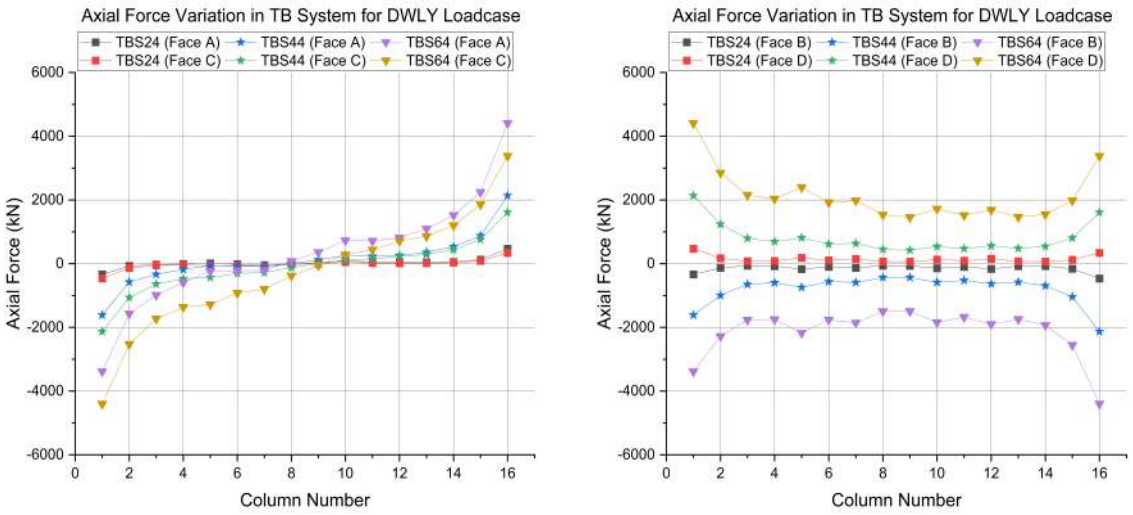

(a) Axial Force Variation in Face A and C (b) Axial Force Variation in Face B and D

Figure 6.25: Axial Force Variation of TB buildings for DWLY Loadcase

From the results depicted in the figures above, it can be seen that as the number of storeys in tubular buildings increases, the variation in axial forces between two opposed faces increases. Maximum axial force variation is detected in the corners of each face, and a substantial rise in axial force variation is noted at columns 5, 7, 10, and 12. Primary beams connect the columns at these positions to the core of tubular buildings. Consequently, abrupt jumps in axial force variation are observed in these places.

6.4 Outrigger and Belt Truss (OR) System

Results of outrigger and belt truss structural system buildings OB7S24, OB17S44, OB27S64 and OBS27&59S64 in terms of base shear, time period, modal participating mass ratio, story displacement and inter-story drift ratio are presented and discussed in this section.

6.4.1 Base Shear

Base shear for various lateral load cases in OB7S24, OB17S44, OB27S64 and OBS27&59S64 are shown in Figures 6.26a, 6.26b, 6.26c and 6.26d respectively. Story shear for various lateral load cases in SM1S24, SM1S44 and SM1S64 are shown in Figures 6.27a, 6.27b, 6.27c and 6.27d respectively.

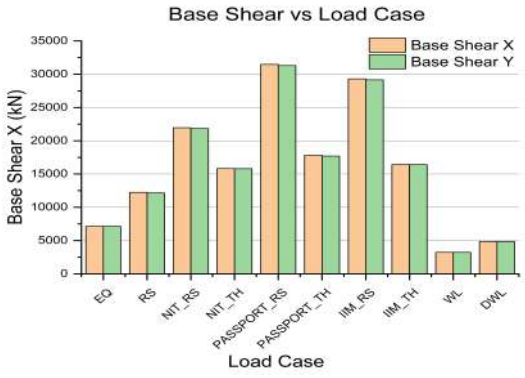

(a) Base Shear of OR7S24

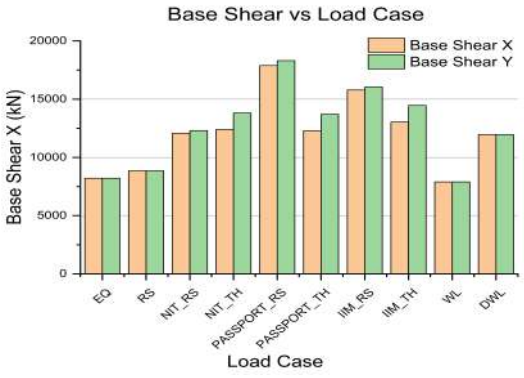

(b) Base Shear of OR17S44

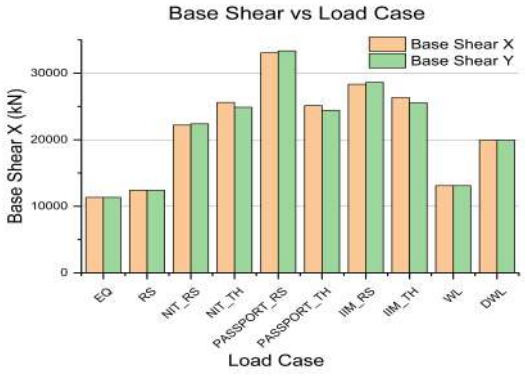

(c) Base Shear of OR27S64

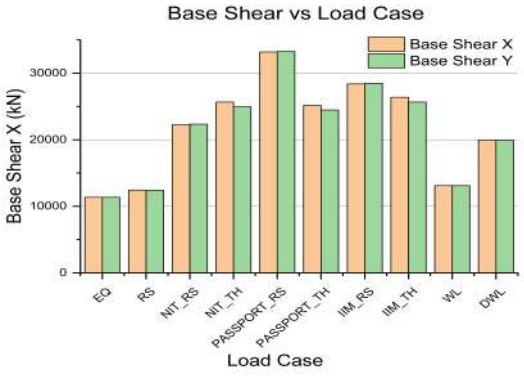

(d) Base Shear of OR27&59S64

Figure 6.26: Base Shear of OR Tall Buildings

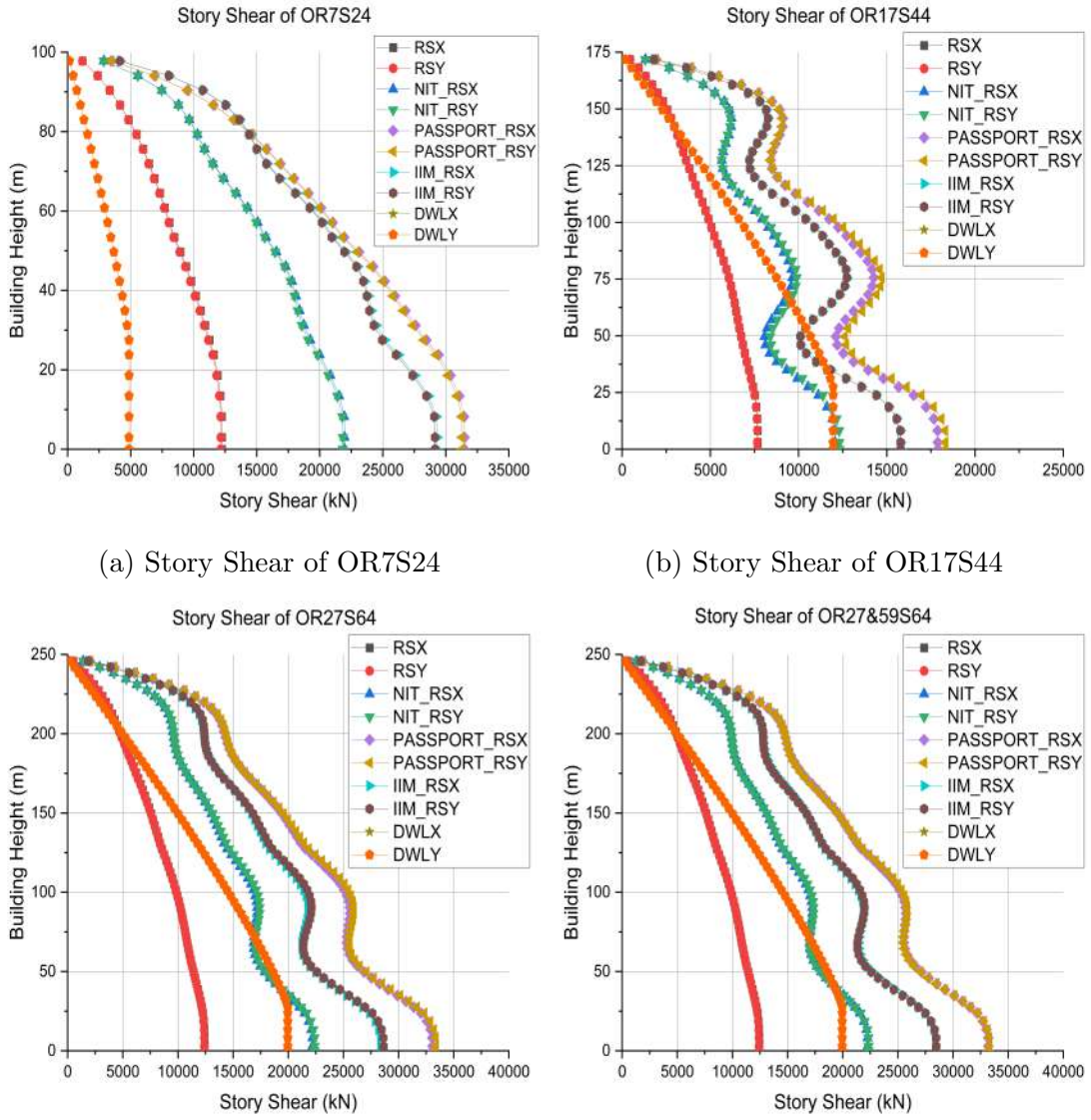

(a) Story Shear of OR7S24

(b) Story Shear of OR17S44

(c) Story Shear of OR27S64

(d) Story Shear of OR27&59S64

Figure 6.27: Story Shear of OR Tall Buildings

From the results of Fig. 6.16 and Fig. 6.17, base shear of NIT_RS, PASSPORT_RS, IIM_RS and DWL are between 159.8% to 204.6%, 238.4% to 275.6%, 193.7% to 235.2% and 71.2% to 163.3% of RS load case respectively. This shows that, PASSPORT_RS from SSRSA gives maximum base shear and base shear due to DWL load case from DGF analysis increases exponentially as building height increases from 24 story SM1 tall building to 64 story SM1 tall building.

6.4.2 Natural Time Period and Modal Participating Mass Ratio

In accordance with clause 7.7.5.2 of IS 1893 (Part 1):2016[47], for the analysis of earthquake shaking in the considered direction, the number of modes shall be such that the sum of their modal masses is at least 90% of the overall seismic mass. The natural time period and modal participation mass ratios for OB7S24, OB17S44, OB27S64 and OBS27&59S64 are depicted in Tables 6.13, 6.14, 6.15 and 6.16, respectively. Based on the results of these tables, it can be stated that the number of modes addressed for analysis in all models is adequate for earthquake load analysis.

Table 6.13: Time Period and Modal Participating Mass Ratio of OR7S24

Mode	**Time Period (Sec)**	**UX**	**UY**	**SumRZ**
1	2.02	0.00	0.80	0.00
2	2.01	0.81	0.00	0.00
3	1.81	0.00	0.00	0.84
4	0.73	0.08	0.00	0.00
5	0.73	0.00	0.09	0.00
6	0.72	0.00	0.00	0.06
7	0.34	0.00	0.00	0.03
8	0.32	0.04	0.00	0.00
9	0.31	0.00	0.04	0.00
10	0.26	0.00	0.00	0.02
11	0.23	0.02	0.00	0.00
12	0.23	0.00	0.02	0.00

Table 6.14: Time Period and Modal Participating Mass Ratio of OR17S44

Mode	**Time Period (Sec)**	**UX**	**UY**	**RZ**
1	5.194	0.00	0.77	0.00
2	5.09	0.77	0.00	0.00
3	4.573	0.00	0.00	0.81
4	1.823	0.00	0.10	0.00
5	1.808	0.10	0.00	0.00
6	1.758	0.00	0.00	0.07
7	0.888	0.00	0.00	0.04
8	0.83	0.00	0.05	0.00
9	0.83	0.05	0.00	0.00
10	0.645	0.00	0.00	0.02
11	0.585	0.02	0.00	0.00
12	0.584	0.00	0.02	0.00

Table 6.15: Time Period and Modal Participating Mass Ratio of OR27S64

Mode	**Time Period (Sec)**	**UX**	**UY**	**RZ**
1	6.396	0.00	0.74	0.00
2	6.244	0.74	0.00	0.00
3	5.427	0.00	0.00	0.80
4	2.24	0.00	0.12	0.00
5	2.2	0.12	0.00	0.00
6	1.96	0.00	0.00	0.09
7	1.113	0.00	0.05	0.00
8	1.103	0.05	0.00	0.00
9	1.103	0.00	0.00	0.04
10	0.804	0.00	0.00	0.02
11	0.799	0.00	0.02	0.00
12	0.798	0.02	0.00	0.00

Table 6.16: Time Period and Modal Participating Mass Ratio of OR27&59S64

Mode	**Time Period (Sec)**	**UX**	**UY**	**RZ**
1	6.44	0.00	0.74	0.00
2	6.29	0.74	0.00	0.00
3	5.47	0.00	0.00	0.79
4	2.24	0.00	0.12	0.00
5	2.20	0.12	0.00	0.00
6	1.98	0.00	0.00	0.09
7	1.10	0.00	0.00	0.05
8	1.10	0.00	0.06	0.00
9	1.09	0.06	0.00	0.00
10	0.80	0.00	0.00	0.01
11	0.78	0.00	0.01	0.00
12	0.78	0.01	0.00	0.00

Figure 6.28 depicts the time period for the first three modes of vibration in buildings OR7S24, OR17S44, OR27S64 and OR27&59S64. From Fig. 6.28, it can be deduced that the probability of torsional mode of vibration occurring as the first fundamental mode of vibration of OR tall building is less compared to SM1 tall buildings. Time period values of TB tall buildings are less in 24 story tall buildings and larger in case of 44 and 64 story tall buildings compared to SM1 tall buildings.

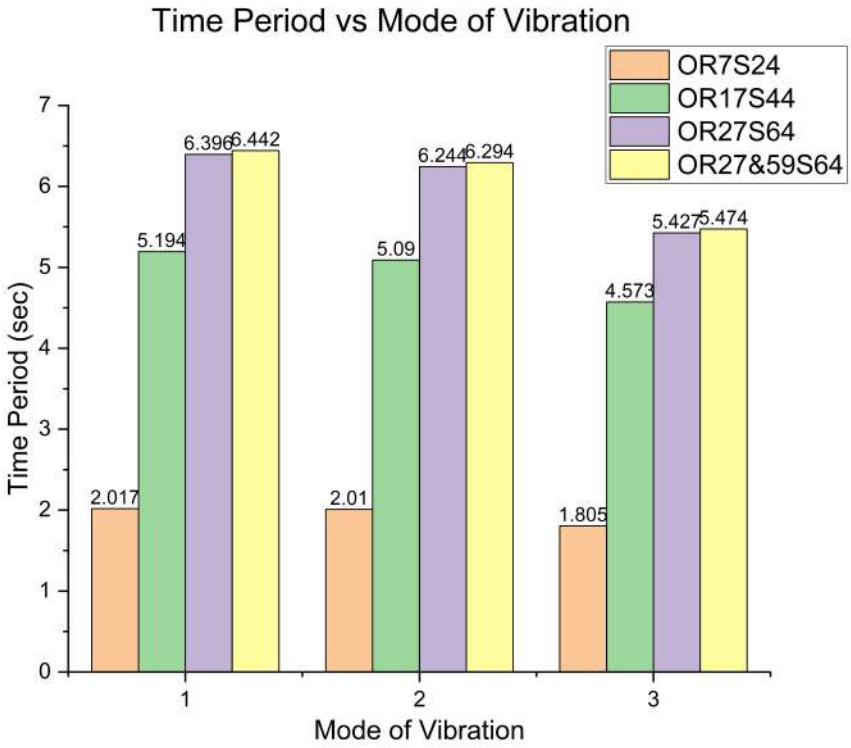

Figure 6.28: Time Period of OR Tall Buildings

6.4.3 Story Displacements

In accordance with clause 20.5 of IS 456: 2000[44] and table 6 of IS 800: 2007[45], the displacement of the top storey of any building must be less than (building height)/500. So, the allowable maximum top storey displacement for models OR7S24, OR17S44, OR27S64 and OR27&59S64 are 195.6 mm, 269.6 mm and 343.6 mm, respectively. The Figures 6.29a, 6.29b, 6.29c and 6.29d depict the story displacements of OR7S24, OR17S44, OR27S64 and OR27&59S64 tall buildings under various combinations of lateral loads respectively.

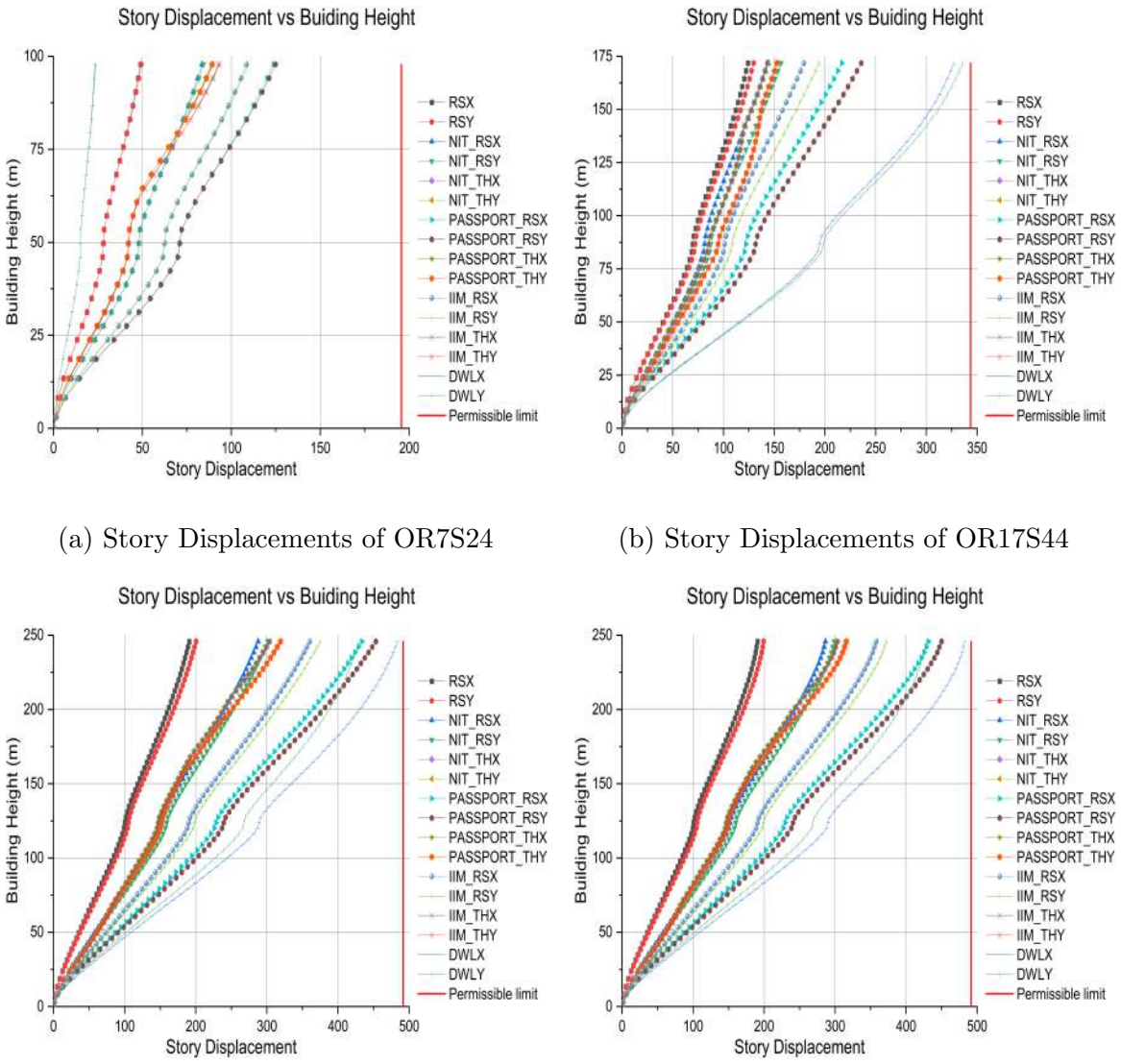

(a) Story Displacements of OR7S24

(b) Story Displacements of OR17S44

(c) Story Displacements of OR27S64

(d) Story Displacements of OR27&59S64

Figure 6.29: Story Displacements of OR Tall Buildings

From the results of story displacements, it can be determined that the story displacements of all OR tall structures fall within the allowable range. As the number of stories increases, the wind load combination utilising the DWL load case from the DGF analysis becomes increasingly significant, and the displacement of the top story owing to this load combination approaches the allowable limit. On floors where outriggers are provided, the amount of incremental story displacement decreases.

6.4.4 Inter-Story Drift Ratio

According to clause 7.11 of IS 1893: 2016[47], the permitted limit for inter-story drift ratio of a structure under service loads is 0.004 times the height of each level. In addition, IS 16700: 2017[48] stipulates that the permitted maximum inter-story drift ratio of factored earthquake load combinations for tall buildings must not exceed storey height/250. Thus, allowable maximum ISDR for models OR7S24, OR17S44, OR27S64 and OR27&59S64 is 0.0148. Figures 6.30a, 6.30b, 6.30c and 6.30d represent the ISDR for OR7S24, OR17S44, OR27S64 and OR27&59S64 tall structures for various load combinations under maximum codal requirements of IS 1893: 2016[47] and IS 16700: 2017[48].

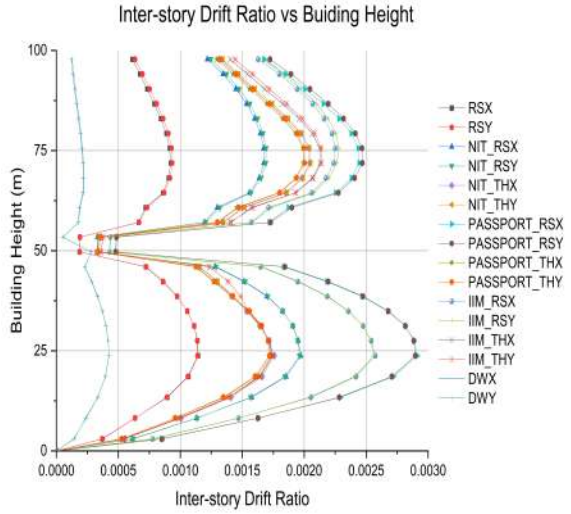

(a) ISDR of OR7S24

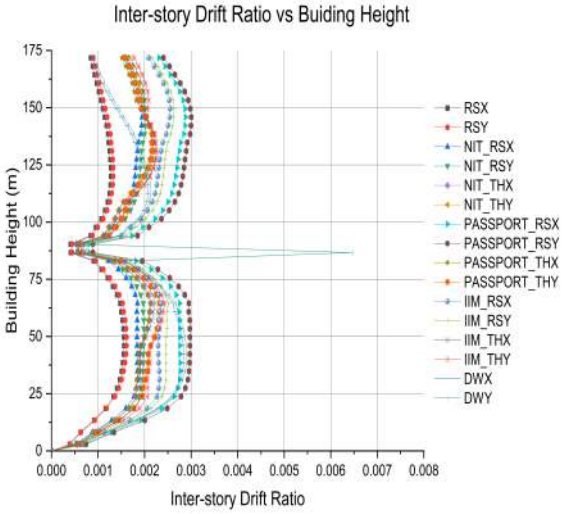

(b) ISDR of OR17S44

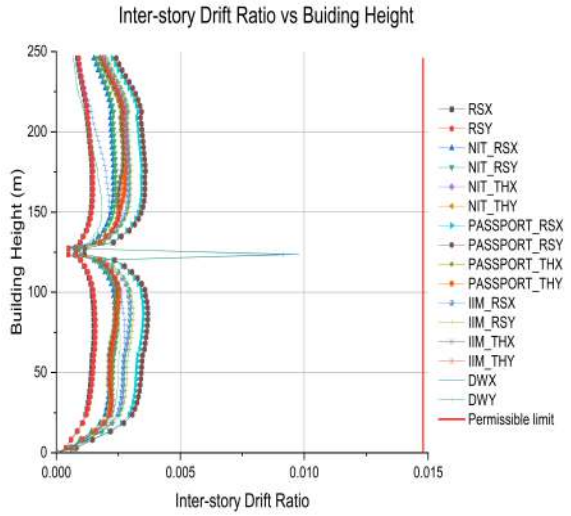

(c) ISDR of OR27S64

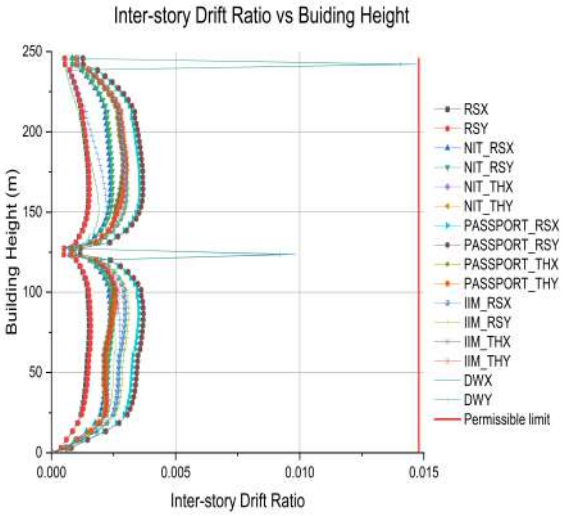

(d) ISDR of OR27&59S64

Figure 6.30: ISDR of OR Tall Buildings

It is seen that ISDR for all TB buildings are within limits and maximum ISDR is recorded in case of PASSPORT RS load case. Exponent spike in ISDR due to DWL load cases and abrupt decrease in ISDR owing to all seismic load cases are noticed in all OR steel-concrete tall buildings at the story where outriggers are placed.

6.5 Comparison between Lateral Load Resisting Systems

Structural engineers' ultimate goal is to design tall structures with sufficient strength, stiffness, stability, and cost-effectiveness. In this section, the strength and stiffness parameters of the structural Wall-Moment Frame system, the Tubular system, and the Outrigger and Belt Truss systems addressed in this study will be compared, and the most efficient structural system will be presented.Out of the three structural wall configurations SM1, SM2, and SM3, the SM1 configuration is chosen for comparison with other structural systems due to its superior performance in terms of strength, stiffness, and cost. In the case of a 64-story outrigger (OR) system, the OR27&59S64 building model is excluded because it requires two outriggers while having comparable strength and stiffness to the OR27S64 model.

6.5.1 Comparison of Base Shear with various LLRS

Critical lateral load case such as PASSPORT_RS and DWL along with Response Spectrum (RS) load case from IS 1893 (Part 1): 2016[47] are selected for comparison of base shear with different LLRS. Base Shear in three LLRS (SM, TB and OR) with 24 story, 44 story and 64 story steel-concrete tall buildings are presented in Figures 6.31, 6.32 and 6.33 respectively.

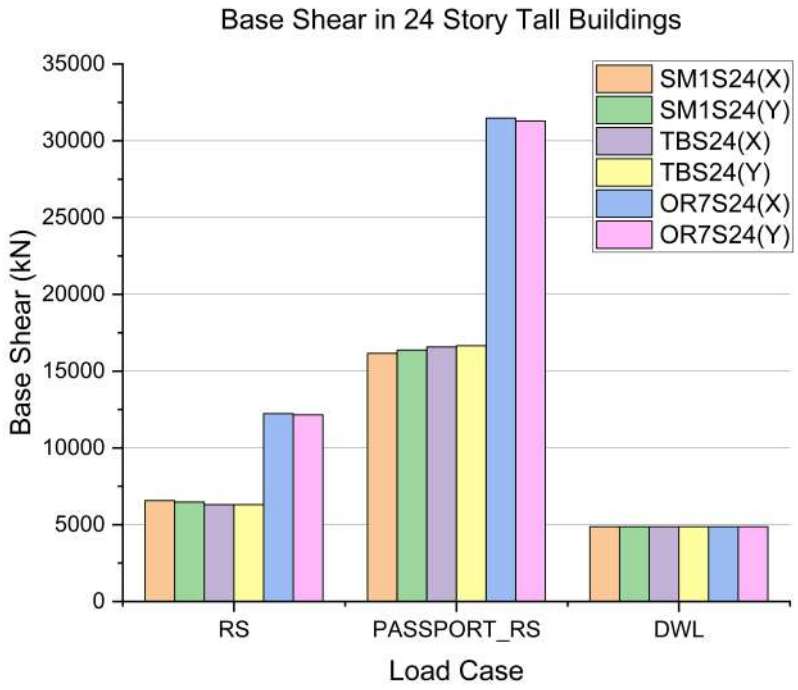

Figure 6.31: Base Shear in 24 Story Tall Buildings

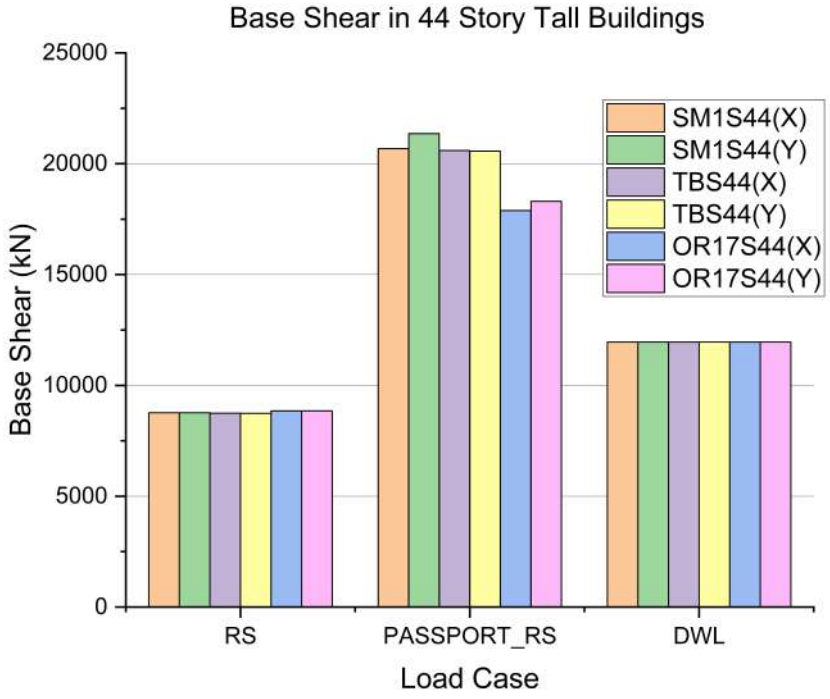

Figure 6.32: Base Shear in 44 Story Tall Buildings

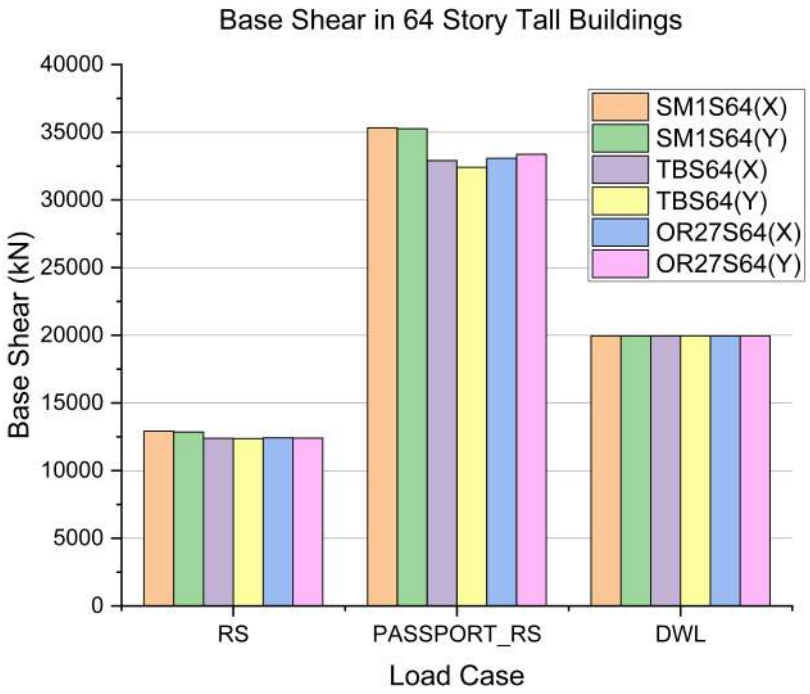

Figure 6.33: Base Shear in 64 Story Tall Buildings

The highest shear at the base owing to the PASSPORT RS load case is observed in all three LLRS and for all story counts. In 44-story and 64-story tall buildings, the SM system has the highest base shear and the OR system has the lowest base shear. In the case of 24-story tall buildings, the base shear owing to seismic lateral load cases (RS and PASSPORT RS) escalated exponentially, resulting in an outrigger system with the highest base shear in RS and PASSPORT RS load cases among the three LLRS.

6.5.2 Comparison of Lateral Force Distribution in Structural Walls and Columns with various LLRS

Walls and columns play a significant role in resisting lateral loads. To investigate the relative contribution of structural walls and columns in resisting crucial lateral loads, the lateral forces of the lowest story in structural walls and columns are added separately and shown in tabular format. The Tables 6.17, 6.18, and 6.19 relate the contribution of structural walls in resisting lateral loads to the combined lateral forces resisted by structural walls and columns in buildings of 24, 44, and 64 stories, respectively.

Table 6.17: Structural Wall Contribution in Resisting Lateral Loads for 24 Story Buildings

Structural Wall Contribution in Resisting Lateral Loads						
Load Case	**Force in X direction (Fx)**			**Force in Y direction (Fy)**		
	Σ Fx (SW+ Col)	**Σ Fx (SW)**	**% Contribution**	**Σ Fy (SW+ Col)**	**Σ Fy (SW)**	**% Contribution**
SM1S24						
DWLX	4868.3	3974.3	81.6	676.0	558.6	82.6
DWLY	676.0	549.7	81.3	4868.3	4037.3	82.9
PASSPORT_RSX	-16260.6	-13597.7	83.6	-350.3	-258.1	73.7
PASSPORT_RSY	-137.0	-46.9	34.3	-16565.6	-14040.0	84.8
TBS24						
DWLX	2379.5	1762.0	74.1	337.6	253.4	75.1
DWLY	341.4	253.1	74.1	2352.1	1763.1	75.0
PASSPORT_RSX	-6711.7	-4932.3	73.5	-231.7	-190.3	82.1
PASSPORT_RSY	-132.0	-46.4	35.1	-6668.3	-4954.0	74.3
OR7S24						
DWLX	4868.3	3600.2	74.0	676.0	511.4	75.7
DWLY	676.0	499.3	73.9	4868.3	3686.8	75.7
PASSPORT_RSX	-31484.6	-23429.3	74.4	-895.3	-600.6	67.1
PASSPORT_RSY	-732.3	-306.5	41.9	-31326.3	-23860.2	76.2

Table 6.18: Structural Wall Contribution in Resisting Lateral Loads for 44 Story Buildings

Structural Wall Contribution in Resisting Lateral Loads						
Load Case	**Force in X direction (Fx)**			**Force in Y direction (Fy)**		
	Σ Fx (SW+ Col)	**Σ Fx (SW)**	**% Contribution**	**Σ Fy (SW+ Col)**	**Σ Fy (SW)**	**% Contribution**
SM1S44						
DWLX	11958.5	8701.3	72.8	1485.1	1109.9	74.7
DWLY	2335.7	1982.6	84.9	12021.0	9115.5	75.8
PASSPORT_RSX	-20756.3	-15371.7	74.1	-956.3	-665.3	69.6
PASSPORT_RSY	-567.3	-251.4	44.3	-21700.6	-16591.0	76.5
TBS44						
DWLX	6125.8	3662.7	59.8	769.3	469.5	61.0
DWLY	772.2	462.6	59.9	6098.0	3713.3	60.9
PASSPORT_RSX	-9970.0	-5930.8	59.5	-620.1	-477.2	77.0
PASSPORT_RSY	-319.2	-143.2	44.8	-9906.5	-5998.1	60.5
OR17S44						
DWLX	11958.5	9903.7	82.8	1485.1	1241.9	83.6
DWLY	1485.1	1228.0	82.7	11958.5	10014.9	83.7
PASSPORT_RSX	-17894.7	-14992.5	83.8	-1063.0	-953.6	89.7
PASSPORT_RSY	-654.3	-491.5	75.1	-18314.8	-15494.3	84.6

Table 6.19: Structural Wall Contribution in Resisting Lateral Loads for 64 Story Buildings

Structural Wall Contribution in Resisting Lateral Loads						
Load Case	**Force in X direction (Fx)**			**Force in Y direction (Fy)**		
	Σ Fx (SW+ Col)	**Σ Fx (SW)**	**% Contribution**	**Σ Fy (SW+ Col)**	**Σ Fy (SW)**	**% Contribution**
SM1S64						
DWLX	19957.7	13989.8	70.1	2349.3	1693.6	72.1
DWLY	2349.4	1644.1	70.0	19957.7	14409.8	72.2
PASSPORT_RSX	-33501.5	-23766.3	70.9	-1993.0	-1379.7	69.2
PASSPORT_RSY	-1234.8	-701.7	56.8	-34185.8	-25055.2	73.3
TBS64						
DWLX	10684.3	5125.7	48.0	1260.7	620.1	49.2
DWLY	1268.0	610.0	48.1	10615.0	5205.6	49.0
PASSPORT_RSX	-17174.0	-8189.1	47.7	-1372.5	-998.7	72.8
S64	-789.1	-377.5	47.8	-16775.4	-8169.4	48.7
OR27S64						
DWLX	19957.7	13989.8	70.1	2349.3	1693.6	72.1
DWLY	2349.4	1644.1	70.0	19957.7	14409.8	72.2
PASSPORT_RSX	-33501.5	-23766.3	70.9	-1993.0	-1379.7	69.2
PASSPORT_RSY	-1234.8	-701.7	56.8	-34185.8	-25055.2	73.3

Percentage contribution of structural walls in 24, 44 and 64 story tall buildings in x and y direction forces are shown in Figures 6.34, 6.35 and 6.36 respectively.

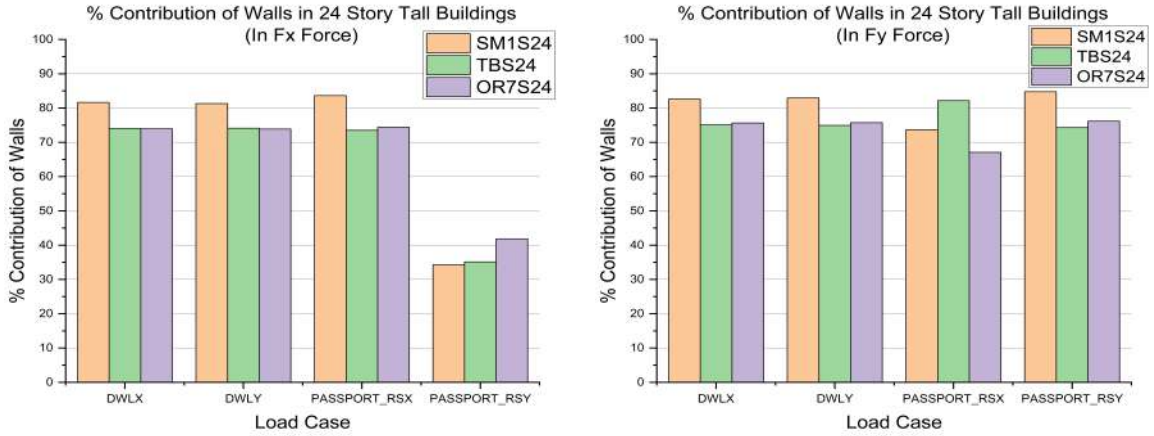

(a) % Contribution in Forces in X direction (b) % Contribution in Forces in Y direction

Figure 6.34: % Contribution of Structural Walls in 24 Story Tall Buildings against Lateral Loads

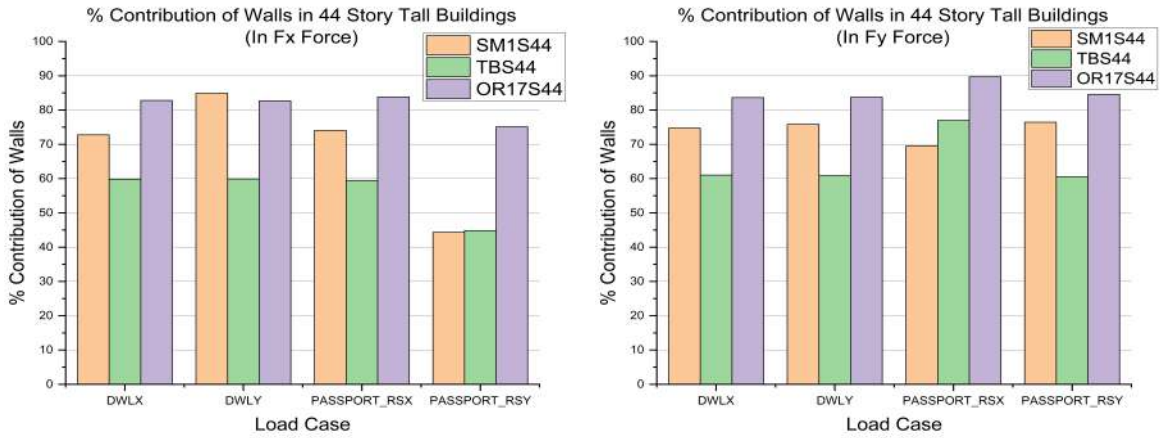

(a) % Contribution in Forces in X direction (b) % Contribution in Forces in Y direction

Figure 6.35: % Contribution of Structural Walls in 44 Story Tall Buildings against Lateral Loads

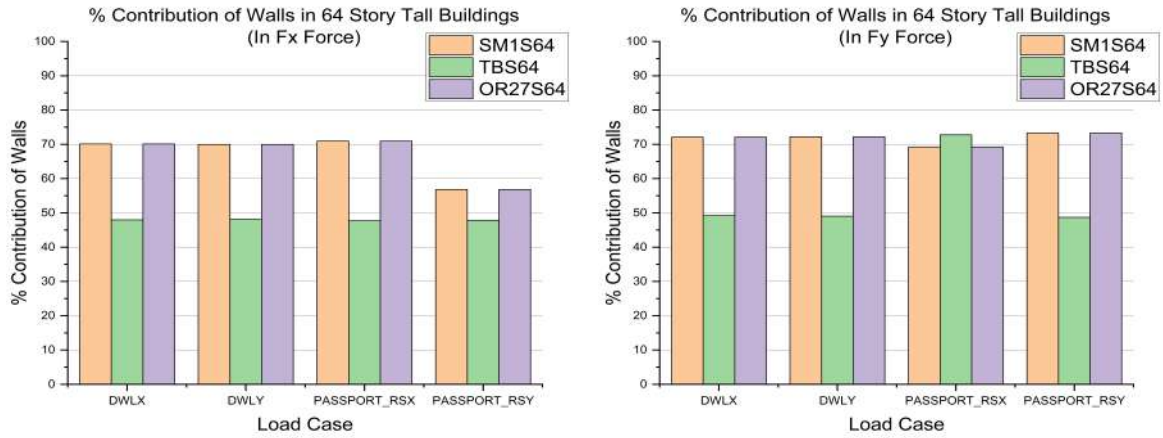

(a) % Contribution in Forces in X direction (b) % Contribution in Forces in Y direction

Figure 6.36: % Contribution of Structural Walls in 64 Story Tall Buildings against Lateral Loads

On the basis of the percentage contribution of structural walls in resisting lateral loads, structural walls in the tubular system contribute the least, as the majority of lateral loads are resisted by closely spaced columns, whereas structural walls in the SM and OR systems contribute significantly more in resisting lateral loads than those in the TB system. Also, as the number of stories increases, the percent contribution of structural walls in all LLRS diminishes.

6.5.3 Time Period and Mode of Vibrations

Controlling the torsional mode of vibration in the design of tall buildings with 24 stories proved challenging in this investigation. Figures 6.37, 6.38 and 6.39 shows time period of the first three mode of vibrations.

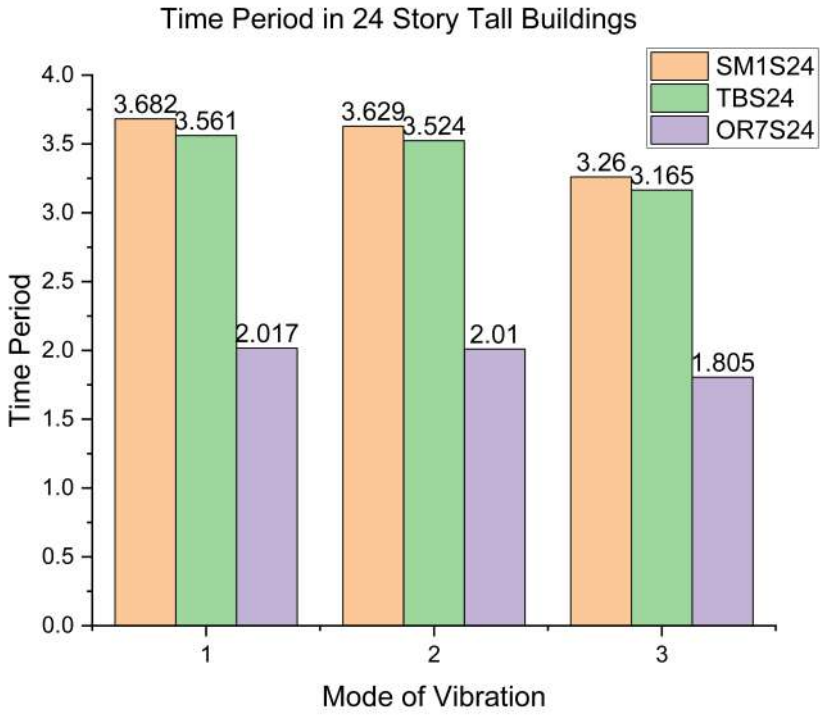

Figure 6.37: Time Period of 24 Story Tall Buildings

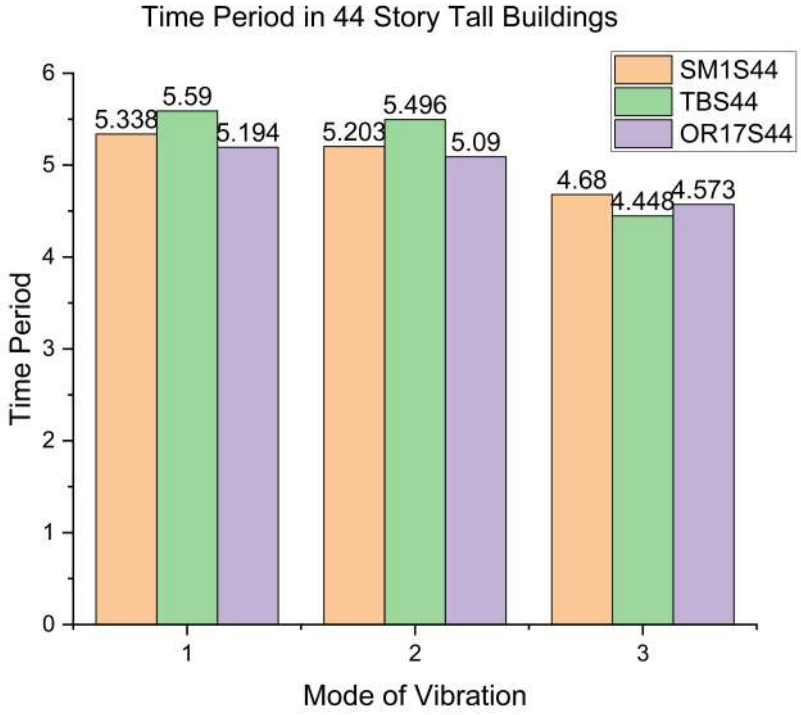

Figure 6.38: Time Period of 44 Story Tall Buildings

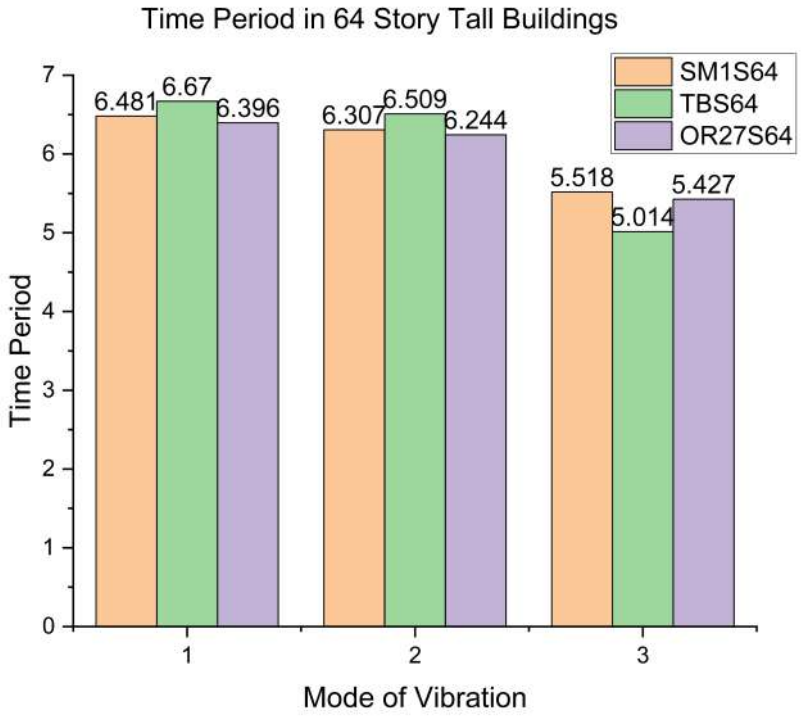

Figure 6.39: Time Period of 64 Story Tall Buildings

From these figures, it can be depicted that time period for the first two translational mode of vibration in case of tubular system results into higher value compared to SM and OR system but tubular systems performs better to resist third mode of rotational vibrations in 24 story tall buildings compared to SM and OR systems.

6.5.4 Story Displacement

Critical load case combination for story displacement in all three systems with 24 story, 44 story and 64 story tall buildings are PASSPORT_RSY, DWLY and DWLX respectively. Story displacement for three LLRS SM, TB and OR for 24, 44 and 64 story tall buildings are shown in Figures 6.40, 6.41 and 6.42 respectively. Top story displacements in all buildings are presented in fig. 6.43.

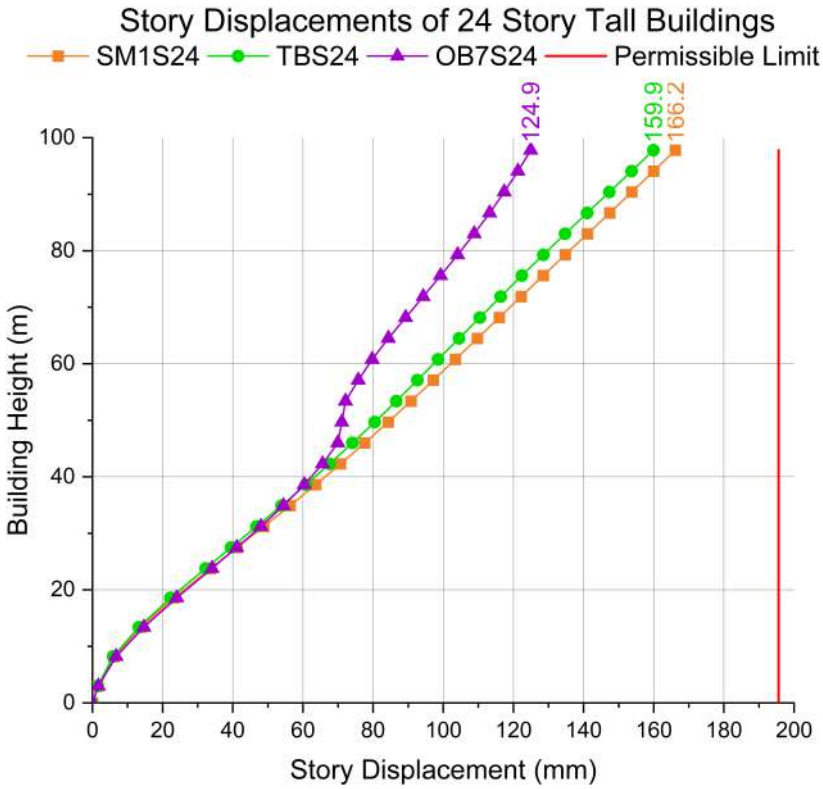

Figure 6.40: Story Displacements of 24 Story Tall Buildings

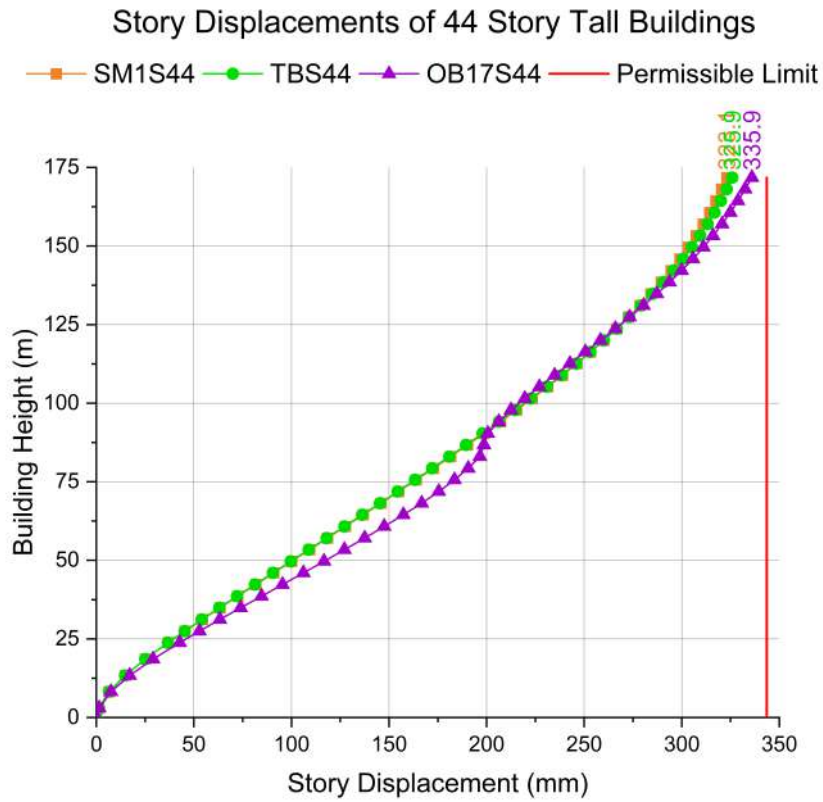

Figure 6.41: Story Displacements of 44 Story Tall Buildings

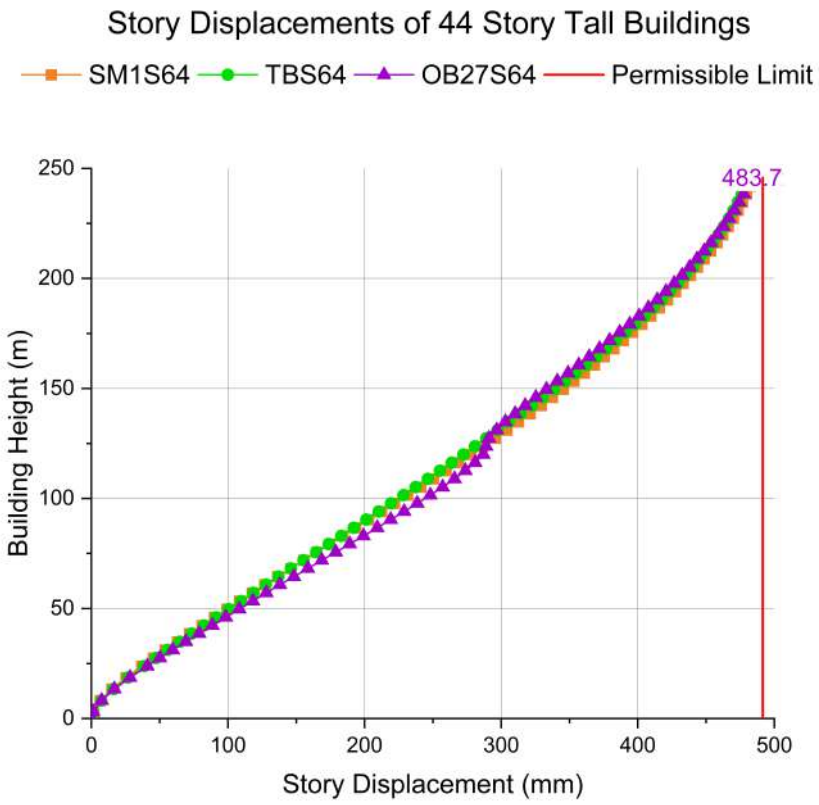

Figure 6.42: Story Displacements of 64 Story Tall Buildings

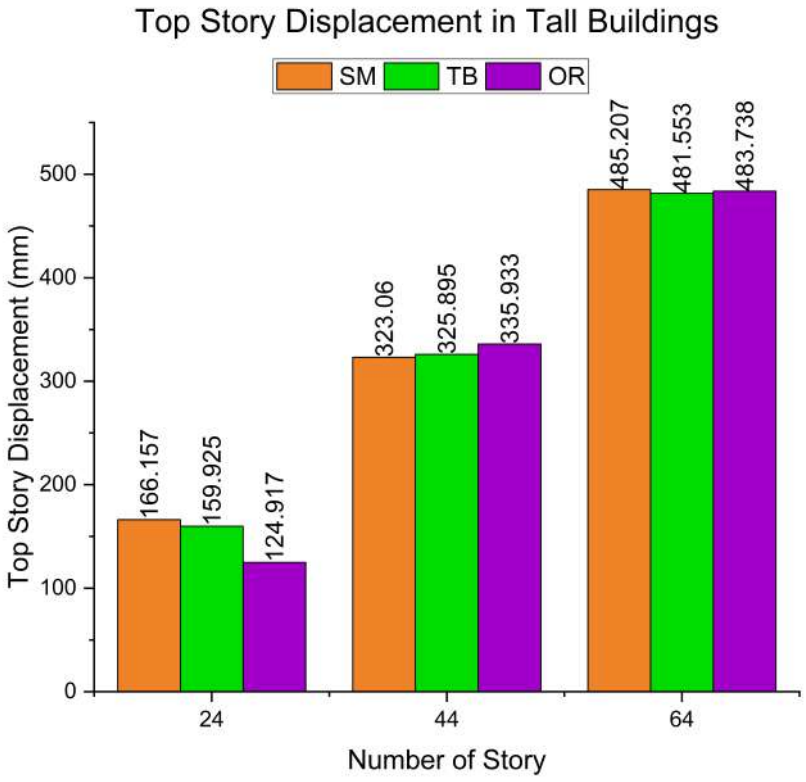

Figure 6.43: Top Story Displacements of Tall Buildings

From the results of story displacements and top story displacements, it can be inferred that as building height increases, story displacements approach the legal limits, and this parameter is beginning to control building design. In 24- and 64-story buildings, outrigger systems result in smaller story displacements compared to SM and TB systems.

6.5.5 Inter-Story Drift Ratio

According to clause 7.11 of IS 1893: 2016[47], the permitted limit for inter-story drift ratio of a structure under service loads is 0.004 times the height of each level. Thus, allowable maximum ISDR for all models is 0.0148. Lateral load combinations due to PASSPORT_RSY load case becomes predominant in the inter-story parameters for all tall building models except 44 and 64 story outrigger system tall buildings. ISDR in three LLRS SM, TB and OR for 24, 44 and 64 story tall buildings are shown in Figures 6.44, 6.45 and 6.46 respectively. Maximum ISDR in all buildings is presented in Fig. 6.47.

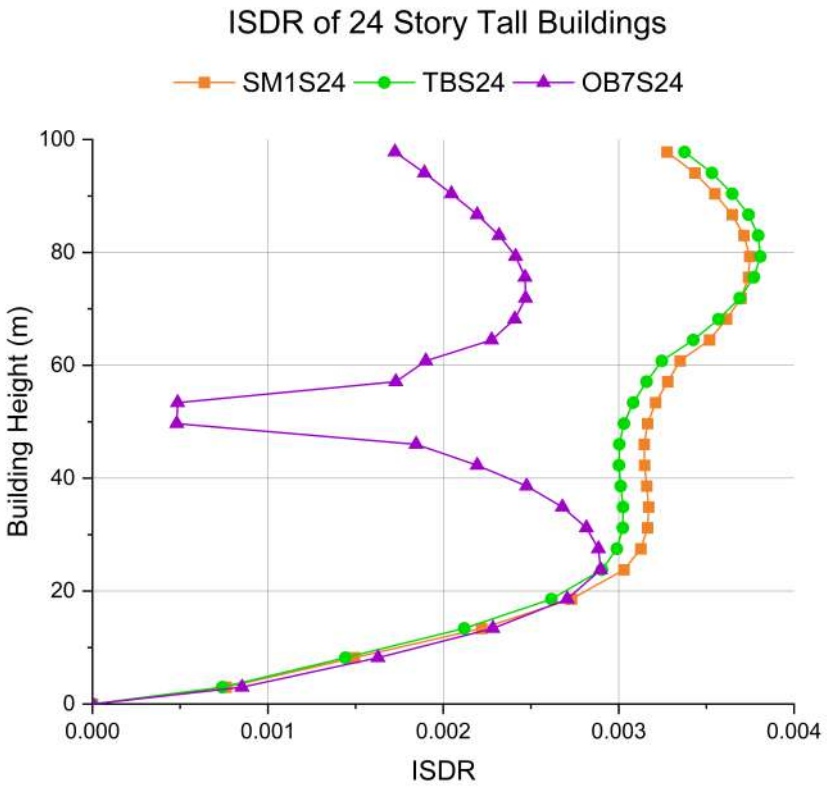

Figure 6.44: ISDR of 24 Story Tall Buildings

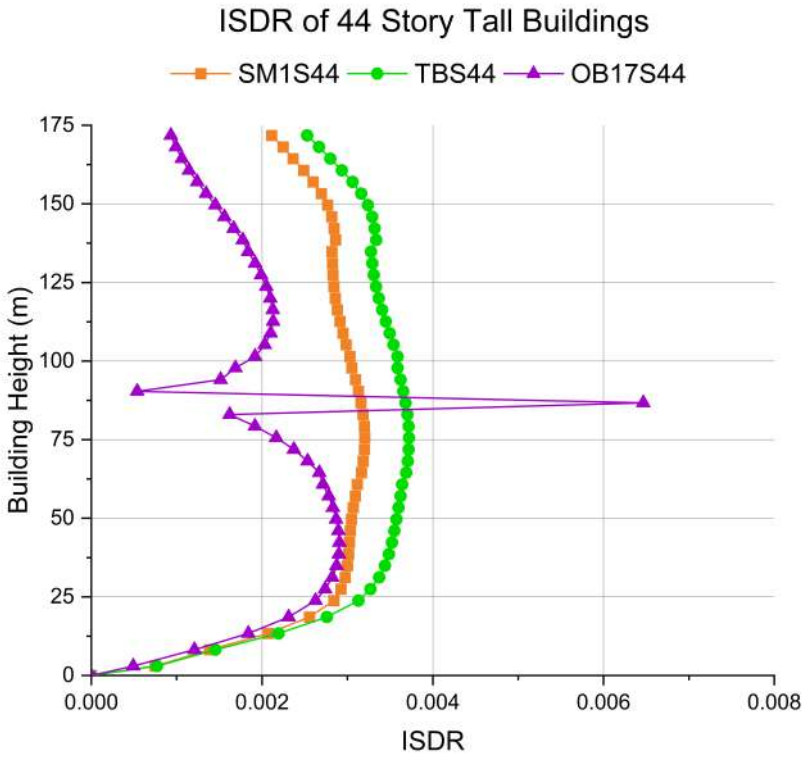

Figure 6.45: ISDR of 44 Story Tall Buildings

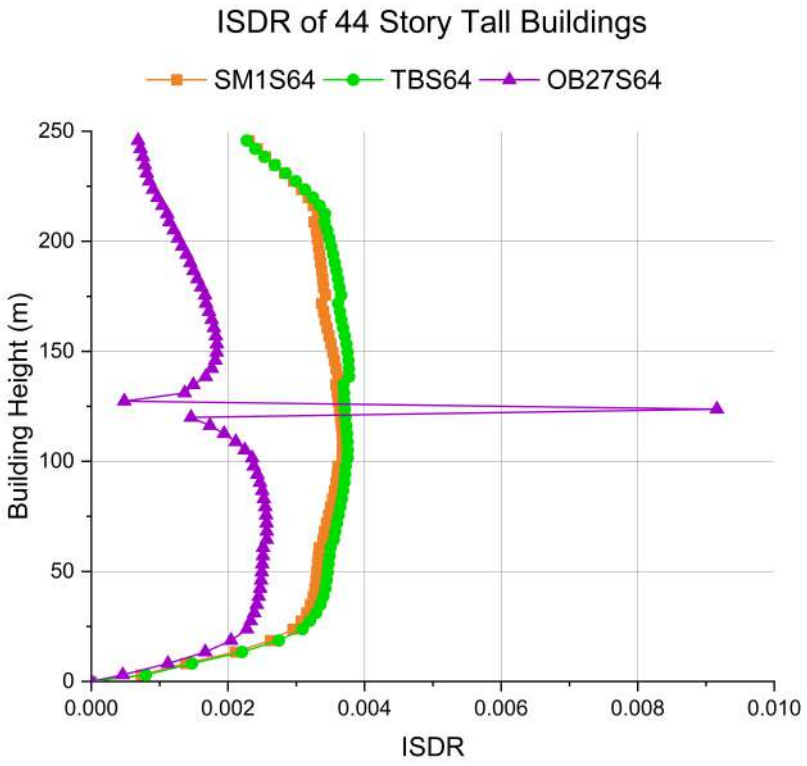

Figure 6.46: ISDR of 64 Story Tall Buildings

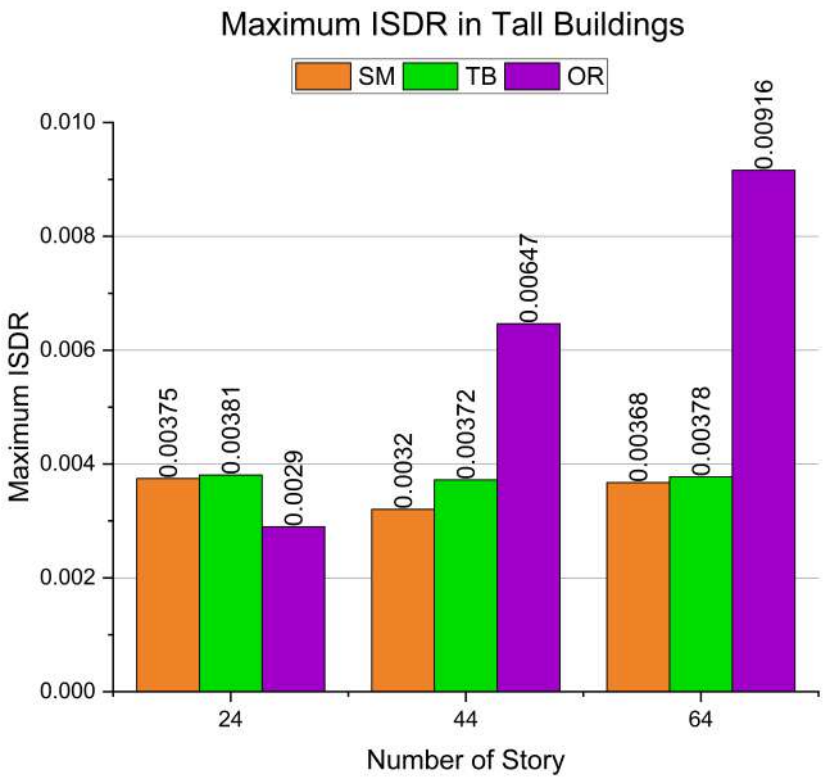

Figure 6.47: Maximum ISDR of Tall Buildings

In 44 and 64 story tall buildings, OR systems exhibit the most inter-story drift compared to SM and TB systems due to DWL load combinations, but OR systems exhibit the lowest ISDR in 24 story buildings due to PASSPORT RS load combinations. This demonstrates that wind load combinations have a significant impact on outrigger systems in taller buildings. The sudden increase in ISDR in OR systems is observed at the floor where outrigger is provided.

6.5.6 Structural Weight

The cost of the project is crucial to the development of tall structures. As a considerable number of structural materials are needed in the construction of tall buildings, optimising the quantity of structural materials and increasing cost efficiency is one of the most important aspects of the intelligent, sustainable, and cost-effective design of tall structures. In Table 6.20, the quantities of M60 concrete and Fe540 structural steel in per square metre of tall building's floor plans are provided.

Table 6.20: Quantity of Concrete and Steel in Tall Buildings

Story	**Building Model**	**M60 Concrete** (m^3/m^2)	**Fe540 Steel** (**kg**/m^2)
24	SM1S24	0.138	119.45
	TBS24	0.135	115.73
	OR7S24	0.138	224.62
44	SM1S44	0.152	145.82
	TBS44	0.156	148.04
	OR17S44	0.137	135.43
64	SM1S64	0.163	219.86
	TBS64	0.178	226.69
	OR27S64	0.149	214.18

Concrete quantity and structural steel in all tall buildings are presented in Figures 6.48 and 6.49 respectively.

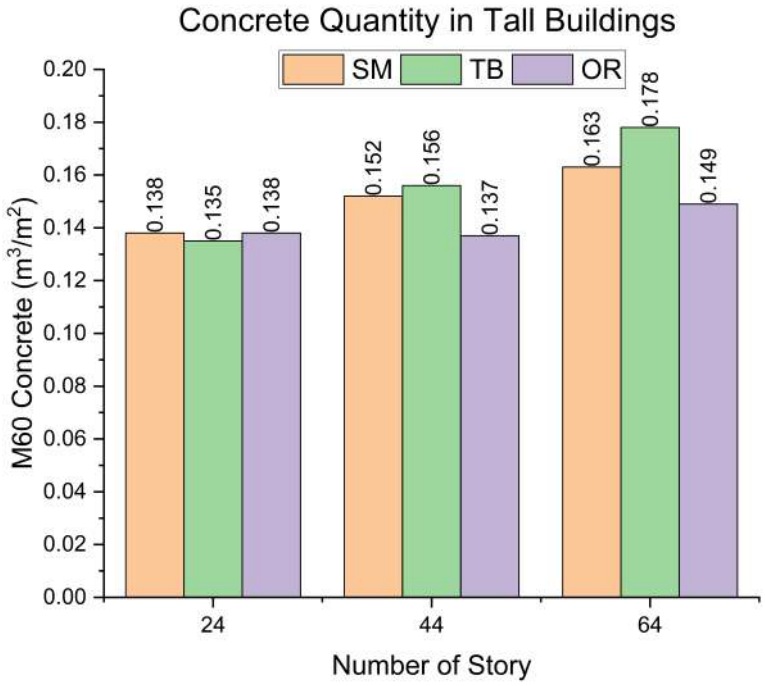

Figure 6.48: M60 Concrete Quantity in Tall Buildings

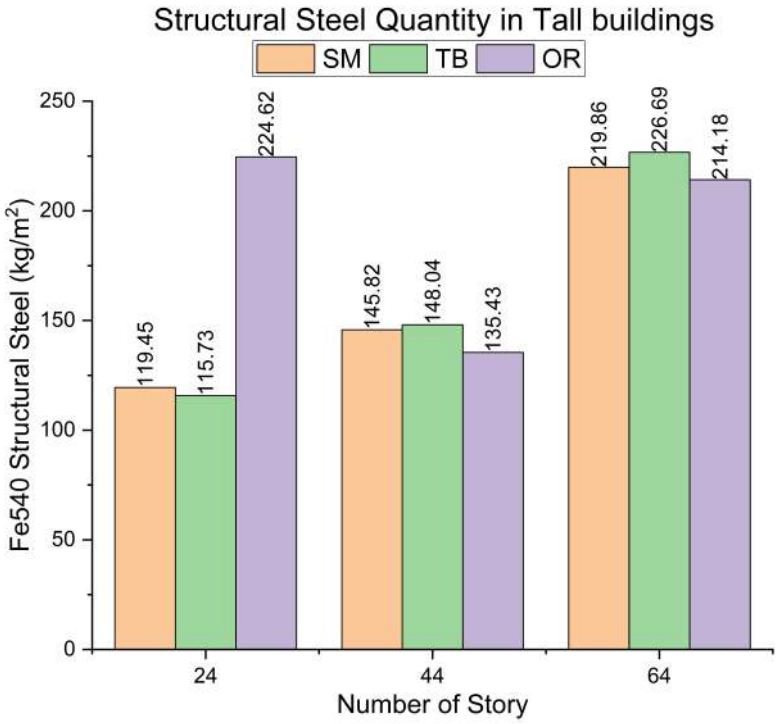

Figure 6.49: Fe540 Structural Steel Quantity of Tall Buildings

From the quantity estimation of concrete and structural steel used in all three LLRS, it can be deduced that outrigger systems are most economic system in case of 44 and 64 story buildings while tubular system is the most economic in 24 story tall buildings. Structural wall-Moment Frame system lies in between outrigger and tubular systems in all 24, 44 and 64 story tall buildings.

6.6 Summary

This section presents and discusses the base shear, storey shear, time period, modal participating mass ratio, story displacements, and inter-story drift ratio of the structural wall-moment frame system, the tubular system, and the outrigger and belt truss system. This chapter also compares several lateral load resisting systems based on serviceability characteristics, lateral load distribution between columns and structural walls, and structural weight.

Chapter 7

Summary, Conclusion and Future scope of work

7.1 Summary

Various lateral load-resisting structural systems employed in concrete, steel, and steel-concrete composite tall structures have been studied in the present major project work report. The case studies of existing super-tall buildings around the world as well as literatures related to the structural wall-moment frame system, tubular system, outrigger system, and wind load in tall buildings are studied during present study. Structural Wall-Moment Frame System, Tubular System and Core with Outriggers and Belt Truss System are considered to study their behaviour in tall buildings of varying height.

A parametric analysis of along and across wind loads on tall structures with identical floor plans and aspect ratios ranging from 1:1 to 1:3 is carried out. For estimating wind loading on buildings, IS 875 (Part 3): 2015 code-specified static wind load analysis and dynamic wind load analysis utilising the gust factor method for the along and across wind loadings are adopted. In the absence of wind tunnel testing, a wind time history analysis can be performed utilising the Tokyo Polytechnic University (TPU) Aerodynamic Wind Pressure Database for the building under consideration. In present study, the procedure for calculating along and across wind time history loads using wind pressure coefficients from the TPU database is illustrated.

This study investigated the analysis and design of 24, 44, and 64-story tall buildings with a 48 m x 48 m floor plan with structural wall-moment frame, tubular, and outrigger & belt

truss structural systems. The evaluation of gravitational and lateral loads due to earthquakes and wind as well as structural element design methodology are presented in this report. Static and dynamic wind load analysis are carried out as per IS 875 (Part 3): 2015 for along and across wind load estimation. The seismic loads are evaluated using equivalent static analysis and dynamic response spectrum analysis as specified in IS 1893 (Part 1): 2016 as well as site-specific response spectrum and time history analysis. The software ETABS is utilised for modelling, analysis, and design of tall buildings. The selection of load combinations is based on the recommendations of applicable Indian standards. The design of composite structural members adheres to AISC 360-10[35], whereas the design of other structural components adheres to relevant Indian standard requirements.

A study is conducted to compare response of tall buildings with different location of structural walls in structural wall-moment frame structural system. The shear lag effect in tubular systems is also studied for tall buildings considered in this study. The optimal number of outriggers in 64-story tall buildings is also determined. On the basis of analysis results such as code-specified and dynamic time periods, base shear owing to earthquake and wind loads, structural wall contribution in resisting lateral loads, story displacements, and drift ratio due to lateral loadings, all three structural systems are compared. The performance of three structural systems for 24, 44 and 64 story buildings is assessed based on design considerations including appropriate structural member dimensions and material consumption.

7.2 Conclusions

Based on parametric study carried out for estimation of along and across wind loading on tall buildings with different dimensions using static and dynamic analysis as per IS 875 (Part 3): 2015 and using wind tunnel based TPU database, following conclusions are derived.

1. The along wind forces due to dynamic gust factor (DGF) method are 148 to 267.5 percent of along wind forces due to static wind load analysis (SWLA) which shows importance of dynamic wind load analysis using gust factor compared to static wind load analysis in design of tall buildings.

2. In square plan buildings, along wind load due to maximum sum, peak coefficient, and mean coefficient methods based on TPU database are between 69.7% to 128.8%, 125.7% to 186.9%, and 34.8% to 56.4% respectively and across winds are 89.3% to 521.8%, 272.1% to 1711.7%, and 1.3% to 13.3% compared to dynamic gust factor method, compared to dynamic gust factor method.

3. When wind is flowing along longer dimension of rectangular shape buildings, along wind forces from wind time history methods based on TPU database are between 14.8% to 56.7% of along wind forces due to dynamic gust factor method and across wind forces are between 162.8% to 1276.8% of across wind forces due to dynamic gust factor method.

4. When wind is flowing along shorter dimension of rectangular shape buildings, along wind forces from wind time history methods based on TPU database are between 79.6% to 133.6% of along wind forces due to dynamic gust factor method and across wind forces are between 6.3% to 586.6% of across wind forces due to dynamic gust factor method.

5. In tall buildings with a square plan, the dynamic gust factor method as well as the maximum sum of pressure coefficient approach based on TPU database are preferred for evaluating along wind loads, whilst the maximum sum of pressure coefficient approach based on TPU database is more reliable for evaluating across wind loading.

6. In rectangular-shaped tall buildings, the dynamic gust factor (DGF) method as per IS 875 (Part 3): 2015 is more dependable and safer than other approaches for evaluating along and across wind loading.

Based on comparison of analysis results and structural design of 24 story, 44 story and 64 story steel-concrete composite tall buildings with Structural Wall-Moment Frame (SWMF), Tubular (TB) and Outrigger & Belt frame (OR) structural systems, following conclusions are derived.

1. Shear walls and columns sizes in SM2 and SM3 models of structural wall-moment frame system are between 100% to 128% and 83.33% to 100% respectively compared to SM1 model of structural wall-moment frame system. Similar trend is

also observed in beam section sizes. Compared to the SM1 and SM3 systems, the SM2 system has larger structural member sections and a higher displacement of the top story. While the SM3 system provides the smallest section sizes for structural components but it does not meet the criteria of 90 percent magnitude of the third torsional mode of vibration time period relative to the first two translational modes in 24-story buildings. Therefore,out of the three shear wall configurations for the wall-frame (SM) system, the SM1 configuration is selected for comparing lateral load resisting structural system in tall buildings considered subsequently for other structural systems.

2. Primary beam sections in tubular systems are the smallest, whereas the larger beam sections are found on outrigger floors. Minimum perimeter and interior column sections are observed in tubular systems for 24-story buildings, whereas outrigger systems provide minimum column section sizes for 44- and 64-story structures.

3. Load combinations due to Passport office (located in Ahmedabad) site-specific response spectrum load case are the governing load combinations for design of shear walls in all three structural systems for all story tall buildings. Governing load combinations for columns in all three structural systems are load combinations due to Passport office site-specific response spectrum and dynamic wind load cases.

4. Base shear due to Passport office site-specific response spectrum and dynamic wind load cases are between 225.9% to 289.2% and 71.03% to 155.7% of base shear due to IS 1893 (Part 1): 2016 response spectrum load case respectively in all the three structural systems. This proves that maximum base shear in all the three structural systems is due to Passport office site-specific response spectrum load case. The maximum base shear in tubular and outrigger systems are 102.56% and 194.74% for 24 story, 99.6% and 86.4% for 44 story and 93.62% and 93.16% for 64 story tall buildings compared to structural wall-moment frame system. It is observed that outrigger systems gives least base shear in 44 and 64 story buildings but it gives larger base shear compared to structural wall-moment frame and tubular systems in 24 story tall buildings.

5. Under the effect of lateral loads due to the site-specific response spectrum, a sudden

drop is observed in the increase of story shear between three-quarters and one-fourth of the building's height for all structural systems.

6. Structural walls contribution in resisting lateral loads for structural wall-moment frame, tubular and outrigger & belt truss structural systems are between 69% to 84%, 47% to 72% and 67% to 89% of total lateral load resisting system (Columns + Walls) for 24, 44 and 64 story buildings respectively. As the number of story increases, contribution of structural walls in resisting lateral load decreases. In contribution of structural walls in resisting lateral loads, outrigger & belt truss structural system gives maximum contribution and tubular structural system gives the least contribution.

7. Tubular structural system has the longest time period among the three structural systems considered; however, the probability of torsional mode of vibration occurring as the first mode of vibration in tubular systems is the lowest, which becomes the governing criterion for 24-story wall-frame and outrigger system tall buildings. To avoid torsional mode of vibration as the first mode of vibration in the outrigger system for 24-story tall buildings, it is observed that very large sections of structural members are provided, which has a negative impact on the cost-effectiveness of the outrigger & belt truss structural system for 24-story tall buildings. However, by changing location of outrigger at mid-height to top of buildings, cost-effectiveness of outrigger structural system can be improved for 24 story building.

8. Top story displacement is the important criteria for design of tall buildings. While comparing top story displacements of tubular and outrigger & belt truss structural system with wall-frame structural system, it is 96.23% and 75.2% for 24 story, 100.88% and 103.97% for 44 story and 99.3% and 99.7% for 64 story tall buildings respectively. In 44- and 64-story wall-frame, tubular, and outrigger systems, building design is governed by top story displacement, but in 24-story tall structures, design is governed either by torsional mode of vibration time period values or by structural member strength requirements.

9. All tall buildings with structural wall-moment frame and tubular structural systems have the highest inter-story drift ratios for the Passport office site-specific response

spectrum load case. Maximum inter-story drift ratios in structural wall-moment frame and tubular structural systems are minimal and within the acceptable range. In the case of outrigger systems, however, the largest inter-story drift ratios are caused by dynamic wind load case, and as the number of stories increases, this ratio approaches the maximum allowable limit of inter-story drift ratio 0.0148.

10. According to the concrete and steel quantity estimations, the structural wall-moment frame system and tubular system are the most efficient structural systems for a 24-story tall building. The cost-effectiveness of an outrigger structural system can be improved by changing the outrigger story from mid-height to the optimal location within the building. The outrigger structural system is the most cost-effective lateral load resisting system for 44-story and 64-story tall buildings considered in present study.

7.3 Future scope of work

The present study can be further extended to include following aspects:

- Study of other lateral load resisting structural systems such as diagrid, space truss system, mega column system, tube-in-tube system, hybrid systems etc.
- Study on tall buildings with varying floors plan configuration such as rectangular plan, circular plan, cross-sections with chamfering at corners and various building forms such as tapered, twisted, setback, etc.
- Optimum location and numbers of outriggers for different height of tall buildings
- Incorporation of secondary effects such as creep, shrinkage, axial shortening etc.
- Comparison of one-step analysis and time derived stage construction analysis

Bibliography

[1] Ahamad S. A. and Pratap K. V., "Dynamic analysis of G+20 multi storied building by using shear walls in various locations for different seismic zones by using Etabs," Materials Today: Proceedings, vol. 43, pp. 1043–1048, 2020, doi: 10.1016/j.matpr.2020.08.014.

[2] Alhaddad W., Halabi Y., Xu H., and Lei H. G., "A comprehensive introduction to outrigger and belt-truss system in skyscrapers," Structures, vol. 27, no. June, pp. 989–998, 2020, doi: 10.1016/j.istruc.2020.06.028.

[3] Alinejad H. and Kang T. H.-K., "Engineering Review of ASCE 7-16 Wind-Load Provisions and Wind Effect on Tall Concrete-Frame Buildings," Journal of Structural Engineering, vol. 146, no. 6, p. 04020100, 2020, doi: 10.1061/(asce)st.1943-541x.0002622.

[4] Aly A. M. and Abburu S., "On the design of high-rise buildings for multihazard: Fundamental differences between wind and earthquake demand," Shock and Vibration, vol. 2015, 2015, doi: 10.1155/2015/148681.

[5] Asadi E. and Adeli H., "Diagrid: An innovative, sustainable, and efficient structural system," Structural Design of Tall and Special Buildings, vol. 26, no. 8, pp. 1–11, 2017, doi: 10.1002/tal.1358.

[6] Choi H. S., Ho G., Joseph L., Mathias N., and CTBUH, "CTBUH Height Criteria," Outrigger Design for High-Rise Buildings, pp. 80–82, 2020, doi: 10.1201/9781315661971-13.

[7] Dabbaghchian I., Mirghaderi S. R., and Sayadi S., "Comparison of seismic behavior of the eccentric and conventional diagrid systems," Structural Design of Tall and Special Buildings, vol. 30, no. 3, pp. 1–19, 2021, doi: 10.1002/tal.1824.

[8] Elansary A. A., Metwally M. I., and El-Attar A., "Staged construction analysis of reinforced concrete buildings with different lateral load resisting systems," Engineering Structures, vol. 242, no. March 2020, p. 112535, 2021, doi: 10.1016/j.engstruct.2021.112535.

[9] Fu F., "Bracing, Diagrid, 3D Space Frame, and Mega Frame Structural Systems in Tall Buildings," Design and Analysis of Tall and Complex Structures, pp. 137–175, 2018, doi: 10.1016/b978-0-08-101018-1.00005-8.

[10] Fu F., "Tube System in Tall Building," Design and Analysis of Tall and Complex Structures, pp. 109–135, 2018, doi: 10.1016/b978-0-08-101018-1.00004-6.

[11] Gupta V., Rawat S., Mittal R. K., and Muthukumar G., A Brief Review of Structural Aspects of IS 16700:2017, vol. 38. Springer Singapore, 2020. doi: 10.1007/978-981-13-7615-3-7.

[12] Heshmati M., Khatami A., and Shakib H., "Seismic performance assessment of tubular diagrid structures with varying angles in tall steel buildings," Structures, vol. 25, no. January, pp. 113–126, 2020, doi: 10.1016/j.istruc.2020.02.030.

[13] Ilgın H. E., Ay B. Ö., and Gunel M. H., "A study on main architectural and structural design considerations of contemporary supertall buildings," Architectural Science Review, vol. 64, no. 3, pp. 212–224, 2021, doi: 10.1080/00038628.2020.1753010.

[14] İnam İ. E., Çeribaşı S., and Karapınar I. S., "Determining the optimum outrigger locations for steel tall buildings by using time history analyses," Structural Design of Tall and Special Buildings, vol. 30, no. 7, pp. 1–16, 2021, doi: 10.1002/tal.1843.

[15] Jafari M. and Alipour A., "Methodologies to mitigate wind-induced vibration of tall buildings: A state-of-the-art review," Journal of Building Engineering, vol. 33, no. June 2020, p. 101582, 2021, doi: 10.1016/j.jobe.2020.101582.

[16] Jeong S. Y., Alinejad H., and Kang T. H.-K., "Performance-Based Wind Design of High-Rise Buildings Using Generated Time-History Wind Loads," Journal of Structural Engineering, vol. 147, no. 9, p. 04021134, 2021, doi: 10.1061/(asce)st.1943-541x.0003077.

[17] Kavyashree B. G., Patil S., and Rao V. S., "Evolution of Outrigger Structural System: A State-of-the-Art Review," Arabian Journal for Science and Engineering, no. 0123456789, 2021, doi: 10.1007/s13369-021-06074-9.

[18] Khy K., Chintanapakdee C., Warnitchai P., and Wijeyewickrema A. C., "Modified response spectrum analysis to compute shear force in tall RC shear wall buildings," Engineering Structures, vol. 180, no. September 2018, pp. 295–309, 2019, doi: 10.1016/j.engstruct.2018.11.022.

[19] Kumar K. S., "Wind loading on tall buildings: Review of Indian Standards and recommended amendments," Journal of Wind Engineering and Industrial Aerodynamics, vol. 204, no. May, p. 104240, 2020, doi: 10.1016/j.jweia.2020.104240.

[20] Lacidogna G., Nitti G., Scaramozzino D., and Carpinteri A., "Diagrid systems coupled with closed- and open-section shear walls: Optimization of geometrical characteristics in tall buildings," Procedia Manufacturing, vol. 44, no. 2019, pp. 402–409, 2020, doi: 10.1016/j.promfg.2020.02.277.

[21] Liu C., Li Q., Lu Z., and Wu H., "A review of the diagrid structural system for tall buildings," Structural Design of Tall and Special Buildings, vol. 27, no. 4, pp. 1–10, 2018, doi: 10.1002/tal.1445.

[22] Kumawat M. S. and Kalurkar L. G., "Analysis and Design of Multistory," International Journal of Structural and Civil Engineering Research, vol. 3, no. 2, pp. 125–137, 2014.

[23] Mir M. A. and Kyoung S. M., "Structural Developments in Tall Buildings: Current Trends and Future Prospects," Architectural Science Review, vol. 50, no. 3, pp. 37–41, 2011, doi: 10.3763/asre.200.

[24] Moon K. S., "Comparative efficiency of structural systems for steel tall buildings," International Journal of Sustainable Building Technology and Urban Development, vol. 5, no. 3, pp. 230–237, 2014, doi: 10.1080/2093761X.2014.948099.

[25] Ren X., Bai Q., Yang C., and Li J., "Seismic behavior of tall buildings using steel–concrete composite columns and shear walls," Structural Design of Tall and Special Buildings, vol. 27, no. 4, pp. 1–13, 2018, doi: 10.1002/tal.1441.

[26] Reshma T. V., Sankalpasri S. S., Tanu H. M., and Nirmala M. V., "Multistorey Building Analysis and Its Behavior because of Shear Wall Location Underneath completely different Seismal Zones," IOP Conference Series: Earth and Environmental Science, vol. 822, no. 1, 2021, doi: 10.1088/1755-1315/822/1/012044.

[27] Samadi M. and Jahan N., "Comparative study on the effect of outrigger on seismic response of tall buildings with braced and RC wall core. I: Optimum level and examining modal response spectrum analysis reliability," Structural Design of Tall and Special Buildings, vol. 30, no. 8, pp. 1–15, 2021, doi: 10.1002/tal.1848.

[28] Samadi M. and Jahan N., "Comparative study on the effect of outrigger on seismic response of tall buildings with braced and Wall Core. II: Determining seismic design parameters," Structural Design of Tall and Special Buildings, vol. 30, no. 9, pp. 1–13, 2021, doi: 10.1002/tal.1855.

[29] Sarcheshmehpour M., Estekanchi H. E., and Moosavian H., "Optimum seismic design of steel framed-tube and tube-in-tube tall buildings," Structural Design of Tall and Special Buildings, vol. 29, no. 14, pp. 1–19, 2020, doi: 10.1002/tal.1782.

[30] Abdelrazaq A., "Validating the Structural Behavior and Response of Burj Khalifa," International Journal of High-Rise Buildings, vol. 1, no. 1, pp. 37–51, 2012, [Online]. Available: www.ctbuh.org.

[31] Poon D. C. K., Hsiao L. E., Zhu Y., Zuo S., and Fu G., "Structural analysis and design challenges of the Shanghai Center," Structures Congress 2010, pp. 3088–3103, 2010, doi: 10.1061/41130(369)277.

[32] Abdelrazaq A., "The Challenges of Delivering Iconic Tall Buildings Across the World: A Global Technology Transfer," Global Interchanges: Resurgence of the Skyscraper City, pp.449-55, 2015.

[33] Bungale T.. "Structural Analysis and Design of Tall Buildings: Steel and Composite Construction", CRC Press, Boca Raton, FL, 2016.

[34] Bungale T.. "Tall Building Design: Steel, Concrete, and Composite Systems", CRC Press, Boca Raton, FL, 2016.

[35] ANSI/AISC 360-10. "Specification for Structural Steel Buildings", American Institute of Steel Construction, Illinois, Chicago, 2010.

[36] ACI 318-14 and ACI 318R-14. "Building Code Requirements and Commentary on Building Code Requirements for Structural Concrete", American Concrete Institute, Farmington Hills, MI, 2014.

[37] ASCE 7-16. "Minimum design loads for building and other structures", The American Society of Civil Engineers, Reston, Virginia, 2010.

[38] NBC 2016 (Volume 1). "National Building Code of India", Bureau of Indian Standards, New Delhi, 2016.

[39] NBC 2016 (Volume 2). "National Building Code of India", Bureau of Indian Standards, New Delhi, 2016.

[40] MBBL – 2016, "Model Building Bye-Laws", Ministry of Urban Development, New Delhi, 2016.

[41] IS 875 (Part 1) : 1987. "Code of Practice for Design Loads (Other Than Earthquake) for Buildings and Structures, Part 1 : Dead Loads", Bureau of Indian Standards, New Delhi, 1987.

[42] IS 875 (Part 2) : 1987. "Code of Practice for Design Loads for Buildings and Structures, Part 2 : Imposed Loads", Bureau of Indian Standards, New Delhi,1987.

[43] IS 875 (Part 3) : 2015. "Design Loads (Other Than Earthquake) for Buildings and Structures – Code of Practice, Part 3 : Wind Loads", Bureau of Indian Standards, New Delhi,2015.

[44] IS 456 : 2000. "Plain and Reinforced Concrete – Code of Practice", Bureau of Indian Standards, New Delhi, 2000.

[45] IS 800 : 2007. "General Construction in Steel – Code of Practice", Bureau of Indian Standards, New Delhi, 2007.

[46] IS 13920 : 2016. "Ductile Design and Detailing of Reinforced Concrete Structures Subjected to Seismic Forces – Code of Practice", Bureau of Indian Standards, New Delhi, 2016.

[47] IS 1893 (Part 1) : 2016. "Criteria for Earthquake Resistant Design of Structures, Part 1 : General Provisions and Buildings", Bureau of Indian Standards, New Delhi, 2016.

[48] IS 16700 2017. "Criteria for Structural Safety of Tall Concrete Buildings", Bureau of Indian Standards, New Delhi, 2017.

[49] Patel S. R., "Performance based Wind Analysis of Diagrid Structural Systems," Major Project Report, Department of Civil Engineering, Institute of Technology, Nirma University, Ahmedabad, 2019.

[50] Modi D., "Hybrid Structural System for High Rise Buildings," Major Project Report, Department of Civil Engineering, Institute of Technology, Nirma University, Ahmedabad, 2017.

[51] Khatri N., "Performance based Deisgn of Different Structural Systems in High Rise Structures," Major Project Report, Department of Civil Engineering, Institute of Technology, Nirma University, Ahmedabad, 2016.

[52] Gurule A. V., "Comparison of Structural Systems for Composite Construction in High Rise Building," Major Project Report, Department of Civil Engineering, Institute of Technology, Nirma University, Ahmedabad, 2014.

[53] Saiyed M. S., "High-Rise Structural Systems in Steel," Major Project Report, Department of Civil Engineering, Institute of Technology, Nirma University, Ahmedabad, 2011.

[54] Jivani D. K., "Analysis and Design of Shear Wall Building using Site Specific Response Spectrum," Major Project Report, Department of Civil Engineering, Institute of Technology, Nirma University, Ahmedabad, 2008.

[55] Jamdar R. R., "Study on Characterization of Wind and its Effects on Structures," Major Project Report, Department of Civil Engineering, Institute of Technology, Nirma University, Ahmedabad, 2014.

[56] Aerial View of Burj Khalifa (2017). Available: https://www.maritimegateway.com/wp-content/uploads/2017/04/A-landmark-taller-than-Burj-Khalifa-on-Mumbai-waterfront-scaled.jpg.

[57] CTBUH Tallest Building List Database. Available: https://www.skyscrapercenter.com/building/shanghai-tower/56.

[58] CTBUH Tallest Building List Database. Available: https://www.skyscrapercenter.com/building/432-park-avenue/13227.

[59] Marcus S, Mena H, Yalnız F and Shırley C. “432 Park” in.,” Structure Magazine, pp.32-33, 2018.

[60] ”Tokyo Polytechnic aerodynamic database”, The 21st Century COE program wind effects on tall building and urban Environment. Available: http://db.wind.arch.t-kougei.ac.jp/?msclkid=7aa9fc43ce8511ecb6c3114315fca828

Appendix A

A List of Paper Presented

1) Patel Jenish Y. and Patel Paresh V., "Parametric Study on Design of Steel-Concrete Composite Tall Buildings", International Conference on Research & Developement in Civil Engineering (23^{rd} and 24^{th} December, 2021), SVKM's Institute of Technology, Dhule, Maharashtra. ISBN:978-93-5636-226-0, pp. 24.

Appendix B

A List of Paper Accepted

1) Patel Jenish Y. and Patel Paresh V., "Comparative Study of Outrigger and Wall-Frame Structual Systems in Steel-Concrete Composite Tall Buildings", Innovation in Smart and Sustainable Infrastructure (23^{rd} to 25^{th} August, 2022), PDEU, Gandhinagar, Gujarat. **(Full Paper Submitted)**

2) Patel Jenish Y. and Patel Paresh V., "Comparison of behaviour of Shear Wall-Moment Frame and Framed Tube structural systems of Tall Buildings", International conference on Advancement in Structural & Geotechnical Engineering (25^{th} to 27^{th} August, 2022), Indus University, Ahmedabad, Gujarat. **(Abstract Accepted)**

3) Patel Jenish Y. and Patel Paresh V., "Site Specific Response Spectrum Analysis of Various Wall-Frame Composite Tall Buildings", 17^{th} Symposium on Earthquake Engineering (14^{th} to 17^{th} November, 2022), Indian Institute of Technology Roorkee, Roorkee, Uttarakhand. **(Abstract Accepted)**

Appendix C

MATLAB Code for Calculation of Dynamic Wind Load from Time History Data

This chapter describes the MATLAB code for calculating the dynamic wind load of a high-rise building with a depth to width to height ratio of 1:2:3 using TPU Aerodynamic Database Time History Data [60].

```
clc;
clear all;
%Plz change file name of loading file below and also replace A123_0
with respective model name
load('A123_time_series_of_point_wind_pressure_0' );
A123_0_results = 'A123_0_results.xlsx';
[r_location total_pts] = size(Location_of_measured_points);
%Now we will differentate points to windward, right sideward,
%leeward and left sideward face points.
%Fist column shows point number, second shows x coordinate of pt
%and third shows x coordinate of pt.
ww_pts = zeros(3,total_pts);
rs_pts = zeros(3,total_pts);
```

```
lw_pts = zeros(3,total_pts);
ls_pts = zeros(3,total_pts);
for i = 1:total_pts
 if Location_of_measured_points(4,i)==1
 ww_pts(1,i) = i;
 ww_pts(2,i) = Location_of_measured_points(1,i);
 ww_pts(3,i) = Location_of_measured_points(2,i);
 elseif Location_of_measured_points(4,i)==2
 rs_pts(1,i) = i;
 rs_pts(2,i) = Location_of_measured_points(1,i);
 rs_pts(3,i) = Location_of_measured_points(2,i);
 elseif Location_of_measured_points(4,i)==3
 lw_pts(1,i) = i;
 lw_pts(2,i) = Location_of_measured_points(1,i);
 lw_pts(3,i) = Location_of_measured_points(2,i);
 else
 ls_pts(1,i) = i;
 ls_pts(2,i) = Location_of_measured_points(1,i);
 ls_pts(3,i) = Location_of_measured_points(2,i);
 end
end
%This will differentiate wind pressure coefficient as per on which
%surface it is acting
samples = Sample_frequency*Sample_period;
ww_coeff = zeros(samples,total_pts);
rs_coeff = zeros(samples,total_pts);
lw_coeff = zeros(samples,total_pts);
ls_coeff = zeros(samples,total_pts);
for i = 1:total_pts
 for j = 1:samples
 if Location_of_measured_points(4,i)==1
 ww_coeff(j,i) = Wind_pressure_coefficients(j,i);
```

```
 elseif Location_of_measured_points(4,i)==2
 rs_coeff(j,i) = Wind_pressure_coefficients(j,i);
 elseif Location_of_measured_points(4,i)==3
 lw_coeff(j,i) = Wind_pressure_coefficients(j,i);
 else
 ls_coeff(j,i) = Wind_pressure_coefficients(j,i);
 end
 end
end
%Lets find pressure points in all 3 directions.
breadth_pts = 0; %Variable for number of pressure tap on windward
side
depth_pts = 0; %Variable for number of pressure tap on sideward
side
height_pts = 0; %Variable for number of pressure tap in vertical
direction
for i=1:total_pts
 if Location_of_measured_points(4,i) == 2
 break;
 else
 breadth_pts = breadth_pts + 1;
 end
end
for i=(breadth_pts+1):total_pts
 if Location_of_measured_points(4,i) == 3
 break;
 else
 depth_pts = depth_pts + 1;
 end
end
height_pts = total_pts/(2*(breadth_pts+depth_pts));
%Exporting general data
```

```
Uh_AverageWindSpeed = str2num(Uh_AverageWindSpeed);
xlswrite(A123_0_results,Building_breadth,'General_data','B2');
xlswrite(A123_0_results,Building_depth,'General_data','B3');
xlswrite(A123_0_results,Building_height,'General_data','B4');
xlswrite(A123_0_results,breadth_pts,'General_data','B5');
xlswrite(A123_0_results,depth_pts,'General_data','B6');
xlswrite(A123_0_results,height_pts,'General_data','B7');
xlswrite(A123_0_results,Sample_frequency,'General_data','B8');
xlswrite(A123_0_results,Sample_period,'General_data','B9');
xlswrite(A123_0_results,samples,'General_data','B10');
xlswrite(A123_0_results,total_pts,'General_data','B11');
xlswrite(A123_0_results,Uh_AverageWindSpeed, 'General_data',
'B12');
xlswrite(A123_0_results,Wind_direction_angle, 'General_data',
'B13');
%Exporting pressure point positions
pressure_pts(:,1) = Location_of_measured_points(3,:);
pressure_pts(:,2) = Location_of_measured_points(4,:);
pressure_pts(:,3) = Location_of_measured_points(1,:);
pressure_pts(:,4) = Location_of_measured_points(2,:);
xlswrite(A123_0_results,pressure_pts,'Pressure_pts','A2');
%Lets find average windward pressure coefficient along height
on time
%sample.
ww_avg_results = zeros(samples,height_pts);
rs_avg_results = zeros(samples,height_pts);
lw_avg_results = zeros(samples,height_pts);
ls_avg_results = zeros(samples,height_pts);
temp=1;
count=0;
for i=1:samples
 for j=1:total_pts
```

```
 count = count+1;
 if count>(2*(breadth_pts+depth_pts))
 count=1;
 temp = temp+1;
 end

 if ww_coeff(i,j)~=0
 ww_avg_results(i,temp) = ww_avg_results(i,temp)+
 ww_coeff(i,j);
 end

 end
 temp = 1;
 count =0;
end
for i=1:samples
 for j=1:height_pts
 ww_avg_results(i,j) = ww_avg_results(i,j)/breadth_pts;
 end
end
%Lets find average right sideward pressure coefficient along
height on time
%sample.
temp=1;
count=0;
for i=1:samples
 for j=1:total_pts
 count = count+1;
 if count>(2*(breadth_pts+depth_pts))
 count=1;
 temp = temp+1;
 end
```

```
 if rs_coeff(i,j)~=0
 rs_avg_results(i,temp) = rs_avg_results(i,temp)+
 rs_coeff(i,j);
 end

 end
 temp = 1;
 count =0;
end
for i=1:samples
 for j=1:height_pts
 rs_avg_results(i,j) = rs_avg_results(i,j)/depth_pts;
 end
end
%Lets find average leeward pressure coefficient along height
on time
%sample.
temp=1;
count=0;
for i=1:samples
 for j=1:total_pts
 count = count+1;
 if count>(2*(breadth_pts+depth_pts))
 count=1;
 temp = temp+1;
 end

 if lw_coeff(i,j)~=0
 lw_avg_results(i,temp) = lw_avg_results(i,temp)+
 lw_coeff(i,j);
 end
```

```
 end
 temp = 1;
 count =0;
end
for i=1:samples
 for j=1:height_pts
 lw_avg_results(i,j) = lw_avg_results(i,j)/breadth_pts;
 end
end
%Lets find average left sideward pressure coefficient
along height on time
%sample.
temp=1;
count=0;
for i=1:samples
 for j=1:total_pts
 count = count+1;
 if count>(2*(breadth_pts+depth_pts))
 count=1;
 temp = temp+1;
 end

 if ls_coeff(i,j)~=0
 ls_avg_results(i,temp) = ls_avg_results(i,temp)+
 ls_coeff(i,j);
 end

 end
 temp = 1;
 count =0;
end
```

```
for i=1:samples
 for j=1:height_pts
 ls_avg_results(i,j) = ls_avg_results(i,j)/depth_pts;
 end
end
ww_peak_results = zeros(samples,height_pts);
rs_peak_results = zeros(samples,height_pts);
lw_peak_results = zeros(samples,height_pts);
ls_peak_results = zeros(samples,height_pts);
%Lets find peak windward pressure coefficient along
height on time
%sample.
temp=1;
count=0;
peak_ww = -10;
for i=1:samples
 for j=1:total_pts
 count = count+1;
 if count>(2*(breadth_pts+depth_pts))
 count=1;
 temp = temp+1;
 peak_ww = -10;
 end

 if ww_coeff(i,j)~=0
 if ww_coeff(i,j) > peak_ww
 peak_ww = ww_coeff(i,j);
 ww_peak_results(i,temp) = peak_ww;
 end
 end

 end
```

```
 temp = 1;
 count =0;
 peak_ww = -10;
end
%Lets find peak right sideward pressure coefficient
along height on time
%sample.
temp=1;
count=0;
peak_rs = -10;
for i=1:samples
 for j=1:total_pts
 count = count+1;
 if count>(2*(breadth_pts+depth_pts))
 count=1;
 temp = temp+1;
 peak_rs = -10;
 end

 if rs_coeff(i,j)~=0
 if rs_coeff(i,j) > peak_rs
 peak_rs = rs_coeff(i,j);
 rs_peak_results(i,temp) = peak_rs;
 end
 end

 end
 temp = 1;
 count =0;
 peak_rs = -10;
end
%Lets find peak leeward pressure coefficient
```

```
along height on time
%sample.
temp=1;
count=0;
peak_lw = -10;
for i=1:samples
 for j=1:total_pts
 count = count+1;
 if count>(2*(breadth_pts+depth_pts))
 count=1;
 temp = temp+1;
 peak_lw = -10;
 end

 if lw_coeff(i,j)~=0
 if lw_coeff(i,j) > peak_lw
 peak_lw = lw_coeff(i,j);
 lw_peak_results(i,temp) = peak_lw;
 end
 end

 end
 temp = 1;
 count =0;
 peak_lw = -10;
end
%Lets find peak left sideward pressure coefficient
along height on time
%sample.
temp=1;
count=0;
peak_ls = -10;
```

```
for i=1:samples
 for j=1:total_pts
 count = count+1;
 if count>(2*(breadth_pts+depth_pts))
 count=1;
 temp = temp+1;
 peak_ls = -10;
 end

 if ls_coeff(i,j)~=0
 if ls_coeff(i,j) > peak_ls
 peak_ls = ls_coeff(i,j);
 ls_peak_results(i,temp) = peak_ls;
 end
 end

 end
 temp = 1;
 count =0;
 peak_ls = -10;
end
ww_min_results = zeros(samples,height_pts);
rs_min_results = zeros(samples,height_pts);
lw_min_results = zeros(samples,height_pts);
ls_min_results = zeros(samples,height_pts);
%Lets find minimum windward pressure coefficient
along height on time
%sample.
temp=1;
count=0;
min_ww = 10;
for i=1:samples
```

```
 for j=1:total_pts
 count = count+1;
 if count>(2*(breadth_pts+depth_pts))
 count=1;
 temp = temp+1;
 min_ww = 10;
 end

 if ww_coeff(i,j)~=0
 if ww_coeff(i,j) < min_ww
 min_ww = ww_coeff(i,j);
 ww_max_results(i,temp) = min_ww;
 end
 end

 end
 temp = 1;
 count =0;
 min_ww = 10;
end
%Lets find minimum right sideward pressure coefficient
along height on time
%sample.
temp=1;
count=0;
min_rs = 10;
for i=1:samples
 for j=1:total_pts
 count = count+1;
 if count>(2*(breadth_pts+depth_pts))
 count=1;
 temp = temp+1;
```

```
 min_rs = 10;
 end

 if rs_coeff(i,j)~=0
 if rs_coeff(i,j) < min_rs
 min_rs = rs_coeff(i,j);
 rs_min_results(i,temp) = min_rs;
 end
 end

 end
 temp = 1;
 count =0;
 min_rs = 10;
end
%Lets find minimum leeward pressure coefficient
along height on time
%sample.
temp=1;
count=0;
min_lw = 10;
for i=1:samples
 for j=1:total_pts
 count = count+1;
 if count>(2*(breadth_pts+depth_pts))
 count=1;
 temp = temp+1;
 min_lw = 10;
 end

 if lw_coeff(i,j)~=0
 if lw_coeff(i,j) < min_lw
```

```
 min_lw = lw_coeff(i,j);
 lw_min_results(i,temp) = min_lw;
 end
 end


 end
 temp = 1;
 count =0;
 min_lw = 10;
end
%Lets find minimum left sideward pressure coefficient
along height on time
%sample.
temp=1;
count=0;
min_ls = 10;
for i=1:samples
 for j=1:total_pts
 count = count+1;
 if count>(2*(breadth_pts+depth_pts))
 count=1;
 temp = temp+1;
 min_ls = 10;
 end


 if ls_coeff(i,j)~=0
 if ls_coeff(i,j) < min_ls
 min_ls = ls_coeff(i,j);
 ls_min_results(i,temp) = min_ls;
 end
 end
```

```
 end
 temp = 1;
 count =0;
 min_ls = 10;
end
height = zeros(2,height_pts);
temp = 1;
for i=1:height_pts
 height(1,i) = i;
 height(2,i) = Location_of_measured_points(2,temp);
 temp=temp+(2*(breadth_pts+depth_pts));
end
time = zeros(samples,1);
for i=1:samples
 time(i,1) = i/Sample_frequency;
end
%Writes average Wind THA for net along wind and across
wind pressure coeff.
net_avg_along_wind_tha = zeros(samples,height_pts);
net_avg_across_wind_tha = zeros(samples,height_pts);
% avg_max_along = 1;
% avg_max_across = 1;
for i=1:samples
 for j=1:height_pts
 net_avg_along_wind_tha(i,j) = ww_avg_results(i,j)
 - lw_avg_results(i,j);
 net_avg_across_wind_tha(i,j) = rs_avg_results(i,j)
 - ls_avg_results(i,j);
 end
end
%Finding absolute maximum along and across sum
coefficient time
```

```
%app1 denotes approach 1 in which time at which base
shear becomes maximum
%is selected
app1_along_sum = zeros(samples,2);
app1_across_sum = zeros(samples,2);
for i=1:samples
 app1_along_sum(i,1) = i;
 app1_across_sum(i,1) = i;
 app1_along_sum(i,2) = sum(net_avg_along_wind_tha(i,:));
 app1_across_sum(i,2) = sum(net_avg_across_wind_tha(i,:));
end
app1_max_along = [app1_along_sum(1,1)
app1_along_sum(1,2)];
app1_max_across = [app1_across_sum(1,1)
app1_across_sum(1,2)];
for i=1:samples
 if abs(app1_max_along(1,2)) < abs(app1_along_sum(i,2))
 app1_max_along(1,1) = app1_along_sum(i,1);
 app1_max_along(1,2) = app1_along_sum(i,2);
 end
 if abs(app1_max_across(1,2)) < abs(app1_across_sum(i,2))
 app1_max_across(1,1) = app1_across_sum(i,1);
 app1_max_across(1,2) = app1_across_sum(i,2);
 end
end
app1_final_maxsum_along_result = zeros(height_pts,2);
app1_final_maxsum_across_result = zeros(height_pts,2);
for i=1:height_pts
 app1_final_maxsum_along_result(i,1) =
 net_avg_along_wind_tha(app1_max_along(1,1),i);
 app1_final_maxsum_along_result(i,2) =
 net_avg_across_wind_tha(app1_max_along(1,1),i);
```

```
 app1_final_maxsum_across_result(i,1) =
 net_avg_along_wind_tha(app1_max_across(1,1),i);
 app1_final_maxsum_across_result(i,2) =
 net_avg_across_wind_tha(app1_max_across(1,1),i);
end
%Exporting Approach 1 results
xlswrite(A123_0_results,height,'Along_wind_THA','B4');
xlswrite(A123_0_results,time,'Along_wind_THA','A6');
xlswrite(A123_0_results,net_avg_along_wind_tha,
'Along_wind_THA','B6');
xlswrite(A123_0_results,height,'Across_wind_THA','B4');
xlswrite(A123_0_results,time,'Across_wind_THA','A6');
xlswrite(A123_0_results,net_avg_across_wind_tha,
'Across_wind_THA','B6');
xlswrite(A123_0_results,app1_max_along,'Final_coeff',
'B4');
xlswrite(A123_0_results,app1_max_across,'Final_coeff',
'B5');
xlswrite(A123_0_results,height(2,:)','Final_coeff',
'A8');
xlswrite(A123_0_results,height(2,:)','Final_coeff',
'D8');
xlswrite(A123_0_results,app1_final_maxsum_along_result,
'Final_coeff','B8');
xlswrite(A123_0_results,app1_final_maxsum_across_result,
'Final_coeff','E8');
%Writes peak Wind THA for net along wind and across
wind pressure coeff.
net_peak_along_wind_tha = zeros(samples,height_pts);
net_peak_across_wind_tha = zeros(samples,height_pts);
for i=1:samples
 for j=1:height_pts
```

```
 net_peak_along_wind_tha(i,j) = ww_peak_results(i,j)
 - lw_min_results(i,j);
 net_peak_across_wind_tha(i,j) = rs_peak_results(i,j)
 - ls_min_results(i,j);
 end
end
%Finding peak along and across sum coefficient time
peak_along_wind = zeros(1,height_pts);
peak_across_wind = zeros(1,height_pts);
for i=1:height_pts
 peak_along_wind(1,i) = net_peak_along_wind_tha(1,i);
 peak_across_wind(1,i) = net_peak_across_wind_tha(1,i);
end
for i=1:samples
 for j = 1:height_pts
 if net_peak_along_wind_tha(i,j) > peak_along_wind(1,j)
 peak_along_wind(1,j) = net_peak_along_wind_tha(i,j);
 end
 if net_peak_across_wind_tha(i,j) > peak_across_wind(1,j)
 peak_across_wind(1,j) = net_peak_across_wind_tha(i,j);
 end
 end
end
%Exporting Peak Wind Force results
xlswrite(A123_0_results,height,'Along_wind_THA','AE4');
xlswrite(A123_0_results,time,'Along_wind_THA','AD6');
xlswrite(A123_0_results,net_peak_along_wind_tha,
'Along_wind_THA','AE6');
xlswrite(A123_0_results,height,'Across_wind_THA','AE4');
xlswrite(A123_0_results,time,'Across_wind_THA','AD6');
xlswrite(A123_0_results,net_peak_across_wind_tha,
'Across_wind_THA','AE6');
```

```
xlswrite(A123_0_results,height(2,:)','Final_coeff','J8');
xlswrite(A123_0_results,peak_along_wind','Final_coeff','K8');
xlswrite(A123_0_results,peak_across_wind',
'Final_coeff','L8');
%Lets find mean wind force coeff
mean_along_wind = zeros(1,height_pts);
mean_across_wind = zeros(1,height_pts);
for i=1:samples
 for j=1:height_pts
 mean_along_wind(1,j) = mean_along_wind(1,j)
 + net_avg_along_wind_tha(i,j);
 mean_across_wind(1,j) = mean_across_wind(1,j)
 + net_avg_across_wind_tha(i,j);
 end
end
for j=1:height_pts
 mean_along_wind(1,j) = mean_along_wind(1,j)/samples;
 mean_across_wind(1,j) = mean_across_wind(1,j)/samples;
end
%Exporting Approach 1 results
xlswrite(A123_0_results,height,'Along_wind_THA','BK4');
xlswrite(A123_0_results,time,'Along_wind_THA','BJ6');
xlswrite(A123_0_results,net_avg_along_wind_tha,
'Along_wind_THA','BK6');
xlswrite(A123_0_results,height,'Across_wind_THA','BK4');
xlswrite(A123_0_results,time,'Across_wind_THA','BJ6');
xlswrite(A123_0_results,net_avg_across_wind_tha,
'Across_wind_THA','BK6');
xlswrite(A123_0_results,height(2,:)','Final_coeff','P8');
xlswrite(A123_0_results,mean_along_wind','Final_coeff','Q8');
xlswrite(A123_0_results,mean_across_wind',
'Final_coeff','R8');
```

Appendix D

Design of Composite Slab

Fig. D.1 shows composite slab considered for design in floor plan and fig. D.2 and fig. D.3 shows metal deck and composite slab support details respectively.

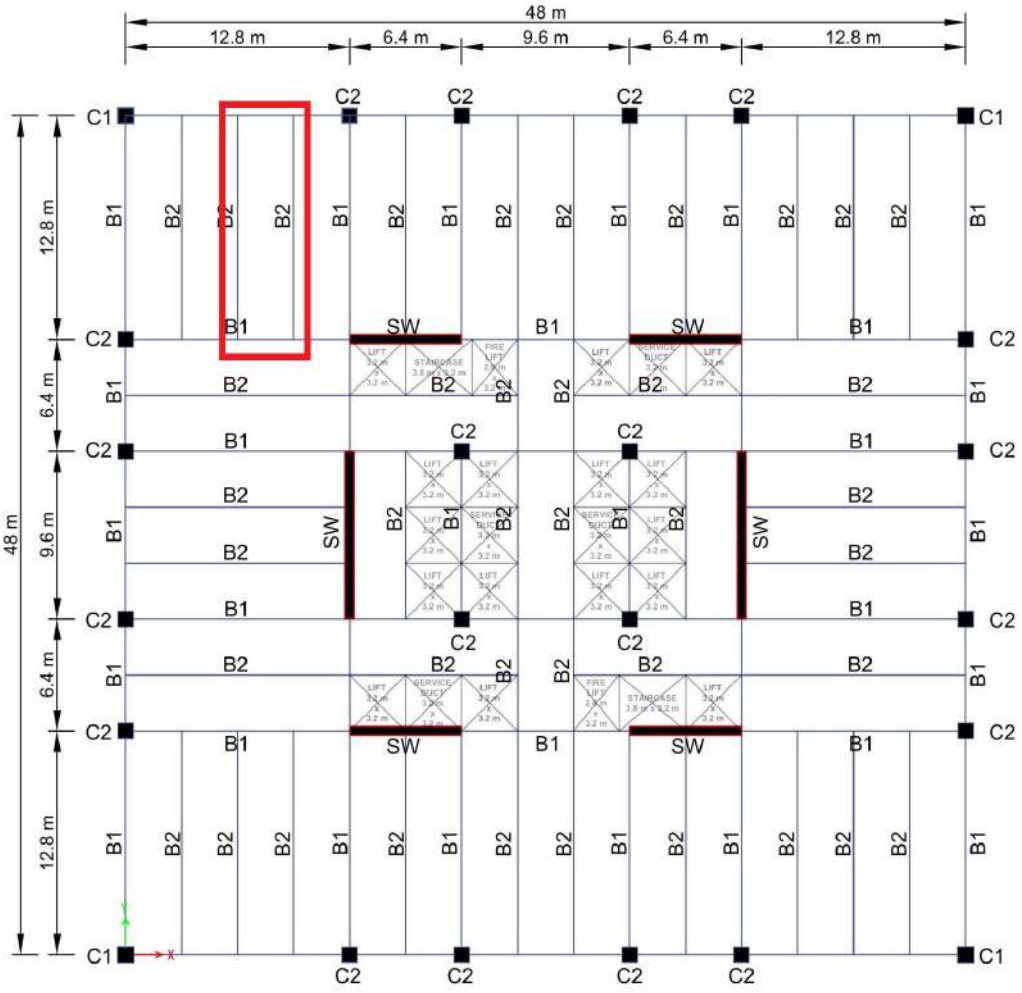

Figure D.1: Composite Slab Plan Details

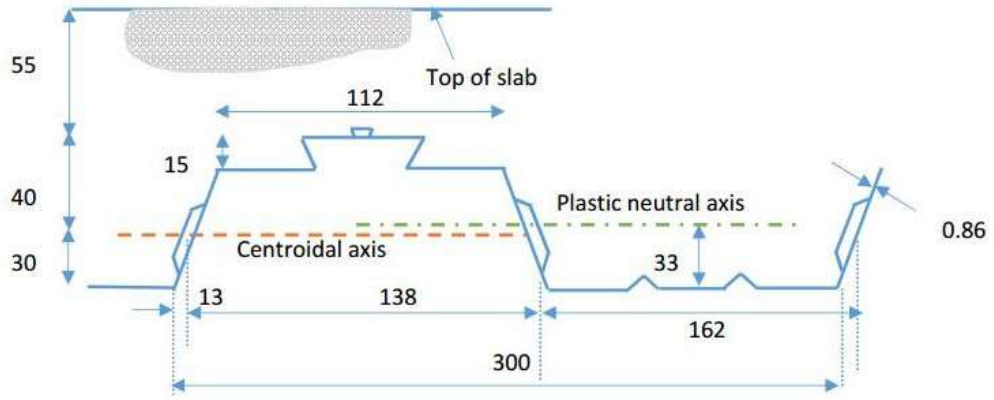

Figure D.2: Metal Deck Details

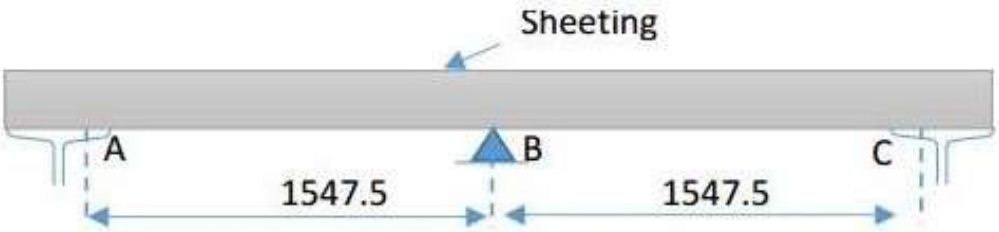

Figure D.3: Composite Slab Support Details

Design calculations for composite slab is given in Table. D.1.

Table D.1: Design of composite slab

General data				
Span of deck	l_x	=	3.2	m
Partial safety factor	γ_{ap}	=	1.15	
Concrete grade	fck	=	70	N/mm2
Total depth of composite slab	D	=	125	mm
Decking sheet data				
Yeild strength of steel	fyp	=	540	N/mm2
Design thickness of sheet	tp	=	0.86	mm
Effective area of cross section	Ap	=	1185	mm2/m
Moment of Inertia	Ip	=	570000	mm4/m

Plastic moment of resistance	Mpa	=	4.92	kNm/m
Distance of centroid above base	e	=	30	mm
Distance of plastic neutral axis above base	ep	=	33	mm
Resistance to vertical shear	Vpa	=	49.2	kN/m
For resistance to longitudinal shear	m	=	184	N/mm2
	k	=	0.053	N/mm2
Modulus of elasticity of steel	Ea	=	200000	N/mm2
Depth of the sheeting	Dp	=	70	mm
Load data				
Description	Load (N/mm2)		Factored Load (N/mm2)	
Imposed Load	5		7.5	
Dead Load	4.375		5.90625	
Construction Load	0.75		1.125	
Profile sheet as shuttering				
Profile deck sheet is propped at centre				
Assume top flange of supporting steel beams		=	0.175	m
Effective length le		=	1547.5	mm
Moments				
Sagging moment		=	1.44808	kNm/m
Hogging moment		=	1.71375	kNm/m
Shear				
Shear force at A		=	5.44043	kN/m
Shear force at B		=	6.52852	kN/m
Design Moment		=	4.27826	kNm/m
Design Shear		=	42.78261	kN/m
Design load at construction stage		=	5.125	kN/m^2
Max deflection at construction stage		=	1.393606	mm
Composite slab				
distance between center of supports		=	3200	mm

clear distance btween supports+eff. Depth of slab					=	3145	mm
effective length Le					=	3145	mm
Design ultimate loading ($w_{u,DL}$ +$w_{u,LL}$)					=	13.4063	kN/m^2
Mid span B.M					=	16.5752	kNm/m
Span for vertical shear calculation					=	3200	mm
Vertical shear at support					=	21.45	kN/m
Ncf					=	556.435	kN/m
Design compressive strength of concrete fck					=	21.6	N/mm^2
X					=	25.761	mm
hc					=	55	mm
Md,rd					=	46.849	kNm/m
Check for vertical shear							
b0					=	162	mm
b					=	300	mm
dp					=	95	mm
Effective area in shear of profile Ap					=	173.72	mm^2
ρ					=	0.01129	Ok
Kv					=	1.505	Ok
Shear stength of concrete Vv,Rd					=	0.3	N/mm^2
Vv,Rd					=	38.2523	kN/m
Check for longitudinal shear							
γ_{vs}					=	1.25	
Ls					=	800	mm
Vi,Rd					=	21.9222	kN/m
Check for serviceability							
Provide 0.4% reinforcement to avoid cracking							
As					=	220	mm^2/m
Reniforment steel	Dia	=	8	mm	@	200	mm c/c
Provided As				=	251.327	mm^2/m	Ok
Span/depth					=	31.8421	Ok

Appendix E

Composite Beam Design as per AISC 360-16

Design calculations for composite beam is given in Table. E.1

Table E.1: Design of Composite Beam as per AISC 360-16

General Data			Remarks
Span of slab	3.2	m	-
Beam span	12.8	m	-
Concrete Grade f'c	60	N/mm2	-
Steel yield Stress Fy	380	N/mm2	-
SteelUltimate Stress Fu	540	N/mm2	-
Diameter of stud dsa	20	mm	-
Shored Construction	No	-	-
Composite Slab Thickness	125	mm	Manufacturer's Data
Deck depth/ rib height	70	mm	
Average rib width wr	162	mm	
Deck sheet weight	0.13	kN/m2	
Dead Loads			
Pre-composite Loads			
Wet concrete slab wight	2.3	kN/m2	MF Data
Beam Self weight	0.5	kN/m2	Assumed

Composite Loads			
Services, partition walls, FF	2	kN/m2	Assumed
Dry concrete slab weight	2.2	kN/m2	MF Data
Live Loads			
Pre-composite Loads			
Construction Load	0.75	kN/m2	Assumed
Composite Loads			
Imposed Load	5	kN/m2	IS 875 : 1987 (Part2)
Composite Deck and Anchor Requirement			
Concrete Grade f'c	60	Ok	AISC I1.3
Deck depth/ rib height	70	Ok	AISC I3.2c
Average rib width wr	162	Ok	AISC I3.2c
Diameter of stud dsa	20	Ok	AISC I8.1
Provided length of stud (mm)	100	Ok	AISC I8.2 and I3.2c
Thickness of flange required	8	mm	AISC I8.1
Concrete Cover above stud	25	Ok	AISC I3.2c
Minimum slab thickness (mm)	121	Ok	AISC I3.2c
Design for Pre-composite Condition			
DL partial safety factor	1.5	-	ASCE 7
IL partial safety factor	1.5	-	ASCE 7
wD	9.376	kN/m	-
wL	2.4	kN/m	-
Mu	361.75872	kNm/m	-
ϕb	0.9	-	AISC I3.2.a
Zx,min	1057.774035	cm3	AISC F2.1
Section Properties			
Select I section	ISWB 450	-	
Zx,prov	1760.59	cm3	SP 6 Handbook
weight w	79.4	kg/m	
Depth h	450	mm	
Width bf	200	mm	

Area A	10115	mm2	SP 6 Handbook
Flange thickness tf	15.4	mm	
Web thickness tw	9.2	mm	
Radius R1	14	mm	
MOI Ix	350576000	mm4	
MOI IY	17067000	mm4	
Pre-composite Deflection			
δnc	46.73950192	mm	-
Allowable deflection	35.55555556	mm	Camber required
Maximum camber allowed	37.39160154	mm	AISC Design Guide 3
Camber provided	55	mm	Ok
Composite Condition			
wD	15.456	kN/m	-
wL	16	kN/m	-
wu	47.184	kN/m	-
Mu	966.32832	kNm/m	-
Effective width b	3.2	m	AISC I3.1a
h/tw	48.91304348	-	-
Plastic distribution check	Ok	-	AISC I3.2a
Effective area of concrete Ac	288000	mm2	-
Stud Compressive force C			
Concrete crushing	14688	kN	AISC Spec. Comm. Eq-C-I3-7
Steel Yeilding	3843.7	kN	AISC Spec. Comm. Eq-C-I3-6
Percentage of composite	50	%	
Stud Compressive force C	1921.85	kN	AISC Spec. Comm. Eq-C-I3-8
PNA Distance x	12.64375	mm	-
a	11.77604167	Ok	AISC Spec. Comm. Eq-C-I3-9
d1	119.1119792	mm	-
d2	6.321875	mm	-
d3	225	mm	-
Py	3843.7	kN	-

Mn	1081.598162	kNm	AISC Spec. Comm. Eq-C-I3-10
ϕbMn	973.4383455	kNm	Ok
Live Load Deflection			
YENA	397.0559896	mm	AISC Spec. Comm. Eq-C-I3-2
ILB	949450021.6	mm4	AISC Spec. Comm. Eq-C-I3-1
δc (mm)	29.45076205	Ok	T. 1604.3 of IBC (ICC, 2015)
δc (mm)	14.72538103	Ok	AISC Design Guide 3
Anchor Design			
Qn	65	N/mm2	AISC Manual T. 3-21
Nos of anchor per rib	2	-	-
Flute spacing	300	mm	MF Data
nflutes	42	-	-
nanchor	29.56692308	-	Ok
Spacings of anchor	300	mm	Ok
Shear Strength Check			
h/tw	48.91304348	-	Ok
Cv1	1	-	AISC Spec. Comm. Eq-G-2-2
ϕVn	943.92	kN	AISC Spec. Comm. Eq-G-2-1
Vu	301.9776	kN	Ok

Appendix F

Design of Steel Beam as per IS 800: 2007

Design calculations for steel beam is given in Table. F.1

Table F.1: Design of steel beam as per IS 800: 2007

DATA INPUT		
Factored Maximum Bending Moment M (kNm)	=	3839
Factored Maximum Shear Force F (kN)	=	1245
Trial I Section Beam	=	I 750x450x40x20
Yield Strength of Member (fy) (N/mm2)	=	540
Is beam Simply Supported (SS) or Cantilever (CA) ?	=	CO
Stiff Bearing Length at Support (b1) (mm)	=	375
SECTION PROPERTIES		
Depth of Section (h) (mm)	=	750
Width of Flange (bf) (mm)	=	450
Thickness of Flange (tf) (mm)	=	40
Thickness of Web (tw) (mm)	=	20
Radius at Root (R1) (mm)	=	0
Depth of web (d) (mm)	=	670
Moment of Inertia about Major Axis (Izz) (mm4)	=	6324825000
Moment of Inertia about Minor Axis (Iyy) (mm4)	=	608000000

Elastic Section Modulus (Zez) (mm3)	=	17032500
Plastic Section Modulus (Zpz) (mm3)	=	20439000
Section Weight w(kN/m)	=	3.93
SECTION CLASSIFICATION		
IS 800 : 2007, Cl.3.7.2 and Cl.3.7.4, TABLE 2		
e	=	0.680413817
b/tf	=	5.625
d/tw	=	33.5
Plastic Section		
CHECK FOR SHEAR BUCKLING		
IS 800 :2007, Cl. 8.4.2		
d/tw	=	33.5
CHECK FOR SHEAR		
IS 800 : 2007, Cl. 8.4		
Av (mm2)	=	15000
Vd (kN)	=	4251
SAFE IN SHEAR		
0.6*Vd (kN)	=	2550.6
Design Beam as Low Shear		
CHECK FOR THE DESIGN CAPACITY OF THE SECTION		
IS 800 : 2007, Cl. 8.2.1.2		
β_b	=	1
Limiting Md (kNm)	=	12542.11364
Md (kNm)	=	10033
SAFE IN BENDING MOMENT		
CHECK FOR WEB BUCKLING AT SUPPORT		
IS 800 : 2007, Cl. 8.7.3.1		
KL (mm)	=	469
r (mm)	=	5.773502692
KL/r	=	81.23318287

fcc (N/mm2)	=	299.1319492
MOI	=	1.34358603
f	=	1.682790287
fcd (N/mm2)	=	84
n1 (mm)	=	375
Ab (mm2)	=	15000
Buckling Resistance Fcdw (kN)	=	1260
SAFE IN WEB BUCKLING AT SUPPORT		
CHECK FOR WEB CRIPPLING OR WEB BEARING		
IS 800 : 2007, Cl. 8.7.4		
n2 (mm)	=	100
Fw (kN)	=	4663
SAFE IN WEB CRIPPLING OR WEB BEARING		